KU LEUVEN

ARENBERG DOCTORAL SCHOOL
Faculty of Science

Beyond Classical Cosmology with the No-Boundary Wave Function

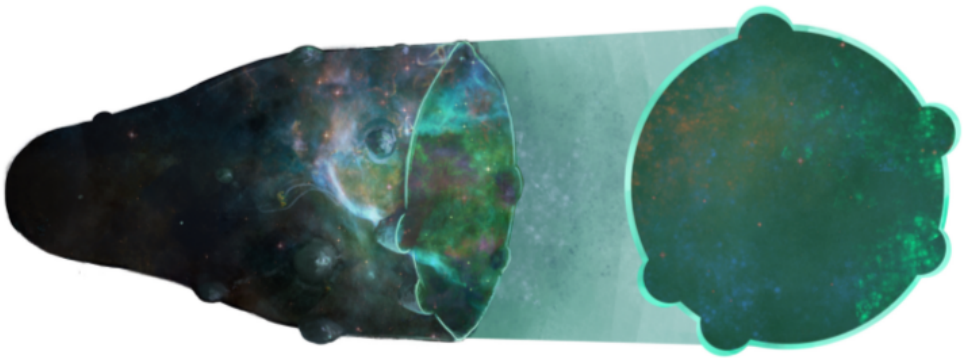

Yannick Vreys

Supervisor:
Prof. dr. T. Hertog

Dissertation presented in partial fulfilment of the requirements for the degree of Doctor of Science (PhD): Physics

September 2017

Beyond Classical Cosmology with the No-Boundary Wave Function

Yannick VREYS

Examination committee:
Prof. dr. A. Van Proeyen, chair
Prof. dr. T. Hertog, supervisor
Prof. dr. C. Maes
Prof. dr. T. Van Riet
Prof. dr. F. Denef
(Columbia University in the City of New York and KU Leuven)
Prof. dr. J. Hartle
(University of California, Santa Barbara)

Dissertation presented in partial fulfilment of the requirements for the degree of Doctor of Science (PhD): Physics

September 2017

© 2017 KU Leuven – Faculty of Science
Uitgegeven in eigen beheer, Yannick Vreys, Celestijnenlaan 200D, B-3001 Leuven (Belgium)

Cover illustration by Nicky Vreys

Alle rechten voorbehouden. Niets uit deze uitgave mag worden vermenigvuldigd en/of openbaar gemaakt worden door middel van druk, fotokopie, microfilm, elektronisch of op welke andere wijze ook zonder voorafgaande schriftelijke toestemming van de uitgever.

All rights reserved. No part of the publication may be reproduced in any form by print, photoprint, microfilm, electronic or any other means without written permission from the publisher.

ACKNOWLEDGEMENTS

As the reader will notice, I refrain from using the pronoun *I* in the main part of this thesis, but instead constantly use the pronoun *we*. This is because research, and especially writing a thesis, is almost never performed alone in a room without contact with the outside world. Here I would like to thank all the people who changed the *I* into a *we*.

First of all I would like to thank my supervisor Thomas Hertog who introduced me five years ago to the fascinating subject of the wave function of the universe and gave me the opportunity to learn after my masterthesis even more about this mysterious object. His guidance and ideas have helped shape this thesis.

Secondly, big thanks should go to all the other people with whom I closely collaborated. Ruben, Nikolay, Sebastian, Jean-Luc, Pablo and Gabriele, thank you for the interesting discussions and collaborations! Thanks should also go to all the other members of the high energy group in Leuven for organising interesting discussion sessions and seminars, and also for making the general working atmosphere so enjoyable. I would also like to thank Pierre for reading through the introduction and correcting my language mistakes. The members of my examination committee should not be forgotten here, because they made the effort to go through this thesis and showed me the missing gaps in the introduction.

Because *all work and no play makes Jack a dull boy* I would also like to thank the people who did not directly contribute to this thesis, but without whom this adventure would never have worked out. All the people of the ITF should get a big thank you here for making coming to work a real pleasure! Special mention should go to Kristof for organising the ITF Christmas band and (board)game nights, Alexandre for getting everyone to lunch for two years, Tom for fixing rides to the Sportpaleis, Ruben M for showing me around New York and Brecht for sharing a room in Amsterdam (and together with Ruben having the same sense of "humour"). The people who started their PhD with me, Michiel,

Jesper and Pieter also deserve to be thanked for sharing frustrations about the doctoral diary and other Arenberg Doctoral School regulations. My office mates, Gabriele, Pieter, Jonas and Frederik, thanks for sticking up with me in your office. And last but definitely not least, I have to thank the (social) engine of the sixth floor, Anneleen and Filip, for organizing all the get-togethers, barbecues, parties, for bringing cookies during the coffee break and also for taking care of all the administrative tasks and fixing my computer problems.

Also, outside the ITF group I would like to thank a lot of people for their support and their friendship throughout the years (and I should not forget all the beers and nonsense discussions). So, thank you my friends from 't Kamp: Micha, Maarten, Robin, Niels and Barthel, my friends from the Neanias (and also from DST): Bart, Dries D, Dries V (whom I would also like to thank for the innumerable drives between Leuven and Beverlo), Kobe, Nadia, Niels, and Roeland, my physics buddies: Elise, Janne, Karel, Kasper, Laurens, Michiel, Roald, Ruben D, Simon, Valerie, Yana and the people with whom I shared a house for two years: Katrijn and Marc, Lies, Pieter, Melissa and Thimothy.

Als laatste wil ik graag mijn gehele familie bedanken. Mama en papa, bedankt dat jullie mij altijd hebben gesteund (en ondersteund) in mijn keuze om fysica te gaan studeren, ook al hadden jullie geen idee wat het inhield en wat ik er later mee kon doen (en waarschijnlijk nu nog altijd geen idee hebben). Ook mijn grootouders, tantes en nonkels wil ik bedanken voor het zorgen dat ik een zorgeloze jeugd had en daardoor altijd mijn eigen interesses kon navolgen. In het bijzonder wil ik ook mijn broer, Nicky, bedanken voor het maken van de voorpagina tekening.

Last but not least, bedankt Karen om in mijn leven te komen (iets meer dan) vier jaar geleden. Bedankt voor al je liefde, steun en vertrouwen en om me er altijd aan te herinneren dat ik mijn thesis nog moest schrijven.

ABSTRACT

The goal of quantum cosmology is to find a quantum state that describes the entire evolution of our universe: from the fuzzy quantum dynamics dominating the universe's evolution at early times to the classical cosmological evolution in our spacetime neighbourhood. Classical cosmology emerges in quantum cosmology under certain conditions only. In recent years significant progress has been made to understand the "classical realm" predicted by the No-Boundary Wave Function (NBWF), which will be the main focus of this thesis. However, it has not been understood how to go beyond this and learn something about the quantum realm of the universe as predicted by the NBWF. In this thesis we take a number of steps in this direction.

The NBWF relates on a semiclassical level, Lorentzian de Sitter (dS) solutions to Euclidean Anti-de Sitter (AdS) solutions, which in their turn correspond, using the AdS/CFT conjecture, to a dual field theory defined on their boundary. This allows for a holographic formulation of the NBWF in which the relative weighting of different cosmological histories is given by the partition functions of (Euclidean) AdS/CFT duals. In this thesis we develop this novel holographic form of the NBWF in several directions.

In the first part of this thesis we investigate the emergence of classical cosmological evolution from the boundary field theory and derive a sufficient set of conditions to obtain classical, Lorentzian bulk evolution at large spatial volumes. This derivation is based on the construction of a new wave function in terms of asymptotic variables, which are related to the sources of the dual field theory. With this new wave function it is possible to define new classicality conditions using the vacuum expectation values (vevs) from the dual boundary theory.

In the second part of this thesis we look at the physics of eternal inflation, a regime where the dynamics of the theory is governed by large quantum fluctuations that get produced together with their backreaction on the geometry,

meaning that the background does not evolve classically any more and that we therefore cannot get information about the global structure of the universe using the available techniques of the NBWF. With the use of the holographic NBWF proposal, it is possible to have an alternative calculation of the no-boundary measure, which is not plagued by the absence of a classical background. We show that it is possible to deduce some properties of the global structure of eternal inflation, by considering as a toy model a field theory living on a double squashed three-sphere. Both the squashed spheres and eternal inflation have highly curved regions and a high overall anisotropy. We start by calculating Euclidean AdS solutions that have the boundary of a squashed sphere and compare these with the free $O(N)$ model. We find that the free energies of the two theories are remarkably similar, if we do not consider scalar excitations. We also comment on a universal property for CFTs on a squashed sphere. Namely, the field theory free energy has a local maximum in terms of the squashing parameter at zero squashing. Properties like this can be translated, using the holographic no-boundary conjecture, to cosmological spaces, with the result that the measure is peaked around isotropic universes, suggesting that holography predicts a smooth exit from eternal inflation. This is verified by the explicit calculation of the interacting $O(N)$ model on the squashed sphere, which gives a distribution function that is globally peaked at the round sphere with zero scalar deformation with a low amplitude for geometries with negative scalar curvature.

In the last part of this thesis we track the classical histories predicted by the NBWF back in time to the moment that the classicality conditions are not satisfied any more. Here, quantum-mechanical effects should be taken into account, making it possible that a classically forbidden transition happens between classical patches of cosmological evolution. We study these transitions by constructing complex saddle points that connect two classically evolving regions. The probabilities for transitions are then found to be the actions of these saddle points. We observe that universes at large values of the potential prefer a symmetric transition, while universes with a small value for the potential have a higher likelihood to transition to universes with a larger value of the potential.

BEKNOPTE SAMENVATTING

Het doel van kwantumkosmologie is het vinden van een kwantumtoestand die de gehele evolutie van ons Universum kan beschrijven: vanaf het begin van het Universum waarin de evolutie gedomineerd wordt door de wetten van de kwantummechanica tot de klassieke kosmologische evolutie in onze ruimtetijd omgeving. Klassieke Universa kunnen in de kwamtumkosmologie slechts onder zeer specifieke omstandigheden ontstaan. De afgelopen jaren is er veel vooruitgang geboekt met het begrijpen van het klassieke regime dat wordt voorspeld door de Hartle-Hawking golffunctie, ook wel de "No-Boundary Wave Function" genoemd of afgekort NBWF – een golffunctie voor het universum waarop onze focus zal liggen in deze thesis. Het is echter nog niet goed begrepen hoe we voorbij dit klassieke regime kunnen gaan en iets kunnen leren over het kwantumregime van het Universum, zoals voorspeld door de NBWF. In deze thesis zullen we een paar stappen zetten in deze richting.

De NBWF relateert op een semiklassiek niveau, Lorentziaanse de Sitter (dS) oplossingen met Euclidische anti-de Sitter (AdS) oplossingen, die op hun beurt weer overeenkomen, met behulp van de AdS/CFT conjectuur, met een duale veldentheorie gedefinieerd op de AdS rand. Hierdoor kan de NBWF op een holografische manier geformuleerd worden door de relatieve waarschijnlijkheidsverdeling van verschillende kosmologische geschiedenissen te geven door partitiefuncties van de (Euclidische) AdS/CFT duale. In deze thesis zullen we deze nieuwe holografische beschrijving van de NBWF verder uitwerken in verschillende richtingen.

In het eerste deel van deze thesis gaan we de emergentie van klassieke kosmologische evolutie onderzoeken vanuit de veldentheorie op de rand en zullen we een voldoende set van condities afleiden om klassieke, Lorentziaanse bulk evolutie te verkrijgen op grote ruimtelijke volumes. Deze afleiding is gebaseerd op de constructie van een nieuwe golffunctie in termen van asymptotische variabelen die gerelateerd zijn aan de bronnen van de duale veldentheorie. Met deze nieuwe golffunctie is het mogelijk om nieuwe klassikaliteitsvoorwaarden te

definiëren door gebruik te maken van de vacuumsverwachtingswaarden van de duale veldentheorie.

In het tweede deel van deze thesis zullen we kijken naar de fysica achter *eeuwige inflatie*, een regime waar de dynamica van de kosmologische evolutie beheerst wordt door grote kwantumfluctuaties die geproduceerd worden samen met hun invloed op de evolutie van de achtergrond geometrie. Dit betekent dat de achtergrond niet meer klassiek evolueert en dat we hierdoor geen informatie kunnen bemachtigen over de globale structuur van het Universum met de huidige technieken van de NBWF. Echter, met behulp van de holografische NBWF, is het mogelijk om een alternatieve berekening uit te voeren van de NBWF waarschijnlijkheidsverdeling die niet wordt belemmerd door de afwezigheid van een klassieke achtergrond. We tonen aan dat het mogelijk is om enkele eigenschappen van de globale structuur van eeuwige inflatie af te leiden door te kijken naar een vereenvoudigd model dat bestaat uit een veldentheorie die leeft op een dubbel gedeformeerde drie-sfeer. Zowel de gedeformeerde sfeer als eeuwige inflatie hebben regios met een grote kromming en hebben ook een grote totale anisotropie. We starten met het berekenen van Euclidische AdS oplossingen die als rand een dergelijke gedeformeerde sfeer hebben. Deze vergelijken we dan met het vrije $O(N)$ vector model. We vinden dat de vrije energieën van de twee theoriën opmerkelijk veel gelijkenissen vertonen, als we geen scalaire excitaties beschouwen. We merken ook een universele eigenschap op voor conforme veldentheorieën op gedeformeerde sferen. We zien namelijk dat de vrije energie van de veldentheorie altijd een lokaal maximum heeft in functie van de deformatie parameter en dit maximum bereikt als er geen deformatie is. Zo een eigenschappen kunnen vertaald worden, door gebruik te maken van de holografische NBWF conjectuur, naar kosmologische ruimtes, met het resultaat dat de waarschijnlijkheidsverdeling gepiekt is rond isotrope Universa. Dit suggereert dat holografie voorspelt dat het regime van eeuwige inflatie toch niet zo eeuwig is. Dit is geverifieerd door de expliciete berekening van de partitiefunctie van het interagerende $O(N)$ model op de gedeformeerde sfeer, die een distributiefunctie geeft die globaal piekt rond de ronde sfeer zonder scalaire excitaties met een lage amplitude voor geometrieën met negatieve scalaire kromming.

In het laatste deel van deze thesis kijken we naar wat er gebeurt als we de klassieke geschiedenissen, die voorspeld worden door de NBWF, terug in de tijd evolueren tot op het moment dat de klassikaliteitsvoorwaarden niet meer voldaan zijn. Op dit moment zouden kwantummechanische effecten in rekening gebracht moeten worden, zodat het mogelijk wordt dat er een transitie, die klassiek verboden is, tussen twee niet-geconnecteerde klassieke regio's van kosmologische evolutie plaatsvindt. We bestuderen deze transities door complexe zadelpunten te construeren die twee klassiek evoluerende regio's verbinden. De

waarschijnlijkheden van deze transities zijn dan geassocieerd aan de acties van deze zadelpunten. We observeren dat Universa met grote waardes van de potentiaal een symmetrische overgang verkiezen, terwijl Universa met een kleine waarde van de potentiaal een grotere waarschijnlijkheid hebben om over te gaan naar Universa met een hogere waarde van de potentiaal.

CONTENTS

CHAPTER 1

INTRODUCTION

The beginning of the 20th century marked the birth of modern physics with the discovery of both quantum mechanics and the theory of General Relativity (GR). Both theories changed the way we think about nature and shaped the course of research. Quantum mechanics taught us that at the shortest length scales the physical laws as envisioned by Newton, do not hold any more. Instead it was found that objects should be described by complex wave functions in a Hilbert space obeying the Schrödinger equation.

On the other hand, the discovery of the theory of GR by Albert Einstein affects only the largest scales in the universe. The Einstein field equations couple the geometry of space-time to matter, meaning that not only space gets curved by massive objects, but also that the motion of these objects is determined by the curvature of space-time. In our everyday lives the curvature is weak enough that we cannot tell the difference between an object moving according to the laws of GR or to the ones of Newton. But the effect is more obvious at cosmological scales. For example, the motion of Mercury around the Sun can be completely understood only with Einstein's field equations.

At larger scales the importance of GR becomes even more apparent. The evolution of the universe itself can only be described with the use of GR. Friedman and Lemaître independently understood this and wrote down the equations that govern the evolution of the size of the universe. Lemaître realised that according to his equations and the rudimentary data available at that time, the universe was expanding. Nowadays it is known that this expansion is accelerating and is best described by a positive cosmological constant Λ that can be viewed as a repulsive gravitational force, pushing test particles away in

an empty universe. Universes that have such a positive cosmological constant are called de Sitter (dS) universes.

If the universe is expanding today, this means that going back in time we eventually reach a hot, dense phase where all the matter in the universe is located in one point – a state which Lemaître called the primeval atom, but later became more famously known as the Big Bang. It should be clear that at this point GR alone is not enough to give a complete description of this state, quantum-mechanical effects should start playing an important role. That is, we need to combine gravity and quantum mechanics into a theory of quantum gravity to describe the Big Bang!

Such a well-established quantum theory of gravity does not yet exist, but there is a good candidate in String Theory, which states that the fundamental building blocks are not the fields of the Standard Model, but extended string-like objects. One of the predictions of String Theory is that the world is actually 10-dimensional, with 6 dimensions being curled up or compactified. This compactification can be done in approximately 10^{500} ways. All of them are expected to break the symmetries of String Theory in a different way, leading to a landscape of possible vacua.

How can physics lead to any predictions when there are so many universes possible? String Theory does not give any explanation why one vacuum should be preferred over another one. In other words, String Theory is only a theory of the dynamics and does not say anything about the initial state of the universe. It is this idea that led people like Hawking and Hartle[1], Linde [2] and Vilenkin[3] to propose an initial quantum-mechanical state of the universe, the central object of this thesis. To get the main idea, we can take a look at quantum mechanics, where the relevant object is the quantum-mechanical wave function ψ whose evolution is governed by the Schrödinger equation:

$$i\hbar \frac{\partial \psi(t)}{\partial t} = H\psi(t) \ . \tag{1.1}$$

From this it can be seen that the dynamics of ψ is governed by the Hamiltonian H. However, this is not enough to determine the complete evolution of ψ, to this end it is necessary to know from which state to start, i.e. what the initial state ψ_0 is. Only with both the Hamiltonian and the initial state it is possible to know the complete evolution of ψ.

The proposal for the initial state we will focus on in this thesis is the one by Hartle and Hawking, also called the No-boundary Wave Function (NBWF) [1, 4]. The goal of this thesis will be to use this to go beyond the predictions of classical cosmology and learn something about the quantum regime of the universe as predicted by the NBWF. Other approaches aimed at learning something about

the early quantum epoch of the universe made use of holography to describe the cosmic singularity [5, 6, 7] or to describe the strongly interacting inflationary period [8, 9].

In the next section we will see what the exact definition of the NBWF is and how a semiclassical approximation can be used to obtain properties for classical universes. If we take into account our observations of the universe, the NBWF predicts that we live in a universe that is eternally inflating. The discussion in Section 1.1.3 will show how this observation means that the classical evolution of the background breaks down. This means that to accurately describe the NBWF in this eternally inflating regime, we need to go beyond the classical approximation. One possible way is to use the holographic principle to relate calculable CFT partition functions to the NBWF. The exact method to achieve this will be explained in Section 1.2.2. In Section 1.3 we will elaborate on the problems that we will solve in this thesis by posing three questions that will serve as the main guidelines for this thesis.

1.1 A quantum state of the universe

1.1.1 Quantum Gravity

The easiest way to see how the NBWF is defined is to start with the Feynman path integral construction in ordinary quantum mechanics. There the propagator that takes a particle with position x' at time t' to position x at time t is given by

$$\psi = \langle x, t | x', t' \rangle = N \int \mathcal{D}x(t) \mathrm{e}^{iS[x(t)]/\hbar} \,, \tag{1.2}$$

with N an overall normalisation constant and S the classical Lorentzian action of the particle. The meaning of this path integral is as follows: one sums over all the possible paths from x' at time t' that reach x at time t and weighs each path by the exponential of its classical action. It can be shown that ψ obeys the time-dependent Schödinger equation given in (1.1).

A particular state of interest in quantum mechanics is the ground state, which is the lowest eigenfunction of the Hamiltonian. In the path integral formalism this state gets selected by going to a Euclidean version of the path integral

$$\psi_0 = N \int \mathcal{D}x(\tau) \mathrm{e}^{-I_{\mathrm{E}}[x(\tau)]/\hbar}, \tag{1.3}$$

where I_{E} is the Euclidean action obtained by sending $t \to -i\tau$ in S.

It is this formalism that Hawking and Hartle used to formulate quantum gravity[1]. They defined the quantum-mechanical state of the universe as the equivalent of the ground state wave function in non-relativistic quantum mechanics:

$$\Psi(h_{ij},\chi) = \int_{\mathcal{C}} \mathcal{D}g\mathcal{D}\phi \exp(-I_{\mathrm{E}}[g(x),\phi(x)]/\hbar) \quad . \tag{1.4}$$

It is a function on the space of three-geometries $h_{ij}(\vec{x})$ and matter field configurations $\chi(\vec{x})$ on a closed, spacelike three-surface Σ. The gravitational Euclidean action I_{E} contains the Einstein-Hilbert term and a positive cosmological constant Λ, together with a scalar field that has a potential $V(\phi)$, which we will assume to behave quadratically for small ϕ. It is given by

$$I_{\mathrm{E}} = -\int \mathrm{d}^4x\sqrt{g}\left[\frac{1}{2\kappa^2}(R-2\Lambda) - \frac{1}{2}(\nabla\phi)^2 - V(\phi)\right] + \frac{1}{\kappa^2}\int \mathrm{d}^3x\sqrt{h}K \ , \tag{1.5}$$

where h and K are the induced metric and extrinsic curvature on Σ. The integration in (1.4) is over all four-geometries g_{ij} and matter fields ϕ that match respectively h_{ij} and χ on the final spatial hypersurface.[1]

An important part of the description are the boundary conditions that the paths of integration should satisfy, denoted in (1.4) by $\mathcal{C}$. It was argued in [4] that only compact metrics with regular matter fields should be considered in the path integral. This means that the universe is completely self-contained and has no boundaries. It is the reason this quantum state is also called the no-boundary wave function (NBWF).

Just like non-relativistic quantum states obey the Schrödinger equation, the NBWF obeys a functional equation called the Wheeler-DeWitt (WDW) equation. To derive its form, we start from the ADM decomposition of the metric [10]

$$\mathrm{d}s^2 = (N^2 + N_iN^i)\mathrm{d}\lambda^2 + 2N_i\mathrm{d}x^i\mathrm{d}\lambda + g_{ij}\mathrm{d}x^i\mathrm{d}x^j \ , \tag{1.6}$$

where N and N_i are lapse functions, λ an affine time parameter and g_{ij} the metric on the spacelike hypersurface Σ. After inserting this into the Euclidean action of Ψ, the WDW equation can be obtained by noticing that the wave function is time reparametrisation invariant (meaning that $\delta\Psi/\delta N = 0$), which results in

$$\int_{\mathcal{C}} \mathcal{D}g\mathcal{D}\phi \left(\frac{\delta I_{\mathrm{E}}}{\delta N}\right) \exp(-I_{\mathrm{E}}[g(x),\phi(x)]/\hbar) = 0 \ , \tag{1.7}$$

where $\frac{\delta I_{\mathrm{E}}}{\delta N}$ gives the Hamiltonian, H, of GR. This means that the NBWF obeys the operator version of the Hamiltonian constraint $H = 0$. From this

[1] The space consisting of all possible three-geometries is called superspace.

classical constraint the WDW can be obtained by first writing it in terms of the coordinates of the wave function and its conjugate momenta and then by replacing these momenta by their functional operator form. For general actions with a Einstein-Hilbert term, cosmological constant and matter, this is [2]

$$\left\{-G_{ijkl}\hbar^2\frac{\partial}{\partial h_{ij}h_{kl}}+h^{1/2}\left[-{}^{(3)}R+2\Lambda-\kappa^2 T_{nn}\left(\frac{\partial}{\partial\phi},\phi\right)\right]\right\}\Psi[h_{ij},\chi]=0\ , \tag{1.8}$$

where ${}^{(3)}R$ is the Ricci scalar associated with the three-metric h_{ij}, T_{nn} the energy-stress tensor associated with the matter content projected in a direction normal to Σ, and G_{ijkl} is understood to be the metric on superspace.

We should note that there are some problems with the above stated definition of the NBWF. First of all, the gravitational measure in the path integral (1.4) is not rigorously defined, making it unclear how to perform the exact integration. Another problem is that the Euclidean action is unbounded both from above and below[11], rendering the integral possibly divergent. How can we get any information from this formulation with all these problems? In the next section we will see that it is possible to approximate the path integral to get some useful results, using a saddle point approximation, while in Section 1.2.2 a proposal is given to calculate the full wave function using holography.

1.1.2 Semiclassical solutions

Even though we saw that it is an almost impossible task to calculate the full NBWF using the path integral, there are some useful things that we can deduce from it. One of these is how to obtain predictions for observations of our classical universe. For this we need to know when a quantum state predicts classical evolution. This happens when the probability, given by the quantum state, is high for trajectories that exhibit patterns of classical correlation in time, governed by deterministic dynamical laws. For example, when I throw a ball, it will behave classically when its quantum state predicts histories for its trajectories that coincide with Newton's laws.

To find if the NBWF gives such histories we first apply the method of steepest descent (also called the saddle point method), which gives an approximation of the NBWF in the limit of small $\hbar$. The resulting approximative NBWF is given by a sum of terms of the form

$$\Psi[h_{ij},\chi]\approx\exp\{(-I_{\mathrm{R}}[h,\chi]+iS[h,\chi])/\hbar\}. \tag{1.9}$$

[2] Notice that we ignored the issue of the ordering of operators. Because this will not play a role for us, we chose the most convenient ordering.

Here $I_{\mathrm{R}}[h,\chi]$ and $-S[h,\chi]$ are the real and imaginary parts of the extremized Euclidean action $I_{\mathrm{E}}[h,\chi]$ of a saddle point history (g,ϕ) on a compact 4-disk M with one boundary Σ. Because these are the fields we integrate over, they should match the real values (h_{ij},χ) on Σ and have to be regular on the disk, rendering (g,ϕ) generally complex in the interior (which is the reason they are called *fuzzy instantons*). The NBWF is a real function which means that the sum over saddle points should include the complex conjugate of each saddle.

Not all the solutions that can be found are going to lead to classical correlated universes. To see which ones become classical, we have to look at the Wheeler-DeWitt equation (1.8), which can schematically be written as

$$\left(-\frac{\hbar^2}{2}\nabla^2+\mathcal{V}(q^A)\right)\Psi[q^A]=0\ , \tag{1.10}$$

here q^A represents all the coordinates in superspace[3], ∇^2 contains the second derivatives with respect to the three-metric as well as with respect to the scalar field, while $\mathcal{V}$ contains all the other (non-derivative) terms.

If we insert the semiclassical approximation (1.9) into the WDW equation we get an equation which resembles the Hamilton-Jacobi equation

$$-\frac{1}{2}(\nabla I_{\mathrm{E}})^2+\mathcal{V}(q^A)=0\ , \tag{1.11}$$

and an equation for the integral curves[4]

$$G_{AB}\frac{1}{N}\frac{\mathrm{d}x^A}{\mathrm{d}\lambda}=\nabla_A I_{\mathrm{E}}(q^A)\ , \tag{1.12}$$

where x^A represents the coordinates in the bulk of the saddle point that reduce to q^A at the final hypersurface. By inserting the real and imaginary parts of the action, the first equation also splits into a real and imaginary part, respectively given by

$$-\frac{1}{2}(\nabla I_{\mathrm{R}})^2+\frac{1}{2}(\nabla S)^2+\mathcal{V}(q^A)=0\ , \tag{1.13a}$$

$$\nabla I_{\mathrm{R}}\cdot\nabla S=0\ . \tag{1.13b}$$

Together with (1.12), the first of these equations reduces to the Lorentzian Hamilton-Jacobi equations for $S(q^A)$ when

$$|\nabla I_{\mathrm{R}}|\ll|\nabla S|\ . \tag{1.14}$$

[3]For example: $q=(h_{ij},\chi)$.

[4]This equation comes from looking at how the momentum acts on Ψ.

This is the classicality condition which determines if solutions are deemed classical or not. With these classicality conditions the momenta follow the classical Hamilton-Jacobi equations, giving classical evolution along the Lorentzian direction

$$p_A = \nabla_A S(q^A) \ . \tag{1.15}$$

In the semiclassical approximation it is possible to have a well-defined probability distribution, which gives the probability to have a classical history in a region B of superspace

$$P(B) = \int_{q^A \epsilon B} dq^A \mu(q^A) |\Psi(q^A)|^2 \ , \tag{1.16}$$

where $\mu(q^A)$ is the measure associated with the probability distribution. This measure is constructed using a Hamiltonian formalism and involves the trajectories of the classical solutions[12, 13]. For this reason the measure, and consequentially the probability distribution itself, is only defined at the semiclassical level. Notice that this measure gives diverging probabilities if one has a uniform distribution[13], so it is the combination of both the wave function and its semiclassical measure that gives reasonable results. In practice we can ignore the measure and look for peaks in the wave function itself when asking for predictions. If the peak is sufficiently strong, one would expect any sensible measure constructed from the wave function to have the same peak. Therefore we will associate with each classical solution a probability distribution given by $P(q^A) \sim e^{-2I_{\mathrm{R}}(q^A)/\hbar}$. It makes sense to use the real part of the Euclidean action, because it is approximately constant along integral curves of $S(q^A)$ according to (1.13b).

For a slowly varying scalar field the main contribution to the real part of the action will be given by the Euclidean part of the saddle point [14]:

$$I_{\mathrm{R}}(\chi) \sim -\frac{1}{V(\chi)} \ . \tag{1.17}$$

From this we can see that universes with a smaller scalar field, close to the minimum of the potential, are more probable than universes with a lot of matter content. This might seem counter-intuitive, because to undergo the amount of inflation necessary for our universe we need large scalar fields. However, if we take into account that our observations are limited to our Hubble volume and that we therefore cannot observe entire histories, the probability distribution shifts and predicts the correct amount of inflation [15]. Practically, this gets done by conditioning on a description of the local observational situation, i.e. instead of calculating the probability distributions coming from the NBWF

$P(q^a)$, we should calculate $P(q^A|\text{us})$. These are called top-down probabilities, whereas probabilities that come directly from the NBWF are called bottom-up. The top-down probabilities will play an important role later on.

Because the classical solutions discussed until now are complex, they do not describe the classical Lorentzian universes that are predicted by the NBWF, these are instead given by what are called classical histories. The classical solutions only provide the Cauchy data for the Lorentzian histories obtained as the integral curves of $S(q^A)$. The real, classical, Lorentzian histories predicted by the NBWF are therefore not the same as the complex saddle points that determine their probabilities. Furthermore, the relations between superspace coordinates and momenta (1.15) mean that to leading order in $\hbar$, and at any one time, the predicted classical histories do not fill classical phase space. Rather, they lie on a surface of half the dimension of the classical phase space.

Before we can get to some examples, we need to realise that practical calculations are almost impossible for general superspace. Therefore, the degrees of freedom are usually limited to what is called mini-superspace. A well-studied example is the one where only a scale factor $a(\lambda)$ in a homogeneous, isotropic FLRW space is considered[5], together with a homogeneous scalar field $\phi(\lambda)$. The complete Euclidean action for these models is given by

$$I_{\mathrm{E}}[a,\phi] = \frac{6\pi^2}{\kappa^2}\int \mathrm{d}\lambda\, N\left\{-a\left(\frac{1}{N}\frac{\mathrm{d}a}{\mathrm{d}\lambda}\right)^2 - a + \frac{\kappa^2 a^3}{3}\left(\frac{1}{2}\left(\frac{1}{N}\frac{\mathrm{d}\phi}{\mathrm{d}\lambda}\right)^2 + V(\phi)\right)\right\}\,, \tag{1.18}$$

where we introduced $\kappa^2 = 8\pi G_N$ and absorbed the cosmological constant into the scalar field potential. By varying the action with respect to the scale factor, the scalar field and the lapse function N we get the following equations of motion respectively

$$\frac{1}{N^2}\frac{\mathrm{d}^2 a}{\mathrm{d}\lambda^2} + \frac{a\kappa^2}{3}\left(V(\phi) + \left(\frac{1}{N}\frac{\mathrm{d}\phi}{\mathrm{d}\lambda}\right)^2\right) = 0\,, \tag{1.19a}$$

$$\frac{1}{N^2}\frac{\mathrm{d}^2\phi}{\mathrm{d}\lambda^2} + \frac{3}{aN^2}\frac{\mathrm{d}a}{\mathrm{d}\lambda}\frac{\mathrm{d}\phi}{\mathrm{d}\lambda} - \frac{\partial V(\phi)}{\partial\phi} = 0\,, \tag{1.19b}$$

$$\left(\frac{1}{N}\frac{\mathrm{d}a}{\mathrm{d}\lambda}\right)^2 - 1 + \frac{\kappa^2 a^2}{3}\left(-\frac{1}{2}\left(\frac{1}{N}\frac{\mathrm{d}\phi}{\mathrm{d}\lambda}\right)^2 + V(\phi)\right) = 0\,. \tag{1.19c}$$

[5]This means that in (1.6) we take $g_{ij}dx^i dx^j = a(\lambda)^2 d\Omega_3^2$, with $d\Omega_3^2$ the metric on the round three-sphere, and we choose a gauge such that $N_i = 0$

As mentioned before, the solutions to these equations of motion will be complex. In order to obtain the action in (1.18) we had to choose a gauge such that $N_i = 0$, but left N undefined. We can now define a new coordinate $\mathrm{d}\tau = N\mathrm{d}\lambda$, which we can take to be complex by letting N become complex.[6] At the endpoint of integration the scale factor and scalar field should reach their classical values b and χ respectively, which happens at $\tau = \upsilon = x_{\mathrm{TP}} + it$, the endpoint of integration. We defined here the turning point x_{TP} as the $x-$coordinate along which the solutions should become classical. The starting point of integration is called the South Pole[7], it is here that the no-boundary initial conditions of regularity should be satisfied. In the mini-superspace model these amount to requiring the following at the South Pole

$$a(\tau = 0) = 0, \qquad \phi'(\tau = 0) = 0 \ , \tag{1.20}$$

where a $'$ represents a derivative with respect to τ. Notice that $a(0) = 0$ is only a curvature singularity, not a coordinate singularity and that around $\tau = 0$ the space looks like $\mathbb{R}^4$. With these boundary conditions we are ready to solve the equations of motion.

There are some regions in phase space for which the mini-superspace equations of motion can be solved analytically, namely where the scalar field is so small it doesn't affect the evolution of the scale factor, or when the scalar field is so large we can use the slow-roll approximation to simplify the equations of motion [16, 14]. However, most of the time we have to resort to numerical techniques to solve (1.19).

The precise methods that we will use rely heavily on the numerical exploration of parameter space by [14]. That is, we start with a complex scalar field ϕ at the South Pole

$$\phi(\tau = 0) = \phi_0 \mathrm{e}^{i\theta} \ , \tag{1.21}$$

with ϕ_0 the parameter that we will use to label the different classical solutions and θ a phase that we can vary in order to get real $\phi(\upsilon)$. We then have to solve the equations in the complex τ-plane along a contour from the SP to $\tau = \upsilon$. The easiest path one can follow, is first to go along the horizontal axis to $\tau = x_{\mathrm{TP}}$ and then up along the vertical Lorentzian axis to reach the endpoint $\tau = \upsilon$. To obtain classical solutions that obey the classicality conditions at large volume, we can fine-tune both θ and x_{TP}. An example of such a classical solution for $\phi_0 = 3.5$ and $V = 3 + \phi^2$ is shown in Figure 1.1, where in the top

[6] The complexity of τ can also be seen from the analyticity of the solutions $a(\lambda)$ and $\phi(\lambda)$, which means that the integration can be done anywhere in the complex time plane, as long we do not cross a singularity.

[7] In the no-boundary proposal the question of what happened before there was time is as relevant as what is south of the south pole.

figure the behaviour of the real and imaginary parts of ϕ is plotted, while in the bottom figure the real and imaginary parts of a are plotted.[8]

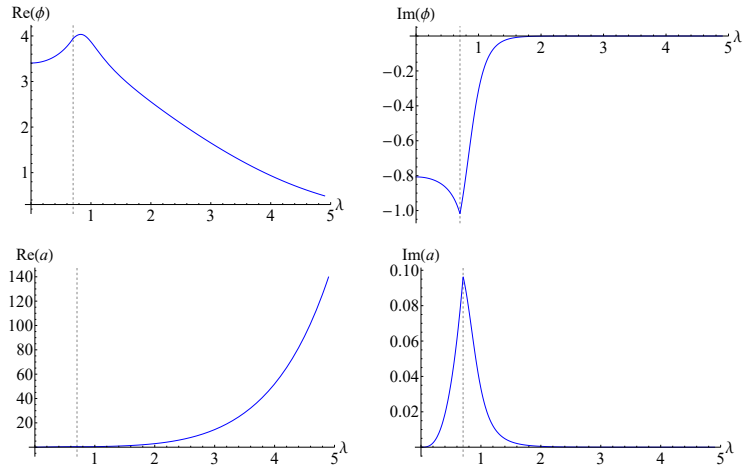

Figure 1.1: The top row shows the behaviour of the real (right) and imaginary (left) parts of ϕ while the bottom row shows both the real (right) and imaginary (left) part of a. These are functions of λ, which parametrises the length of the path, which first runs horizontally to the point $\tau = x_{\mathrm{TP}} = 0.7$ and then up along the vertical axis where the imaginary parts of ϕ and a rapidly decay. To reach a classical solution, the initial phase of the scalar field had to be fine-tuned to be $\theta = -0.233$.

To evaluate the classical histories, we have to look at the values of b and χ together with their momenta at the boundary and evaluate their real part back in time using the Lorentzian equations of motion for minisuperspace

$$\ddot{a} + \frac{a\kappa^2}{3}\left(\dot{\phi}^2 - V(\phi)\right) = 0 \,, \tag{1.22a}$$

$$\ddot{\phi} + 3\frac{\dot{a}}{a}\dot{\phi} + \frac{\partial V(\phi)}{\partial \phi} = 0 \,, \tag{1.22b}$$

$$\dot{a}^2 + 1 - \frac{\kappa^2 a^2}{3}\left(\frac{\dot{\phi}^2}{2} + V(\phi)\right) = 0 \,, \tag{1.22c}$$

where $\dot{}$ denotes a derivative with respect to the Lorentzian time coordinate t. The NBWF now has the remarkable property that solutions obeying the

[8] From now on we will always take in our numerical solutions $\kappa = 1$ and put the cosmological constant $\Lambda = 3$, which means that the de Sitter length $l_{\mathrm{dS}} = 1$.

classicality conditions have an early period of inflation driven by the scalar field ϕ [14, 16]. For a quadratic potential we obtain the following classical histories in this regime [9]

$$\chi(t) = \phi_0 - \sqrt{\frac{2}{3}}\frac{mt}{\kappa} \ , \tag{1.23a}$$

$$b(t) = \sqrt{\frac{3}{2}}\frac{1}{m\kappa\phi_0}\exp\left(\frac{\kappa m\phi_0}{\sqrt{6}}t - \frac{1}{6}m^2t^2\right) \ , \tag{1.23b}$$

where m stands for the mass of the scalar field. Two typical results for $m = \sqrt{2}$ are shown in Figure 1.2: in blue a history with a classical bounce characterised by a minimal value for a with a maximal scalar field, and in red a history depicting a classical singularity that shows how χ diverges when b goes to 0.

The bouncing histories are very intriguing, if we follow these back in time we reach a region where the classicality conditions are not satisfied any more. It was shown in [17] that if we enter this region it is possible to have a quantum-mechanical transition to another bouncing universe. This can best be compared with a particle moving in a potential well: according to classical mechanics this particle will always stay trapped inside the well, but according to quantum mechanics, the particle – which is actually described by a wave packet – can tunnel outside the well, while there is also a possibility it just stays inside the well. That is, part of the wave packet gets transmitted through the wall, while the rest is reflected by it. In the same way there could be a quantum transition between one bouncing universe and another one through the classically forbidden region.

Before we continue, let us summarise this subsection. We showed how it is possible to find semiclassical solutions of the NBWF. If they obey the classicality conditions, these can be used to obtain the classical histories predicted by the NBWF. These histories will always have a period of inflation. In general, the NBWF will prefer the ones that have less inflation, unless we take the top-down probabilities, which are probabilities conditioned on some part of our data[15]. We will see that this has some far-reaching implications if quantum-mechanical fluctuations of the background solutions are taken into account. Namely, when the value of the scalar field is large enough, as predicted by the top-down weighting of the NBWF, inflation will last eternally. What exactly this means will be discussed in the next section.

In the rest of this thesis we will work in units where $\hbar = 1$ and $\Lambda = \pm 3$, where the positive sign is for dS spaces and the negative one for AdS spaces, unless

[9] These solutions can be found by assuming that ϕ is large and the slow-roll conditions $\ddot{\phi} < 1$ and $\dot{\phi}^2 < V(\phi)$ are satisfied in (1.22).

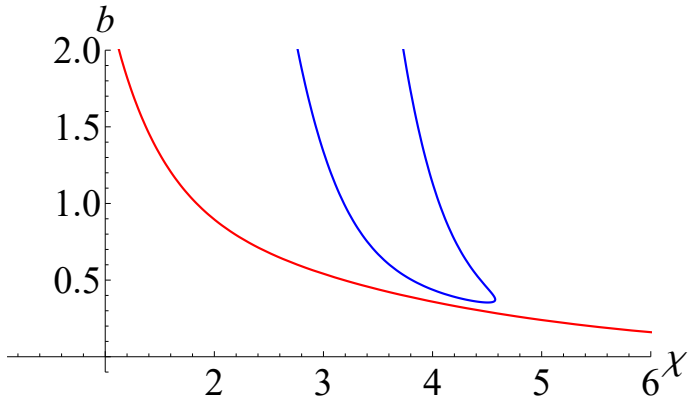

Figure 1.2: Two examples of classical histories in the (b, χ)-plane. The blue history shows a bouncing history associated with an initial scalar field $\phi_0 = 3.5$, while in red a singular history is depicted that comes from an initial scalar field $\phi_0 = 1.9$.

mentioned otherwise. This means that the reduced Planck mass is given by $M_{\rm P} \equiv \sqrt{\frac{\hbar c}{8\pi G_{\rm N}}} = 1/\kappa$.

1.1.3 The NBWF and eternal inflation

To fully understand the evolution of the universe, we need to study the quantum-mechanical fluctuations of the background fields. They are the seeds for the galaxy and star formation that follows inflation. However, it was found in the early eighties that they can have some serious implications for the evolution of the universe. Namely, when a scalar field starts rolling down its potential, there is a chance that due to quantum fluctuations, there will be a position in space where, in a unit of time, it fluctuates higher up its potential than it was rolling down. The field will then again initiate an inflationary regime in which this process can repeat itself. Because inflation increases the volume of space, there will always be a lot of regions that are not in causal contact with each other. Therefore, if this process happens somewhere it will not affect the physics of those other regions. The available regions where the inflaton can independently fluctuate upwards increase every timestep. This means that if the probability of a quantum fluctuation in a small patch with respect to the creation of such patches is just right, the universe will always be inflating somewhere, this is called eternal inflation. The fact that inflation could lead to eternally inflating universes was pioneered in the early eighties by Linde, Steinhardt and Vilenkin

[18, 19, 20]. In [21, 22] it was shown that most inflationary models with a sufficiently flat potential exhibit this feature. Eternal inflation occurs in any inflationary regime where the amplitude of density perturbations becomes $\mathcal{O}(1)$ for some values of the field.[10]

If, during reheating, the scalar field breaks the symmetry group of the matter present[11], the idea of different causally disconnected universes means that this symmetry could be broken in different ways, leading to different physics in each of these mini-universes [18]. In this way eternal inflation can be linked to the many possible vacua of the multiverse in string theory.

The general picture associated with eternal inflation is the one in Figure 1.3. Different inflating mini-universes are shown with possibly different physical laws (indicated by the different colours). One can see that eternal inflation predicts a highly inhomogeneous and anisotropic universe that contains an infinite amount of mini-universes. It has even been argued that eternal inflation causes a fractal-like structure [24, 25].

Eternal inflation typically happens when the inflaton potential has an extremely flat patch relative to the value of the potential

$$\left(\frac{\mathrm{d}V}{\mathrm{d}\phi}\right)^2 < \kappa^6 V^3 \ . \tag{1.24}$$

The NBWF predicts that in such models long wavelength fluctuations have a large amplitude, because the variance of Gaussian NBWF probabilities for linear fluctuations is proportional to the reciprocal of (1.24)[15]. This can be seen not only as an indication of the breakdown of linearised perturbation theory in a regime of eternal inflation, but also of the assumption that there is an approximately classical background. A calculation in perturbation theory of the expected fractional change in the volume $\mathcal{V}(t)$ of a surface of constant scalar field, due to the combined effect of all fluctuations outside the horizon, yields[15, 17]

$$\left\langle \frac{\delta\mathcal{V}}{\mathcal{V}_0}(t) \right\rangle \approx \frac{1}{8\pi^2\kappa^6} \frac{V^3(t)}{(\mathrm{d}V/\mathrm{d}\phi)^2} \ , \tag{1.25}$$

where $\mathcal{V}_0(t) = 2\pi^2 b^3(t)$ is the volume of a constant field surface. In the regime of eternal inflation the volume of reheating can differ significantly from the reheating volume of the classical background.

[10] A historical overview of the evolution of eternal inflation together with a lot of useful references can be found in [23].

[11] e.g. supersymmetry

Because in the top-down weighting of the NBWF large scalar fields dominate, (1.24) will in general be satisfied.[12] It therefore seems that quantum fluctuations and their backreaction dominate the evolution of the universe on the large scales associated with eternal inflation, making it unlikely one could get information about the global structure of eternally inflating universes with the methods described above[17].[13]

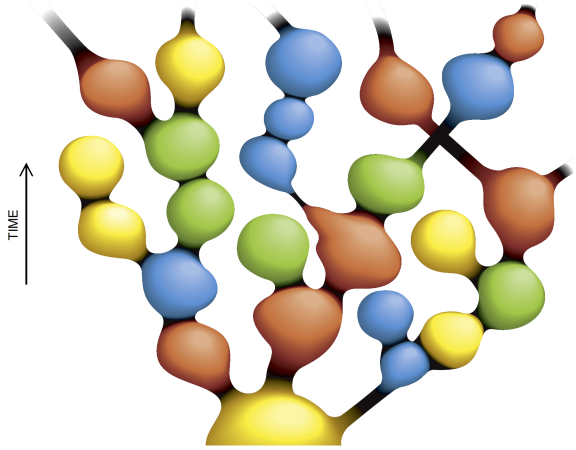

Figure 1.3: This figure resembles the growth of the multiverse, where different mini-universes branch off from the original mother universe. Each mini-universe can have different laws of physics due to different symmetry-breaking in each bubble. Figure by A. Linde [27].

1.2 A holographic quantum state of the universe

In the previous section we saw that the classical evolution of the background metric does not hold any more when we incorporate the effects of quantum fluctuations into the NBWF, meaning that we have to find a method to do calculations in the quantum regime of the NBWF, beyond tree-level. From the path integral perspective it is not yet clear how this can be achieved, but luckily, there is a way around this by using the holographic correspondence to

[12] For a quadratic potential the regime of eternal inflation happens when $\chi > 1/\sqrt{m}$.

[13] To really get information about probabilities in quantum theory we need a certain amount of coarse graining. In this way, if we sum over all fluctuation modes that leave the horizon in eternal inflation, one recovers an approximately homogeneous background with small fluctuations on short scales. This makes it possible to compute predictions for e.g. CMB fluctuations [26].

define a holographic NBWF. How holography is defined and how it is exactly implemented into the NBWF will be discussed in this section.

1.2.1 The holographic principle

The holographic principle is one of the biggest breakthroughs in theoretical physics in the last 20 years. It is understood to be the conjectured duality between gravity theories in d dimensions and quantum field theories in one dimension less, meaning that like a hologram all the information from the bulk actually lives on the boundary [28, 29]. The first example that achieved this was found by Maldacena [30] and related string theory on $AdS_5 \times S^5$ with $\mathcal{N} = 4$ super Yang-Mills theory with $SU(N)$ gauge group in 4 dimensions. This relation was proven to be valid in a low energy limit, where the curvature of the background, on which the strings live, must be large compared to the length of the strings and that the quantum corrections on the string theory side are small. This can be reduced to saying that 't Hooft coupling $\lambda \equiv g_{\mathrm{YM}}^2 N$ should be much larger than 1, while taking $g_{\mathrm{YM}} \to 0$ and $N \to \infty$. Here g_{YM} is the coupling constant of the dual field theory that is related to the string coupling constant by $4\pi g_{\mathrm{string}} = g_{\mathrm{YM}}^2$, and N is the rank of the field theory gauge group, which on the string theory side corresponds to the number of D3-branes – special 4-dimensional objects often used in String Theory. On the field theory side a large 't Hooft coupling corresponds to taking a large effective coupling. This means that weakly coupled gravity is dual to strongly interacting Super Yang Mills. The correspondence then states in its strongest version that the duality is valid for every value of λ for large N. Because of this pioneering example the holographic correspondence is sometimes also called AdS/CFT.

Witten made the correspondence more precise by introducing a dictionary to relate observables of the field theory to observables in an AdS space [31]. More precisely, he asserted that the supergravity (or if one wants to take into account quantum corrections, a string theory) partition function in terms of the boundary values of the fields should be interpreted as the generating functional of conformal field theory correlation functions, where the sources are given by the boundary field values, i.e.

$$Z_{\mathrm{SUGRA}}(\alpha) = \left\langle \exp \int_{\Sigma} \alpha \mathcal{O} \right\rangle_{\mathrm{CFT}} . \tag{1.26}$$

The value of α can be found by studying the near-boundary behaviour of the fields. For example, when there is a scalar field with a quadratic potential, we have

$$\phi = \alpha \mathrm{e}^{-\lambda_- r} + \beta \mathrm{e}^{-\lambda_+ r} , \tag{1.27}$$

from which we can see that α has scaling dimension λ_- which roughly corresponds to the conformal weight of the dual operator.[14] The exponential falloffs are related to the mass of the scalar field by

$$\lambda_\pm = \frac{d}{2}\left(1 \pm \sqrt{1 + \frac{4m^2}{d^2}}\right) . \tag{1.28}$$

Because there is a coupling $\int \alpha\mathcal{O}$ on the CFT side, the conformal dimension of the vacuum expectation value (vev) $\mathcal{O}$ will be $d - \lambda_- = \lambda_+$.

These holographic relations were soon well understood when the gravity theory had a negative cosmological constant, but we know that our universe is best described by a positive cosmological constant, so what about a holographic de Sitter space? There are a few subtleties that make a dS/CFT correspondence a little more difficult. First of all, for AdS space the fields asymptote at spatial infinity, while for dS universes the asymptotia are at future and past infinity. Secondly, it is much more difficult to construct dS vacua from string theory than AdS vacua. There are only a handful of explicit constructions known and they are not stable, but metastable dS vacua, e.g. [32]. There are also other arguments, based on the finiteness of the dS entropy, that claim that dS spaces can only exist for a finite amount of time[33], so that it would be bizarre to construct something at its future infinity. But then where would the boundary on which the corresponding degrees of freedom can live be?

Strominger [34] was one of the first to conjecture how a dS/CFT duality could work. Because a stringy realisation of dS space was missing back then, he analysed the asymptotic symmetries of de Sitter space and related them to a Euclidean CFT on a sphere of one dimension lower (following the analogous derivation by Brown and Henneaux for AdS_3 and CFT_2 [35]). He noticed that there is only one CFT dual to dS, in spite of its past and future boundary. Gravity correlators with points at past infinity are CFT correlators on the sphere, while insertion of gravity operators with points at future infinity correspond to inserting operators at the antipodal points of the sphere.

The dual CFT does not need to be unitary, as can be seen from the expansion of the scalar field near past or future infinity which has the same form as the scalar field in AdS (1.27), but with r replaced by t and $\lambda_\pm$ now given by

$$\lambda_\pm = \frac{d}{2}\left(1 \pm \sqrt{1 - \frac{4m^2}{d^2}}\right) . \tag{1.29}$$

[14] This can be seen by going to Poincaré coordinates $ds^2 = \frac{1}{z^2}(dt^2 + dx_i dx^i)$ and see how the components of ϕ rescale under a coordinate rescaling $z \to az$.

This leads to the same relationship between dS variables and CFT observables as in the AdS/CFT case. Then, indeed, when the mass becomes too large the conformal weight of the corresponding operator will become complex.

Approximately 10 years after Strominger came up with the dS/CFT correspondence, Anninos and Hartman conjectured together with Strominger an explicit realisation of the correspondence, relating Vasiliev's higher-spin gravity in four-dimensional dS space to the large N limit of the Euclidean $Sp(N)$ vector model on the spacelike boundary of dS space at future timelike infinity [36]. Vasiliev gravity with a positive cosmological constant is an extension of ordinary gravity that includes, besides a scalar field with mass $m^2 = 2/l_{\text{dS}}^2$, fields with spins going up to infinity, which makes it impossible to write down a Lagrangian description of the theory[37]. On the other hand, the free version of the $Sp(N)$ model is described by the action

$$I_{Sp(N)}^{\text{free}} = \frac{1}{8\pi} \int \mathrm{d}^3x \, \Omega_{ab} g^{ij} \, \partial_i \chi^a \, \partial_j \chi^b, \quad \Omega_{ab} = \begin{pmatrix} 0 & \mathbb{1}_{\frac{N}{2} \times \frac{N}{2}} \\ -\mathbb{1}_{\frac{N}{2} \times \frac{N}{2}} & 0 \end{pmatrix} , \quad (1.30)$$

with χ^a a real N-component anti-commuting scalar and N an even number. This explicit realisation of the dS/CFT duality relates massless higher-spin fields on the gravity side to $Sp(N)$-singlet conserved currents of even spin s, of the form

$$J^s_{\mu_1 \mu_2 \ldots \mu_s} = \sum_{k=0}^{s} c_{sk} \Omega_{ab} \partial_{(\mu_1 \ldots \mu_k} \chi^a \partial_{\mu_{k+1} \ldots \mu_s)} \chi^b \, , \quad (1.31)$$

where c_{sk} can be found by solving the conservation equation for the currents. For $s = 0$ the scalar operator $J_0 = \Omega_{ab} \chi^a \chi^b$ of the $Sp(N)$ model is related to the scalar field with mass $m^2 = 2/l_{\text{dS}}^2$ on the gravity side. The interacting model is obtained by adding a double trace deformation $(\chi \cdot \chi)^2$, which causes the theory to flow to its interacting IR fixed point. The free and interacting theory are both dual to the same gravity theory, but with different boundary conditions. The interacting theory is dual to Vasiliev theory with fixed α on the boundary, while the free theory is dual to Vasiliev space with fixed β on the boundary, which is related to the theory with fixed α by a Legendre transform. The latter is also called alternate quantisation[38].[15]

The explicit model was realised after Klebanov and Polyakov showed that minimal, bosonic Vasiliev theory in AdS, consisting only out of massless even spin fields, is dual to the singlet sector of the $O(N)$ vector model[39]. This vector model consists of N scalar fields that transform as vectors under $O(N)$

[15] A more detailed explanation can be found in Chapter 3.

transformations. This duality has the following relation between N and Λ

$$N \sim \frac{1}{\Lambda G_N} \ , \tag{1.32}$$

from which we can see that the $1/N$ expansion on the CFT side is mapped to the perturbative expansion on the AdS gravity side, which runs in powers of the Newton's constant. Anninos, Hartman and Strominger showed that both the free and critical $O(N)$ and $Sp(N)$ model are related to each other by analytically continuing $N \to -N$. This continuation is related to the existing analytic continuation that transforms Vasiliev gravity in AdS to dS by (1.32), giving an explicit realisation of the dS/CFT correspondence.

In the meantime, Maldacena proposed the use of a wave function of the universe to formulate a dS/CFT correspondence [40], stating that the wave function itself should be dual to the CFT partition function. Later on, this formulation of the duality was extensively studied and combined with the Vasiliev/$Sp(N)$ correspondence to calculate the wave function of Vasiliev space by calculating the $Sp(N)$ partition function in[41, 42]. These authors tested the correspondence by deforming the field theory on the boundary in many different ways, e.g. mass deformations and deformations of the background away from an isotropic three-sphere. Some of these results will be generalised in Chapters 3 and 5.

1.2.2 The holographic no-boundary measure

Can the methods described above be used to implement a holographic dictionary for the NBWF? The answer to this was formulated by Hartle and Hertog in [43], where they took the first steps in constructing such a dictionary. Let us see how their formulation works.

It all starts with the observation that the metric has a complex time coordinate, τ, over which we have to integrate the fields. Different contours for this integral give different geometric representations of the saddle point, each giving the same amplitude for the boundary configuration (h_{ij}, χ). This freedom in the choice of contour gives physical meaning to a process of analytic continuation – not of the Lorentzian histories themselves, but of the saddle points that define their probabilities.

In [43, 44] this freedom of choice of contour was used to identify two different useful representations of the general saddle points corresponding asymptotically to de Sitter universes. The first representation was already used above in the description of the semiclassical solutions. These solutions converged to real Lorentzian solutions that were asymptotically dS, while their interior behaved as if Λ and V were positive. In the other (AdS) representation the Euclidean

part of the interior geometry behaves as if these quantities were negative, and specifies in this way a regular AdS domain wall. Asymptotically Lorentzian de Sitter (dS) universes and Euclidean anti-de Sitter (AdS) spaces are in this way connected by the wave function. This connection can be made explicit using the asymptotic form of the saddle point solutions. For convenience in the next chapter it will be useful to define a variable η by [16]

$$\eta(\tau) = i\eta_0 e^{i\tau} = i\eta_0 \mathrm{e}^{-y+ix}, \tag{1.33}$$

with η_0 a scale which we leave free here, but fix in the next chapter. The large volume expansion of the general complex solution of the Einstein equations can be written as [45, 46]

$$g_{ij} = \frac{1}{\eta^2}\left(\gamma_{ij} + \eta^2\gamma_{(2)ij} + \eta^{3-\sigma}\gamma_{(-)ij} + \eta^3\gamma_{(3)ij} + \eta^{3+\sigma}\gamma_{(+)ij} + \mathcal{O}\left(\eta^4, \eta^{4\pm\sigma}\right)\right) , \tag{1.34a}$$

$$\phi = \eta^{\lambda_-}\gamma^{\lambda_-/2\sigma}\alpha - \frac{\eta^{\lambda_+}}{\sigma}\gamma^{-\lambda_+/2\sigma}\beta + \mathcal{O}\left(\eta^{\lambda_\pm+1}\right) , \tag{1.34b}$$

where $\sigma \equiv \lambda_+ - \lambda_-$, with $\lambda_\pm$ defined in (1.29), and γ is the determinant of γ_{ij}. Notice that the expansion of the scalar field looks slightly different than what was shown in (1.27) for AdS space. The asymptotic expansions only tell us that there are undefined coefficients, given by γ_{ij}, $\gamma_{(3)ij}$, α and β, so we are allowed to change these as long as they stay undefined. The way they are written here is the most convenient notation for the next chapter. All the other coefficients are defined as a function of these.

We saw that to get real classical solutions, the phases of the fields at the SP are tuned so that the fields become real along the Lorentzian line $x = x_{\mathrm{TP}}$ for small η. Equations (1.34) show that along this curve the complex saddle point tends to a real, asymptotically dS history. However, since the expansions are analytic functions of η, there is an alternative asymptotically vertical contour located at $x_{\mathrm{A}} = x_{\mathrm{TP}} - \pi/2$ along which the metric g_{ij} is also real, but with the opposite signature. Along this contour the saddle point geometry (1.34a) is asymptotically Euclidean AdS. Hence a contour which first runs along the $x = x_{\mathrm{A}}$ line and then cuts horizontally to the endpoint $\tau = \upsilon$ provides a representation of the saddle points in which their interior geometry consists of a regular Euclidean AdS domain wall that makes a smooth transition to an asymptotically dS universe.

Figure 1.4 illustrates this for a saddle point in which the scalar field $\phi(0)$ at the SP at $\tau = 0$ is significantly displaced from the minimum of its potential. The

[16] Notice that here we already put $\Lambda = 3$, if this would not have been the case, we would have to define η as $\eta = i\eta_0 e^{i\tau\sqrt{\Lambda/3}}$.

dS contour first runs along the real axis to a turning point at $x_{\rm TP} = \pi/2V(\phi_0)$ and then vertically to the endpoint υ. The AdS contour starts vertically but gradually moves away from the dS contour to $x = x_{\rm A}$ at large y. Along this part of the contour the saddle point is an asymptotically AdS, spherically symmetric domain wall with a complex scalar field profile in the radial direction y. The complex transition region along the horizontal branch of the contour smoothly interpolates between the AdS and the dS domain. This contour has the same endpoint υ, the same action, and makes the same predictions, but the saddle point geometry is different.

The real part of the Euclidean action along $x = x_{\rm A}$ has the usual AdS divergences for large y. However, along the $x = x_{\rm TP}$ curve the real part of the action is asymptotically constant and hence does not grow parametrically with y. Therefore, the horizontal branch of the AdS contour regulates the divergences of the AdS action.

It can be shown [43] that for general saddle points the divergent terms in the action of the horizontal part are precisely the regulating counterterms plus a universal phase factor $S_{\rm ct}$. Moreover, the action integral along the horizontal branch of the AdS contour does not contribute to the amplitude in the large y limit[43]. This means that the probabilities for all Lorentzian asymptotically dS histories in the NBWF are fully specified by the regularised action of the interior asymptotic AdS regime of the saddle points. Specifically,

$$I_{\rm E}[\eta(\upsilon), h_{ij}, \chi] = -I^{\rm reg}_{\rm aAdS}[\bar{\gamma}_{ij}, \bar{\alpha}] + iS_{\rm ct}[\eta(\upsilon), h_{ij}, \alpha] + \mathcal{O}\left(\eta(\upsilon)\right) \ . \tag{1.35}$$

Here $I^{\rm reg}_{\rm aAdS}$ is the $y \to \infty$ limit of the regulated asymptotic AdS action. Given $(\eta(\upsilon), h_{ij}, \chi)$, one can calculate the barred quantities $\bar{\alpha}$ and $\bar{\gamma}_{ij}$ as the coefficients in the Fefferman-Graham expansion of the saddle points along the asymptotic AdS branch of the contour. The overall sign change of the three-metric gives the Euclidean AdS metric and therefore $\bar{\gamma}_{ij} = \gamma_{ij}$ and $\bar{\alpha} = \alpha {\rm e}^{-i\frac{\pi}{2}\lambda_-}$. The minus sign in front of $I^{\rm reg}_{\rm aAdS}$ in (1.35) is connected to the fact that the NBWF behaves as a decaying wave function along the AdS branch of the contour [47]. Now the relation between AdS theories and CFTs (1.26) can be used to yield the following holographic form of the semiclassical NBWF in the large volume limit

$$\Psi[h_{ij}, \chi] = Z^{-1}_{\rm QFT}[\bar{\gamma}_{ij}, \bar{\alpha}] \exp(iS_{\rm ct}[h_{ij}, \chi]/\hbar) \ , \tag{1.36}$$

where the arguments (h_{ij}, χ) of the wave function enter as expected, as external sources $(\bar{\gamma}_{ij}, \bar{\alpha})$ of the field theory and we have temporarily reinstated $\hbar$. This relation was, in the spirit of AdS/CFT, conjectured to hold beyond the semiclassical level. Another way to look at this would be to turn this relation around and use the partition function to identify a well-defined wave function, which at the semiclassical level is given by the NBWF[43].

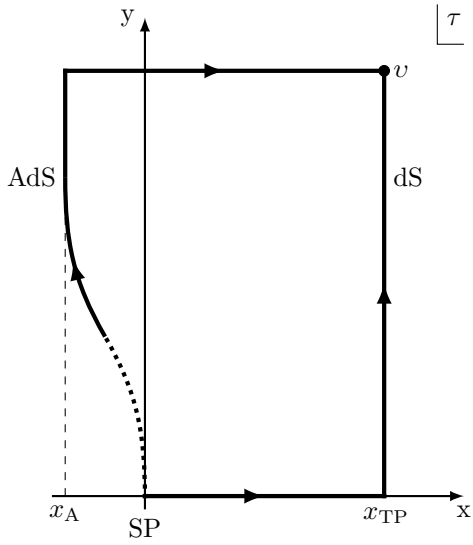

Figure 1.4: Two representations in the complex τ-plane of the same no-boundary saddle point associated with an inflationary universe. Along the vertical part of the AdS contour the geometry is an asymptotically AdS, spherically symmetric domain wall with a complex scalar field profile. Along the vertical branch of the dS contour the saddle point tends to a Lorentzian, inflationary universe. The logarithm of the amplitude of this universe is given by the AdS domain wall action. The horizontal branch of the AdS contour connecting AdS to dS automatically regularises the AdS action.

1.3 Three not so easy questions

In this thesis we will study the boundaries of the semiclassical approximation of the NBWF and try to go beyond these, by making use of two techniques, the first one – on which our main focus will be – is the holographic no-boundary proposal. We will among other things, study its implications for classical histories and eternal inflation. The other technique will be the construction of quantum transitions between different histories; in this way we hope to probe the quantum nature of the classical solutions. As a guideline we will try to answer three questions that can increase our understanding of quantum cosmology. Due to the nature of these questions we will rely heavily on a numerical analysis to give adequate answers.

For the first question we will extend the holographic principle for the NBWF

and provide some clear entries for its holographic dictionary. In particular we will be interested in answering the following question: "*Can we derive a sufficient set of conditions on the Euclidean boundary theory in dS/CFT for it to predict classical, Lorentzian bulk evolution at large spatial volumes?*". In other words, what do the classicality conditions become from a holographic perspective?

This is a highly non-trivial question, because the classical solutions identified in the previous sections are all rendered classical by the large phase factor in (1.36). This large phase is not present in the holographic theory due to the addition of counterterms that cancel the divergent phase. We will show in Chapter 2 that we can construct a new wave function consisting of variables that make sense from an asymptotic perspective, i.e. an asymptotic wave function. This wave function can be used to derive a sharper set of classicality conditions in terms of variables very naturally related to the CFT ones, giving an answer to the first question.

In Chapter 3 we start our study of double squashed spheres, by looking at the behaviour of field theories on this curved manifold and gravitational theories that have a double squashed three-sphere boundary. These theories are interesting for multiple reasons. First of all, studying field theories on curved backgrounds can teach us something about their universal properties, which we will review in Chapter 4. Further, studying both gravitational theories and field theories on the same boundary can teach us something about the gauge/gravity duality. More precisely, we will look in Chapter 3 at gravitational theories with a negative cosmological constant and use the Klebanov-Polyakov prescription to compare these to the $O(N)$ vector model to see how many similarities we can find.

In Chapter 5, we will then relate the AdS/CFT calculation from Chapter 3 to the dS/CFT correspondence, using the relation between dS and AdS coming from the NBWF, described above. The CFT that we will relate our dS results to will be the critical $O(N)$ model on a double squashed sphere. In this way it is possible to see how good the gravitational theory and the field theoretical partition function agree, which will serve as a test of our correspondence. With this we can come to the most important reason to study squashed spheres. From a cosmological perspective, these namely give rise to highly anisotropic universes with regions of negative curvature. This means that they have some properties of the overall geometry of an eternally inflating universe. This leads us to the second question we want to answer: "*What can we learn about eternal inflation using the holographic no-boundary proposal?*". In Chapter 5 we will state that the field theory partition function on the double squashed sphere should resemble the NBWF of an eternally inflating universe, from which it is otherwise impossible to infer anything due to the breakdown of the classical evolution of the background geometry.

Finally, for the last question we want to study, we will look at the breakdown of classicality in another way. Namely, we will abandon in Chapter 6 the holographic approach and instead study what happens when we follow a classical solution back in time until we reach the point where the classicality conditions are not satisfied any more. From [17] we know that it is possible to have a quantum transition at this point to another patch of classical solutions. The question we want to ask can now be formulated as: "*What are the probabilities to have a quantum-mechanical transition from one classical solution to another?*". This amounts to the question of what happens when we go back in time. To answer this we construct new saddle point solutions that make the connection between the different classical universes, from whose action we can interfere the transition probabilities.

A summary of all the results presented here will follow in Chapter 7, together with an outlook toward possible new directions and extensions of this work.

CHAPTER 2

LORENTZIAN CONDITIONS IN HOLOGRAPHIC COSMOLOGY

In this chapter we will explore the first question posed in the introduction: "*Can we derive a sufficient set of conditions on the Euclidean boundary theory in dS/CFT for it to predict classical, Lorentzian bulk evolution at large spatial volumes?*". We saw in the introduction that classical solutions should obey the classicality conditions (1.14), which state that the phase of the solutions should vary much faster than its amplitude in all directions in superspace. This is an analogous statement as the prediction of classical behaviour of a particle in a WKB state in non-relativistic quantum mechanics. Our concern will be to find how these classicality conditions can be defined using the holographic no-boundary measure (1.36). That is, we can reformulate our question as: "*What do the classicality conditions become in the dual field theory?*".

The derivation of the classicality conditions that was done explicitly in the introduction does not simply carry over to the dual partition function. The large phase factor in (1.9) that was crucial for the classicality conditions (1.14) to hold, is absent in the partition function, cancelled by the addition of counterterms. This renders the question stated above highly non-trivial.

The key feature of our answer to the main question of this chapter is an asymptotic wave function in terms of superspace coordinates $(\bar{\gamma}_{ij}, \bar{\alpha})$, that are natural and meaningful from an asymptotic viewpoint and in particular enter as sources in the partition function. We will show that the relation between this asymptotic wave function and the original one resembles and generalises the Fourier transformation between a quantum-mechanical wave function in

momentum and position space. Since this involves a map between two symplectic manifolds we will work in the Hamiltonian formulation of the theory, where the symplectic structure is manifest. This will be further explained in Section 2.1.

We note that a calculation in the same spirit was done in the context of AdS holography in [48], where variables on phase space were identified that make the variational problem well-defined. These variables were found to be related by a canonical transformation to the original AdS fields and momenta. It was established that this transformation is equivalent to holographic renormalisation. Furthermore, the generating function of this canonical transformation coincides exactly with the local boundary terms that regularise the AdS action. In the next section we show that this conclusion carries over to the dS case where the local boundary terms appear to play a physical role as discussed above.

In Section 2.2 we will discuss in detail how the classicality conditions emerge from the asymptotic wave function, giving an answer to our first question. Because the asymptotic coordinates are related to the sources and vevs of the dual theory we will interpret these asymptotic classicality conditions from a dual viewpoint as a restriction on the vevs. In Section 2.3 we will use the minisuperspace approximation to illustrate the difference between the two classicality prescriptions.

This chapter is based on work with R. Monten and T. Hertog published in [49].

2.1 Asymptotic Wave Function

We start by deriving the NBWF as a function of a new set of variables that remain finite and physically meaningful in the large volume limit. These variables come in canonically conjugate pairs so they are related to the original fields and momenta through a canonical transformation.

2.1.1 The Hamiltonian NBWF

We work with the ADM form of the saddle point metrics (1.6) and with the NBWF in Hamiltonian form,

$$\Psi(h_{ij},\chi) \propto \int \mathcal{D}g_{ij}\mathcal{D}\phi\mathcal{D}\pi^{ij}_{(g)}\mathcal{D}\pi_{(\phi)}\mathcal{D}N\mathcal{D}N^i \; e^{\frac{1}{\hbar}\int \mathrm{d}\lambda \int \mathrm{d}^3x \; \left[i\pi_{(\phi)}\dot{\phi}+i\pi^{ij}_{(g)}\dot{g}_{ij}-\sqrt{g}\left(NH+N^iH_i\right)\right]} \,, \tag{2.1}$$

where $\pi_{(\phi)}$ and $\pi^{ij}_{(g)}$ are the conjugate momenta of the scalar field and the metric, a dot means a derivative with respect to λ and we introduced

$$\begin{aligned} H =& \frac{2\kappa^2}{g}\left(\pi^{ij}_{(g)}\pi_{(g)ij} - \frac{\mathrm{Tr}(\pi_{(g)})^2}{2}\right) + \frac{(\pi_{(\phi)})^2}{2g} + \frac{1}{2\kappa^2}\left(-{}^{(3)}R + 2\Lambda\right) \\ &+ \frac{1}{2}g^{ij}\partial_i\phi\partial_j\phi + V(\phi) \ , \\ H_i =& -2i\mathcal{D}^j\left(\frac{\pi_{(g)ij}}{\sqrt{g}}\right) + i\frac{\pi_{(\phi)}}{\sqrt{g}}\partial_i\phi \ , \end{aligned} \tag{2.2}$$

with $\mathcal{D}^j$ the covariant derivative on slices of constant λ, and ${}^{(3)}R$ the three dimensional Ricci scalar constructed from g_{ij}. Performing the Gaussian integrations over $\pi_{(\phi)}$ and $\pi^{ij}_{(g)}$ by substituting their extremising values yields the original action (1.5).

Variation of the action with respect to N and N_i yields the first-class Hamiltonian and momentum constraints. One can use the gauge freedom of coordinate reparametrisations to fix the values of these fields, e.g. $N^i = 0$ and $N = 1$. Concerning the lapse, a change $N(\lambda) \to N(\lambda) + f'(\lambda)$ can be absorbed in a redefinition of the time coordinate λ to keep the metric invariant. However, the constraint that the range of λ remains unchanged means $\upsilon = \int_0^1 N\mathrm{d}\lambda$ is invariant under gauge transformations. To differentiate between the physical data υ and all other – gauge dependent – information in N, we introduce the following variables

$$\tau(\lambda) = \int_0^\lambda \mathrm{d}\lambda' \ N(\lambda') \ , \qquad\qquad \int \mathcal{D}N(\lambda) \to \int \mathcal{D}\tau(\lambda) \ . \tag{2.3}$$

The only physical information contained in $\tau(\lambda)$ is $\tau(1) = \upsilon$. Therefore, the path integral over N reduces to a physically irrelevant constant of proportionality – the volume of the gauge group – and an ordinary integral $\int \mathrm{d}\upsilon$ over all possible values of $\int \mathrm{d}\lambda \ N(\lambda)$.[1]

[1]This can also be seen from an explicit discretisation of the measure. Writing

$$\int \mathcal{D}N = \lim_{J\to\infty}\int\left(\prod_{m=0}^{J}\mathrm{d}N_m\right) , \tag{2.4}$$

where the subscript m labels the λ-slice, one can consider the following change of variables:

$$M_m \equiv \sum_{n=0}^{m} N_n \ , \qquad\qquad \prod_{m=0}^{J}\mathrm{d}N_m = \prod_{m=0}^{J}\mathrm{d}M_m \ . \tag{2.5}$$

The asymptotic momenta in the Hamiltonian version of the action can be expressed in terms of the coefficients in the Fefferman-Graham (FG) expansion (1.34) as follows:

$$\begin{aligned}\pi_{(\phi)} &= i\sqrt{g}\left(\phi' - N^i\partial_i\phi\right)\\ &= -\lambda_-\alpha\gamma^{\lambda_+/2\sigma}\eta^{-\lambda_+} + \lambda_+\frac{\beta}{\sigma}\gamma^{-\lambda_-/2\sigma}\eta^{-\lambda_-} + \mathcal{O}\left(\eta^{-\lambda_++1}\right)\ , \end{aligned} \tag{2.7a}$$

$$\begin{aligned}\pi_{(g)}{}^i{}_j &= \pi^{ik}_{(g)}g_{kj} = i\frac{\sqrt{g}}{2\kappa^2}\left(K^{ik} - Kg^{ik}\right)g_{kj}\\ &= \frac{\sqrt{g}}{2\kappa^2}\Big[-2\delta^i_j - \eta^2\left(\gamma_{(2)}{}^i{}_j - \gamma_{(2)}\delta^i_j\right) - \lambda_-\eta^{3-\sigma}\left(\gamma_{(-)}{}^i{}_j - \gamma_{(-)}\delta^i_j\right)\\ &\quad -\frac{3}{2}\eta^3\left(\gamma_{(3)}{}^i{}_j - \gamma_{(3)}\delta^i_j\right) - \lambda_+\eta^{3+\sigma}\left(\gamma_{(+)}{}^i{}_j - \gamma_{(+)}\delta^i_j\right) + \mathcal{O}\left(\eta^4\right)\Big]\ , \end{aligned} \tag{2.7b}$$

where prime denotes a derivative with respect to τ and K_{ij} is the extrinsic curvature given by

$$K_{ij} = \frac{1}{2N}\left(\dot{g}_{ij} - \mathcal{D}_iN_j + \mathcal{D}_jN_i\right)\ . \tag{2.8}$$

These relations follow from the on-shell expression of the momenta in terms of time derivatives of the fields and will be useful below to motivate the change of coordinates we apply there.

Note that the equations of motion of the momenta provide an alternative way to determine the coefficients in the FG expansion order by order, with γ_{ij}, $\gamma_{(3)ij}$, α and β as the only independent coefficients [46]. For instance, the equation for $\pi_{(\phi)}$ implies $\lambda_\pm = 3/2\left(1 \pm \sqrt{1 - 4m^2/9}\right)$, which is exactly what we expect from (1.29). Similarly, the leading-order equation for $\pi^{ij}_{(g)}$ is satisfied if $\Lambda = 3$ (remember that we are working in units of the de Sitter length) and the next orders imply

$$\gamma_{(-)ij} = -\frac{\kappa^2}{4}\gamma^{\lambda_-/\sigma}\alpha^2\gamma_{ij}\ , \qquad \gamma_{(2)ij} = \left(R_{(\gamma)ij} - \frac{1}{4}R_{(\gamma)}\gamma_{ij}\right)\ ,$$

The second equation follows from the fact that the Jacobian is 1, since the transformation matrix is triangular with only 1's on the diagonal. One can now easily separate the physical quantity $v = M_J$ from the rest. Hence for $m < J$, M_m has no physical significance and we can gauge it away. Therefore,

$$\int \mathcal{D}N = \lim_{J\to\infty}\int\left(\prod_{m=0}^{J-1}\mathrm{d}M_m\right)\mathrm{d}M_J = \lim_{J\to\infty}\int\left(\prod_{m=0}^{J-1}\mathrm{d}M_m\right)\mathrm{d}v \propto \int \mathrm{d}v\ . \tag{2.6}$$

$$\gamma_{(+)ij} = -\frac{\kappa^2}{4}\gamma^{-\lambda_+/\sigma}\frac{\beta^2}{\sigma^2}\gamma_{ij} \ , \tag{2.9}$$

where $R_{(\gamma)ij}$ and $R_{(\gamma)}$ are the Ricci tensor and scalar constructed from γ_{ij}. Finally, defining $\pi^{ij}_{(\gamma)}$ as the coefficient of the $\mathcal{O}(\eta^3)$-term in (2.7b), i.e. $\pi^{ij}_{(\gamma)} \equiv \frac{3\sqrt{\gamma}}{4\kappa^2}(\gamma_{(3)}\gamma^{ij} - \gamma^{ij}_{(3)})$, we note that the Hamiltonian and momentum constraints require that

$$\mathrm{Tr}\ \pi_{(\gamma)} = \frac{\lambda_+\lambda_-\alpha\beta}{\sigma} \ , \qquad \mathcal{D}^j_{(0)}\pi_{(\gamma)ij} = \frac{1}{2\sigma}(\lambda_-\alpha\partial_i\beta + \lambda_+\beta\partial_i\alpha) \ . \tag{2.10}$$

2.1.2 Canonical transformation to asymptotic coordinates

We now proceed by describing the canonical transformation to variables that are meaningful asymptotically. Inspired by the FG expansions (1.34), we introduce a new set of coordinates and conjugate momenta $(\Gamma_{ij}, \Pi^{ij}_{(\Gamma)}, A, B, \eta)$ on extended phase space as follows:

$$\begin{aligned}
g_{ij} &\equiv \frac{1}{\eta^2}\left[\Gamma_{ij} + \eta^2\left(R_{(\Gamma)ij} - \frac{1}{4}R_{(\Gamma)}\Gamma_{ij}\right) - \frac{\kappa^2}{4}\eta^{3-\sigma}A^2\Gamma^{\lambda_-/\sigma}\Gamma_{ij}\right. \\
&\qquad \left. + \frac{2\kappa^2}{3\sqrt{\Gamma}}\eta^3(\Pi_{(\Gamma)}\Gamma_{ij} - 2\Pi_{(\Gamma)ij}) - \frac{\kappa^2}{4\sigma^2}\eta^{3+\sigma}B^2\Gamma^{-\lambda_+/\sigma}\right] \ , \\
\pi^{ij}_{(g)} &\equiv \frac{1}{2\kappa^2}\frac{\sqrt{\Gamma}}{\eta}\left[-2\Gamma^{ij} + \eta^2\left(R^{ij}_{(\Gamma)} - \frac{1}{4}R_{(\Gamma)}\Gamma^{ij}\right)\right] + \frac{\sigma-2}{8}\eta^{2-\sigma}A^2\Gamma^{3/2\sigma}\Gamma^{ij} \\
&\quad + \frac{\eta^2}{3}\left(\Pi_{(\Gamma)}\Gamma^{ij} - \Pi^{ij}_{(\Gamma)}\right) - \frac{\sigma+2}{8\sigma^2}\eta^{2+\sigma}B^2\Gamma^{-3/2\sigma}\Gamma^{ij} \ , \\
\phi &\equiv A\Gamma^{\lambda_-/2\sigma}\eta^{\lambda_-} - \frac{B}{\sigma}\Gamma^{-\lambda_+/2\sigma}\eta^{\lambda_+} \ , \\
\pi_{(\phi)} &\equiv -\lambda_- A\Gamma^{\lambda_+/2\sigma}\eta^{-\lambda_+} + \frac{\lambda_+}{\sigma}B\Gamma^{-\lambda_-/2\sigma}\eta^{-\lambda_-} \ ,
\end{aligned} \tag{2.11}$$

where $R_{(\Gamma)}$ is the Ricci scalar associated with the metric Γ_{ij} and Γ is its determinant. We raise and lower indices of the new phase space coordinates by acting with Γ_{ij} and its inverse Γ^{ij}.

Note that $(\Gamma_{ij}, \Pi^{ij}_{(\Gamma)}, A, B)$ are functions of the scale factor variable η, but $\Gamma_{ij} \to \gamma_{ij}$, $\Pi^{ij}_{(\Gamma)} \to \pi^{ij}_{(\gamma)}$, $A \to \alpha$ and $B \to \beta$ when $\eta \to 0$. The η-dependence merely incorporates the higher order terms in the FG expansions.[2]

Since we only consider compact three-geometries, we can fix the scale of η in (1.33) by choosing $\eta_0 = 1/\sqrt{\mathrm{Vol}(h_{ij})}$. This guarantees that Γ_{ij} has volume 1 at late times.

What we would like to find, is a generating function f, such that

$$\pi^{ij}_{(g)}\mathrm{d}g_{ij} + \pi_{(\phi)}\mathrm{d}\phi + \sqrt{g}H\frac{\mathrm{d}\eta}{\eta} = \Pi^{ij}_{(\Gamma)}\mathrm{d}\Gamma_{ij} + B\mathrm{d}A + \sqrt{\Gamma}\tilde{H}\frac{\mathrm{d}\eta}{\eta} + \mathrm{d}f + \mathcal{P}(\eta)\ , \tag{2.12}$$

where $\mathcal{P}(\eta)$ is a function consisting of $\mathrm{d}A$, $\mathrm{d}B$, $\mathrm{d}\Gamma$ and $\mathrm{d}\Pi_{(\Gamma)}$ terms that cannot be written in the form of one of any of the other terms in (2.12). We will find that $\mathcal{P}(\eta)$ is higher order in η, as expected. Using the definition of the dynamical asymptotic variables (2.11), the left-hand side of (2.12) can be expressed in terms of Γ_{ij}, $\Pi^{ij}_{(\Gamma)}$, A and B. For the scalar field variables we get

$$\begin{aligned}\pi_{(\phi)}\mathrm{d}\phi = B\mathrm{d}A - \mathrm{d}\left(\lambda_-\Gamma^{3/2\sigma}\eta^{-\sigma}\frac{A^2}{2} - \frac{\lambda_-}{\sigma}AB + \frac{\lambda_+}{\sigma^2}\Gamma^{-3/2\sigma}\eta^{\sigma}\frac{B^2}{2}\right)\\ + \left(\frac{\lambda_-}{4}\eta^{-\sigma}A^2\Gamma^{3/2\sigma} + \frac{\lambda_+}{4\sigma^2}\eta^{\sigma}B^2\Gamma^{-3/2\sigma}\right)\Gamma^{ij}\mathrm{d}\Gamma_{ij}\\ - \left(\frac{3\lambda_-}{2}A^2\Gamma^{3/2\sigma}\eta^{-\sigma} - 2\frac{\lambda_+\lambda_-}{\sigma}AB + \frac{3\lambda_+}{2}\frac{B^2}{\sigma^2}\Gamma^{-3/2\sigma}\eta^{\sigma}\right)\frac{\mathrm{d}\eta}{\eta}\ ,\end{aligned} \tag{2.13}$$

where we have used that $\sqrt{g}$ can be expanded as $\sqrt{\Gamma}/\eta^3$ and terms of higher order in η,

$$\begin{aligned}\sqrt{g} = \frac{\sqrt{\Gamma}}{\eta^3}\left(1 + \frac{\eta^2 R_{(\Gamma)}}{8} - \frac{\eta^{3-\sigma}3\kappa^2\Gamma^{\lambda_-/\sigma}A^2}{2} + \frac{\eta^3\kappa^2\Pi_{(\Gamma)}}{3\sqrt{\Gamma}}\right.\\ \left. - \frac{\eta^{3+\sigma}3\kappa^2\Gamma^{-\lambda_+/\sigma}}{8\sigma^2} + \mathcal{O}\left(\eta^4\right)\right)\ .\end{aligned} \tag{2.14}$$

[2]The η-dependence of the new variables guarantees that (2.11) holds exactly at all times. Specifically, A contains all terms that are higher order in η such like the higher order terms of the form η^{λ_-+n} with $n > 0$. Similarly the corrections to B are of the form η^{λ_++n}. The same goes for Γ_{ij}.

Similarly, the gravitational part of the symplectic form is

$$\pi^{ij}_{(g)}\mathrm{d}g_{ij} = -\frac{2}{\kappa^2}\mathrm{d}\sqrt{g} + \left[\frac{1}{2\kappa^2}\frac{\sqrt{\Gamma}}{\eta}\left(\frac{1}{2}R_{(\Gamma)}\Gamma^{ij} - R^{ij}_{(\Gamma)}\right) - \frac{\lambda_-}{4}\eta^{-\sigma}A^2\Gamma^{3/2\sigma}\Gamma^{ij}\right.$$
$$\left. + \Pi^{ij}_{(\Gamma)} - \frac{\lambda_+}{4\sigma^2}\eta^{\sigma}B^2\Gamma^{-3/2\sigma}\Gamma^{ij}\right]\mathrm{d}\Gamma_{ij} + \left(-\frac{1}{2\kappa^2}\frac{\sqrt{\Gamma}}{\eta}R_{(\Gamma)}\right.$$
$$\left. + \frac{3\lambda_-}{2}\eta^{-\sigma}A^2\Gamma^{3/2\sigma} - 2\Pi_{(\Gamma)} + \frac{3\lambda_+}{2\sigma^2}\eta^{\sigma}B^2\Gamma^{-3/2\sigma}\right)\frac{\mathrm{d}\eta}{\eta} + \mathcal{P}(\eta)\ , \tag{2.15}$$

where $\sqrt{g}$ is given in (2.14). Adding these expressions one sees that the terms proportional to $A^2\mathrm{d}\Gamma_{ij}$ and $B^2\mathrm{d}\Gamma_{ij}$ cancel. Furthermore, the term proportional to $\sqrt{\Gamma}/\eta$ in (2.15) is a total derivative,

$$\frac{1}{2\kappa^2}\frac{\sqrt{\Gamma}}{\eta}\left[\left(\frac{1}{2}R_{(\Gamma)}\Gamma^{ij} - R^{ij}_{(\Gamma)}\right)\mathrm{d}\Gamma_{ij} - R_{(\Gamma)}\frac{\mathrm{d}\eta}{\eta}\right] = \mathrm{d}\left(\frac{1}{2\kappa^2}\frac{\sqrt{\Gamma}}{\eta}R_{(\Gamma)}\right)\ . \tag{2.16}$$

Finally, expanding $\sqrt{g}$ in the first term of (2.15) using (2.14), one obtains (2.12) with

$$f = \frac{\sqrt{\Gamma}}{\kappa^2}\left(\frac{-2}{\eta^3} + \frac{1}{4\eta}R_{(\Gamma)}\right) + \frac{\sigma}{4}\eta^{-\sigma}\Gamma^{3/2\sigma}A^2 - \frac{2}{3}\Pi_{(\Gamma)} + \frac{\lambda_-}{\sigma}AB$$
$$- \frac{1}{4\sigma}\Gamma^{-3/2\sigma}\eta^{\sigma}B^2\ , \tag{2.17}$$

and

$$\sqrt{\Gamma}\tilde{H}\frac{\mathrm{d}\eta}{\eta} = \sqrt{g}H\frac{\mathrm{d}\eta}{\eta} + 2\left(\frac{\lambda_+\lambda_-}{\sigma}AB - \Pi_{(\Gamma)}\right)\frac{\mathrm{d}\eta}{\eta}\ . \tag{2.18}$$

Furthermore, $\mathcal{P}(\eta)$ indeed only contains terms that are higher order in η. Note that the additional term in the new Hamiltonian $\tilde{H}$ vanishes exactly when the Hamiltonian constraint is applied. This means that the physical constraint remains the same, as it should.

2.1.3 A new wave function $\tilde{\Psi}$

We now implement the asymptotically canonical transformation to the variables $(\Gamma_{ij}, \Pi^{ij}_{(\Gamma)}, A, B, \eta)$ at the level of the wave function and write the NBWF in

terms of these new variables. In the $\eta \to 0$ limit, this reduces to an asymptotic wave function $\tilde{\Psi}_{as}$ which is a function of (γ_{ij}, α).[3]

The exponent in the Hamiltonian version (2.1) of the path-integral has the same structure as the symplectic one-form in (2.12), with differentials replaced by time derivatives, and without the $\mathcal{P}(\eta)$ term in (2.12). Including this as a correction to the new Hamiltonian $\tilde{H}$ which vanishes in the $\eta \to 0$ limit, we can use (2.12) to rewrite the exponent in (2.1) in terms of the new variables. Furthermore, since the Jacobian of a canonical transformation equals one, the measure is left invariant.[4] Hence we can write, for $\eta_* = \eta(\upsilon)$,

$$\Psi(h_{ij},\chi) \propto \int_{\mathcal{C}} \mathcal{D}\Gamma_{ij}\mathcal{D}\Pi^{ij}_{(\Gamma)}\mathcal{D}A\mathcal{D}B\mathrm{d}\log(\eta_*)\ \mathrm{e}^{\frac{i}{\hbar}\int \mathrm{d}\eta \int \mathrm{d}^3x\ \frac{\mathrm{d}f}{\mathrm{d}\eta}(\Gamma_{ij},\Pi^{ij}_{(\Gamma)},A,B,\eta)}$$

$$\cdot\, \mathrm{e}^{+\frac{i}{\hbar}\int \mathrm{d}\eta \int \mathrm{d}^3x\ \left(B\frac{\mathrm{d}A}{\mathrm{d}\eta}+\Pi^{ij}_{(\Gamma)}\frac{\mathrm{d}\Gamma_{ij}}{\mathrm{d}\eta}+\sqrt{\Gamma}\frac{\tilde{H}}{\eta}\right)}\ , \tag{2.19}$$

where the integral is still over the class $\mathcal{C}$ of histories that obey the no-boundary conditions of regularity and compactness and that match (h_{ij}, χ) on the boundary Σ. That is,

$$g_{ij}(\eta_*,\Gamma_{ij},\Pi^{ij}_{(\Gamma)},A,B) = h_{ij}, \qquad \phi(\eta_*,\Gamma_{ij},\Pi^{ij}_{(\Gamma)},A,B) = \chi\ . \tag{2.20}$$

Solving the conditions (2.20) yields an expression of the boundary values of the momenta in terms of the old coordinates, the new coordinates and η_*,

$$\Pi^{ij}_{(\Gamma)}(\Gamma_{ij},A,h_{ij},\chi,\eta_*)\ , \qquad B(\Gamma_{ij},A,h_{ij},\chi,\eta_*)\ . \tag{2.21}$$

The term with the generating function is a boundary term at $\eta = \eta_*$. Substituting the solutions (2.21) in f defines a new function $\tilde{f}$ that does not depend on the momenta but is a function of the coordinates only – both the original ones and the new asymptotic coordinates,

$$\tilde{f}(\Gamma_{ij},A,h_{ij},\chi,\eta) = \frac{\sqrt{\Gamma}}{\kappa^2\eta_*^3}\left[1+\eta_*^2\left(\Gamma^{ij}h_{ij}+\frac{R_{(\Gamma)}}{2}\right)\right] - \frac{\sigma}{2}\eta_*^{-\sigma}A^2\Gamma^{3/2\sigma}$$

$$+\,\sigma\eta_*^{-\lambda_+}A\chi\Gamma^{\lambda_+/2\sigma} - \frac{\lambda_+}{2}\frac{\sqrt{\Gamma}}{\eta_*^3}\chi^2\ . \tag{2.22}$$

Finally, by inserting the identities

$$\int \mathcal{D}A = \int \mathrm{d}A_* \int_{A(\eta_*)=A_*} \mathcal{D}A\ , \quad \int \mathcal{D}\Gamma_{ij} = \int \mathrm{d}\Gamma_{*ij} \int_{\Gamma_{ij}(\eta_*)=\Gamma_{*ij}} \mathcal{D}\Gamma_{ij}\ , \tag{2.23}$$

[3] The connection between wave functions in terms of different, canonically related variables is described in more detail and more generally in Appendix A.1.

[4] This again only holds up to $\mathcal{O}(\eta)$. We will not consider those correction terms because they are higher order in $\hbar$.

in the wave function we can take the generating function $\tilde{f}$ outside the path integral, because it depends only on the (fixed) boundary values. This yields

$$\Psi(h_{ij},\chi) = \int \mathrm{d}\Gamma_{*ij}\mathrm{d}A_*\mathrm{d}\log(\eta_*)\ \mathrm{e}^{\frac{i}{\hbar}\int \mathrm{d}^3x\ \tilde{f}(\Gamma_{*ij},A_*,h_{ij},\chi,\eta_*)}\ \tilde{\Psi}(\Gamma_{*ij},A_*,\eta_*)\ , \tag{2.24}$$

with the no-boundary wave function $\tilde{\Psi}(\Gamma_{*ij},A_*,\eta_*)$ in terms of the asymptotic variables given by

$$\tilde{\Psi}(\Gamma_{*ij},A_*,\eta_*) \equiv \int_{\mathcal{C}} \mathcal{D}\Gamma_{ij}\mathcal{D}\Pi^{kl}_{(\Gamma)}\mathcal{D}A\mathcal{D}B\ \mathrm{e}^{\frac{i}{\hbar}\int \mathrm{d}\eta\int \mathrm{d}^3x\ \left(B\frac{\mathrm{d}A}{\mathrm{d}\eta}+\Pi^{ij}_{(\Gamma)}\frac{\mathrm{d}\Gamma_{ij}}{\mathrm{d}\eta}+\sqrt{\Gamma}\frac{\tilde{H}}{\eta}\right)}\ . \tag{2.25}$$

Since the transformation to new coordinates is canonical for $\eta \to 0$, the structure of the path integral representing the new wave function $\tilde{\Psi}$ is similar to that of the original wave function, only with the new Hamiltonian $\tilde{H}$ replacing the original H.

The relation (2.24) can be inverted by considering (2.12) in the other direction, with the generating function f subtracted from both sides. A similar derivation, starting by inverting the relations (2.11), then yields

$$\tilde{\Psi}(\Gamma_{*ij},A_*,\eta_*) = \int \mathrm{d}h_{ij}\mathrm{d}\chi\ \mathrm{e}^{-\frac{i}{\hbar}\int \mathrm{d}^3x\ \tilde{f}(\Gamma_{*ij},A_*,h_{ij},\chi,\eta_*)}\Psi(h_{ij},\chi)\ . \tag{2.26}$$

The derivation of (2.24) together with the definition of $\tilde{\Psi}$ is the central result of this chapter. The new wave function is obtained from the original wave function by a transformation that generalises the Fourier transform. The generating function f is a finite polynomial, given in (2.17). Furthermore, since the dynamical η-dependent asymptotic variables tend to constants at late times, $\tilde{\Psi}$ converges to the asymptotic wave function $\tilde{\Psi}_{\mathrm{as}}(\gamma_{ij},\alpha)$ where (γ_{ij},α) do not depend on η. This is the form of the wave function of the universe that is directly related to and potentially computed with dS/CFT techniques.

To gain further intuition about the relation between the two formulations of the wave function, we consider the semiclassical approximation of both $\Psi(h_{ij},\chi)$ and $\tilde{\Psi}(\Gamma_{*ij},A_*,\eta_*)$. In the semiclassical approximation $\Psi(h_{ij},\chi)$ can be written as

$$\Psi(h_{ij},\chi) \propto \mathrm{e}^{-\frac{1}{\hbar}I^{\mathrm{O.S.}}[h_{ij},\chi]}\ , \tag{2.27}$$

where $I^{\mathrm{O.S.}}$ is the extremized, on-shell action of a regular compact saddle point, i.e. an extremising solution to the equations of motion, that satisfies the boundary condition that $g_{ij} = h_{ij}$ and $\phi = \chi$ at the boundary Σ where $\eta = \eta_*$. For simplicity we assume here there is only one such saddle point.

Similarly, we substitute the semiclassical form of $\tilde{\Psi}(\Gamma_{*ij}, A_*, \eta_*)$ in (2.24),

$$\int \mathrm{d}\Gamma_{*ij}\mathrm{d}A_*\mathrm{d}\log(\eta_*)\ \mathrm{e}^{\frac{i}{\hbar}\int \mathrm{d}^3x\ \tilde{f}(\Gamma_{*ij},A_*,h_{ij},\chi,\eta_*)}\mathrm{e}^{-\frac{1}{\hbar}\tilde{I}^{\mathrm{O.S.}}[\Gamma_{*ij},A_*,\eta_*]}\ . \tag{2.28}$$

Solving the remaining integral in the steepest descent approximation yields the following relations,

$$i\int \mathrm{d}^3x\frac{\partial\tilde{f}}{\partial\Gamma_{*ij}} = \frac{\partial\tilde{I}}{\partial\Gamma_{*ij}}\ ,\quad i\int \mathrm{d}^3x\frac{\partial\tilde{f}}{\partial A_*} = \frac{\partial\tilde{I}}{\partial A_*}\ ,\quad i\int \mathrm{d}^3x\frac{\partial\tilde{f}}{\partial\eta_*} = \frac{\partial\tilde{I}}{\partial\eta_*}\ . \tag{2.29}$$

We denote the solutions of these equations by $\boldsymbol{\Gamma}_{*ij}$, $\boldsymbol{A}_*$ and $\boldsymbol{\eta}_*$. They are functions of the original data, h_{ij} and χ. The semiclassical approximation thus gives the following relation between the two extremising actions,

$$I^{\mathrm{O.S.}}[h_{ij},\chi] = \tilde{I}^{\mathrm{O.S.}}[\boldsymbol{\Gamma}_{*ij},\boldsymbol{A}_*,\boldsymbol{\eta}_*] - i\int \mathrm{d}^3x\ \tilde{f}(\boldsymbol{\Gamma}_{*ij},\boldsymbol{A}_*,h_{ij},\chi,\boldsymbol{\eta}_*)\ . \tag{2.30}$$

It is important to notice that in the above equation h_{ij}, χ, $\boldsymbol{\Gamma}_{*ij}$, $\boldsymbol{A}_*$ and $\boldsymbol{\eta}_*$ are related to each other by (2.29), no new variables have been introduced here.[5] One can use this to determine the behaviour of the on-shell actions in the large volume limit. The asymptotic behaviour of the action $I^{\mathrm{O.S.}}(h_{ij},\chi)$ in terms of the asymptotic expansions given in (1.34) is known to be

$$I^{\mathrm{O.S.}} \approx \frac{i}{\kappa^2}\int \mathrm{d}^3x\ \sqrt{\gamma}\left(\frac{2}{\eta_*^3} - \frac{R_{(\gamma)}}{4\eta_*} - \frac{\kappa^2}{4\sigma}\left[\alpha^2\sigma^2\gamma^{\lambda_-/\sigma}\eta_*^{-\sigma} - \beta^2\gamma^{-\lambda_+/\sigma}\eta_*^{\sigma}\right] + \mathcal{O}(\eta_*)\right)$$
$$+ I_{\mathrm{IR}}\ , \tag{2.31}$$

where I_{IR} is an η_*-independent constant that depends on the non-asymptotic behaviour of the on-shell action, i.e. on the value of the fields around the SP. Hence, the diverging terms in the on-shell action I are equal to those of the generating function (2.17). This means there are no diverging terms left in $\tilde{I}$: the on-shell action is regulated by the canonical transformation to asymptotically meaningful coordinates, as expected.[6] This is of course consistent with the usual counterterms employed in dS/CFT, which are given by

$$S_{\mathrm{ct}}[h,\chi] = -\frac{2i}{\kappa^2}\int \mathrm{d}^3x\sqrt{h} + \frac{i}{2\kappa^2}\int \mathrm{d}^3x\sqrt{h}\ {}^{(3)}R + \frac{i\lambda_-}{2}\int \mathrm{d}^3x\sqrt{h}\ \chi^2 + \dots\ , \tag{2.32}$$

where the dots refer to additional scalar counterterms that enter for certain scalar masses only. The divergent parts of the counterterms S_{ct} are equal to those of f.

[5] The relations between these variables is in leading order $h_{ij} \approx \boldsymbol{\Gamma}_{*ij}\boldsymbol{\eta}_*^{-2}$ and $\chi \approx \boldsymbol{A}_*\boldsymbol{\eta}_*^{\lambda_-}$

[6] This can also be seen by writing $\tilde{I}^{\mathrm{O.S.}} = -i\int(\Pi^{ij}_{(\Gamma)}\mathrm{d}\Gamma_{ij} + B\mathrm{d}A + \sqrt{\Gamma}\tilde{H}\mathrm{d}\eta/\eta)$. The Hamiltonian $\tilde{H}$ vanishes on-shell, as a result of the Hamiltonian constraint, and the other terms in the on-shell action remain finite, by virtue of the finiteness of the asymptotic variables. Therefore, $\tilde{I}^{\mathrm{O.S.}}$ cannot diverge.

2.1.4 Implications for dS/CFT

The relation between the semiclassical actions in (2.30) is reminiscent of the relation (1.35) between the action computed in the dS and in the AdS representations of the NBWF saddle points and leads, in the large volume limit, to the following chain of equalities,

$$\tilde{I}^{\text{O.S.}}[\Gamma_{*ij}, A_*, \eta_*] = I^{\text{O.S.}}[h_{ij}, \chi] - iS_{\text{ct}} = -I^{\text{reg}}_{\text{aAdS}}[\bar{\gamma}_{*ij}, \bar{\alpha}_*] \ , \tag{2.33}$$

where $\bar{\gamma}_{ij}$ and $\bar{\alpha}$ are the natural variables from an AdS viewpoint, defined below (1.35), and thus *locally related* to the argument of the wave function. Using (1.36) this leads to the following formulation of a semiclassical dS/CFT correspondence

$$\tilde{\Psi}_{\text{as}}(\gamma_{ij}, \alpha) = \frac{1}{Z_{\text{QFT}}(\bar{\gamma}_{ij}, \bar{\alpha})} \ , \tag{2.34}$$

where we remind the reader that Z_{QFT} is the partition function of a deformation of a Euclidean AdS/CFT dual. This is both a more elegant and a cleaner formulation of dS/CFT than (1.36), since it is stated purely in terms of quantities that are available in the dual QFT. There is no need to involve the local counterterms in the bulk. Evaluating the wave function at finite scale factor rather than asymptotically loosely corresponds to adding a UV regulator υ in the boundary theory. In what follows we fix the overall scale of the boundary metric to have volume one. This is consistent with $\text{Vol}(\Gamma_{ij}) \to 1$, as implied by our choice of η_0 above.

The variables with a bar differ from the original variables by a phase only. More specifically, $\bar{\gamma}_{ij}$ and $\bar{\alpha}$ are the coefficients that are real in the FG expansion in the asymptotic AdS domain. Whereas η is real on the dS part of the contour, the radial AdS variable $z = -i\eta$. Using the analyticity of (1.34), one can write the FG expansions in terms of z and the barred variables, with

$$\bar{\Gamma}_{ij} = \Gamma_{ij} \ , \quad \bar{\Pi}^{ij}_{(\Gamma)} = i\Pi^{ij}_{(\Gamma)} \ , \quad \bar{A} = \mathrm{e}^{-i\pi\lambda_-/2}A \ , \quad \bar{B} = \mathrm{e}^{-i\pi\lambda_+/2}B \ . \tag{2.35}$$

Notice that there is an extra i in front of the momentum of Γ, this means that the expansions themselves know that going from the dS representation to the AdS representation changes the momenta from Lorentzian to Euclidean signature. The expectation value of the CFT stress tensor is dual to the subleading falloff of the metric and the bulk scalar field corresponds to the expectation value of the dual scalar operator,

$$\langle \mathcal{T}^{ij}(\vec{x}) \rangle = \frac{\delta}{\delta \bar{\gamma}_{ij}} \log Z_{\text{QFT}} \approx \frac{\delta \tilde{I}^{\text{O.S.}}[\Gamma_{*ij}, A_*, \eta_*]}{\delta \Gamma_{*ij}} \to -\bar{\pi}^{ij}_{(\gamma)}(\vec{x}) \ , \tag{2.36a}$$

$$\langle \mathcal{O}(\vec{x})\rangle = \frac{\delta}{\delta\bar{\alpha}} \log Z_{\rm QFT} \approx e^{i\pi\lambda_-/2} \frac{\delta \tilde{I}^{\rm O.S.}[\Gamma_{*ij}, A_*, \eta_*]}{\delta A_*} \to -\bar{\beta}(\vec{x}) \ . \tag{2.36b}$$

Here $\bar{\pi}^{ij}_{(\gamma)}$ and $\bar{\beta}$ are the asymptotic values of $\bar{\Pi}^{ij}_{(\Gamma)}$ and $\bar{B}$ on the extremising solution for $\upsilon \to i\infty$, i.e. $\eta_* \to 0$.

The phase factors in the relations (2.35) between the asymptotic coefficients on the dS and the AdS branches means the vevs in the dual are in general complex when the argument of the dS wave function is real. This sharpens the question whether the emergence of classical space-time evolution in the large volume limit along the dS branch can be understood from the dual partition function.

2.2 Classicality 2.0

The NBWF in its usual form in terms of the variables (h_{ij}, χ) oscillates very rapidly in the large volume limit. The large phase factor means the classicality conditions (1.14) hold almost automatically, so that the wave function predicts that (h_{ij}, χ) evolves classically. In fact, the classical behaviour can be understood as a consequence of the Wheeler-DeWitt equation in the large volume regime and therefore applies to any wave function in terms of these variables that satisfies the Hamiltonian constraint.

By contrast the wave function $\tilde{\Psi}$ need not oscillate and has no exponent that diverges in the large volume limit. This leads to the question whether it obeys the classicality conditions (1.14) at large volume. The derivation done in the introduction [14] of the conditions required for a wave function to predict classical evolution is general and applies also to the wave function in terms of the new asymptotic variables. Asymptotically, the classicality conditions in the latter formulation are

$$|\nabla_{A_*} \tilde{I}_{\rm R}| = |{\rm Im} B_*(\vec{x})| \ll |{\rm Re} B_*(\vec{x})| = |\nabla_{A_*} \tilde{S}| \ , \tag{2.37a}$$

$$|\nabla_{\Gamma_{*ij}} \tilde{I}_{\rm R}| = |{\rm Im}\Pi^{ij}_{(\Gamma)}(\vec{x})| \ll |{\rm Re}\Pi^{ij}_{(\Gamma)}(\vec{x})| = |\nabla_{\Gamma_{*ij}} \tilde{S}| \ . \tag{2.37b}$$

These conditions are stronger than the original classicality conditions (1.14), derived from the NBWF in its usual 'bulk' form. In particular, the original conditions do not involve the subleading coefficients in the Fefferman-Graham expansion. From the dual viewpoint they involve the sources only whereas (2.37) are requirements on the vevs.

This means that the ensembles of classical histories predicted by both wave functions may not be identical. We investigate and confirm this in the next

section in a minisuperspace approximation in which we can verify the classicality conditions and identify the ensemble explicitly.

This difference does not point towards an inconsistency; certain variables may exhibit classical behaviour when others do not. One may ask, however, given two different notions of classicality, which one is more physical? While the original classicality conditions are natural from the point of view of an observer in the bulk it is clear that holography suggests the new set of stronger conditions (2.37) is in fact more accurate and appropriate in quantum gravity.

2.3 Minisuperspace model

In this section we compute the ensemble of classical histories predicted by $\tilde{\Psi}$ in a minisuperspace model in Section 1.1.2, which consists of a closed, homogeneous, isotropic FLRW metric described by a scale factor a, coupled to a single scalar field ϕ with a quadratic potential V and positive cosmological constant. The relevant equations of motion are given by (1.19).

In [14] the exact same model was studied, they identified a one-parameter set of saddle point geometries consisting of a slightly deformed Euclidean four-sphere that makes a smooth transition through a complex intermediate region, to a Lorentzian inflationary history in which the scalar field slowly rolls down to the minimum of its potential. Those saddle points were found to obey the usual classicality conditions in the large volume limit, leading [14] to conclude that the usual NBWF in this minisuperspace model describes a one-parameter family of inflationary universes that are asymptotically de Sitter. We now generalise this analysis and compare with the classical predictions of $\tilde{\Psi}$ at large volume.

2.3.1 Minisuperspace wave function $\tilde{\Psi}$

We first construct the minisuperspace wave function $\tilde{\Psi}$. The Fefferman-Graham expansions (1.34) in the minisuperspace approximation reduce to

$$a = \frac{\gamma}{\eta} + \frac{\eta}{4\gamma} - \frac{\kappa^2\alpha^2}{16\pi^2}\gamma^{\frac{9}{\sigma}-2}\eta^{2-\sigma} + \frac{\kappa^2\gamma_{(3)}}{36\pi^2\gamma}\eta^2 - \frac{\kappa^2\beta^2}{16\pi^2\sigma^2}\gamma^{-\frac{9}{\sigma}-2}\eta^{2+\sigma} + \mathcal{O}\left(\eta^3\right) \ ,$$

$$\phi = \frac{\alpha}{\sqrt{2}\pi}\gamma^{3\lambda_-/\sigma}\eta^{\lambda_-} - \frac{\beta}{\sqrt{2}\pi\sigma}\gamma^{-3\lambda_+/\sigma}\eta^{\lambda_+} + \mathcal{O}\left(\eta^{\lambda_-+1}\right) \ , \tag{2.38}$$

where we have defined[7] $\gamma_{ij} \equiv \gamma^2 \Omega_{ij}$. The momenta conjugate to a and ϕ can be found from $\pi_{(a)} = -12\pi^2 i a a'/\kappa^2$ and $\pi_{(\phi)} = 2\pi^2 i a^3 \phi'$. All coefficients in the expansions (2.38) are given in terms of $(\alpha, \beta, \gamma, \gamma_{(3)})$ by the equations of motion. As before we define time dependent functions $\Gamma(\eta)$, $\Pi_{(\Gamma)}(\eta)$, $A(\eta)$ and $B(\eta)$ such that[8] $\Gamma \to 1$, $\Pi_{(\Gamma)} \to \pi_{(\gamma)}$, $A \to \alpha$ and $B \to \beta$ for $\eta \to 0$. This allows us to write the expansions as a finite polynomial. The symplectic form (2.12) becomes

$$\pi_{(a)} \mathrm{d}a + \pi_{(\phi)} \mathrm{d}\phi + H \frac{\mathrm{d}\eta}{\eta} = \Pi_{(\Gamma)} \mathrm{d}\Gamma + B \mathrm{d}A + \tilde{H} \frac{\mathrm{d}\eta}{\eta} + \mathrm{d}f + \mathcal{P}(\eta) \ , \tag{2.39}$$

where $\mathcal{P}$ contains higher order terms in η and where the new Hamiltonian $\tilde{H}$ and generating function f are given by

$$\tilde{H} = H - \Gamma \ \Pi_{(\Gamma)} + \frac{2m^2}{\sigma} AB \ , \tag{2.40}$$

$$f = -\frac{4\pi^2 \Gamma^3}{\kappa^2 \eta^3} + \frac{3\pi^2 \Gamma}{\kappa^2 \eta} + \frac{\lambda_-}{\sigma} AB - \frac{\Gamma \Pi_{(\Gamma)}}{3} + \frac{\sigma}{4} \Gamma^{9/\sigma} A^2 \eta^{-\sigma} - \frac{1}{4\sigma} \Gamma^{-9/\sigma} B^2 \eta^{\sigma} \ , \tag{2.41}$$

and the wave function $\tilde{\Psi}$ in terms of the asymptotic variables can be written as

$$\tilde{\Psi}(\Gamma_*, A_*, \eta_*) = \int_{\mathcal{C}} \mathcal{D}\Gamma \mathcal{D}\Pi_{(\Gamma)} \mathcal{D}A \mathcal{D}B \ \mathrm{e}^{i \int B \mathrm{d}A + i \int \Pi_{(\Gamma)} \mathrm{d}\Gamma + i \int \frac{\mathrm{d}\eta}{\eta} \tilde{H}(\Gamma, \Pi_{(\Gamma)}, A, B)} \ , \tag{2.42}$$

where $\tilde{f}$ is obtained from f by substituting the momenta $(B, \Pi_{(\Gamma)})$ in terms of the coordinates (Γ, A, a, ϕ), yielding

$$\tilde{f}(\Gamma_*, A_*, b, \chi, \eta_*) = \frac{\pi^2 \Gamma_*^3}{\eta_*^3} \left(\frac{8}{\kappa^2} - \lambda_+ \chi^2 \right) - \frac{12\pi^2 b \Gamma_*^2}{\kappa^2 \eta_*^2} + \sigma A_* \chi \sqrt{2} \pi \Gamma_*^{3\lambda_+/\sigma} \eta_*^{-\lambda_+}$$
$$+ \frac{6\pi^2 \Gamma_*}{\kappa^2 \eta_*} - \frac{\sigma}{2} A_*^2 \Gamma_*^{9/\sigma} \eta_*^{-\sigma} \ , \tag{2.43}$$

and where $\tilde{H}$ now includes the higher order terms in η coming from $\mathcal{P}$, namely

$$\mathcal{P}(\eta) = -\eta^2 \left(\frac{\Pi_{(\Gamma)}}{12\Gamma^2} + \frac{3}{16}(\sigma - 1) A^2 \Gamma^{9/\sigma - 3} \eta^{-\sigma} - \frac{3}{16\sigma^2}(\sigma + 1) B^2 \Gamma^{-9/\sigma - 3} \eta^{\sigma} \right) \mathrm{d}\Gamma$$

[7] We use in this section the same notation as in the previous sections for simplicity, but be aware that their meaning is not completely the same. For example, γ is not the determinant of γ_{ij} any more. The same goes for the other variables.

[8] γ can be fixed to one by an appropriate choice of η_0 in (1.33). Furthermore, $\pi_{(\gamma)}$ is related to $\gamma_{(3)}$ as before.

$$
\begin{aligned}
&- \frac{\kappa^2}{1728\pi^2\sigma^3}\Gamma^{-4-18/\sigma}\eta^{3-2\sigma}\Big(-4\Gamma\Pi_{(\Gamma)} - 9(\sigma-1)A^2\Gamma^{9/\sigma}\eta^{-\sigma} \\
&+9(\sigma+1)B^2\Gamma^{-9/\sigma}\eta^{\sigma}\Big) \times \Big(4\sigma\Gamma(\Gamma \mathrm{d}\Pi_{(\Gamma)} - \Pi_{(\Gamma)}\mathrm{d}\Gamma) \\
&+ 9A\Gamma^{9/\sigma}\eta^{-\sigma}((2\sigma-9)A\mathrm{d}\Gamma - 2\sigma\Gamma\mathrm{d}A) \\
&+ \frac{9}{\sigma^2}B\Gamma^{-9/\sigma}\eta^{\sigma}((2\sigma+9)B\mathrm{d}\Gamma - 2\sigma\Gamma\mathrm{d}B)\Big) \ . \qquad (2.44)
\end{aligned}
$$

Finally the relation between the different on-shell actions in the semiclassical approximations becomes

$$
I_{\mathrm{extr}}(b,\chi) = \tilde{I}_{\mathrm{extr}}(\boldsymbol{\Gamma}_*, \boldsymbol{A}_*, \boldsymbol{\eta}_*) - i\tilde{f}(\boldsymbol{\Gamma}_*, \boldsymbol{A}_*, b, \chi, \boldsymbol{\eta}_*) \ . \qquad (2.45)
$$

The minisuperspace approximation allows for an explicit calculation of the actions which shows that all divergences of I_{extr} are indeed contained in $\tilde{f}$.

2.3.2 Classical Predictions

Our main motivation to evaluate $\tilde{\Psi}$ in the minisuperspace approximation is to explicitly verify the differences between the classical predictions of both formulations of the NBWF implied by the bulk classicality conditions (1.14) expressed in terms of (h_{ij}, χ) or the asymptotic ones (2.37) in terms of (γ_{ij}, α).

Applied to the minisuperspace model, the classicality conditions in terms of the asymptotic variables (2.37) require that asymptotically classical universes must have real β and real $\gamma_{(3)}$. The latter condition follows from the former, because the Hamiltonian constraint implies $\Gamma\Pi_{(\Gamma)} = 2m^2AB/\sigma$. Since Γ_* and A_* are real, $\Pi_{(\Gamma *)}$ has to be real if B_* is real, and vice versa.

To evaluate $\tilde{\Psi}$ we first solve the equations of motion subject to the above (no-) boundary conditions. The saddle points can be viewed as solutions $(a(\tau), \phi(\tau))$ in the complex τ-plane, as discussed in Section 1.1.2. Remember from that same section that we label the solutions with $\phi_0 = |\phi(\tau = 0)|$, and that we have to numerically fine-tune the phase θ of the initial scalar field and the turning point x_{TP}. In [14] it was found that for each value of ϕ_0, there is a single value of θ as well as a vertical line labeled by x_{TP} along which the solutions become real and Lorentzian, satisfying the classicality conditions.

We have performed a more systematic analysis of the classical predictions which we summarise in Figure 2.1 where we show, for three values of the scalar mass m^2, the values $(x_{\mathrm{TP}}, \theta)$ in function of ϕ_0 for which the saddle points become real

at large times y. As can be seen, there are in general multiple one-parameter families of solutions. This generalises the results obtained in [14], where only the solutions depicted in red were found.[9]

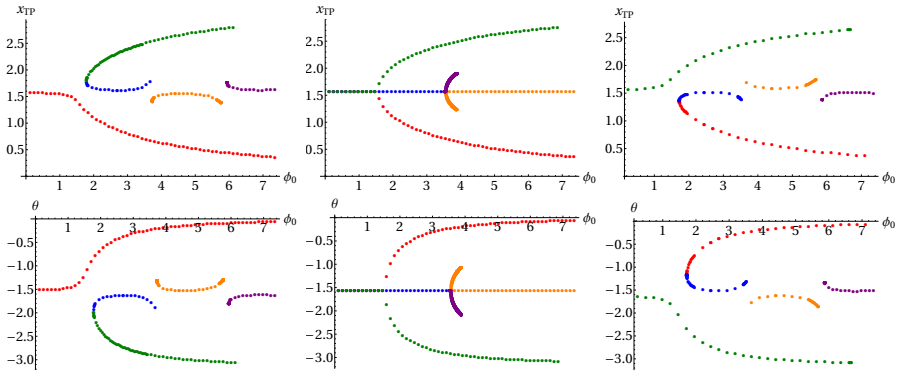

(a) $m = 1.4$ **(b)** $m = \sqrt{2}$ **(c)** $m = 1.43$

Figure 2.1: Each semiclassical contribution to the NBWF in the minisuperspace approximation can be characterised by three numbers: ϕ_0, the absolute value of the scalar field at the SP; θ, the phase of the scalar field at the SP; and $x_{\rm TP}$ the real part of v. This figure shows the values of θ and $x_{\rm TP}$ as a function of ϕ_0 for which both $a(\tau)$ and $\phi(\tau)$ become real and the solutions asymptote to de Sitter space as $y \to \infty$. The colours indicate different continuously connected sets of solutions that differ only in their relative position in the $(x_{\rm TP}, \theta)-$plane. The solutions in red were previously found in [14]. Depending on the mass of the scalar field, the map of the solutions looks slightly different. We show this for three values of m; from left to right 1.4, $\sqrt{2}$ and 1.43.

The parameters specifying the solutions change continuously with the value of the scalar field mass. The conformally coupled scalar with $m^2 = 2$ is a special value for which the space of solutions has an enhanced symmetry. This can be explained analytically, as described in Appendix A.2.

With the solutions found above, the asymptotic wave function $\tilde{\Psi}$ can be constructed. It suffices to find the relation between the asymptotic parameters (dual to the sources) and the initial conditions denoted by ϕ_0, in order to interpret the solutions above as saddle points of $\tilde{\Psi}$. In Figure 2.2 we show α as a function of ϕ_0 for the solutions found in Figure 2.1. This figure shows that the correspondence between ϕ_0 and α is not one-to-one. Instead, it can happen that multiple saddle point solutions contribute to $\tilde{\Psi}(\alpha)$ for a single value of α,

[9] Our result is consistent with observations in dimensions other than four [50] and for different potentials [51].

even within each of the "branches" identified in Figure 2.1. We return to this point below.

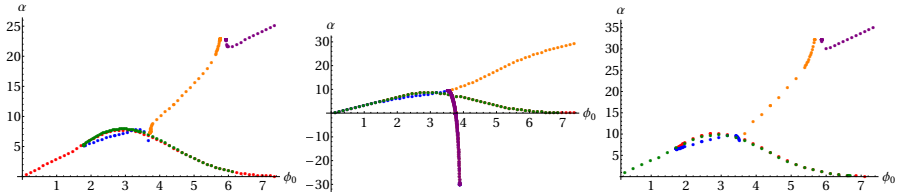

(a) $m = 1.4$ **(b)** $m = \sqrt{2}$ **(c)** $m = 1.43$

Figure 2.2: The value of α, the coefficient of the leading falloff of the scalar field profile, versus ϕ_0, the absolute value of the scalar field on the SP, for the semiclassical contributions to the minisuperspace NBWF shown in Figure 2.1. The colour of each branch coincides with the colour used there. Notice that the red and green branches almost completely coincide.

We now consider the classicality conditions, starting with their original formulation. Figure 2.3 shows the ratio of the gradients of the real and imaginary parts of the action with respect to the usual variables (b, χ) for the solutions with $m = 1.43$. The other values of the scalar mass give very similar results. If the ratio of the derivatives plotted in Figure 2.3 is small, the usual NBWF predicts that the corresponding homogeneous, isotropic configuration (b, χ) evolves classically at large volume. As anticipated in Section 2.2, all solutions satisfy these classicality conditions.

Notice that the values in these figures are of the expected order of magnitude. Because the imaginary part of the action goes as $S \sim \frac{1}{\eta_*^3}$ while I_{R} remains of order 1, we expect that $|\nabla I_{\mathrm{R}}/\nabla S| \sim \eta_*^3$, giving the resulting values of the classicality conditions. However, the semiclassical solutions indicated in red seem to do parametrically better than this. We will see that this distinction between the saddle points carries over to $\tilde{\Psi}$ and appears to be physically meaningful.

Next, we evaluate the classicality conditions in terms of asymptotic variables. Figure 2.4 shows the ratio of the imaginary part of β to its real part as a function of ϕ_0 for three different masses of the scalar field.[10] A number of points are important. First, the scale on the y-axis is very different from the scale in Figure 2.3 – the ratio is a lot larger. In fact, for some solutions the ratio is of order 1 or even larger. Hence these solutions do not obey the more stringent classicality conditions in terms of asymptotic variables. More precisely,

[10] From the holographic point of view, it would be more natural to plot these as functions of α, but in this way it is easier to compare these results with the classicality conditions in bulk variables.

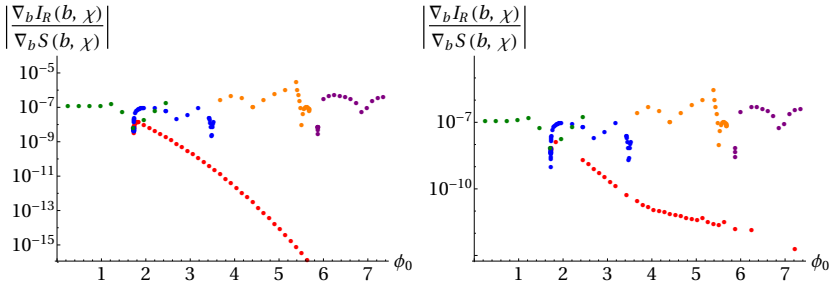

(a) In terms of the derivative w.r.t. b **(b)** In terms of the derivative w.r.t. χ

Figure 2.3: The classicality conditions in terms of the variables (b, χ) for the scalar field solutions with $m = 1.43$ given in the rightmost panel of Figure 2.1, evaluated at $\eta_* = \mathrm{e}^{-6} \approx 2 \cdot 10^{-3}$. Each contribution is indicated in the same colour as in Figure 2.1. As expected, all solutions satisfy (1.14) and are hence predicted to behave classically asymptotically.

none of the solutions that were previously unknown are classical. A remarkable observation is that for small ϕ_0 there are no solutions at all that are predicted to behave classically, even though a perturbative analysis based on the original classicality conditions leads to the opposite conclusion [14]. Note also that for the conformal mass, the red and green branch coincide again and correspond to classical solutions. This was to be expected due to the symmetry of this case (see Appendix A.2). It is interesting to observe that a small breaking of this symmetry – for example changing the mass from $\sqrt{2}$ to 1.4 or 1.43 – has a drastic effect on the behaviour of the green branch.

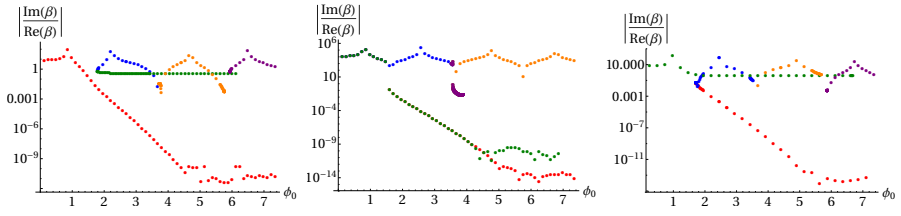

(a) $m = 1.4$ **(b)** $m = \sqrt{2}$ **(c)** $m = 1.43$

Figure 2.4: The classicality conditions in terms of the asymptotic variables, (2.37). From left to right the ratios of the imaginary part of β to its real part are plotted in function of ϕ_0 for three different masses 1.4, $\sqrt{2}$ and 1.43. The colours are the same as in Figure 2.1.

At a technical level, the discrepancy between the classical predictions of Ψ and $\tilde{\Psi}$ can be traced to the generating function. In particular, the comparison shows

that the seemingly classical behaviour of the new solutions in terms of the usual variables is entirely due to the growing phase factor in the usual NBWF, which is a universal surface term that is the generating function. This is absent in $\tilde{\Psi}$ – and in the dual partition function – and the new classicality conditions are not sensitive to this. Instead they are more stringent and depend on the interior dynamics and on the quantum state, which are encoded asymptotically e.g. in β. Therefore, they appear more physical from a dual perspective.

However, we should emphasise that classicality conditions derived à la WKB are inherently approximate.[11] They are only a sufficient condition for classical evolution to be predicted. It is therefore possible that classical evolution holds in the regime where the new, more stringent set of classicality conditions break down. To verify this, however, one would need to evolve the entire wave function. Alternatively, it is also possible that the breakdown of classicality conditions is an indication of large quantum effects, possibly induced by the scalar field in a regime which exhibits features of eternal inflation. This would mean that in fact the inequality in the old classicality conditions must be made stronger. It would be very interesting to explore this question further.

The last figure of this section shows the relative probabilities of the different classical histories predicted by the NBWF, which are given by $\sim \mathrm{e}^{-2I_{\mathrm{R}}}$. In general the solution with the most negative real part of the on-shell action provides the dominant contribution to the wave function. In Figure 2.5 we show the real part of the action for each family of saddle points, whether classical or not. Notice that for $m^2 = 2$ the green and the red branch coincide perfectly as a consequence of the enhanced symmetry. Figure 2.5 shows that the action of the new solutions is of the same order of magnitude as the previously known solutions in red.[12] At first sight it seems non-trivial to decide which saddle point dominates for a given ϕ_0.

However, the new set of asymptotic classicality conditions selects a unique saddle point solution for each value of α. Specifically Figure 2.4 shows that the only classical saddle point solutions are on the red branch for sufficiently large ϕ_0. These solutions are denoted with a full black line in Figure 2.5. Setting conditions on asymptomatically classical behaviour, therefore, restores the NBWF prediction of a one-parameter set of classical homogeneous isotropic universes with relative probabilities, for which the action is approximated by $I_{\mathrm{R}} \sim -\frac{1}{V(\phi)}$, favouring a low amount of scalar field driven inflation, as was expected from the introduction.

[11] They are an inequality and it is not clear how precisely their formulation in different bases should be related.

[12] The results shown in Figure 2.1 for the green branch of solutions with $m = 1.4$ are numerically unstable. We do not expect the apparent divergence to be physical, which should thus not be interpreted as a non-normalisable direction of the probability density.

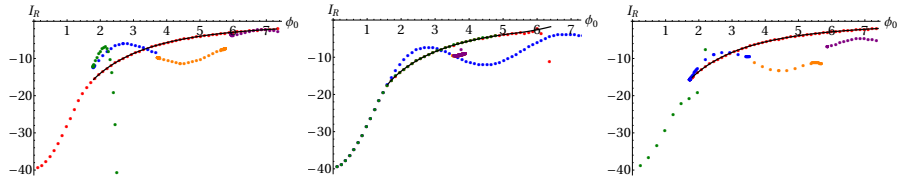

(a) $m = 1.4$ **(b)** $m = \sqrt{2}$ **(c)** $m = 1.43$

Figure 2.5: The real part of the action versus ϕ_0, the absolute value of the scalar field at the SP. This specifies the relative probabilities of the solutions shown in Figure 2.1. The colours coincide with the colours used there. For the case $m^2 = 2$ the red and the green branch coincide. The full black curve shows the solutions that obey both sets of classicality conditions.

2.4 Discussion and outlook

In this chapter we successfully gave an affirmative answer to the first question posed in the introduction, namely: "*Can we derive a sufficient set of conditions on the Euclidean boundary theory in dS/CFT for it to predict classical, Lorentzian bulk evolution at large spatial volumes?*". The conditions we found put a requirement on the vevs corresponding to the external sources in the dual partition function. This in turn leads to a restriction on the values of the sources and on the path integral defining the partition functions if the dual theory is to be compatible with the asymptotic semiclassical structure implied by the WDW equation.

To derive the new set of classicality conditions, we first expressed the bulk wave function for large spatial volumes in terms of the sources of the dual partition function. This enabled us to put forward a sharper formulation of dS/CFT in which the wave function of the universe is directly related to the dual partition function.

The conditions under which the boundary theory predicts classical bulk evolution are stronger than the criteria usually employed in quantum cosmology. We illustrated this in a minisuperspace model comprising homogeneous, isotropic histories in gravity coupled to a scalar field, where we identified several families of histories which are predicted to behave classically according to the old classicality conditions but do not obey the new conditions. Besides a number of exotic histories in which the initial scalar field is large, these also include histories which are relatively small perturbations of empty de Sitter in which the scalar field is small everywhere. This appears to be a generalisation to light scalars of the prediction [14] in the Hartle-Hawking state for heavy scalars that

empty de Sitter is an isolated point in the ensemble of asymptotically classical histories.

The discussion in this chapter was restricted to the NBWF for 4-dimensional dS for the sake of clarity and because the connection between dS and AdS representations of saddle points in this case was worked out explicitly in [43]. Generalisation to other space-time dimensions will be the subject of further research. The canonical transformations that we used can be performed for higher dimensions, as has been worked out in [48] for AdS. Furthermore, it would be interesting to see if the basis change we apply is also valid for other wave function proposals, such as the tunneling wave function [20, 47].

CHAPTER 3

ADS/CFT ON SQUASHED SPHERES

In this chapter we will start our exploration of double squashed spheres. Our goal will be to investigate gravitational theories that asymptote to a double-squashed sphere boundary and CFTs living on this boundary. The main reason to use these solutions is to learn something about highly anisotropic, cosmological spaces. In the end we will use the results from the CFT to get more information about the non-classically, eternal inflation phase of the NBWF. Because the holographic NBWF relates on a semiclassical level the cosmological relevant solutions with Euclidean AdS spaces, we will start by studying these. That is, in this chapter we will focus on gravitational theories with a negative cosmological constant together with the $O(N)$ vector model in one dimension less.

We should note that these squashed spheres are not only useful in a cosmological setting. For example, coupling a quantum field theory to background fields is a powerful tool which can be utilised to gain insights into the dynamics of the theory. The background metric couples naturally to the conserved energy momentum tensor operator of the CFT. Studying deformations of the background could therefore learn us something about the universal character of CFTs.

Another application for the squashed spheres, can be found in the AdS/CFT duality. One can use the squashed spheres to test how far the duality can be deformed away from the usual conformally flat class of manifolds. On the other hand, with the gauge/gravity duality GR solutions can be used to learn something about CFTs, or alternatively, it becomes possible to study quantum gravity aspects by using their dual CFTs.

This Chapter is based on work with N. Bobev, G. Conti and T. Hertog published in [52, 53].

3.1 Setup

The squashed three spheres on which we will consider CFTs and their holographic duals, can be written as

$$\mathrm{d}s^2 = \frac{r_0^2}{4}\left((\sigma_1)^2 + \frac{1}{1+B}(\sigma_2)^2 + \frac{1}{1+A}(\sigma_3)^2\right) , \tag{3.1}$$

where r_0 is an overall radius for which we choose the normalisation $r_0 = 1$, and σ_i, with $i = 1, 2, 3$ are the left-invariant one-forms of $SU(2)$ given by

$$\begin{aligned} \sigma_1 = -\sin\psi \mathrm{d}\theta + \cos\psi \sin\theta \mathrm{d}\phi \ , \qquad \sigma_2 = \cos\psi \mathrm{d}\theta + \sin\psi \sin\theta \mathrm{d}\phi \ , \\ \sigma_3 = \mathrm{d}\psi + \cos\theta \mathrm{d}\phi \ , \end{aligned} \tag{3.2}$$

with $0 \leq \theta \leq \pi$, $0 \leq \phi \leq 2\pi$ and $0 \leq \psi \leq 4\pi$.

An interesting CFT to study is the three-dimensional $O(N)$ vector model, for which we already saw in Section 1.2 that it is dual to Vasiliev higher-spin gravity in AdS_4, see also [54, 39, 55]. Here we will not consider higher-spin gravitational theories directly. Instead, we will aim for a qualitative comparison between the physics of the $O(N)$ model on the squashed sphere in (3.1) and Einstein gravity with AdS boundary conditions. To do so, we first numerically construct new solutions of general relativity with a negative cosmological constant that are regular everywhere and have a double squashed sphere of the form (3.1) as their boundary. Our solutions are generalisations of the well known AdS Taub-NUT and Taub-Bolt solutions [56, 57]. Comparing the thermodynamic properties of these new solutions with the partition function of the free $O(N)$ model as a function of the two squashing parameters A and B, we find that both systems exhibit a qualitatively similar behaviour over the entire configuration space of boundary geometries. On the other hand, they differ in specific features such as the NUT to Bolt transition at large positive values of the squashing parameters, which is evidently absent in the free dual theory. Afterwards we repeat our analysis, but now with the addition of a scalar field with a non-zero mass in the gravitational theory. This corresponds in the field theory to adding a source for a current. The current we are interested in in the $O(N)$ model will have conformal dimension one, which is less than 3/2, meaning that the source for this term is not dual to the leading order term of ϕ, but to the subleading one, i.e. the scheme of alternate quantization comes into play[38].

The region of superspace where the Ricci scalar on the boundary is negative is particularly intriguing. In general, the Ricci scalar of a double squashed three sphere of the form (3.1) is given by

$$R = \frac{6 + 8A + 8B + 2AB(6 - AB)}{(1 + A)(1 + B)}, \tag{3.3}$$

which is symmetric in A and B. For $B = 0$ there is a single region $A < -3/4$ where R is negative. Adding a second squashing, however, leads to an additional $R < 0$ region associated with large positive values of both A and B. This is illustrated in Figure 3.1.

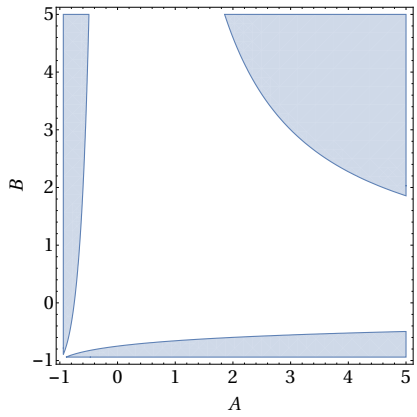

Figure 3.1: The shaded blue region is where the Ricci scalar, R, becomes negative. For one squashing there is only one place where R changes sign, but away from these points there are for given A or B two regions where R is negative.

Before we proceed with the details of our analysis, it is worth mentioning that supersymmetric CFTs on the squashed S^3 have been studied recently in the context of supersymmetric localisation [58, 59, 60] (see also [61, 62] for some applications of these results as well as [63, 64, 65] for holographic studies in this context). We emphasise that in this approach, in order to preserve supersymmetry, one has to turn on background gauge fields for the R-symmetry in addition to the curved metric. This differs from our construction here, since we are not concerned with supersymmetric theories and thus in general we do not have an R-symmetry at our disposal and the curved metric in (3.1) is the only background field. In particular our gravitational solutions are different from the supergravity backgrounds constructed in [66], since those solutions are supersymmetric and have non-trivial electromagnetic fields. An explicit comparison between the supersymmetric and non-supersymmetric case was made in [67].

The rest of this chapter is organised as follows. After a brief review of the class of known solutions of general relativity with a single squashed S^3 boundary we find new solutions with a double squashed S^3 boundary in Section 3.2 with and without scalar field. In Section 3.3 we study the thermodynamic properties of these new solutions. In Section 3.4 we switch gears and analyse the free $O(N)$ model on the double squashed S^3 and compare its behaviour with the thermodynamics of our new gravity solutions in Section 3.5 and conclude with a discussion and some avenues for future work in Section 3.6.

3.2 Double squashed AdS Taub-NUT/Bolt

In this section we discuss four-dimensional solutions of general relativity with a negative cosmological constant with Euclidean signature that have a squashed sphere as their asymptotic boundary coming from the action given by (1.5). We will consider both the case with and without a massive scalar field. When there is only one squashing and no scalar field, i.e. $B = 0$ in (3.1), these backgrounds are well-known and can be thought of as extensions of the usual asymptotically flat Taub-NUT and Taub-Bolt solutions [56, 57]. We review these backgrounds in Section 3.2.1 and present their generalisation in Section 3.2.2 and finally see what happens when a scalar field is added in Section 3.2.3.

3.2.1 Single squashed AdS Taub-NUT/Bolt

The AdS Taub-NUT/Bolt solutions are a family of solutions that are asymptotically AdS for which the metric is given by [68] (see also [69])

$$\mathrm{d}s^2 = 4n^2V(\rho)(\sigma_3)^2 + \frac{\mathrm{d}\rho^2}{V(\rho)} + (\rho^2 - n^2)(\sigma_1^2 + \sigma_2^2)\ , \tag{3.4}$$

where the one-forms σ_i are defined in (3.2) and V is given by

$$V \equiv \frac{(\rho^2 + n^2) - 2m\rho + l^{-2}(\rho^4 - 6n^2\rho^2 - 3n^4)}{\rho^2 - n^2}\ , \tag{3.5}$$

with n denoting the NUT charge, m the generalised mass and l the AdS length scale ($l^2 = -\Lambda/3$). The asymptotic behaviour for $\rho \to \infty$ of the metric in (3.4) is locally the same as the one for AdS_4. The only difference being that the boundary is a squashed S^3 with a single squashing parameter. Comparing the boundary metric with the metric on the squashed sphere in (3.1) one finds that

$$\frac{1}{4(1+A)} = \frac{n^2}{l^2}\ , \qquad B = 0\,. \tag{3.6}$$

There are now two subclasses of topologically distinct solutions. The first set consists of the NUT solutions, which are defined by requiring that there is a zero dimensional fixed point set. Furthermore, the Dirac-Misner string should be unobservable and there should be no conical defect around $\rho = n$. These requirements restrict the mass parameter m to be [70, 68]

$$m_{\rm n} = n - \frac{4n^3}{l^2} \ . \tag{3.7}$$

This mass parameter makes the space around $\rho = n$ look like the origin of a smooth $\mathbb{R}^4$. Notice that there is a special case when we put $n = l/2$, the squashing at the boundary disappears and we recover the usual AdS_4 space. Appropriately in this case we find that the mass $m_{\rm n}$ in (3.7) vanishes.

The second set of solutions is called the Bolt solutions, these are characterised by a two dimensional fixed point set. This is achieved by requiring that there is a Bolt, i.e. a topological S^2, at $\rho = \rho_{\rm b} > n$, and no conical singularities. These two conditions lead to the following identities

$$V(\rho_{\rm b}) = 0, \qquad V'(\rho_{\rm b}) = \frac{1}{2n} \ . \tag{3.8}$$

From the first condition in (3.8) one finds that the mass of the Bolt should satisfy

$$m_{\rm b} = \frac{\rho_{\rm b}^2 + n^2}{2\rho_{\rm b}} + \frac{1}{2l^2}\left(\rho_{\rm b}^3 - 6n^2\rho_{\rm b} - 3\frac{n^4}{\rho_{\rm b}}\right) \ . \tag{3.9}$$

The second condition in (3.8) yields a relation between $\rho_{\rm b}$ and n and l:

$$\rho_{\rm b\pm} = \frac{l^2}{12n}\left(1 \pm \sqrt{1 - 48\frac{n^2}{l^2} + 144\frac{n^4}{l^4}}\right) \ . \tag{3.10}$$

Therefore there are two branches of real solutions, if the discriminant is positive. This positivity condition combined with the requirement that $\rho_{\rm b} > n$ restricts the existence of the Bolt solutions to the region of parameter space where [1]

$$0 < \frac{n^2}{l^2} \leq \left(\frac{n^2}{l^2}\right)_{\rm crit} = \frac{2 - \sqrt{3}}{12} \approx 0.089 \ . \tag{3.11}$$

In particular this implies that the AdS Taub-Bolt solutions do not exist in the same region of parameter space with Euclidean AdS_4 which is obtained by setting $n = l/2$.

[1] Expressed in terms of the parameter A this range is $A > A_{\rm crit} = 5 + 3\sqrt{3}$.

There is a Hawking-Page-type topology changing phase transition which occurs at[2]

$$\left(\frac{n^2}{l^2}\right)_{\text{HP}} = \frac{1}{28+8\sqrt{10}} \approx 0.0188\ . \tag{3.12}$$

For values of n^2/l^2 lower than this critical value the Taub-Bolt solution is the dominant one, whereas for larger values of n^2/l^2 the Taub-NUT solution is thermodynamically preferred. The thermodynamic properties of these solutions are reviewed in more detail in Section 3.3.2 below.

3.2.2 Double squashings

Having reviewed the well-known AdS-Taub-NUT and Taub-Bolt solutions, we are ready to tackle the more serious problem of finding asymptotically locally AdS_4 backgrounds which have the same NUT/Bolt topology but asymptote to the squashed sphere in (3.1) with two non-vanishing squashing parameters.

We start by imposing a metric Ansatz compatible with the isometries of the sphere at the asymptotic boundary[3]

$$\mathrm{d}s^2 = l_0(r)^2\mathrm{d}r^2 + l_1(r)^2\sigma_1^2 + l_2(r)^2\sigma_2^2 + l_3(r)^2\sigma_3^2\ . \tag{3.13}$$

We then plug this Ansatz into the equations of motion derived from the action in (1.5) and derive a system of non-linear second order differential equations for the metric functions $l_a(r)$. Since we were not able to solve these equations analytically we resorted to a perturbative analysis near the asymptotic boundary and near the NUT/Bolt locus. In addition to that we exhibit numerical solutions which interpolate between these two asymptotic regions. Some technical details pertaining to this analysis are presented in Appendix B.1.[4]

To avoid confusion we emphasise that in order to construct numerical solutions to the equations of motion, we have found it easier to choose a different gauge, $l_0(r) = 1$, for the radial coordinate as compared to the analytic solution in (3.4). We adopt this gauge for most of the following discussion.

[2] In terms of the squashing parameter A this value is at $A_{\text{HP}} = 6 + 2\sqrt{10}$.

[3] We assume that the full four-dimensional solutions have the same isometries as the asymptotic boundary.

[4] This appendix already takes into account the scalar field that we will add in the following subsection. The relevant equations for this subsection can be found by putting $V = -3$ and $\phi = 0$.

UV expansion

We start by considering an expansion at large values of r which, employing holographic terminology, we call UV expansion. The UV expansion will be the same for both the NUT and Bolt solutions, since in both cases the non-trivial information is encoded in the interior of the solutions, i.e. the IR. The UV expansion is of the standard Fefferman-Graham type and thus we are dealing with asymptotically, locally AdS_4 solutions. The leading order terms in the metric for large r are given by

$$\mathrm{d}s^2 = \mathrm{d}r^2 + \mathrm{e}^{2r}\left(A_0^2\sigma_1^2 + B_0^2\sigma_2^2 + C_0^2\sigma_3^2\right) \ . \tag{3.14}$$

Notice that we have implemented the gauge $l_0(r) = 1$ and from now on we fix the cosmological constant to be $\Lambda = -3$ or alternatively the AdS_4 length scale $l = 1$. Taking this as the starting point, the UV expansion at large r of the metric functions takes the form

$$\begin{aligned} l_1(r) = A_0\mathrm{e}^r + A_k\mathrm{e}^{(1-k)r} \ , \qquad l_2(r) = B_0\mathrm{e}^r + B_k\mathrm{e}^{(1-k)r} \ , \\ l_3(r) = C_0\mathrm{e}^r + C_k\mathrm{e}^{(1-k)r} \ , \end{aligned} \tag{3.15}$$

where the sum over k goes over all positive integers.

With this Ansatz at hand one can plug the series expansion (3.15) into the Einstein equations and solve them order by order in powers of e^r. The results of this procedure are summarised in Appendix B.1, see Equation (B.4). The important upshot of this analysis is that the UV expansion without scalar field, is controlled by five independent parameters $\{A_0, B_0, C_0, A_2, B_2\}$. It turns out that the Einstein equations are invariant under constant shifts of r and we can use this freedom to eliminate one of the five parameters. We make the choice

$$A_0 = \frac{1}{2} \ . \tag{3.16}$$

Comparing the asymptotic form of the metric with the metric (3.1) on the double squashed sphere, one can find the following relation between the squashing parameters A and B and the leading order coefficients B_0 and C_0

$$A = \frac{1}{4C_0^2} - 1 \ , \qquad B = \frac{1}{4B_0^2} - 1 \ . \tag{3.17}$$

The remaining independent subleading coefficients, A_3 and B_3, stay undetermined. As we discuss in Appendix B.1 their values are ultimately fixed by imposing regularity conditions (either a NUT or a Bolt) in the bulk of the full solution of the nonlinear equations of motion. To understand how to do this we now move on to the analysis of the two possible regular IR expansions.

NUTs

From the analytic AdS-Taub-NUT solution presented in Section 3.2.1, we know that close to the NUT locus the space should look like the origin of $\mathbb{R}^4$ without any conical singularity. We will impose the same condition when looking for new solutions. However, in our IR expansion we will not impose any other restrictions on the metric functions $l_i(r)$, i.e. we will look for solutions where all l_i are distinct. If we take r^* to indicate the location of the NUT, the metric around this point, to leading order in $(r - r^*)$, should be

$$\mathrm{d}s^2 = \mathrm{d}r^2 + \frac{(r-r^*)^2}{4}(\sigma_1^2 + \sigma_2^2 + \sigma_3^2) \ . \tag{3.18}$$

This defines the first order terms of the IR expansion. The gauge choice, $l_0(r) = 1$, that we used in the UV expansion is globally well-defined and is already implemented in the above metric. The Ansatz for the IR expansion then becomes

$$\begin{aligned} l_1(r) &= \frac{1}{2}(r-r^*) + \beta_{k+1}(r-r^*)^{k+1} \ , \\ l_2(r) &= \frac{1}{2}(r-r^*) + \gamma_{k+1}(r-r^*)^{k+1} \ , \\ l_3(r) &= \frac{1}{2}(r-r^*) + \delta_{k+1}(r-r^*)^{k+1} \ , \end{aligned} \tag{3.19}$$

where k runs from 1 to ∞. Plugging this into the Einstein equations and solving them order by order in $(r - r^*)$ leads to a consistent series solution which is controlled by two real constants γ_3 and β_3. All other constants β_k, γ_k and δ_k, can be expressed in terms of these two parameters. In particular we find that all coefficients of even powers of $(r - r^*)$ vanish. The parameter r^* is spurious since it can be shifted to any value by a constant shift of the radial variable r.

The IR expansion in (3.19) can be used as an initial condition to integrate the equations of motion numerically to the UV. We will thus get a two-parameter family of solutions that are controlled by γ_3 and β_3. There are two distinct classes of solutions. The first class consists of regular solutions for which the metric functions $l_{1,2,3}(r)$ grow exponentially and the boundary metric is a sphere with two non-trivial squashing parameters as in (3.1). We also find a class of singular solutions for which one or more of the metric functions $l_{1,2,3}(r)$ vanish at some finite value of r which leads to a curvature singularity. We will ignore the second class of solutions since they do not seem to be of physical relevance.

Two representative examples of these classes of solutions are shown in Figure 3.2. In the right panel of the figure we present an example of a singular

solution, while in the left panel an example of a regular AdS-Taub-NUT solution with two different squashing parameters of the boundary S^3 is shown. We have constructed numerous such numerical solutions and we will analyse their properties in Section 3.3 and Section 3.5. For more details on the construction of these solutions we refer to Appendix B.1.

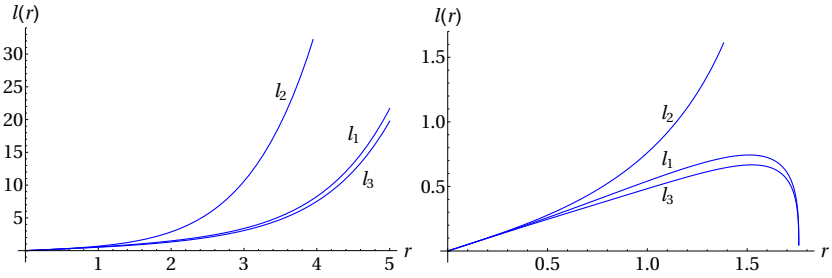

Figure 3.2: Two typical solutions with a NUT in the IR. Left: a solution with $\beta_3 = 1/12$ and $\gamma_3 = 1/6$ for which all the l_i keep on growing exponentially. This is an AdS-Taub-NUT solution with a double squashed sphere boundary geometry. Right: a solution with $\beta_3 = 1/12$ and $\gamma_3 = 3/14$, for which there is a singularity where $l_1(r) = l_3(r) = 0$ at a finite value of r. Here we have chosen $r^* = 0$.

Bolts

To find generalisations of the AdS-Taub-Bolt solutions from Section 3.2.1, we have to impose that there is a two dimensional fixed point set of the Killing vector ∂_ψ. We take this locus to be at $r = r^*$. The geometry in the neighbourhood of r^* is determined by a metric on $\mathbb{R}^2 \times S^2$. Therefore the metric around r^* should take the form

$$\mathrm{d}s^2 = \mathrm{d}r^2 + \frac{(r-r^*)^2}{4}\sigma_3^2 + \beta_0\sigma_1^2 + \gamma_0\sigma_2^2 \ . \tag{3.20}$$

We have again implemented the gauge choice $l_0(r) = 1$. Our Ansatz for the IR expansion of the Bolt solutions thus becomes

$$\begin{aligned} l_1(r) &= \beta_0 + \beta_k(r-r^*)^k \ , \\ l_2(r) &= \gamma_0 + \gamma_k(r-r^*)^k \ , \\ l_3(r) &= \frac{1}{2}(r-r^*) + \delta_{k+1}(r-r^*)^{k+1} \ , \end{aligned} \tag{3.21}$$

where the integer k goes from 1 to ∞. With this at hand we proceed as before. We substitute the expansion (3.21) in the Einstein equations and solve them

order by order in $(r - r^*)$. The details of this procedure are summarised in Appendix B.1, see in particular equation (B.3). The leading order analysis leads to $\beta_0 = \gamma_0$ and one finds non-vanishing coefficients only for the odd powers of $(r - r^*)$ for l_3 and even powers for l_1 and l_2. The rest of the expansion coefficients in (3.21) are determined in terms of two parameters which can be chosen to be γ_0 and γ_4.

Constructing numerical AdS-Taub-Bolt solutions of the nonlinear equations of motion is very similar to the NUT solutions discussed in Section 3.2.2. One has to use the series expansion in (3.21) with γ_0 and γ_4 as independent integration parameters. Again, one finds two classes of solutions. The regular ones are the generalisations of the AdS-Taub-Bolt solutions we are after and one can read off the squashing parameters A and B from the UV expansion of the numerical solutions after using the relations (3.17). A typical regular AdS-Taub-Bolt solution with two non-vanishing squashing parameters is presented in the left panel of Figure 3.3. There are also singular solutions which we ignore from now on. An example of the latter is shown in the right panel of Figure 3.3.

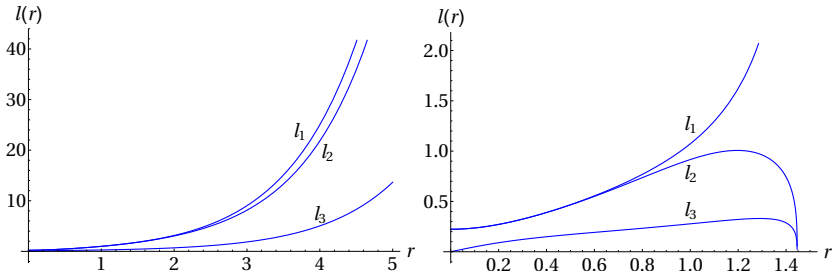

Figure 3.3: Two representative solutions with a Bolt in the IR. Left: a solution with $\gamma_0 = \frac{1}{2\sqrt{5}}$ and $\gamma_4 = -2.84169$ for which all the l_i keep on growing exponentially. This is an AdS-Taub-Bolt solution. Right: a solution with $\gamma_0 = \frac{1}{2\sqrt{5}}$ and $\gamma_4 = -2.84633$, for which there is a singularity where $l_2(r) = l_3(r) = 0$ at a finite value of r. We have chosen $r^* = 0$.

Despite their similarity with the NUT solutions, the regular AdS-Taub-Bolt backgrounds are more subtle because there are two branches of such solutions. To understand these branches better, it is worthwhile to focus briefly on the solutions with a single squashing parameter by setting $B = 0$. This condition imposes the following relation between the two independent IR parameters

$$\gamma_4 = -\frac{11 + 24\gamma_0^2}{384\gamma_0^3} \ . \tag{3.22}$$

Since we have an analytic solution for $B = 0$, namely the AdS-Taub-Bolt background of Section 3.2.1, we can also express the squashing parameter A as

a function of γ_0.

$$A = 9\gamma_0^2 + \frac{3}{4\gamma_0^2} + 5\,. \tag{3.23}$$

It is now clear that for every positive value of A there are two different values of γ_0. This is illustrated in the left panel of Figure 3.4. At the critical value $\gamma_0 = \frac{1}{\sqrt{2\sqrt{3}}} \approx 0.537285$ one finds a minimum of the function in (3.23) and the value $A = 5 + 3\sqrt{3} \approx 10.1962$ at this point is precisely the minimum value of A below which there are no AdS-Taub-Bolt with a single squashing parameter. The branch of solutions with a value of γ_0 greater/smaller than the critical value will be dubbed "positive"/"negative" respectively. To construct numerical solutions with non-vanishing B we proceed as follows. We choose values of γ_0 and γ_4 that lie on the analytic curve (3.22) characterising solutions with $B = 0$ and we change γ_4 to explore the full parameter space in the (γ_0, γ_4) plane. In this manner we can always keep track of which branch of solutions the resulting numerical solution belongs to. In the right panel of Figure 3.4 we show part of the region in the (γ_0, γ_4) plane where there are regular AdS-Taub-Bolt solutions. The "negative" branch solutions are depicted in red while the "positive" branch is in blue.

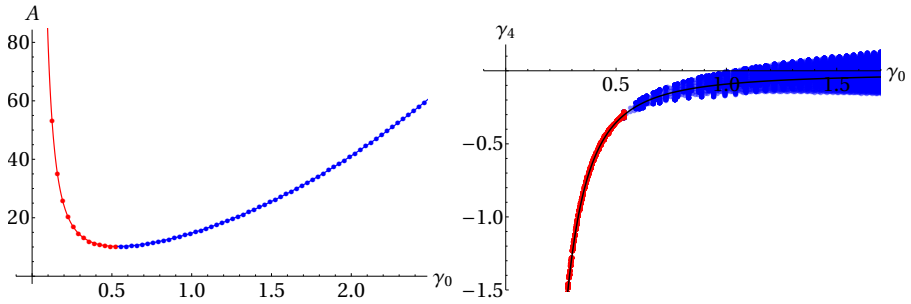

Figure 3.4: Left: The squashing parameter A as a function of γ_0 for the single squashed AdS-Taub-Bolt solutions; the solid curve is the analytic result in (3.23). Right: the range of values of (γ_0, γ_4) for which there is a regular AdS-Taub-Bolt solution with two nontrivial squashing parameters; the solid curve is the relationship in (3.22).

3.2.3 Double squashings and scalar field

Let us now consider an extra generalisation to the previous results, namely AdS-Taub-NUT/Bolt solutions with a massive scalar field. We choose the potential $V(\phi) = -2 - \cosh(\sqrt{2}\phi)$, which already includes a negative cosmological constant.

This potential comes from a consistent truncation of the low energy limit of M-Theory compactified to $AdS_4 \times S^7$ [71].

The equations of motion can again be found by varying the action with respect to the three scale factors and the scalar field and results in (B.1) in Appendix B.1. To tackle the full equations of motion, we use the same method as in the no scalar field case: expand the solutions around the IR and numerically evolve them to the UV. The IR and UV expansions of the scale factors l_i will have the same form as described above in (3.19), (3.21) and (3.15). The IR expansion of the scalar field will behave the same for the NUT and Bolt geometries and looks like

$$\phi(r) = \phi_0 + \phi_k (r - r*)^k \ , \tag{3.24}$$

where k goes from 2 to ∞ and only takes even values. The only free parameter in the scalar field expansion is ϕ_0, the coefficient of the higher order terms are a function of this single parameter. Due to the backreaction of the scalar field to the metric, the higher order terms in the scale factors, l_i, will also depend on ϕ_0, as described in Appendix B.1. Thus there are in total, for both the NUT and the Bolt solutions, three parameters that can be used to explore parameter space.

The UV expansion of the scalar field is given by [5]

$$\phi(r) = \frac{\bar{\alpha}}{(A_0 B_0 C_0)^{1/3}} e^{-r} + \frac{\bar{\beta}}{(A_0 B_0 C_0)^{2/3}} e^{-2r} + \mathcal{O}(e^{-3r}) \ . \tag{3.25}$$

Notice that this expansion is slightly different from the one in Chapter 2, because here we already put $\eta_0 = 1/\sqrt{\text{Vol}(h_{ij})}$. In Figure 3.5 an example for an AdS-NUT solution is shown, in the left panel the behaviour of the scalar field is depicted and in the right panel the three different scale factors are shown. Again we find solutions that do not reach the asymptotic boundary, but these will be ignored.

It is interesting to look at the dispersion relation between $\bar{\alpha}$ and $\bar{\beta}$, because these will be related to respectively the vev and its source in the dual field theory. For different values of the squashing A these can be found in Figure 3.6. The most interesting part of this plot is that $\bar{\beta}$ goes to a constant for large $\bar{\alpha}$ when the squashing is $A > -3/4$ [6]. Further, there is a regime where at the same value of $\bar{\beta}$ there are two values of $\bar{\alpha}$. For squashings smaller than $A < -3/4$, $\bar{\beta}$ doesn't converge any more, but diverges. $A = -3/4$ is precisely the value of the squashing when R changes sign. When the squashing is large enough, the Bolt solutions appear, whose behaviour is shown in the left panel

[5] Remember that a bar over the quantity indicates that it is an AdS variable.

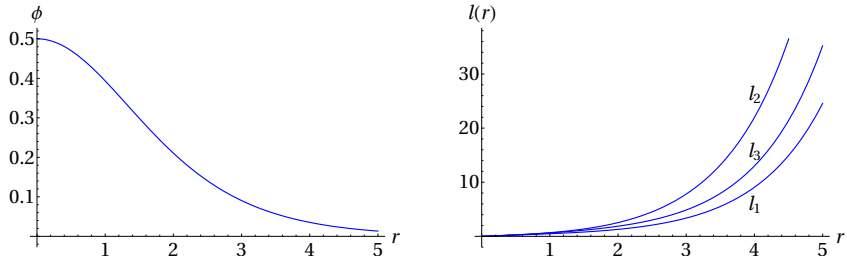

Figure 3.5: Example of an AdS-NUT solution with scalar field and two squashings with initial conditions $\phi_0 = 1/2$, $\beta_4 = -2/10$, $\gamma_4 = -23/120$. Left: the evolution of the scalar field. Right: the three different scale factors.

of Figure 3.6. The solutions with more negative values of $\bar{\beta}$ correspond to the "positive" branch Bolt solutions, while the other solutions, which are almost indistinguishable from the NUT solutions, are related to the "negative" branch.

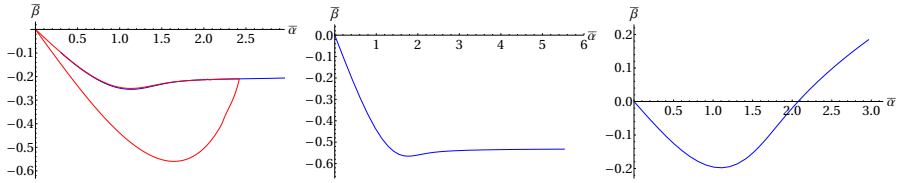

(a) $A = 40.0$ **(b)** $A = 0$ **(c)** $A = -0.85$

Figure 3.6: These figures show $\bar{\alpha}$ as a function of $\bar{\beta}$ for different squashings. Blue depicts the NUT solutions, while red represents the Bolt solutions. The more negative bolt solutions in the left panel are related to the "positive" branch, while the other bolt solutions correspond to the "negative" branch.

3.3 From NUTs to Bolts: Thermodynamics and phase transitions

In Section 3.2 we found a new class of solutions of the Einstein equations which extends the known AdS-Taub-NUT/Bolt solutions. In this section we study their thermodynamic behaviour by evaluating their regularised Euclidean on-shell action. This also sets the stage for a holographic comparison with the field theory results for the free energy in Section 3.4.

3.3.1 Renormalising the action

The evaluation of the action can get simplified by inserting the equations of motion into the Euclidean action (1.5) to get the on-shell action (with $l_0(r) = 1$)

$$I_{\mathrm{E}}^{\mathrm{O.S.}} = -\frac{16\pi^2}{\kappa^2}\int \mathrm{d}r\; l_1(r)l_2(r)l_3(r)V(\phi(r)) \\ -\frac{16\pi^2}{\kappa^2}\Big(l_2(r)l_3(r)l_1'(r) + l_1(r)l_3(r)l_2'(r) + l_1(r)l_2(r)l_3'(r)\Big)_{r=r_{\mathrm{c}}}\,, \tag{3.26}$$

where r_{c} is the cut-off radius at which we take the boundary $\partial\mathcal{M}$.

As usual for asymptotically locally AdS space, the value of the on-shell action diverges, and one needs to implement a regularisation procedure. We apply the usual tools of holographic renormalisation which were used for the NUT/Bolt solutions of Section 3.2.1 in [68] (see also [72] and [73] for a review). This procedure amounts to adding infinite counterterms to the action in (3.26) that make it finite on-shell. These counterterms are universal for a given gravitational theory and thus we can simply apply the results of [68, 73] to our setup. The counterterms are given by

$$S_{\mathrm{ct}} = \frac{1}{\kappa^2}\int_{\partial\mathcal{M}} d^3x\sqrt{h}\left(2 + \frac{\mathcal{R}}{2} + \frac{\kappa^2}{2}\phi^2\right)\,, \tag{3.27}$$

where $\mathcal{R}$ is the scalar curvature of the boundary metric h_{ij}. Evaluating this counterterm action yields

$$S_{\mathrm{ct}} = 4\pi^2\frac{2({l_1}^2{l_2}^2 + {l_2}^2{l_3}^2 + {l_1}^2{l_3}^2) + 2{l_1}^2{l_2}^2{l_3}^2(4+\kappa^2\phi^2) - {l_1}^4 - {l_2}^4 - {l_3}^4}{\kappa^2 l_1 l_2 l_3}\,. \tag{3.28}$$

Substituting our asymptotic expansions of the functions $l_i(r)$ and the scalar field, (3.15) and (3.25), gives[6]

$$S_{\mathrm{ct}} = \frac{8\pi^2}{\kappa^2}\Big(4A_0B_0C_0\mathrm{e}^{3r} - \frac{1}{4A_0B_0C_0}\Big(A_0^4 + B_0^4 + C_0^4 - 2B_0^2C_0^2 - 2A_0^2B_0^2 \\ - 2A_0^2C_0^2 + 2\kappa^2(A_0B_0C_0)^{4/3}\bar{\alpha}^2\Big)\mathrm{e}^r - \frac{16\pi^2\kappa^2}{3}\bar{\alpha}\bar{\beta} + \mathcal{O}(\mathrm{e}^{-r})\Big)_{r=r_{\mathrm{c}}}\,. \tag{3.29}$$

[6] Notice that to expand the scalar field, we have to assume that it rolled down its potential such that potential gets approximated by $V(\phi) \approx -3 - \phi^2 + \dots$.

The asymptotic form of the original on-shell gravitational action in (3.26) reads

$$I_{\rm E}^{\rm O.S.} = -\frac{8\pi^2}{\kappa^2}\Bigg(4A_0B_0C_0\mathrm{e}^{3r} - \frac{1}{4A_0B_0C_0}\Big(A_0^4+B_0^4+C_0^4-2B_0^2C_0^2-2A_0^2B_0^2 \\ -2A_0^2C_0^2+2\kappa^2(A_0B_0C_0)^{4/3}\bar{\alpha}^2\Big)\mathrm{e}^r+\mathcal{O}(1)\Bigg)_{r=r_{\rm c}} . \tag{3.30}$$

As expected the sum

$$I_{\rm E}^{\rm ren} = I_{\rm E} + S_{\rm ct} , \tag{3.31}$$

remains finite in the $r = r_{\rm c} \to \infty$ limit and thus this sum can serve as a good regularised on-shell action.

Since our gravitational solutions are constructed numerically, evaluating the regularised on-shell action $S_{\rm ren}$ is tricky. The difficulty comes from the fact that one has to add a large positive and a large negative number and this could lead to numerical instabilities. To remedy this, we found it useful to employ the following strategy. From (3.30) we know how the on-shell action diverges at large values of r. We can thus evaluate numerically this on-shell action at large but finite values of r and fit the resulting values to the function

$$f = D\mathrm{e}^{3r_c} + E\mathrm{e}^{2r_c} + F\mathrm{e}^{r_c} + G + H\mathrm{e}^{-r_c} + I\mathrm{e}^{-2r_c} . \tag{3.32}$$

We can then read of the coefficients D, E, and F and use the first three terms in (3.32) as our numerical counterterm action that should be added to S to produce a finite result. If there is no scalar field, the value of G is the final value for the renormalised action.

If there is a non-zero scalar field present we have to do some more work. Because in the dual theory we want to analyse the deformation by an operator of dimension $\Delta = 1$,the scheme of alternate quantization comes into play and we have to evaluate the action in terms of $\bar{\beta}$. To achieve this we have to perform a Legendre transform by adding the following term [38, 74]

$$S_- = -\int_{\partial\mathcal{M}} \mathrm{d}^3x\sqrt{h}\phi\pi_\phi , \tag{3.33}$$

where π_ϕ is the canonical momentum of ϕ at the boundary

$$\pi_\phi = \frac{1}{\sqrt{h}}\frac{\delta(I_{\rm E}+S_{\rm ct})}{\delta\phi} = \partial_r\phi + \phi . \tag{3.34}$$

After plugging in the asymptotic expansions in this term, we get

$$S_- = 16\pi^2\bar{\alpha}\bar{\beta} + \mathcal{O}(\mathrm{e}^{2r}) . \tag{3.35}$$

Thus to get the complete action, we have to add to G the constant parts from (3.29) and (3.35).

As a consistency check of our numerical results we should find that the coefficient E in (3.32) is approximately 0. We found that this value usual was of the order of $\mathcal{O}(10^{-10})$, but became bigger, up to order $\mathcal{O}(10^{-4})$, for squashings close to -1.

3.3.2 Single squashed NUTs and Bolts

To test our numerical methods further, we compare them with the known, analytic results for the regularised on-shell action of the AdS-Taub-NUT and Bolt solutions with a single squashed S^3 on the boundary, with zero scalar field [68].

The regularised on-shell action for the Taub-NUT/Bolt solutions of Section 3.2.1 can be found by plugging the metric (3.4) into the action (1.5) and adding the counterterms given in (3.27). This yields the following result [68]:

$$I_{\mathrm{E}}^{\mathrm{O.S.}} = \frac{32\pi^2 n}{\kappa^2 l^2}(l^2 m + 3n^2\rho_+ - \rho_+^3) \ . \tag{3.36}$$

In this formula one has to plug in the value of m corresponding to the NUT (3.7) or Bolt (3.9) solution. The value for ρ_+ corresponds to the minimum possible value of ρ, i.e. the location of the fixed point of the Killing vector ∂_ψ.

For the NUT solutions we have to substitute $\rho_+ = n$ and $m = m_n$ (3.7). This gives a general expression for the NUT actions which we, from now on, write as a function of A

$$I_{\mathrm{E}}^{\mathrm{NUT}} = \frac{4\pi^2(1+2A)}{(1+A)^2} \ , \tag{3.37}$$

where we have set $\kappa^2 = 1$ and $l = 1$. In the left plot of Figure 3.7 we compare the analytic single squashed, Taub-NUT action (in red) as a function of A with the action (in blue dots) obtained from our numerical methods described in Section 3.3.1 above. It is clear from this figure that the numerical procedure reproduces the analytical results with a very good accuracy.

We can repeat this comparison for the Bolt solutions. To find the analytic results, we just have to plug in the Bolt mass parameter m_b from (3.9) and the positive or negative Bolt radius $\rho_{b\pm}$ from (3.10) into m and ρ_+ respectively. This gives two different values for the Bolt action

$$I_{\mathrm{E}}^{\pm} = \frac{4\pi^2}{27(A+1)}\left(17 - \left(1 \pm \sqrt{\frac{(A-10)A-2}{(A+1)^2}}\right)A^2 \pm 2\sqrt{\frac{(A-10)A-2}{(A+1)^2}}\right.$$

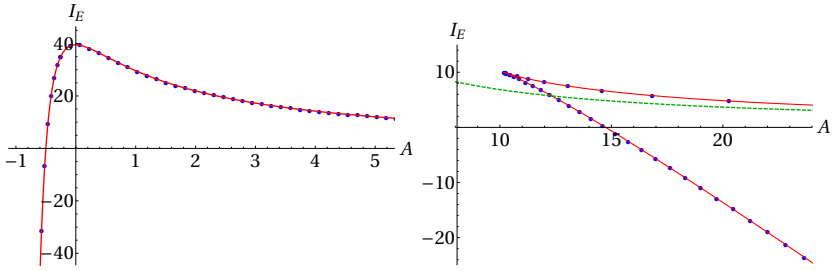

Figure 3.7: Left: The analytic Taub-NUT action for a single squashing at the boundary in red compared with the results from our numerical techniques in blue. Right: Idem for the Taub-Bolt action.

$$+2\left(8\pm 5\sqrt{\frac{(A-10)A-2}{(A+1)^2}}\right)A\Bigg)\,, \tag{3.38}$$

where $I_{\rm E}^{+}$ corresponds to the positive branch and $I_{\rm E}^{-}$ to the negative branch of solutions. For both of these branches, the analytic (full red line) and the numerical results (blue dots), are shown in the right plot of Figure 3.7. In the same figure we also plot the on-shell action of the NUT solution (dashed green curve) for comparison. Again, there is excellent agreement between the numerical and analytical calculations, giving us confidence in our numerical techniques.

It is clear from Figure 3.7 that there is a phase transition from the NUT to the Bolt solutions as one increases the value of A. This phase transition is similar to the Hawking-Page one and to find the precise value of the squashing parameter at which it occurs, one has to compare the regularised on-shell action for the two types of solutions, i.e. the solution with the lower on-shell action is the thermodynamically preferred one. For $A < A_{\rm crit} = 5+3\sqrt{3} \approx 10.2$ there are only NUT solutions. The Bolt solutions with higher on-shell action are the ones from the "negative" branch with action $I_{\rm E}^{-}$. They are never thermodynamically preferred. The "positive" branch Bolt solutions with action $I_{\rm E}^{+}$ become thermodynamically favoured for $A > A_{\rm HP} \equiv 6+2\sqrt{10} \approx 12.3$. The precise value $A_{\rm HP}$ is obtained by solving the algebraic equation $I_{\rm E}^{+} = I_{\rm E}^{\rm NUT}$.

3.3.3 Double squashed NUTs and Bolts

Having some faith in our numerical techniques, it is time to apply them to the new asymptotically AdS_4 solutions with two squashing parameters that we constructed in Sections 3.2.2 and 3.2.3. First, we discuss the case without the scalar field, which we will add again in the next subsection.

Since we do not have analytic solutions, we evaluate the regularised on-shell action numerically as described in Section 3.3.1. The resulting on-shell action for the AdS-Taub-NUT solutions is plotted in Figure 3.8. It is clear from this plot that the on-shell action exhibits a global maximum at $A = B = 0$. If one considers slices of constant B, there is a maximum around $A = 0$ for positive B and at $A = B$ for negative B and vice versa for slices of constant A. A similar analysis can be done for the AdS-Taub-Bolt solutions with two squashings. As discussed in Section 3.2.2, we have two branches of Bolt solutions, both of which exist only in a limited region in the (A, B) plane. The regularised on-shell action for the two branches of solutions is plotted in Figure 3.9.

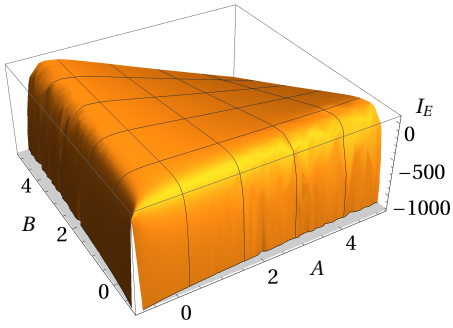

Figure 3.8: The regularised on-shell action of the AdS-Taub-NUT solutions as a function of the two squashing parameters.

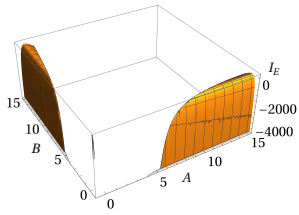

(a) The positive branch Bolt solutions

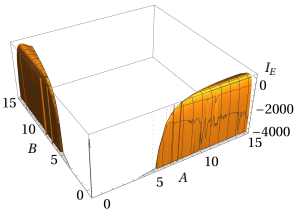

(b) The negative branch Bolt solutions

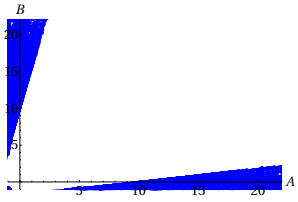

(c) The region in the (A, B) plane where the Bolt solutions exist.

Figure 3.9: The regularised on-shell action of the two branches of the AdS-Taub-Bolt solutions as a function of the two squashing parameters and the region in the (A, B) plane for which the solutions exist.

Equipped with the regularised on-shell action, we can ask which of the solutions is thermodynamically favoured in various regions of parameter space. This is not immediately clear and to illustrate the result better, we have compared the

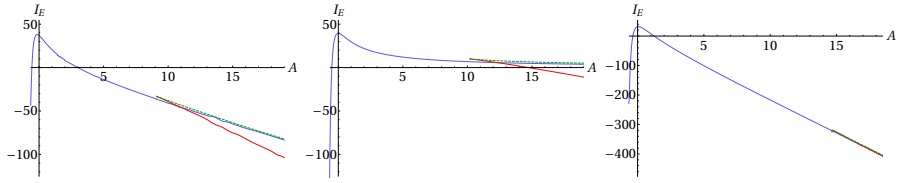

(a) $B = -0.2$ **(b)** $B = 0$ **(c)** $B = 0.8$

Figure 3.10: The regularised on-shell action for the NUT and Bolt solutions as a function of A for slices of constant B. The NUT action is plotted in blue, the negative branch Bolt action is in dashed green while the positive branch is in red.

on-shell action for the NUT and Bolt solutions by choosing slices of constant B and plotted the action as a function of A. Some representative results are presented in Figure 3.10. What we find, is that for any fixed value of B_0 the Taub-Bolt solutions exist only for values of A larger than a finite critical value $A_{\text{crit}}(B_0)$. In addition there is always a Hawking-Page type phase transition at some $A_{\text{HP}}(B_0) > A_{\text{crit}}(B_0)$. Thus we conclude that the new AdS-Taub-Bolt solutions exhibit a qualitatively similar behaviour to the analytic Bolt solutions with $B = 0$ across the entire configuration space of boundary geometries parameterised by (A, B). It is useful to note that $A_{\text{HP}}(B_0)$ increases for increasing B_0. Finally, notice that for negative B_0, the maximum value of the action as a function of A moves away from $A = 0$.

3.3.4 Scalar field thermodynamics

Finally, let us see how the addition of a scalar field adjusts the thermodynamical phase transitions. The behaviour of the actions changes drastically when we add a scalar field. If the deformation $\bar{\beta}$ is small enough, the action around small A behaves similar as the no-scalar field case (see Figure 3.11a), but for large A the Hawking-Page type phase transition changes completely (see Figure 3.11d). First of all, the NUT solutions stop existing for large squashings. Before this critical point gets reached, they become multivalued for fixed values of A. The region of existence of the Bolt solutions, in the meantime, gets shifted to larger squashings, while the non-dominant negative-branch Bolt solutions also become multivalued. The appearance of multiple solutions for a fixed value of A can be understood from Figure 3.6, where we see that for fixed A and $\bar{\beta}$ there correspond multiple values of $\bar{\alpha}$.

The solutions that arise due to the multiple solutions with a fixed $\bar{\beta}$ and A all have a higher free energy, therefore these solutions do not seem to play an

important role in the quantum gravity path integral. However, it was shown in [75, 7] that in AdS/CFT one should sum over bulk geometries in the Euclidean theory. For example, correlators for the subdominant geometries can play an important role and even help to restore black hole unitarity. For this reason it would be interesting to study these subdominant contributions to understand their explicit meaning and see if their contribution is bigger than anticipated.

When the absolute value of the deformation gets increased even more, the domain of existence of NUT solutions shrinks more and more, until there is only a small region around $A = 0$ where the NUT solutions exist. Notice that around this region they also become multivalued. The minimal squashing for which the Bolt solutions exist, shifts to larger values of the squashing, such that there are squashings for which there are no solutions. This can be seen in the right panels of Figure 3.11.

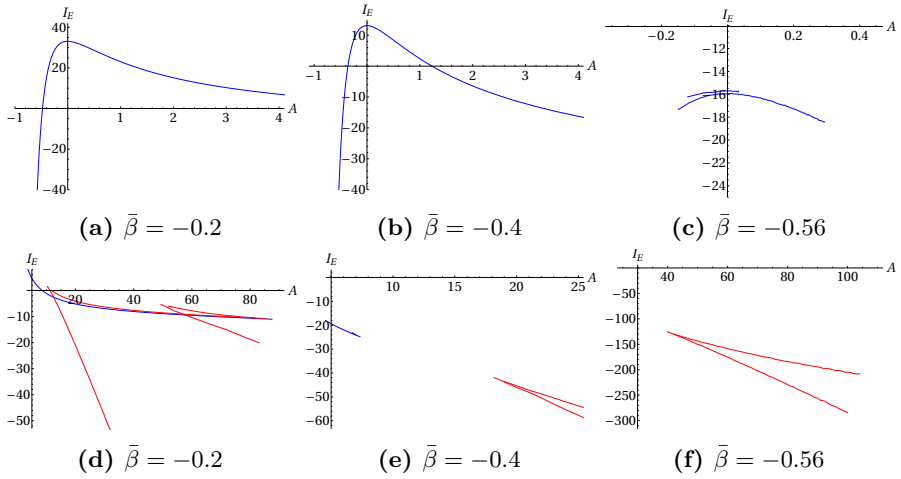

Figure 3.11: The free energy as a function of the squashing for different values of $\bar{\beta}$. The blue line is given by the NUT solutions, while the red lines represent the Bolt solutions. In the upper row we zoomed in on the region $A \in [-1, 5]$ while in the bottom row we highlighted the NUT to Bolt transitions.

3.4 The $O(N)$ model on the double squashed sphere

Studying the holographic, dual field theory description of the gravitational solutions described in the previous two sections is a non-trivial problem. One

approach could be to embed these solutions as backgrounds in string or M-theory and identify a dual CFT in which to phrase the question. An example of how this could be achieved, is to think of the NUT/Bolt solutions as deformations of the $AdS_4 \times S^7$ solution of eleven-dimensional supergravity. In this case the dual field theory is the ABJM SCFT and we are faced with the problem of evaluating the partition function of this theory at strong coupling upon a supersymmetry breaking deformation. This is a formidable problem which we will not attempt to solve here. Instead, we will focus on a simplified model of this setup where we consider a free vector-like theory on the double-squashed sphere in (3.1). In particular, we focus on evaluating the partition functions, or free energy, of the free $O(N)$ model as a function of the two squashing parameters A and B and the mass m of the scalar fields.

The free $O(N)$ vector model in three dimensions is conjectured to be described holographically by a higher-spin Vassiliev theory in AdS_4 with certain specific boundary conditions [54, 39, 55]. This four-dimensional theory is very different from pure Einstein gravity with a negative cosmological constant. Despite this difference, we find that there are many qualitative similarities between the behaviour of the free energy of the free $O(N)$ vector model and the action of the gravitational solutions in Section 3.2 as a function of A and B. Similar results were found in [76] for the case of S^3 boundaries with a single squashing parameter, i.e. $B = 0$.

3.4.1 The method

The action for the free, three-dimensional $O(N)$ vector model in Euclidean signature is given by

$$I_{O(N)} = \frac{1}{2}\int \mathrm{d}^3x\sqrt{g}\left(\partial_\mu\phi_a\partial^\mu\phi^a + \frac{R}{8}\phi_a\phi^a + m^2\phi_a\phi^a\right) . \tag{3.39}$$

Here we are assuming that the N scalar fields ϕ_a, $a = 1, \ldots, N$, are conformally coupled and have mass m. We will assume that the metric is given by the squashed sphere metric in (3.1) with Ricci scalar R given by (3.3). One of our interests will be to study the spin zero current $\frac{1}{2}\phi_a\phi^a$, which has conformal dimension one. Because this is less than 3/2, we had to use the alternate quantization in the previous section.

The partition function for this model is given by

$$Z_{O(N)} = \int \mathcal{D}\phi e^{-I_{O(N)}} . \tag{3.40}$$

To find the free energy of this theory we have to evaluate the Gaussian integral in (3.40). This amounts to computing the following determinant

$$F_{O(N)} = -\log Z_{O(N)} = \frac{N}{2}\log\left(\det\left[\frac{-\nabla^2 + m^2 + \frac{R}{8}}{r_0^2\Lambda^2}\right]\right) , \tag{3.41}$$

where r_0 is the radius of the sphere (3.1) (which we set to 1 from now on) and Λ is the cutoff used to regularise the UV divergences in this theory. These divergences arise from infinite covariant counterterms written in terms of the metric and curvature scalar of the squashed sphere. Since we are dealing with a CFT in three dimensions there are no conformal anomalies and thus the divergences for large Λ can be schematically written in the form

$$\text{divergences} \approx D\Lambda^3 + E\Lambda^2 + F\Lambda \ . \tag{3.42}$$

It is not accidental that we chose the same notation for the coefficients in (3.32) and (3.42). The role of Λ in the CFT is played by the radial cutoff e^{r_c} used in holographic renormalisation. The cubic and linear terms in (3.42) arise from the covariant counterterms $\Lambda^3\int d^3x\sqrt{g}$ and $\Lambda\int d^3x\sqrt{g}R$ respectively. There is no covariant counterterm that will lead to a quadratic divergence and thus we should have $E = 0$ in (3.42).

Our goal is to calculate (3.41). There are two technical obstacles along the way. First, one has to find the spectrum of the scalar Laplacian ∇^2 for the metric in (3.1). Second, since this operator is infinite dimensional, one has to perform an infinite sum and regularise the divergences described above to evaluate the determinant in (3.41).

To address the first problem we can use the fact that the metric in (3.1) is a homogeneous metric on S^3 and thus one can use algebraic techniques to find the spectrum of the Laplacian. When one of the squashing parameters vanishes, say $B = 0$, the spectrum of the scalar Laplacian can be found in closed analytic form, see for example [77, 78]. When both squashing parameters are turned on, the problem becomes harder and one has to resort to numerical techniques. The procedure to find the eigenvalues of the scalar Laplacian for the double squashed sphere is outlined in Appendix B.2. The upshot of the analysis is that we are able to determine this spectrum numerically to (in principle) any desired accuracy.

To regularise the infinite sum in (3.41) one may be tempted to use an analytic approach like ζ-function regularisation [79, 76, 80]. However, this method is not well-adapted to situations where the spectrum of the Laplacian is known only numerically. Therefore, we will use a heat-kernel type regularisation, which can be implemented numerically and was discussed in some detail in [41]. Here

we briefly summarise this approach. Because in the next chapter we are also interested in theories with a single Dirac fermion, we shall immediately include these in our treatment.

The free energy of the free $O(N)$ model and the fermion can be written as

$$F = 2\left(\frac{-1}{2}\right)^f N^{f-1} \log\det[\mathfrak{D}/\Lambda^f] \,, \tag{3.43}$$

where $\mathfrak{D}$ is the conformal Laplace operator (3.41) or the Dirac operator (4.35), with $f = 1$ for fermions and $f = 2$ for scalar fields. The regularisation we adopt proceeds by rewriting (3.43) using a heat-kernel[7]

$$\log\det[\mathfrak{D}/\Lambda^f] = \sum_i \int_{1/\Lambda^2}^{\infty} \frac{\mathrm{d}t}{t} \mathrm{e}^{-t\lambda_i^{3-f}} \,, \tag{3.44}$$

where the sum is over all eigenvalues, λ_i, of the operator $\mathfrak{D}$. The resulting determinant captures all modes with energies lower than the cutoff Λ. The contributions of modes with eigenvalues above the cutoff is exponentially small. To see this, note that for the low lying modes, i.e. $\lambda_i/\Lambda^f \ll 1$, we have

$$\int_{1/\Lambda^2}^{\infty} \frac{\mathrm{d}t}{t} \mathrm{e}^{-t\lambda_i^{3-f}} = \Gamma(0, \lambda_i^{3-f}/\Lambda^2) = -\log(\lambda_i^{3-f}/\Lambda^2) + \mathcal{O}(\lambda_i^{3-f}/\Lambda^2) \,, \tag{3.45}$$

where $\Gamma(a, z)$ is the incomplete Euler-Gamma function. For the higher modes, i.e. $\lambda_i/\Lambda^f \gg 1$, we find

$$\Gamma(0, \lambda_i^{3-f}/\Lambda^2) = \mathrm{e}^{-\lambda_i^{3-f}/\Lambda^2} \left(\frac{1}{\lambda_i^{3-f}/\Lambda^2} + \mathcal{O}\left(\frac{1}{(\lambda_i^{3-f}/\Lambda^2)^2}\right)\right) \,. \tag{3.46}$$

Using this kernel, it can be shown that the divergences are going to appear when t is integrated over small values. To keep track of the divergences, we split the integral over t into an UV and IR part

$$\log\det[\mathfrak{D}/\Lambda^f] = \det_{\mathrm{UV}} + \det_{\mathrm{IR}} \,, \tag{3.47}$$

where

$$\det_{\mathrm{UV}} \equiv \int_{1/\Lambda^2}^{\delta} \frac{\mathrm{d}t}{t} \sum_i k_i e^{-t\lambda_i^{3-f}} \,, \tag{3.48a}$$

$$\det_{\mathrm{IR}} \equiv \sum_i k_i \int_{\delta}^{\infty} \frac{\mathrm{d}t}{t} \mathrm{e}^{-t\lambda_i^{3-f}} = \sum_i k_i \Gamma(0, \lambda_i^{3-f}\delta) \,. \tag{3.48b}$$

[7] See [81] for a review of heat kernel methods.

Here k_i is the degeneracy of eigenvalue λ_i and δ is an arbitrarily chosen small number that we can vary in order to get better convergence of the numerical results.

While the sum in $\det_{\rm IR}$ converges, in general, quite fast, the sum in $\det_{\rm UV}$ contains all the divergences and should be treated with care. The approach we adopt, is to numerically evaluate $\det_{\rm UV}$ for many values of Λ and fit the diverging results to the function in (3.42). The divergences obtained in this way are removed by hand and the remaining finite result is added to the finite value of $\det_{\rm IR}$ to obtain the desired result for the free energy. As a consistency check, we find that there is no dependence of the finite result on Λ and that the coefficient E in (3.42) is vanishing with good numerical accuracy.

To test our numerical method, it is instructive to calculate the free energy of the free $O(N)$ model on the round three sphere when all the scalars are massless, i.e. $A = B = m = 0$. The eigenvalues λ_i of the conformal Laplacian in (3.41) and their multiplicities k_i are given by

$$\lambda_i = i^2 - \frac{1}{4} \,, \qquad k_i = i^2 \,, \tag{3.49}$$

where $i \geq 1$. After setting[8] $N = 1$, we can plug this into our numerical machinery and find

$$F = -(\det_{\rm UV} + \det_{\rm IR}) \approx 0.0638070552 \,. \tag{3.50}$$

The free energy of a conformally coupled scalar field on S^3 can be computed analytically by using ζ-function regularisation, see for example [80]. The result is

$$F = \frac{1}{16}\left(2\log 2 - \frac{3\zeta(3)}{\pi^2}\right) \approx 0.0638070548 \,. \tag{3.51}$$

Comparing this analytic results with (3.50) we see a very good agreement. This gives us confidence in our numerical methods and in the next section we will apply them for the squashed sphere.

3.4.2 The results

Let us start with studying the single squashed sphere with massless scalars, by setting $B = m = 0$. The eigenvalues of the conformal Laplacian for this metric are known analytically, e.g [77, 78] (see also [67] for an extension of this result

[8] For simplicity all the results we show below are for $N = 1$, to obtain the results for higher N, one just has to multiply the free energy by N.

to squashed spheres in higher dimensions) and are labelled by two integers i and q

$$\lambda_{i,q} = \left(i^2 + A(i-1-2q)^2 - \frac{1}{4(1+A)} \right), \tag{3.52}$$

where $q = 0, 1, \ldots, i-1$ and $i \geq 1$ and they have a multiplicity of $k_i = i$. Since these eigenvalues are known analytically, one can apply the heat-kernel regularisation procedure described above, by using an analytic method to approximate the integral in (3.48) and subtract the UV divergences [41, 42]. The results of this procedure are captured by the solid red line in Figure 3.12.

As described in some detail in Appendix B.2, the eigenvalues of the conformal Laplacian with $B \neq 0$ are not known analytically and we have to resort to numerics. To gain even further confidence in our numerical procedure, we applied it to the case of the single squashed sphere with $B = 0$ and compared the results with the semi-analytic approach of [41, 42]. The outcome of this analysis is summarised in Figure 3.12.

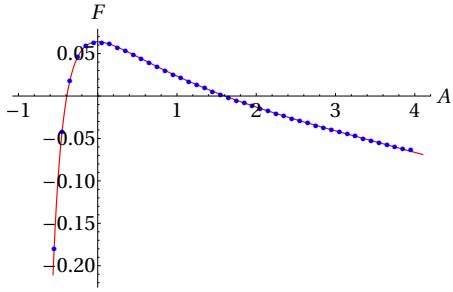

Figure 3.12: The free energy for the squashed sphere with $B = 0$ using our numerical techniques (in blue dots), compared with the semi-analytic approach of [41] (in red).

The numerical results for the free energy of the double squashed three-sphere are presented in Figure 3.13. One immediately recognises some similarities with the regularised on-shell action of the new AdS-Taub-NUT solutions constructed in Section 3.2. For instance, there is a global maximum around $A = B = 0$, and away from this point the free energy has a local maximum around $A = 0$ or $B = 0$ for positive squashings. For negative squashings the maxima are around $A = B$. In Section 3.5 we analyse the differences and similarities between the gravitational and field theories more thoroughly.

There is one more feature in Figure 3.13 we would like to highlight here. The free energy seems to diverge when the Ricci scalar approaches zero. To visualise this better, we plot in Figure 3.14 the region where the exponential of the

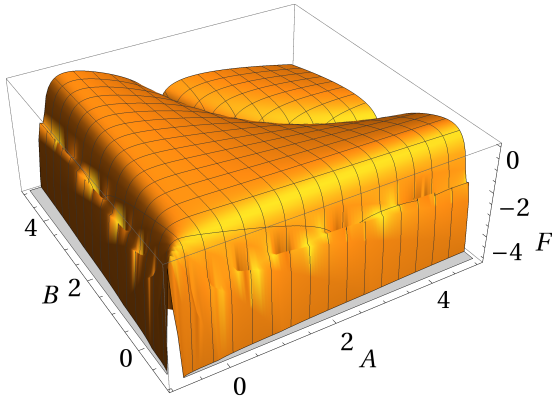

Figure 3.13: The free energy for a free conformally coupled scalar on the double squashed sphere computed using our numerical technique.

free energy becomes zero together with the region where $R = 0$. To see what happens, we have to inspect the IR behaviour of the free energy (3.48b), which is given by a sum over upper incomplete gamma functions $\Gamma(0, \lambda_i \delta)$. From the definition of these (3.45), one can see that if λ_i approaches 0, then $\Gamma(0, \lambda_i \delta)$ diverges. It is not too difficult to see from the discussion in Appendix B.2, that the lowest eigenvalue of the Laplacian ∇^2 always vanishes. Therefore, the first eigenvalue λ_1 of the conformal Laplacian $(-\nabla^2 + \frac{R}{8})$ becomes zero when the Ricci scalar vanishes. This explains the features in Figure 3.14. We should note that there are also "higher order" divergences in Figure 3.13, which are less pronounced. These happen when any of the higher eigenvalues of the Laplacian cancel $R \neq 0$ to give another zero eigenvalue of the conformal Laplacian. These divergences always appear in the regions of the (A, B) plane where the Ricci scalar R in (3.3) is negative.

The divergences give rise to sharp features in the function $F(A, B)$. To illustrate this, we show in Figure 3.15 the free energy as a function of A for a number of different fixed values of B. We show four plots for a small interval of A around $A = 0$. The divergences show up as two sharp negative spikes for small B and they both move to the right when B is increased. The right spike moves much faster to the right and goes to ∞ when B becomes 0, whereas the left spike converges slowly to $A = 0$ when B diverges. We also show three plots of the behaviour at larger A. Here we can only see the right spike, which first moves to ∞ when B approaches 0 and then returns for larger B eventually going to $A = 0$ when $B \to \infty$.

As a final step, let us see what happens when we take a non-zero mass, which acts as a source for the current $\frac{1}{2}\phi_a \phi^a$. The method to calculate the partition

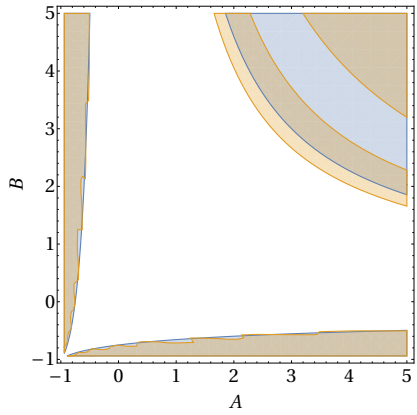

Figure 3.14: Comparison between the region in the (A, B) plane where R is less than 0 (in blue) and the region where the regularised path integral Z vanishes (in orange), which corresponds to a divergent free energy.

function with mass is the same as described above. The resulting free energies as a function of the squashing for different values of m^2 are shown in Figure 3.16, where for simplicity we restricted to one squashing. It is clear that the maximum shifts for smaller m^2, this is in contrast with the gravity result from Figure 3.11, where the maximum stays around zero squashing. Again we see the free energy diverges, whenever $R/8+m^2$ becomes zero. When m^2 becomes more negative, the spike moves to the right, such that when $m^2 = 3/4$ the divergence occurs at zero squashing. Notice that from Figure 3.11 we learned that the region of existence of the Bolt solutions shifted towards larger squashings when we increased the absolute value of the deformation. Could this be related to the shift we see here?

From the partition function it is easy to find the source as a function of the vev by differentiating it with respect to the source, the result for different squashings is shown in Figure 3.17, for which the gravitational counterpart is given by Figure 3.6. We see again that the vev keeps on increasing, while the source converges to a constant for a specific squashing, given by

$$m_{\mathrm{c}}^2 = -1 + \frac{1}{4(1+A)} \ . \tag{3.53}$$

However, the bump that was present on the gravity side cannot be found here. Notice that only a part of the plots correspond to the gravity solutions. For the field theory calculation we can have positive sources, while on the gravity side this doesn't seem to be accessible. Again, there is a qualitative difference

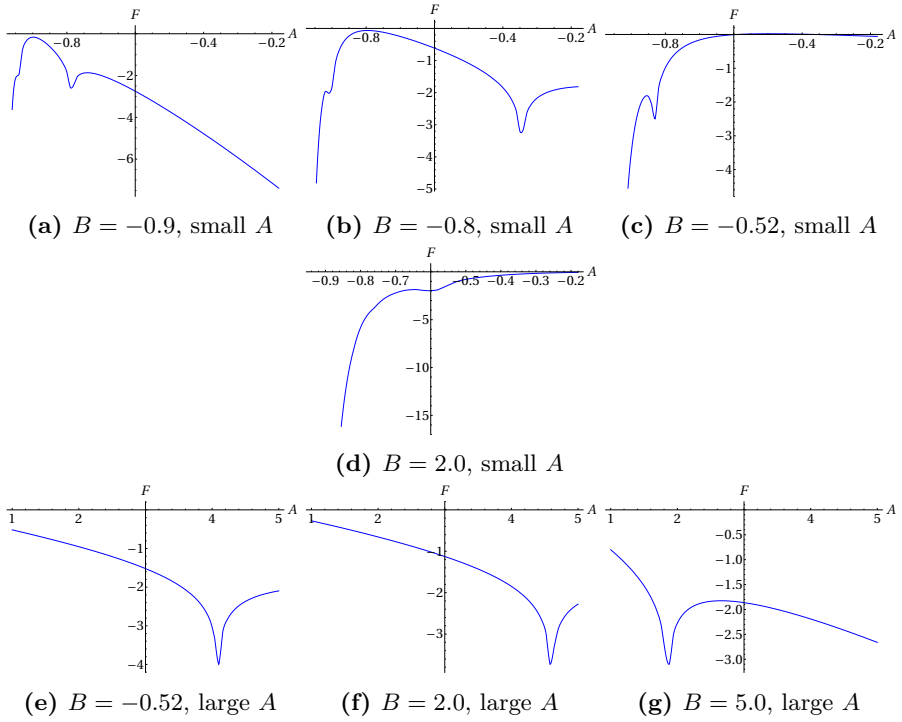

(a) $B = -0.9$, small A **(b)** $B = -0.8$, small A **(c)** $B = -0.52$, small A

(d) $B = 2.0$, small A

(e) $B = -0.52$, large A **(f)** $B = 2.0$, large A **(g)** $B = 5.0$, large A

Figure 3.15: Behaviour of the CFT free energy for fixed B in the region of small and large A.

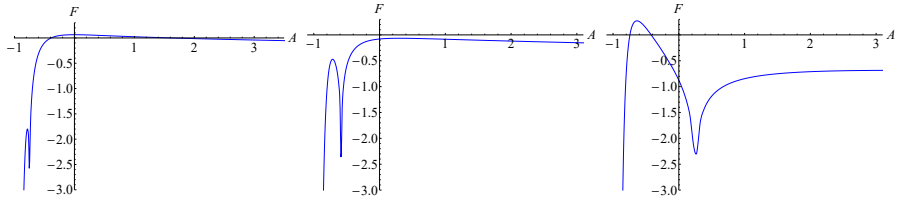

(a) $m^2 = 0.0$ **(b)** $m^2 = -0.4$ **(c)** $m^2 = -0.8$

Figure 3.16: In all these figures the free energy as a function of the squashing is given for different mass deformations.

between the results where $A < -3/4$ and where A is larger. For $A < -3/4$ the region with negative source is not accessible any more, because the minimal value m_c^2 reaches 0 for this squashing. More similarities and differences between the field theory and the gravitational theory will be discussed in the next section.

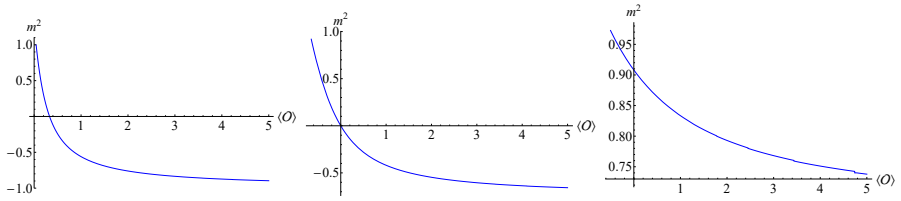

(a) $A = 40.0$ **(b)** $A = 0.0$ **(c)** $A = -0.85$

Figure 3.17: In all these figures we show m^2 as a function of the vev for different squashings.

3.5 Holographic comparison

We can now attempt to compare the regularised on-shell action of our new asymptotically AdS_4 solutions of gravity with a double squashed sphere at the boundary with the free energy of the $O(N)$ vector model on the same squashed sphere. We should emphasise from the start that there is no a priori reason to expect that there is any duality between these two theories. The free $O(N)$ model should be dual to a higher-spin Vasiliev theory in AdS_4 and this theory is very different from pure Einstein gravity with a negative cosmological constant. Nevertheless, the results in [76] suggest that there are some qualitative similarities between these models which we further explore here.

First, let us focus on the case when there is only one non-trivial squashing parameter and no scalar deformations, i.e. $B = 0$. In Figure 3.18 we plot the regularised on-shell action of the corresponding gravitational solution and compare it with the free energy of the free $O(N)$ vector model. We chose to normalise both quantities such that for $A = 0$ they are equal to one and focus on their dependence on the squashing parameter A. There are clear similarities between the two functions in the region $A < 0$. For $A > 0$ the similarity is only qualitative, i.e. both functions decrease as A increases. A notable difference is that the gravitational solutions exhibit a Hawking-Page phase transition for a relatively large positive value of A. Such a phase transition is of course absent in a free quantum field theory. Another notable feature is that the free energy of the CFT diverges for $A = -3/4$ due to the simple fact that the lowest eigenvalue of the conformal Laplacian in (3.41) vanishes at this value of the squashing. There is no corresponding divergence in the gravitational on-shell action. We believe that this discrepancy is entirely due to the fact that we are considering a free CFT. Indeed the large N analysis of the free energy of the interacting three-dimensional $O(N)$ vector model in [76] shows that this divergence in the free energy is removed. We will come back to this in Section

5.3. For large values of A both functions decrease linearly. From our numerical results we can estimate that the ratio of the slopes of these linear functions is approximately 3.7.

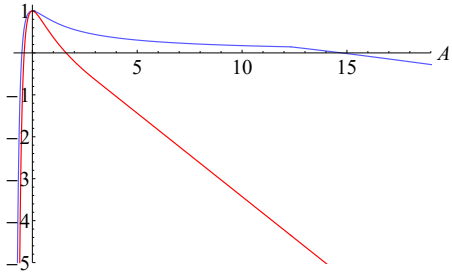

Figure 3.18: Comparison between the free energy of the free $O(N)$ model for $B = 0$ without a scalar deformation and as a function of A(red) and the on-shell action for the analytic AdS-Taub-Nut/Bolt solutions (blue). For the gravitational results we included the phase transition from NUT to Bolt. All results are normalised to give 1 for $A = B = 0$.

Let us now compare the gravitational on-shell action and the field theory free energies when both squashing parameters do not vanish. The regularised bulk on-shell action is presented in Figure 3.8 and the field theory free energy is plotted in Figure 3.13. Some of the similarities between these two figures were already mentioned, the qualitatively similar overall behaviour as well as the global maximum at $A = B = 0$. However, just like in the case of one squashing parameter, we also have differences between the two quantities: the phase transition in the bulk from NUT to Bolt which doesn't appear in the free CFT, the diverging free energy in the free field theory when R becomes 0, and the different asymptotic falloff behaviour for large values of the squashing parameters.

To have a better understanding of the similarities and differences between the gravitational and field theory results, we provide plots of the free energy and on-shell action as a function of A for fixed values of B. This is shown in Figure 3.19 where the CFT results are plotted in red, the on-shell action of the Taub-NUT solutions is in blue and the one for Taub-Bolt solutions is indicated with a green dashed line. From this figure the conclusions of the previous paragraphs are immediately obvious. We see that for $B < 0$ the maxima are around $A = B$, for positive B the maximum is always at $A = B = 0$. The general behaviour for small and large A is also again comparable, but in general the CFT free energy falls off much faster than the bulk on-shell action.

If we add scalar deformations, the comparison becomes more troublesome,

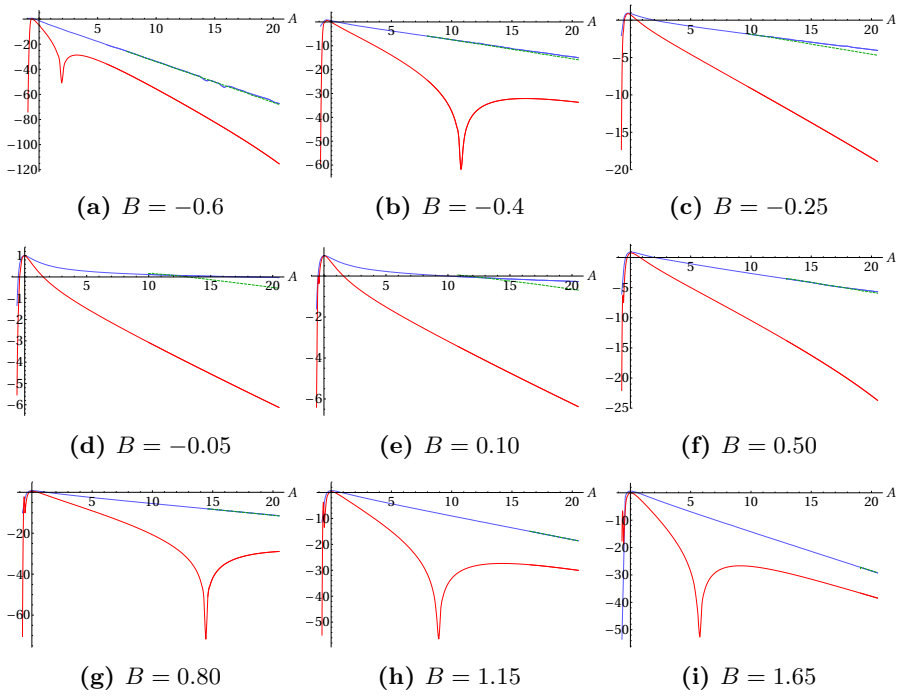

(a) $B = -0.6$ **(b)** $B = -0.4$ **(c)** $B = -0.25$

(d) $B = -0.05$ **(e)** $B = 0.10$ **(f)** $B = 0.50$

(g) $B = 0.80$ **(h)** $B = 1.15$ **(i)** $B = 1.65$

Figure 3.19: Comparison, for different fixed values of B, between the free energy of the CFT (in red), the Taub-NUT (in blue) and Taub-Bolt (in dashed green) on-shell actions. All functions are normalised to give 1 when both squashings parameters are zero.

partially due to the fact that the phase transitions are more complicated. For this reason it is easier to compare the relations between the source and the vev in Figure 3.20. There are a priori not many similarities between the two theories. First of all, as mentioned earlier, the two theories are not exactly related to eachother. Second, the situation is different from the above comparison where the only deformations were the squashings. These squashings are the same for both theories, while the relation between the source and vev with respectively $\bar{\beta}$ and $\bar{\alpha}$ is not clear. The only similarities are that when the vev grows, the source asymptotes to a constant negative value for $A > -3/4$. When $A < -3/4$ the bulk theory dispersion relation does not exhibit this large vev behaviour any more. The field theory still has an asymptotic source when the vev goes to infinity, but this isn't negative any more. A difference that hasn't been discussed yet, is the fact that on the gravitational side zero source corresponds to zero vev, while on the field theory side this is definitely not the case any more.

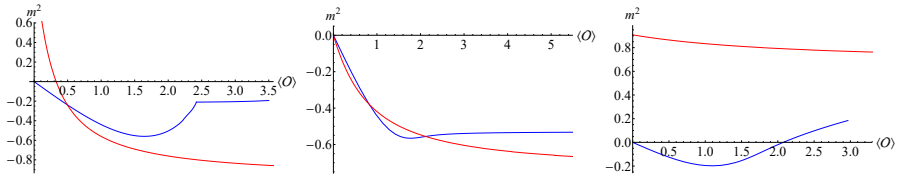

(a) $A = 40.0$ **(b)** $A = 0.0$ **(c)** $A = -0.85$

Figure 3.20: In these figures we show the relation between the vev and the source for both the (dominant) gravitational theory (in blue) and the boundary field theory (in red).

3.6 Discussion and outlook

In this chapter we started our study of squashed spheres by considering gravitational theories with a negative cosmological constant that asymptote to a squashed sphere boundary and the free $O(N)$ model on the same boundary. We have shown that the partition function of the free $O(N)$ model on the double squashed three-sphere with zero mass, as a function of the two squashing parameters, qualitatively reproduces the thermodynamical properties of a new set of Euclidean, asymptotically locally AdS_4 solutions of pure Einstein gravity. We generalised these results even further by adding a scalar field on the gravitational side and a non-zero mass term on the CFT side. New thermodynamical effects on the gravity side were observed, like the appearance of multivalued NUT and Bolt solutions and the shrinking area of valid solutions in parameter space. On the field theory side, the addition of a massterm made peaks in the free energy move in the same way as different values of B seemed to change these. It remains, however, a mystery how to relate the scalar deformations on both sides – if it is even possible.

There are some clear avenues for generalisation of our work. First, it would be interesting to extend our results to higher dimensions. On the gravitational side it should be fairly straightforward to generalise the metric Ansatz in (3.13) and find new solutions of general relativity in higher dimensions. Based on our experience in four dimensions we expect that these backgrounds can be found only numerically. Extending the results of Section 3.4 to higher dimensions, should also be possible. The technical problem here is to find the spectrum of the Laplacian on higher-dimensional squashed spheres. This has been addressed in [67] for a generalisation of the metric in (3.1) with $B = 0$ to higher odd dimensions. Adding additional squashing parameters to the problem will probably be technically cumbersome.

Other possible extensions would be to find the proper dual to the free $O(N)$

models, namely higher-spin Vasiliev theory. In view of the field theory results in Section 3.4 it will therefore be very interesting to construct new solutions of Vasiliev theory which have a squashed S^3 metric on the asymptotic boundary. This will provide new opportunities for quantitative checks of the higher-spin/vector model duality and see if the extensions with a mass term make more sense in these theories. Conversely, it will be desirable to construct proper holographic duals to the gravitational solutions we constructed in Section 3.2. To do this, one has to overcome the technical difficulty in dealing with strongly coupled three-dimensional CFTs, like the ABJM theory, on curved manifolds without resorting to the power of supersymmetry.

Finally, we would also like to study the cosmological implications of the squashed sphere theories. This will be the goal of the Chapter 5, where we apply the holographic no-boundary proposal to the theories studied above.

CHAPTER 4

SOME COMMENTS ON SQUASHED SPHERE PARTITION FUNCTIONS

In general, coupling field theories to background fields can be utilised to learn more about the dynamics of the theory– an idea often used in studying quantum field theories. For example, we saw in the preceding chapter that, when we only considered geometric deformations, the round sphere was a local maximum of the free energy. It is an interesting avenue to study these examples in detail to see if they apply more general and if they can uncover some underlying principle. Properties of CFTs, like the ones we will discus in this chapter, also find relevance in cosmology, because it are these that can be used to learn something about the global structure of eternally inflating universes as we will discus in the next chapter.

We will prove in this chapter that for odd-dimensional CFTs on a conformally flat background metric $\bar{g}_{\mu\nu}$ deformed by a symmetric tensor $\epsilon h_{\mu\nu}$, the free energy of the CFT has the following series expansion for small ϵ

$$F(\epsilon) = F(0) + \frac{\epsilon^2}{2} F''(0) + \mathcal{O}(\epsilon^3)\,, \tag{4.1}$$

where

$$F''(0) = \tilde{G}(\bar{g}_{\mu\nu}, h_{\mu\nu}, d)\, C_{\mathrm{T}}\,, \tag{4.2}$$

and $\tilde{G}(\bar{g}_{\mu\nu}, h_{\mu\nu}, d)$ is a function which depends (see (4.24) below) on the corresponding conformally flat metric $\bar{g}_{\mu\nu}$, the metric deformation $h_{\mu\nu}$ and the spacetime dimension. The real number C_{T} is theory dependent and positive for unitary CFTs. It is often referred to as the "central charge" and determines

the two-point function of the energy-momentum tensor. In particular, for CFTs in Euclidean flat space $\mathbb{R}^d$ with coordinates X_a one has [82][1]

$$\langle T_{ab}(X)\, T_{cd}(0)\rangle_{\mathbb{R}^d} = \frac{1}{\mathcal{S}_{d-1}^2}\frac{C_{\rm T}}{|X|^{2d}}\,\mathcal{I}_{ab,cd}(X)\,, \tag{4.3}$$

where $\mathcal{S}_d = 2\pi^{d/2}/\Gamma[d/2]$ is the area of the unit $(d-1)$-sphere and the tensorial object $\mathcal{I}_{ab,cd}(X)$ reads

$$\mathcal{I}_{ab,cd}(X) = \frac{1}{2}\left(I_{ac}(X)I_{bd}(X) + I_{ad}(X)I_{bc}(X)\right) - \frac{1}{d}\delta_{ab}\delta_{cd}\ , \tag{4.4}$$

where

$$I_{ac}(X) = \delta_{ac} - 2\frac{X_a X_c}{|X|^2}\,. \tag{4.5}$$

The free energy of an odd-dimensional CFT on the round sphere is a useful quantity since it is conjectured to be monotonic decreasing along unitary RG flows for three dimensional CFTs.[2] This F-theorem was proven for three-dimensional CFTs in [85] using entanglement entropy techniques (see [86] for a review and further references), but remains a conjecture for higher-dimensional theories. The squashing deformations of the round sphere metric that we study here, break conformal invariance in the CFT and thus induce an RG flow. This flow is however outside the scope of the established F-theorem, since the induced CFT perturbation is driven by the energy-momentum tensor, which is an operator of spin 2. Nevertheless, it is still natural to expect that the free energy should be a local maximum in the space of deformations controlled by the parameter ϵ in (4.1). This expectation indeed bears out. For CFTs in three dimensions, and the particular metric deformation in (3.1), we are able to explicitly compute the quadratic correction to F in the small ϵ expansion, and find[3]

$$F''_{S^3_\alpha}(0) = -\frac{\pi^2}{48}C_{\rm T}\ . \tag{4.7}$$

For unitary CFTs, the central charge $C_{\rm T}$ is positive and thus the free energy on the round sphere $F(0)$ is a local maximum in the space of squashing deformations given by (3.1).

[1] Note that our convention for $C_{\rm T}$ is the same as in [83], and differs from that in e.g. [82, 84] by a factor of $1/\mathcal{S}_d^2 = \Gamma[d/2]^2/(4\pi^d)$. For example, in our convention, $C_{\rm T} = d/(d-1)$ for a free real scalar field.

[2] For odd-dimensional CFTs the quantity conjectured to be decreasing along the RG flow is [80]

$$\mathcal{F} = (-1)^{(d-1)/2}\log|Z_{S^d}|\,. \tag{4.6}$$

[3] Note that throughout this section, we use the notation $F^{(n)} \equiv d^n F/d\epsilon^n$, i.e. the derivatives are taken with respect to ϵ, not A.

In Section 4.1 we begin with a general discussion of the partition function of odd-dimensional CFTs on deformed conformally flat manifolds. In Section 4.2 we study the partition function of CFTs on the squashed sphere and compute this explicitly by reviewing our results from Chapter 3 together with an explicit computation of the free energy for a free fermion. We conclude in Section 4.3 where we discuss the connection between our study and recent results on the shape-dependence of entanglement entropy in CFTs. We end that section with some comments about the generalisation of our results to more general deformations of the round sphere and an outlook to further work.

This chapter is based on work with N. Bobev and P. Bueno published in [67].

4.1 Partition functions on deformed manifolds

Let us consider the Euclidean partition function of a general CFT on a d-dimensional[4] manifold $\mathcal{M}$ with metric $g_{\mu\nu}$

$$Z = \int \mathcal{D}\varphi \, \mathrm{e}^{-I[\varphi, g_{\mu\nu}]} \,, \tag{4.8}$$

where φ stands schematically for the set of dynamical fields in the theory. We wish to understand how the free energy $F \equiv -\log Z$ changes under small deformations of the metric. Let us parametrise such deformations as

$$g_{\mu\nu} = \bar{g}_{\mu\nu} + \epsilon \, h_{\mu\nu} \,, \tag{4.9}$$

where $\bar{g}_{\mu\nu}$ is some arbitrary reference metric on $\mathcal{M}$, ϵ is a real constant, and $h_{\mu\nu}$ encodes the geometry of the perturbation. If we assume that $|\epsilon| \ll 1$, we can expand the action in a power series in ϵ as follows

$$I[g_{\mu\nu}] = I[\bar{g}_{\mu\nu}] - \frac{\epsilon}{2} \int \mathrm{d}^d x \sqrt{\bar{g}(x)} \, h^{\mu\nu}(x) T_{\mu\nu}(x)$$

$$- \frac{\epsilon^2}{4} \int \mathrm{d}^d x \sqrt{\bar{g}(x)} \left[\frac{h(x)}{2} h^{\mu\nu}(x) T_{\mu\nu}(x) + \int \mathrm{d}^d y \sqrt{\bar{g}(y)} \, h^{\mu\nu}(x) h^{\rho\sigma}(y) \frac{\delta T_{\mu\nu}(x)}{\sqrt{\bar{g}(y)} \delta g^{\rho\sigma}(y)} \right]$$

$$+ \frac{\epsilon^3}{6} \int \mathrm{d}^d x \sqrt{\bar{g}(x)} \left\{ \frac{1}{8} \left(2 h^{\rho\sigma}(x) h_{\rho\sigma}(x) - h^2(x) \right) h^{\mu\nu}(x) T_{\mu\nu}(x) \right.$$

$$\left. - \int \mathrm{d}^d y \sqrt{\bar{g}(y)} \left[\frac{1}{2} h(x) h^{\mu\nu}(x) h^{\alpha\beta}(y) \frac{\delta T_{\mu\nu}(x)}{\sqrt{\bar{g}(y)} \delta g^{\alpha\beta}(y)} \right. \right.$$

[4] We will soon restrict d to be an odd integer.

$$- \int \mathrm{d}^d z \sqrt{\bar{g}(z)} \frac{1}{2} h^{\mu\nu}(x) h^{\rho\sigma}(y) h^{\alpha\beta}(z) \frac{\delta^2 T_{\mu\nu}}{\sqrt{\bar{g}(y)}\sqrt{\bar{g}(z)} \delta g^{\rho\sigma}(y) \delta g^{\alpha\beta}(z)} \Bigg] \Bigg\} + \mathcal{O}(\epsilon^4) \,, \tag{4.10}$$

where, as usual with g and $\bar{g}$, we denote the determinant of the respective metrics, and we have defined $h^{\mu\nu} \equiv -\bar{g}^{\mu\alpha}\bar{g}^{\nu\beta}h_{\alpha\beta}$, $h \equiv \bar{g}^{\mu\nu}h_{\mu\nu}$.[5] We have also used the definition of the stress-energy tensor

$$T_{\mu\nu} \equiv -\frac{2}{\sqrt{g}} \frac{\delta I[\varphi, g_{\mu\nu}]}{\delta g^{\mu\nu}} \,. \tag{4.11}$$

Hence, the partition function on the deformed background reads

$$Z_\epsilon = \int \mathcal{D}\varphi \, \mathrm{e}^{-I[\varphi,\bar{g}_{\mu\nu}] + \frac{\epsilon}{2}\int_{\mathcal{M}} \mathrm{d}^d x \sqrt{\bar{g}}\, h^{\mu\nu}(x) T_{\mu\nu}(x) + \mathcal{O}(\epsilon^2)} \,. \tag{4.12}$$

Now, let us further assume that the free energy is an analytic function of ϵ, i.e. that we can expand it as

$$F(\epsilon) = \sum_{n=0}^{\infty} \frac{\epsilon^n}{n!} F^{(n)}(0) \,. \tag{4.13}$$

A straightforward calculation of the leading correction to $F(0)$ yields

$$\begin{aligned} F'(0) &= -\frac{1}{2} \frac{\int \mathcal{D}\varphi \, \left[\int_{\mathcal{M}} \mathrm{d}^d x \sqrt{\bar{g}}\, h^{\mu\nu}(x) T_{\mu\nu}(x)\right] \mathrm{e}^{-I[\varphi,\bar{g}_{\mu\nu}]}}{\int \mathcal{D}\varphi \, \mathrm{e}^{-I[\varphi,\bar{g}_{\mu\nu}]}} \\ &= -\frac{1}{2} \int_{\mathcal{M}} \mathrm{d}^d x \sqrt{\bar{g}}\, h^{\mu\nu}(x) \left\langle T_{\mu\nu}(x) \right\rangle_{\mathcal{M}} \,. \end{aligned} \tag{4.14}$$

Whenever the one point function of the energy momentum tensor in the CFT on the undeformed space vanishes

$$\left\langle T_{\mu\nu}(x) \right\rangle_{\mathcal{M}} = 0 \,, \tag{4.15}$$

one has $F'(0) = 0$, and thus the background associated to $\bar{g}_{\mu\nu}$ is a local extremum of the free energy. From now on we will assume that (4.15) holds. This is the case for odd-dimensional CFTs placed on a background metric $\bar{g}_{\mu\nu}$ on $\mathcal{M}$ which is conformally flat, like the round three sphere. The fact that $F'(0) = 0$ for small perturbations around the round sphere is in the spirit of the F-theorem in three dimensions [87, 80]. Note, however, that the two statements are not identical since we are considering deformations of the CFT with the energy momentum tensor, which is not a scalar operator.

[5] Note that with this notation, the inverse metric reads: $g^{\mu\nu} = \bar{g}^{\mu\nu} + \epsilon\, h^{\mu\nu} + \mathcal{O}(\epsilon^2)$.

Assuming that (4.15) holds, one finds the following expression for the coefficient of the second order correction to the free energy

$$F''(0) = -\frac{1}{4}\int \mathrm{d}^d y\sqrt{\bar{g}}\int \mathrm{d}^d x\sqrt{\bar{g}}\, h^{\mu\nu}(x)h^{\rho\sigma}(y)\Bigg[\langle T_{\mu\nu}(x)T_{\rho\sigma}(y)\rangle_{\mathcal{M}} + \underbrace{2\langle\frac{\delta T_{\mu\nu}(x)}{\sqrt{\bar{g}(y)}\delta g^{\rho\sigma}(y)}\rangle_{\mathcal{M}}}\Bigg]. \tag{4.16}$$

Analogously, the coefficient of the third order correction reads

$$F'''(0) = -\int \mathrm{d}^d z\sqrt{\bar{g}}\int \mathrm{d}^d y\sqrt{\bar{g}}\int \mathrm{d}^d x\sqrt{\bar{g}}\, h^{\mu\nu}(x)h^{\rho\sigma}(y)h^{\alpha\beta}(y)\times$$

$$\Bigg[\frac{1}{8}\langle T_{\mu\nu}(x)T_{\rho\sigma}(y)T_{\alpha\beta}(z)\rangle_{\mathcal{M}} + \underbrace{\frac{1}{2}\langle\frac{\delta^2 T_{\mu\nu}}{\sqrt{\bar{g}(y)}\sqrt{\bar{g}(z)}\delta g^{\rho\sigma}(y)\delta g^{\alpha\beta}(z)}\rangle_{\mathcal{M}}}$$

$$+\frac{3}{4}\langle\frac{\delta T_{\mu\nu}(x)}{\sqrt{\bar{g}(y)}\delta g^{\rho\sigma}(y)}T_{\alpha\beta}(z)\rangle_{\mathcal{M}}\Bigg] - \frac{1}{2}\int \mathrm{d}^d y\sqrt{\bar{g}}\int \mathrm{d}^d x\sqrt{\bar{g}}\, h(x)h^{\mu\nu}(x)h^{\rho\sigma}(y)\times$$

$$\Bigg[\frac{3}{4}\langle T_{\mu\nu}(x)T_{\rho\sigma}(y)\rangle_{\mathcal{M}} + \underbrace{\langle\frac{\delta T_{\mu\nu}(x)}{\sqrt{\bar{g}(y)}\delta g^{\rho\sigma}(y)}\rangle_{\mathcal{M}}}\Bigg]. \tag{4.17}$$

If the CFT at hand lives in an odd number of dimensions, and the metric $\bar{g}_{\mu\nu}$ on $\mathcal{M}$ is conformally flat, one can show that the terms underlined with a bracket in (4.16) and (4.17) vanish. This is due to the fact that one point functions of local operators in CFTs should vanish in the absence of conformal anomalies.

Since we are interested in deformations of odd-dimensional round spheres, from now on we will ignore the underlined terms in (4.16) and (4.17). In that case, the leading correction to the free energy is quadratic in ϵ with coefficient given by

$$F''(0) = -\frac{1}{4}\int_{\mathcal{M}}\sqrt{\bar{g}}\,\mathrm{d}^d x\int_{\mathcal{M}}\sqrt{\bar{g}}\,\mathrm{d}^d y\,\left[h^{\mu\nu}(x)h^{\rho\sigma}(y)\,\langle T_{\mu\nu}(x)T_{\rho\sigma}(y)\rangle_{\mathcal{M}}\right]. \tag{4.18}$$

Observe that if $\bar{g}_{\mu\nu}$ is the flat metric on $\mathbb{R}^d$, (4.15) is automatically satisfied and C_{T} controls the leading correction to $F(0)$, as it is obvious from (4.3). Now let us take $\mathcal{M}$ to be a (locally) conformally flat manifold, i.e. let us assume it to be related to $\mathbb{R}^d$ through a conformal mapping

$$f : \mathcal{M} \longrightarrow \mathbb{R}^d. \tag{4.19}$$

Then, the metrics of both spaces are related through

$$f_*(\mathrm{d}s^2_{\mathbb{R}^d}) = \Omega^2(x)\mathrm{d}s^2_{\mathcal{M}}\,, \tag{4.20}$$

where f_* is the pullback and $\Omega^2(x)$ the corresponding conformal factor. In odd-dimensional theories, the stress tensors for the theories on $\mathcal{M}$ and $\mathbb{R}^d$ are related through[6]

$$T_{\mu\nu}(x) = \Omega^{d-2}\, M^{ab}_{\mu\nu}\, T_{ab}(X)\,, \quad \text{where} \quad M^{ab}_{\mu\nu} \equiv \frac{\partial X^a}{\partial x^\mu}\frac{\partial X^b}{\partial x^\nu}\,, \tag{4.21}$$

and where we denoted the coordinates in $\mathcal{M}$ and $\mathbb{R}^d$ by $\{x^\mu\}$ and $\{X^a\}$ respectively. For the correlator in the integrand of (4.18), one finds

$$\langle T_{\mu\nu}(x)T_{\rho\sigma}(y)\rangle_{\mathcal{M}} = \Omega^{d-2}(x)\Omega^{d-2}(y)\, M^{ab}_{\mu\nu}(x)M^{cd}_{\rho\sigma}(y)\, \langle T_{ab}(X)T_{cd}(Y)\rangle_{\mathbb{R}^d}\,. \tag{4.22}$$

This expression allows us to write the two-point function on $\mathcal{M}$ in terms of the two-point function on $\mathbb{R}^d$, whose explicit expression is given by (4.3).

To recap, we find that on any odd-dimensional manifold $\mathcal{M}$ for which the map f in (4.19) exists, the free energy behaves, under a small deformation of the metric, as

$$F(\epsilon) = F(0) + \frac{\epsilon^2}{2}F''(0) + \mathcal{O}(\epsilon^3)\,, \tag{4.23}$$

with

$$F''(0) = -\frac{C_{\mathrm{T}}}{4\mathcal{S}^2_{d-1}}\int_{\mathcal{M}}\sqrt{\bar{g}}\,\mathrm{d}^d x\int_{\mathcal{M}}\sqrt{\bar{g}}\,\mathrm{d}^d y\,\times$$
$$\left[h^{\mu\nu}(x)h^{\rho\sigma}(y)\Omega^{d-2}(x)\Omega^{d-2}(y)\, M^{ab}_{\mu\nu}(x)M^{cd}_{\rho\sigma}(y)\,\frac{\mathcal{I}_{ab,cd}(X-Y)}{|X-Y|^{2d}}\right]\,, \tag{4.24}$$

and where in the last term it is understood that we need to write all contributions as functions of $\{x\}$ and $\{y\}$ using the map f defined in (4.19).[7]

A few comments about the third order correction $F'''(0)$ are in order. The terms on the second and fourth lines of (4.17) which are not underlined, depend on the particular CFT of interest only through the constants C_{T}, t_2, and t_4 appearing in the three-point function of the energy momentum tensor — see Appendix C for details. Thus, these contributions are in principle computable for general CFTs. However, the one on the third line depends on the details

[6] In even dimensions, (4.21) generically receives an anomalous contribution — see e.g. [88].

[7] Note that the integral in (4.24) suffers from UV singularities at coincident points $x \to y$. We use the same regularization procedure as in [89, 80] to remove such divergences. See Section 3 of [90] for a more detailed discussion of this type of divergences.

of the CFT at hand and, in particular, on OPE coefficients of local operators with the energy momentum tensor. This leads to the conclusion that it seems hard to obtain an explicit expression for $F'''(0)$ valid for general CFTs. In the examples discussed below, we will be able to estimate $F'''(0)$ for squashed spheres in some specific CFTs, including free theories as well as theories with a weakly curved holographic dual.

4.2 Examples for the squashed three-sphere

In this section, we will apply what we saw in the previous section to our three dimensional spheres with one squashing (with all masses put to zero). We start by doing the explicit calculation of (4.24). Note that in the parametrisation introduced in (4.9), we have the following relation for the small parameter ϵ and the usual squashing parameter A

$$\epsilon = -\frac{A}{1+A} \,. \tag{4.25}$$

At first order in A (which is also first order in ϵ), we can write (3.1) as in (4.9), where $\bar{g}_{\mu\nu}$ is the metric of the round sphere

$$\mathrm{d}s^2_{S^3} = \frac{1}{4}\left[\mathrm{d}\theta^2 + \mathrm{d}\phi^2 + \mathrm{d}\tilde{\psi}^2 + 2\cos\theta \mathrm{d}\phi\mathrm{d}\tilde{\psi}\right] \,. \tag{4.26}$$

For this special choice of deformation of the round sphere, the only non-vanishing component of $h^{\mu\nu}$ reads

$$h^{\tilde{\psi}\tilde{\psi}} = -4 \,. \tag{4.27}$$

Clearly, this is a very symmetric squashing deformation of the metric on the round sphere, which will allow for the explicit results below.

To evaluate the integral in (4.24), we need the explicit form of transformations in (4.20) and (4.21). To find this, we employ a conformal mapping (f^{-1}) from $\mathbb{R}^3$ to S^3 as follows

$$X^1 = \frac{\cos\left(\frac{\phi-\tilde{\psi}}{2}\right)\sin\left(\frac{\theta}{2}\right)}{1-\sin\left(\frac{\phi+\tilde{\psi}}{2}\right)\cos\left(\frac{\theta}{2}\right)} \,, \qquad X^2 = \frac{\sin\left(\frac{\phi-\tilde{\psi}}{2}\right)\sin\left(\frac{\theta}{2}\right)}{1-\sin\left(\frac{\phi+\tilde{\psi}}{2}\right)\cos\left(\frac{\theta}{2}\right)} \,,$$

$$X^3 = \frac{\cos\left(\frac{\phi+\tilde{\psi}}{2}\right)\cos\left(\frac{\theta}{2}\right)}{1-\sin\left(\frac{\phi+\tilde{\psi}}{2}\right)\cos\left(\frac{\theta}{2}\right)} \,. \tag{4.28}$$

In these coordinates, the metric of the round S^3 (4.26) is related to the flat metric on $\mathbb{R}^3$ through

$$f_*(ds^2_{\mathbb{R}^3}) = \Omega^2 ds^2_{S^3} \ , \quad \text{where} \quad \Omega = \frac{1}{2}\left[1 + \delta_{ab} X^a X^b\right] . \tag{4.29}$$

With these ingredients, we are ready to evaluate $F''_{S^3_A}(0)$ using (4.24). A somewhat tedious, but otherwise straightforward, calculation yields

$$F''_{S^3_A}(0) = -\frac{\pi^2}{48} C_{\mathrm{T}} \, . \tag{4.30}$$

Notice that for unitary CFTs, C_{T} is a positive number, which in turn implies that the partition function on the round S^3 is a local maximum in the space of squashing deformations considered here. This observation agrees with the results displayed above in Figures 3.7 and 3.12 that show this for respectively CFTs with an Einstein holographic dual and a free scalar field theory. Our result shows that this holds for general CFTs and, furthermore, that the leading correction to the round sphere result, which is always quadratic in the deformation, is controlled by the central charge C_{T} (4.30).

From these results, we can conclude that for general three-dimensional CFTs, the free energy on a squashed three-sphere with the metric (3.1) is given by

$$F_{S^3_A} = F_{S^3} - \frac{\pi^2 C_{\mathrm{T}}}{96}\epsilon^2 + \mathcal{O}\left(\epsilon^3\right) = F_{S^3} - \frac{\pi^2 C_{\mathrm{T}}}{96}\frac{A^2}{(1+A)^2} + \mathcal{O}\left(\frac{A^3}{(1+A)^3}\right) , \tag{4.31}$$

for small values of the squashing parameter A (or ϵ).

Let us test the accuracy of (4.31) for different theories: the free scalar and fermion and theories that are holographically dual to Einstein gravity.

Free scalar

The results for the scalar can be found by setting $N = 1$ in Section 3.4, where the behaviour of the free energy is plotted in Figure 3.12. From this figure we can see that the round sphere at $A = 0$ leads to a local maximum and it is natural to conjecture that this is true for all allowed values in the range $A > -1$. This is in agreement with our expectations, because according to our general result (4.13), the first derivative of the free energy with respect to the squashing parameter evaluated at $A = 0$ should vanish. We find, with our numeric methods, $F'_{\mathrm{sc},\, S^3_A}(0) \simeq 2.25 \cdot 10^{-11}$. In addition, according to (4.31), we expect to find $-48/\pi^2 F''_{\mathrm{sc},\, S^3_A}(0) = C_{\mathrm{T},\,\mathrm{sc}} = 3/2$. Numerically, we obtain

$-48/\pi^2 F''_{\mathrm{sc},\,S^3_A}(0) \simeq 1.5000004$, which is clearly in very good agreement with the general result (4.31).

From Figure 3.12 we can also see that the free energy becomes a linear function. This linear behaviour for large squashings was also observed and discussed in [91, 76]. In particular, in [91] it was argued that in the limit of $A \gg 1$ the free energy is given by

$$\begin{aligned} F_{\mathrm{sc}} &= -\frac{\zeta(3)}{8\pi^2}A - \frac{1}{24}\log(1+A) + \frac{1}{12}\log(4\pi) + \zeta'(-1) - \frac{\zeta(3)}{8\pi^2} + \mathcal{O}(A^{-1})\,, \\ &\simeq -0.01522A - 0.04167\log(1+A) + 0.03027\,. \end{aligned} \tag{4.32}$$

A fit to our numerical curve yields instead

$$F_{\mathrm{sc}} \simeq -0.01524A - 0.03706\log(1+A) + 0.06587\,. \tag{4.33}$$

It is clear that the leading $\mathcal{O}(\alpha)$ term in our numerical results agrees very well with the result in [91]. This is not the case, however, of the subleading contributions. It would be interesting to identify the source of these discrepancies, which do not seem attributable to numerical errors.

Free fermion

Let us now derive similar results for a free Dirac fermion. The partition function in this case is

$$Z_{\mathrm{f}} = \int \mathcal{D}\psi\, e^{-\int \mathrm{d}^3x\sqrt{g}[\psi^\dagger(i\not{D})\psi]}\,, \tag{4.34}$$

where $\not{D}$ is the Dirac operator on the corresponding curved background. The free energy can be found by solving the Gaussian integral

$$F_{\mathrm{f}} = -\log Z_{\mathrm{f}} = -\log\det\left[\frac{i\not{D}}{\Lambda}\right]\,, \tag{4.35}$$

where, once again, we introduced an energy cutoff Λ. To calculate this determinant we need the eigenvalues of the Dirac operator on the squashed sphere background. These have been found in [79, 92, 93], and read

$$\lambda_{n,q,\,\pm} = \frac{1}{\sqrt{1+A}} \pm 4\sqrt{\frac{n^2(1+A)}{4} - Aq(n-q)}\,, \tag{4.36}$$

where n and q are integers. For the positive branch, denoted by $+$, n goes from 1 to ∞ and q from 0 to n, while for the negative branch, denoted by $-$, n goes

from 2 to ∞ and q from 1 to $n-1$. In evaluating the determinant in (4.35), we have to sum over both branches of the eigenvalues.

To compute the free energy as a function of A, we apply the same numerical procedure used in Section 3.4.1 for the free scalar. Our numerical results are presented in Figure 4.1. We again observe that the round sphere partition function at $A=0$ is a local maximum. However, it is clearly not a global maximum since, interestingly, for large positive values of A, the free energy increases linearly. A fit on this function learns us that

$$F_{\mathrm{f},S^3_A} =\simeq 0.03043A - 0.16551\log(1+A) + 0.20929\,, \quad (\alpha \gg 1)\,. \tag{4.37}$$

Just like for the scalar, an analytic expression was found in [91] for $F_{\mathrm{f},\,S^3_A}$ in this regime. This reads

$$\begin{aligned} F_{\mathrm{f},\,S^3_A} &= \frac{\zeta(3)}{4\pi^2}A - \frac{1}{6}\log(1+A) + \frac{1}{3}\log(4\pi) + 4\zeta'(-1) + \frac{\zeta(3)}{4\pi^2} + \mathcal{O}(A^{-1})\,, \\ &\simeq 0.03045A - 0.16667\log(1+A) + 0.21244\,, \end{aligned} \tag{4.38}$$

which, in this case, agrees very well with our numerical result — see also Figure 4.1.

To gain more confidence in our numerical results, we can again perform some consistency checks. For $A=0$, the partition function for a free Dirac fermion was evaluated analytically in [80] and reads

$$F_{\mathrm{f},\,S^3} = \frac{\log 2}{4} + \frac{3\zeta(3)}{8\pi^2} = 0.21895948\ldots \tag{4.39}$$

With our numerical method for $A=0$, we find $F_{\mathrm{f},\,S^3} \simeq 0.21895949$, which is in excellent agreement with (4.39). The first and second derivatives of the free energy with respect to A, evaluated at $A=0$ are given by $F'_{\mathrm{f},\,S^3_A}(0) = 9.01\cdot 10^{-7}$ and $-48/\pi^2 F''_{\mathrm{f},\,S^3_A}(0) = 2.99999$, respectively. After taking into account that for the free Dirac fermion we have $C_{\mathrm{T},\mathrm{f}} = 3$, these values are in very good agreement with our general results (4.13) and (4.31).

Holography

As a last example, we consider three-dimensional CFTs with an Einstein gravity holographic dual, that has as a boundary the squashed three-sphere. These are of course the AdS-Taub-NUT/Bolt solutions discussed in Section 3.2. Because we are only interested in the behaviour of the free energy around small values of A, we only need to consider the NUT solutions, for which the action is given in

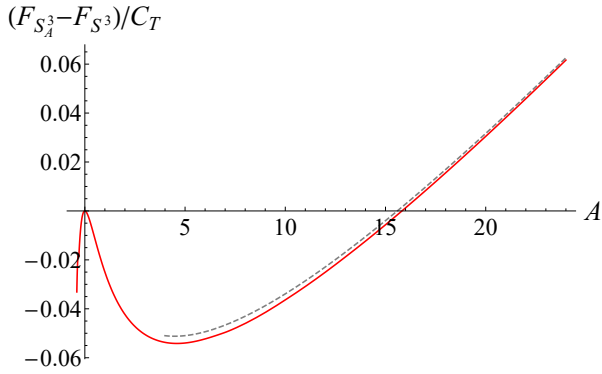

Figure 4.1: The free energy for a free Dirac fermion on the squashed S^3 as a function of the squashing parameter A. The round sphere is not a global maximum, as the free energy grows unbounded after reaching a local minimum for $A_{\rm min} \simeq 4.6228$. For large enough A, the free energy is given by (4.38), which is plotted in a gray, dashed line.

(3.37). To make contact with the field theory around (4.31), we need to express this result in terms of the "central charge" $C_{\rm T}$. For CFTs dual to Einstein gravity one has (see, e.g. [84] and Footnote 1)

$$C_{\rm T} = \frac{48\ell^2}{\pi G} \,. \tag{4.40}$$

Using this and (3.37), it is straightforward to show that the general field theory results (4.13) and (4.31) are obeyed. This is a non-trivial quantitative check of the holographic interpretation of the AdS-Taub-NUT solution. The free energy in (3.37) takes a more suggestive form when rewritten in terms of the parameter ϵ

$$F_{{\rm E},\, S^3_A} = F_{{\rm E},\, S^3} - \frac{\pi^2 C_{\rm T}}{96}\frac{A^2}{(1+A)^2} = F_{S^3} - \frac{\pi^2 C_{\rm T}}{96}\epsilon^2 \,. \tag{4.41}$$

Notice that this is an exact result valid for finite[8] values of A (or ϵ). In particular, this result implies that for three-dimensional CFTs with holographic duals captured by the action in (1.5), the quadratic approximation in (4.13) and (4.31) is exact, and all higher-order corrections in powers of ϵ vanish. Notice also that $A = 0$ is a global maximum for the gravitational free energy (4.41), i.e. the free energy is extremised when the boundary is the round S^3.

[8] Strictly speaking, finite but smaller than the value $A_{\rm HP}$.

Comparison

Let us compare the results for the free energies computed so far. We find it illuminating to study the dependence of the free energy on the squashing parameter by subtracting the value of the free energy on the round sphere and dividing by C_{T}, i.e. by considering the quantity $(F_{S^3_A} - F_{S^3})/C_{\mathrm{T}}$. Indeed, it is natural to normalise the free energy by the central charge C_{T}, given that, as shown in Section 4.1, this quantity controls the leading term in the expansion around $A = 0$. Moreover, it is clear from (4.31) that the round sphere value is a local maximum of $F_{S^3_A}$. In the right panel of Figure 4.2, we plot this normalised free energy as a function of A for the three theories considered in the previous subsections. In addition to that, we present the sum of the free energy of one free boson and one free Dirac fermion. It is unclear to us why the result for this combination is so similar to the one for general CFTs with a holographic dual. The holographic result for the free energy in (4.41) is a simple parabola when parametrised in terms of the squashing parameter ϵ. To this end in the right panel of Figure 4.2 we plot the free energies for the theories discussed above as a function of ϵ.

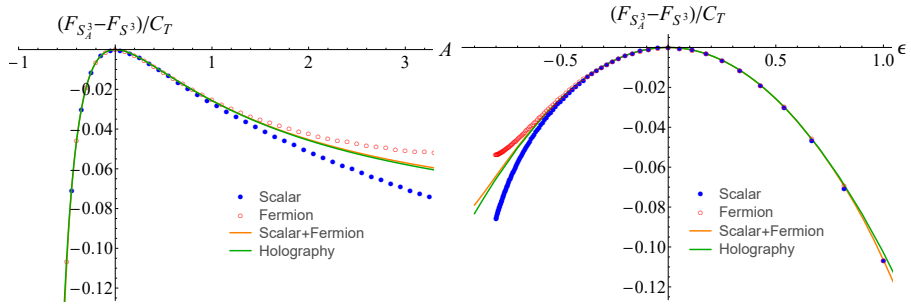

(a) In function of A **(b)** In function of ϵ

Figure 4.2: The normalised free energy $(F_{S^3_A} - F_{S^3})/C_{\mathrm{T}}$ as a function of the squashing parameter A and ϵ for holographic theories dual to Einstein gravity (green solid line), a free scalar (blue dots), a free fermion (red dots) and the combination of both (orange solid line). On the right figure, the holographic curve is the parabola in (4.41).

Some further comments are in order. The quadratic holographic result in (4.41) is a very good approximation for the free boson and fermion in the range $\epsilon \in (-0.5, 0.5)$. This is better than the expected resemblance controlled by the leading order quadratic result. To quantify this better, we can study the

subleading cubic correction to $F_{S^3_A}$

$$\frac{F_{S^3_A} - F_{S^3}}{C_{\mathrm{T}}} = -\frac{\pi^2}{96}\epsilon^2 + q\epsilon^3 + \mathcal{O}\left(\epsilon^4\right) , \tag{4.42}$$

where $q \equiv \frac{F'''(0)}{6C_{\mathrm{T}}}$, as can be seen from (4.13). For the free scalar and free fermion, we can find the coefficient q from our numerical results. A conservative estimate leads to $|q| < 10^{-3}$. Clearly, we have $q = 0$ for theories with holographic duals. This suggests that the cubic correction in (4.42) is either vanishing or has a very small coefficient for general CFTs. Notice that it seems hard to calculate the number q for general CFTs, since this coefficient is determined by the integral in equation (4.17). The various correlation functions (in particular the two-point function terms) appearing in the integrand of (4.17) are theory-specific and, in general, non-vanishing. Thus, the only way to have $q = 0$ is to either have a miraculous cancellation between the five terms in (4.17), or to obtain a zero value of the integrand due to the contractions with the very special form of the perturbation $h^{\mu\nu}$ in (4.27). It would be very interesting to establish whether q vanishes for general theories, or is simply some small non-zero number.

Another notable feature of the numerical results in Figure 4.2 is that the free fermion and free boson curves serve as an "envelope" for the holographic result and the combination of both free fields. In fact, one can check that for a free CFT consisting of any number of free bosons, N_b, and fermions, N_f, the normalised squashed sphere free energy lies between the red and the blue curves in Figure 4.2. We are not able to provide a rigorous explanation of this curious fact, but it is natural to offer some speculations. The higher-order terms in the expansion of $F_{S^3_A}$ around $A = 0$ (or equivalently $\epsilon = 0$) are controlled by some combination of integrated n-point functions of the energy-momentum tensor. Could it be that the free boson and fermion provide an upper and lower bound for such integrated correlators? A hint that this might be true is provided by the three-point function of the energy-momentum tensor.[9] This correlator in general dimension d has three independent tensor structures and is entirely fixed by three independent constants, one of which is C_{T} and the other two are often dubbed t_2 and t_4. For kinematical reasons, in $d = 3$ one finds that $t_2 = 0$. The constant t_4 is bounded above by the value for the free boson, $t_4^{\mathrm{sc}} = 4$, and bounded below by the free fermion value, $t_4^{\mathrm{f}} = -4$, see [82, 94, 95, 84].[10] For CFTs with Einstein holographic duals, one finds $t_4 = 0$ [95, 84]. Of course, the three-point function coefficients C_{T} and t_4 should not determine the full behaviour of the function $F_{S^3_A}$, since higher point functions of $T_{\mu\nu}$ are not simply determined by constants, but are complicated (and in general not known) functions of the conformal invariant cross ratios. Nevertheless, it

[9] See appendix C for a review on the form of such three-point functions.

[10] Notice that the extensive quantities are C_{T} and $C_{\mathrm{T}}t_4$ (as well as $C_{\mathrm{T}}t_2$ when $d \geq 4$).

is tempting to speculate that the free boson and fermion curves in Figure 4.2 provide some analogue of the Hofman-Maldacena bounds [95, 84], which would be valid for odd-dimensional CFTs with a broken conformal invariance induced by the squashing deformation controlled by A.

4.3 Discussion and outlook

Let us end this chapter by discussing a remarkable resemblance between the behaviour of the free energy on the squashed sphere and the entanglement entropy of three-dimensional CFTs from corner regions. The fact that C_{T} provides the "right" normalisation for the free energy — in the sense that the leading contribution is universally controlled by this quantity, and that curves corresponding to very different (presumably general) theories collapse to remarkably close curves — is reminiscent of the behaviour found in [96, 97] for the dependence of the universal contribution to the entanglement entropy of three-dimensional CFTs from corner regions. In both situations, C_{T} controls the leading (quadratic) correction to the most symmetric configuration (round sphere and absence of corner respectively), and in both, the curves corresponding to very different theories collapse to an almost-universal curve when normalised by this quantity. Let us make the connection to entanglement entropy results more precise.

On the one hand, as shown in [98, 99], the universal contribution to the entanglement entropy of a region bounded by a $(d-2)$-sphere is equivalent to the free energy of the corresponding theory on S^d for any odd-dimensional CFT, namely

$$s_{\mathrm{EE}}(S^{d-2}) = -F_{S^d}\,, \quad \text{for odd } d\,. \tag{4.43}$$

On the other hand, a lot of effort has been invested recently in understanding how the entanglement entropy of planar or spherical entangling regions changes under small geometric deformations — see for example [100, 101, 102, 103, 104, 96, 97, 105, 106, 107] and references therein. The result of main interest for us (proven in full generality in [107]) states that, given a general CFT in arbitrary (odd or even) dimensions, if we consider a deformed planar or spherical entangling surface, the leading correction to the entanglement entropy universal term is quadratic in the deformation (schematically)

$$s_{\mathrm{EE}} = s^{(0)}_{\mathrm{EE}} + \frac{\epsilon^2}{2}\, s^{(2)}_{\mathrm{EE}} + \mathcal{O}(\epsilon^3)\,, \tag{4.44}$$

and proportional to the central charge, C_{T}, controlling the stress-tensor two-point function, i.e.

$$s^{(2)}_{\mathrm{EE}} \propto C_{\mathrm{T}}\,, \tag{4.45}$$

where the proportionality constant depends on the explicit details of the geometric deformation.

The similarity between (4.44), (4.45) and (4.13), (4.24) is manifest, and particularly striking in the case of a deformed spherical entangling surface S^{d-2} and a deformed spherical background S^d, in which case (4.43) implies that the leading contributions in (4.13) and (4.44) exactly coincide. Note, however, that the identity (4.43) is in principle only valid for round spheres S^{d-2} and S^d. The fact that the leading correction to the free energy, under geometric perturbations, in odd-dimensional spheres is also controlled by C_{T}, suggests that the relation (4.43) might somehow be extended to a relation between the free energy of CFTs in deformed spheres S^d, and the entanglement entropy of deformed S^{d-2} entangling surfaces. This looks like an intriguing possibility worth further study. Note that a d-dimensional sphere can be deformed in more ways than a $(d-2)$-dimensional one, which means that any putative relation generalizing (4.43) along this lines should no longer be a bijection.

That being said, we would like to notice that the analysis presented above could be repeated for the double squashed spheres from Section 3.4. Following an argument completely analogous to the one in Section 4.1, we can find that the round sphere free energy is a local extremum of the function $F(A,B)$, i.e. $\partial_A F|_{A=B=0} = \partial_B F|_{A=B=0} = 0$. The numerical results in Figure 3.13 are in harmony with this general statement to a very good accuracy. In addition to that, we can extract the following leading order behaviour of the free energy for small values of A and B. The numerical results are in a very good agreement with the following formula (we use $C_{\mathrm{T}} = 3/2$ for the free scalar)

$$F_{S^3}(A,B) = F_{S^3}(0,0) - \frac{\pi^2 C_{\mathrm{T}}}{96}(A^2 + B^2 - AB) + \mathcal{O}\left(A^3, B^3\right) . \tag{4.46}$$

Clearly this is very similar to the result in (4.31) and it is natural to conjecture that (4.46) is valid for general CFTs. This conjecture is also supported by the holographic results from Section 3.2. These numerical holographic results are again in good agreement with (4.46). Finally, we would like to emphasise that if (4.46) holds for general CFTs, it implies that, for unitary theories, the round sphere free energy is a local maximum of $F(A,B)$ in the space of squashing deformations.

Another generalisation would be to extend the entire analysis to higher dimensions. In [67] we found that for general CFTs on a squashed sphere the free energy is a local minimum of the deformation, in accordance to the F-theorem in higher dimensions[80]. This was illustrated by calculating the free energy of the free scalar on the squashed sphere and the higher dimensional extension of the Taub-NUT solutions with Gauss-Bonnet coupling.

Before we continue to the next chapter, let us mention some possible further avenues of research. For starters, it will be desirable to find an analytic method to compute the squashed sphere partition functions. The zeta-function approach employed in [76] might be a good line of attack. With this, it would be interesting to understand whether the speculations about a possible extension of the Hofman-Maldacena type bounds for CFTs on squashed sphere have any merit. Perhaps a more modest goal will be to find a way to compute analytically the third order correction to the free energy in the small ϵ expansion, $F'''(0)$, in (4.17). The numerical results for free theories in three dimensions suggest that this coefficient is a very small number and it is desirable to understand why this is the case. Finally, it would be very interesting to make the tantalizing connections with entanglement entropy for non-spherical regions more precise, and to understand if there is a generalised version of the relation (4.43) between partition functions and entanglement entropies in odd dimensions for deformed spheres.

CHAPTER 5

DS/CFT ON SQUASHED SPHERES AND ETERNAL INFLATION

In the previous chapters we have seen how to construct anisotropic AdS solutions and compared their action with the free energy obtained from the free $O(N)$ vector model. Even though the $O(N)$ model is dual to Vasiliev theory, we found a remarkable resemblance with Einstein gravity. This strengthens our believe that the $O(N)$ calculations can be used to teach us something about eternally inflating Einstein universes, when we only consider geometric and scalar deformations. Using the NBWF, the Euclidean AdS solutions can, on the semiclassical level, be related to cosmological dS universes. This relation, together with the correspondence between AdS and field theories, allows to gather information about cosmology from the inverse of the partition function of the field theory dual to AdS. The explicit translation of these dualities to our results on squashed spheres gives an explicit example of how the holographic NBWF proposal works.

In the context of dS/CFT the squashed spheres enter as the future boundary of homogeneous but anisotropic deformations of de Sitter space. Through dS/CFT the partition function of the free $O(N)$ model as a function of A and B provides a toy model calculation of the NBWF in a minisuperspace model consisting of this set of anistropic cosmologies. The $O(N)$ model has been studied before in what corresponds in the bulk to a number of minisuperspace models, e.g. perturbations of homogeneous, isotropic minisuperspace [41], perturbations of this preserving $SO(3)$ invariance[42], and models with a round $S^1 \times S^2$ future boundary [108].

The ultimate purpose of calculating partition functions on double squashed sphere geometries, is for us their application to the theory of eternal inflation. In the introduction we reviewed that the top-down approach to the NBWF prefers universes with a regime of eternal inflation, in which the dynamics are governed by quantum fluctuations and their backreaction on the background rather than the classical slow roll of the background field. Therefore, the assumption of classical background evolution breaks down in this regime, making it extremely difficult to learn something about the global structure of the universe. With the holographic no-boundary proposal we can capture this regime where the dynamics are governed by quantum fluctuations holographically, if one has full knowledge of the dual partition function. In this way, the partition function on the squashed sphere from the previous chapter seems a good starting point to model an eternally inflating universe. Just as one predicts from a universe dominated by eternal inflation, it has regions of both positive and negative curvature. We will therefore be able to answer the following question: "*Can we get a handle on eternal inflation with the holographic no-boundary wave function?*".

We start by considering the solutions that do not have a scalar field for which it is relatively easy to find how the AdS and dS solutions are related to each other. This will be the topic in Section 5.1. In Section 5.2 we will see if the solutions that we constructed in the previous chapter, can be used for cosmological purposes. In the same section, we will discuss the relevant classical solutions together with their classical histories and probabilities. The field theories that we will use, will be studied in Section 5.3. Finally, we relate our results to the physics of eternal inflation in Section 5.4.

This chapter is based on work with N. Bobev, G. Conti and T. Hertog published in [52] and [53].

5.1 Warming-up: dS/CFT without scalar deformations

In Section 1.2.2 we reviewed how the NBWF saddle points have two different representations, depending on the path in the complex τ-plane along which the equations of motion get integrated. The two possibilities are summarised in Figure 1.4. The usual dS representation is the contour that first runs along the real axis to the turning point $x_{\rm TP}$ and then follows the Lorentzian line until it reaches the endpoint υ. Along this last part the solutions behave like real, asymptotically dS solutions. The AdS representation runs vertically to the turning point $x_{\rm A} = x_{\rm TP} - \pi/2$ from where it follows the imaginary axis; along

this part the solutions behave as a Euclidean AdS domain wall with complex scalar field profile. After this part the contour goes horizontally to the endpoint υ.

The probabilities of the NBWF histories can be found by considering the regularised action of the interior AdS regime of the saddle point using the relation from Section 1.2.2:

$$I_{\rm E} = -I^{\rm reg}_{\rm aAdS} + iS_{\rm ct} \ , \tag{5.1}$$

where $S_{\rm ct}$ is the usual counterterm and $I^{\rm reg}_{\rm aAdS}$ the regularised AdS action. Using the AdS/CFT correspondence, the holographic form of the NBWF on a semiclassical level is

$$\Psi[h_{ij},\chi] = \frac{\exp iS_{\rm ct}[h_{ij},\chi]}{Z_{\rm QFT}[\bar{\gamma}_{ij},\bar{\alpha}]} \ . \tag{5.2}$$

One could conjecture that this holds beyond the semiclassical level, giving an explicit dS/CFT realization, or one could postulate that (5.2) defines a wave function of the universe, specified by the QFT partition function, that on the semiclassical level reduces to the NBWF. In both cases, this shows that dS/CFT relates the argument of the wave function of the universe to external sources in the dual partition function that turn on deformations of the CFT. The dependence of the partition function on the values of these sources, which include the background geometry, yields a holographic measure on the space of asymptotically locally de Sitter universes.

The classical solutions of empty dS space have as turning point $x_{\rm TP} = \pi/2$, which means that the related Euclidean AdS solutions have to follow the contour $\tau = it$. Along this contour the equations of motion reduce to those used in the previous chapter. Therefore, the probabilities for empty dS universes with as a boundary on future infinity a squashed sphere, can immediately be found by using the results of Chapter 3 together with (5.1). It is in this way that Figure 3.13, which shows the free energy of the $O(N)$ model, can be interpreted as the logarithm of the probability distribution $\mathcal{P}(A,B) \equiv |\Psi(A,B)|^2$ as a function of the two squashing parameters A and B. The distribution is normalisable and has a global maximum at the round sphere. The corresponding distribution in Einstein gravity computed via bulk methods follows from our results in Section 3.3.3 and is shown in Figure 3.8 for small values of the squashing parameters and in Figure 3.9 for the large squashings where the Bolt solutions dominate the probabilities. It is striking that both distributions exhibit a qualitatively similar behaviour across the entire configuration space. This is made more explicit in Figure 5.1 where we show and compare three slices of these distributions for

three different values of B, obtained from the AdS results utilising (5.1).[1] This also shows the distributions are significantly broader when B (or A) is small. On the other hand both distributions differ in specific features such as the NUT to Bolt transition at large positive values of the squashing parameters, which is evidently absent in the dual free theory.

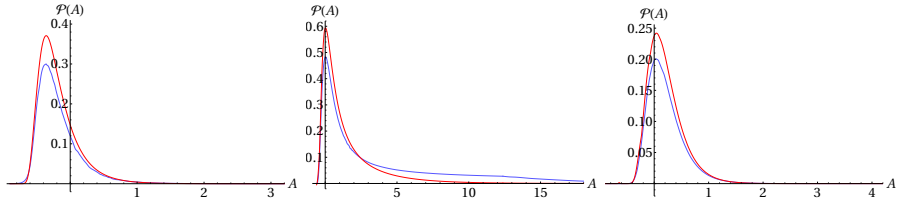

(a) $B = -0.4$ **(b)** $B = 0.05$ **(c)** $B = 1.15$

Figure 5.1: Three constant B slices of the Hartle-Hawking probability distribution $\mathcal{P}(A, B) \equiv |\Psi_{HH}(A, B)|^2$ over a two-parameter family of anisotropic deformations of de Sitter space labelled by the two squashing parameters A and B of the future boundary geometry, in Einstein gravity (blue) and in Vasiliev gravity (red). The distribution in Vasiliev gravity is computed invoking the duality with the free $O(N)$ model at large N. Both distributions exhibit a qualitatively similar behaviour across the entire minisuperspace of boundary configurations and have a global maximum at $A = B = 0$ corresponding to dS space. The normalisation of the slices shown here is such that the integral of the probability distribution $\mathcal{P}(A, B)$ over the (A, B)-plane gives 1. For the CFT we chose $N = 10$. Notice that to obtain these distributions we put $\kappa^2 = 8\pi$ in the gravitational actions.

A particularly interesting region of superspace is the regime of boundary configurations for which the Ricci scalar is negative. The Ricci scalar of a double squashed three sphere of the form (3.1) is given by (3.3) in terms of A and B. If one of the squashings is zero, then $R < 0$ if the remaining squashing parameter is less than $-3/4$. As mentioned earlier, however, adding a second squashing leads to an additional $R < 0$ region associated with large positive values of both A and B. Figure 3.14 shows that along all curves in the (A, B)-plane where $R = 0$ the holographic wave function vanishes. This is expected since the Ricci scalar enters as a mass term in the dual theory. When $R \to 0$ one of the eigenvalues of the scalar Laplacian on the squashed S^3 goes to zero, see (3.41), and since the partition function is proportional to the product of all these eigenvalues it vanishes. This in turn leads to a diverging free energy, and hence the prediction that $\Psi \to 0$ when $R \to 0$. In Figure 5.2 we zoomed in on such a region where the free energy diverges for a specific slice of B. This

[1] To get more meaningful plots we rescaled the actions from Section 3.3 by putting $\kappa^2 = 8\pi$ instead of $\kappa^2 = 1$. In this way the distributions are more spread out so that the falloffs between the two theories can be compared more easily.

figure learns us two things. First, the dS distribution associated with the free energy does not stay zero after the first divergence, instead it starts oscillating, becoming zero whenever another eigenvalue becomes zero. While the zeros of the distribution function become more frequent, the distribution function between these points get exponentially small. The second thing we can see from Figure 5.2, is that the bulk theory also decreases exponentially and thus that the difference between the two theories is actually very similar. In the next section we will discuss how the addition of scalar deformations alters these results.

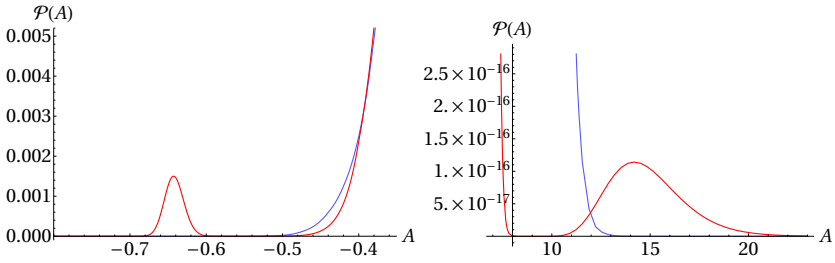

Figure 5.2: Two regimes of a constant $B = 1.15$ slice of the Hartle-Hawking probability distribution over anisotropic deformations of de Sitter space where the curvature of the boundary geometry is negative, in Einstein gravity (blue) and in Vasiliev gravity (red). On the left we zoomed in on the region $A \in [-0.8, -0.4]$ and on the right $A \in [8, 24]$. This second regime where $R(A, B) < 0$ gets introduced by a second squashing corresponding to large positive values of both squashing parameters. The overall amplitude of boundary geometries with a negative scalar curvature is exponentially small in this minisuperspace model. The normalisation, κ^2 and N are chosen to be the same as in Figure 5.1.

5.2 Universes with scalar excitations

5.2.1 Complex saddle points

In Section 1.2.2 it was explained how the de Sitter solutions predicted by the NBWF are related to Euclidean AdS domain-Wall solutions. When the scalar field has mass $m^2 = 2$, the relation between the asymptotic variables from the AdS and from the dS theory is given in the following way:

$$\bar{\gamma_{ij}} = \gamma_{ij} \ , \qquad \bar{\alpha} = -i\alpha \ , \qquad \bar{\beta} = -\beta \ . \tag{5.3}$$

These relations imply that the real Euclidean AdS solutions we considered in Chapter 3, give asymptotically complex scalar fields along the dS contour.

Because the NBWF is a function over real minisuperspace variables (h_{ij}, χ), these AdS solutions are insufficient for our cause.

Following (5.3), to get asymptotically real scalar fields, we need complex AdS solutions to match onto real dS solutions. If the initial scalar field is taken imaginary, the full AdS solution will have an imaginary scalar field profile. These are the solutions that, when going to the de Sitter representation, will give a scalar field that is real in the leading coefficient. This is the second set of saddle point solutions that was discussed in [44].

Changing the scalar field at the SP from real to imaginary also changes the effective potential along the AdS contour:

$$V_{\text{eff}}^{\text{AdS}}(\phi) = -2 - \cosh(\sqrt{2}\phi) \Rightarrow V_{\text{eff}}^{\text{AdS}}(-i\phi) = -2 - \cos(\sqrt{2}\phi) \ . \tag{5.4}$$

Following the connection between the AdS part of the contour and the endpoint, the imaginary ϕ tends again to real values, while the effective potential turns into minus the original AdS one. The fact that the potential behaves as a cosine along the AdS part of the contour has an immediate effect on the possible solutions. To see some of the consequences we refer to Figure 5.3, where in the left plot the original AdS potential is given as a function of real ϕ. It is clear that there is no limitation on the value of the initial value of ϕ; the field will always roll down its potential. In the middle panel we show how the potential looks like when ϕ is imaginary at the SP along the AdS part of the contour. One of the most striking features is that it has a maximum at $\phi_c = \sqrt{2}\pi/2 \approx 2.22$. If the initial value of ϕ is smaller than this value, the scalar field will roll down the potential to the minimum at zero scalar field. For larger values, ϕ will roll down to another vacuum state with non-zero scalar field. Continuing these last solutions to the de Sitter representation will give scalar fields with a non-zero imaginary component. In the right of Figure 5.3 we also show for completeness the effective potential along the dS part of the contour for a purely imaginary field at the SP.

To see more characteristics of this potential, we show in Figure 5.4 the slow roll parameters. In the left panel the first slow-roll parameter $\epsilon = \frac{1}{2}\left(\frac{V'(\phi)}{V(\phi)}\right)^2$ along the de Sitter contour (with positive potential) is plotted. Remarkably, the slow roll condition, $\epsilon \ll 1$, breaks down for large enough ϕ and we do not expect to find inflationary solutions. Using the relation between AdS and dS given by the NBWF, we could in this case determine the exact value of the maximal initial value of ϕ for which it was possible to find inflating de Sitter universes.

We also show the second slow-roll parameter $\eta = \frac{V''}{V}$ in the centre panel. This parameter is usually associated with the duration of inflation. If η is small, the scalar field rolls down the potential long enough, while if it is large, inflation can

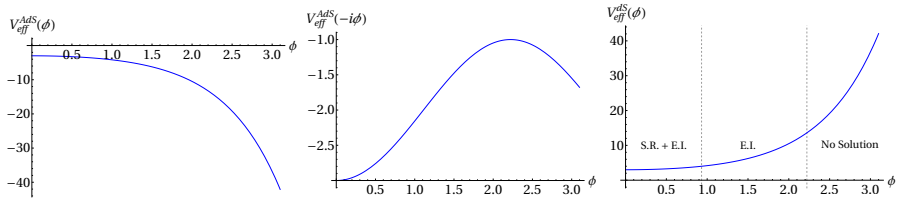

Figure 5.3: In the left panel we show the potential along the AdS contour with real scalar field profile. In the middle panel the potential is shown along the AdS contour with imaginary scalar field profile. The right panel shows the potential along the dS contour, we also distinguished three different regions of the potential: the first region is for small ϕ for which there is both slow roll inflation and eternal inflation, the second region for intermediate ϕ has eternal inflation, the third region with $\phi > \phi_c$ gives no classical solutions.

still happen, but it will not take long. Because η is only smaller than one for small values of ϕ, there is only a limited region of ϕ for which slow-roll inflation can occur.

Because we are ultimately interested in eternally inflating universes, it is interesting to test if the conditions for eternal inflation are satisfied. This can be checked by looking at the ratio ϵ/V, which has to be smaller than one to allow for eternal inflation. From the right panel of Figure 5.4 it is obvious that this condition is always satisfied. Thus for this specific potential, the NBWF will always predict regimes of eternal inflation that will transition directly to asymptotic Λ-dominated universes. A summary of the different regimes in this potential are shown in the right of Figure 5.3. We made the distinction between slow roll and non-slow roll solutions at $\eta = 1$.

We conclude that to get real Lorentzian de Sitter solutions we have to consider imaginary scalar fields along the AdS representation of the saddle points. In this way we will find solutions that have an initial scalar field between 0 and ϕ_c. These are the solutions we will use from now on, which will be discussed intensively in the rest of this section. Adding a squashing is not going to change the conclusions presented here.

5.2.2 Complex solutions

To find the relevant cosmological solutions, we follow the approach discussed in Section 1.1.2. That is, we start at the SP with a scalar field $\phi(0) = \phi_0 e^{i\theta}$, while the initial conditions for the l_is are given by either the NUT- or the Bolt conditions from Section 3.2 (see also Appendix B.1). We then follow a path

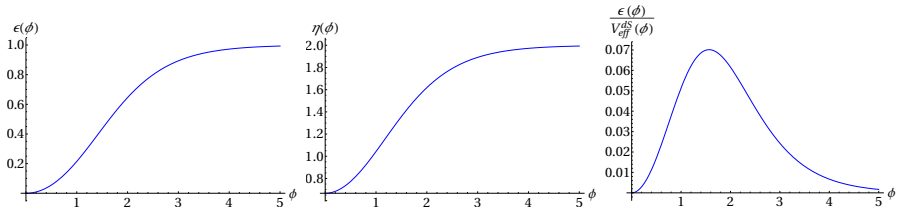

Figure 5.4: In the left panel the first slow roll parameter ϵ along the dS contour is shown. The middle panel shows the second slow roll parameter η along the dS contour and in the right panel ϵ/V is plotted, which gives the condition to have eternal inflation.

into the complex τ-plane that connects the SP to the endpoint υ, where the fields reach their real boundary values (h_{ij}, χ).

Normally, θ and x_{TP} have to be found numerically, but in this case things get simplified due to the potential that is being used. Namely, from the previous sections we know that the solutions along the AdS contour should be purely imaginary. From this we can deduce that θ should be $-\pi/2$.[2] Because the AdS solutions lie along the real vertical axis we can also deduce from Section 1.2.2 that the turning point of the de Sitter contour is at $x_{\text{TP}} = \pi/2$. As explained above, the range of valid, classical solutions only extends to $\phi_0 \approx 2.22$.

In Figure 5.5 an example is shown of a complex NUT solution with two squashings. Due to stability reasons, we chose to follow the AdS contour, i.e. a path that first goes vertically, along which the solutions behave like Euclidean AdS, then followed by the horizontal part that reaches x_{TP}, from where the path is continued vertically again until it reaches υ. Every change in direction is indicated with a grey dotted line. The complex solution shown has $\phi_0 = 0.5$, which is below the critical value ϕ_c and the scalar field rolls down the potential to its vacuum. The asymptotic variables are in this case $\alpha = 0.48$, $A = -0.65$, $B = 1.36$ and $\beta = -0.19i$.

One might worry that due to the limited range of ϕ_0, the values of the asymptotic parameters are also limited in the same way. This does not seem to be the case. Namely, while ϕ_0 approaches ϕ_c, α starts to diverge. This can be seen in Figure 5.6, where the squashings are fixed to $A = 5$ and $B = 0$ and α is plotted as a function of ϕ_0. The dotted black line indicates where ϕ_c is.

It is important to note that all the solutions will have purely imaginary β. This can be seen from the relation between the dS and AdS representation (5.3), from where it is clear that β only changes sign. Thus the imaginary scalar field

[2]The minus sign is there to ensure that the scalar field is positive along the de Sitter contour.

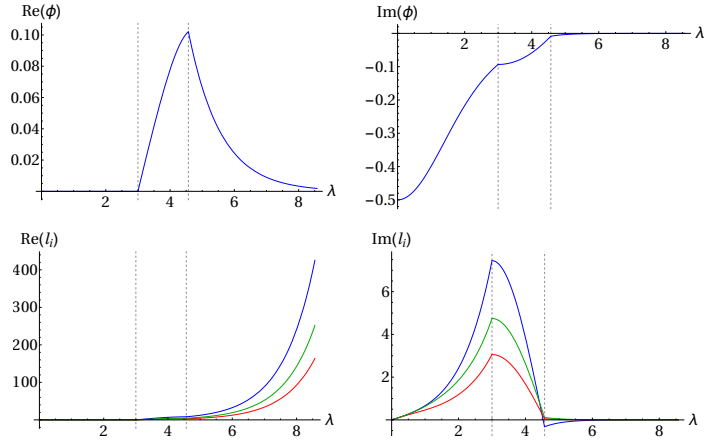

Figure 5.5: In the top the behaviour of the real (left) and imaginary (right) part of the scalar field is shown, while in the bottom the real and imaginary part of the scale factors is plotted. The different colours represent the different scale factors. This is for the NUT initial conditions: $\phi_0 = 1/2$, $\beta_4 = -2/12$ and $\gamma_4 = -22/120$.

along the AdS contour gives real α values, but imaginary values for β. This is a puzzling observation, because the classicality conditions advocated from the asymptotic perspective (2.37), tell us that classical solutions should have real β values! Can we conclude from this that our potential doesn't give access to real classical solutions? Not necessarily, as we discussed in Section 2.3.2, the classicality conditions are only approximate conditions, giving only a sufficient condition for classical evolution to hold. On the other hand, the large imaginary part of β could also signal the presence of large quantum effect. Because we saw that in this kind of potential the conditions for eternal inflation are always satisfied, these could very well be related to each other.

5.2.3 Classical Histories

The classical solutions give initial conditions for the classical histories predicted by the NBWF. In general, for the chosen potential we expect that the solutions are either going to have a singularity or a bounce. In Figure 5.7 two examples of such classical histories are shown that start with NUT initial conditions and evolve to a single squashed three-sphere at late times. In the top row the scale factors shrinks to zero in a finite time when $t \to 0$ and the scalar field diverges at the same moment. In the bottom all the scale factors start growing again

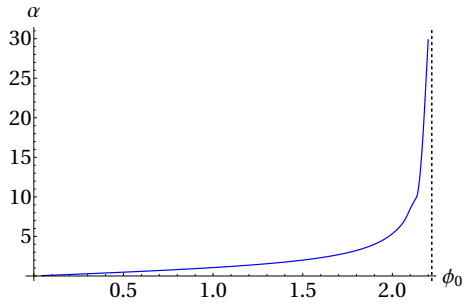

Figure 5.6: The behaviour of α as a function of ϕ_0 for $A = 5$ and $B = 0$. When ϕ_0 approaches ϕ_c, α starts to diverge.

after they reached a minimum value while the scalar field starts rolling down again.

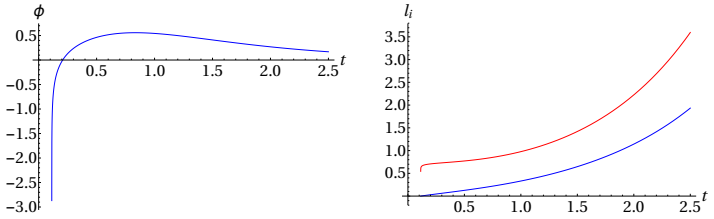

(a) Histories with a classical singularity, with $\phi_0 = 0.5$, $A = 2.3$ and $B = 0$.

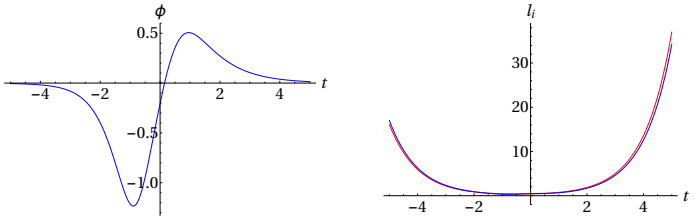

(b) Histories with a classical bounce, with $\phi_0 = 0.5$, $A = 0.16$ and $B = 0$.

Figure 5.7: Two examples of typical classical histories with NUT initial conditions.

An interesting question to study is how the anisotropies change the classical histories. Will the anisotropy drive the classical histories to a singularity or to a bounce? Because the Bolt solutions always have classical singular histories, we

only need to consider NUT solutions in this section. In the left panel of Figure 5.8 the behaviour of the classical histories is given for single squashed universes as a function of the squashing A and the deformation α. Blue indicates those histories for which all the scale factors bounce, while in red the classical histories are shown for which there is a singularity. On the right of that same figure we show for three different values of α inside which region in (A, B)-space the bounces are for two squashings. The smallest triangular shape corresponds to $\alpha = 3/8$, the middle one to $\alpha = 1/4$ and the biggest one to $\alpha = 0$. From the left panel of Figure 5.8 we can deduce that zero squashing has the biggest region of classical histories that bounce. Adding a squashing, decreases the area of bouncing histories, such that for $A < -0.26$ and $A > 1.94$ the only histories that are possible are the singular ones. Thus adding a squashing renders most of the histories unstable, resulting in more singular histories. The same effect can also be observed with two squashing, see the right panel of Figure 5.8. From this figure it is clear that the region in (A, B) space for which there is a bounce shrinks when the scalar field is increased. To really know if singular or bouncing histories are preferred, we have to look at the relative probability with which these occur. The no-boundary measure gives such a probability distribution, so let us discuss this next.

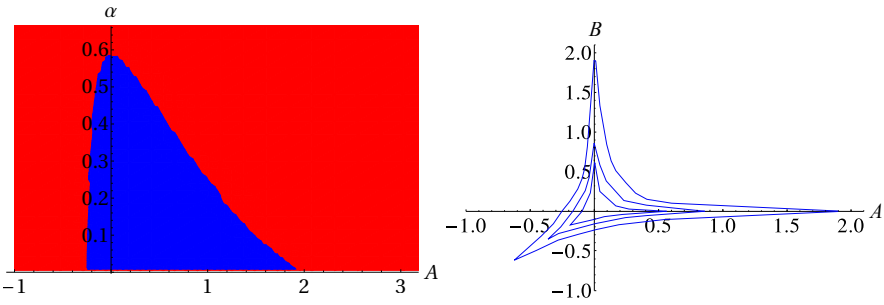

Figure 5.8: In the left panel we show what the behaviour is for classical histories with a single squashing: in red the histories are shown that evolve a singularity in a finite amount of time, in blue the histories that have a classical bounce. In the right panel the behaviour for solutions with a double squashing is depicted. The shapes mark for different values of α the regions inside which the histories have a bounce, outside these shapes they have a singularity. The biggest shape is for $\alpha = 0$, the middle one for $\alpha = 1/4$ and the smallest one for $\alpha = 3/8$.

5.2.4 Probabilities

For classical solutions the action tends to a constant at late times, which can be employed to calculate the probabilities for the classical solutions, given by

$e^{-2I_R(h,\chi)}$. To calculate these actions we can work in two ways. The first one, would be to calculate the AdS action and regularise it with the method described in Section 3.3, or we can calculate the action along the dS contour and take the real part of this. Either method will give the same result.

Because in the previous chapter we wanted to compare the gravitational actions with the free $O(N)$ partition function, we had to work with the alternate quantisation on the gravitational side. This meant that we had to add an extra term to evaluate the action. However, from a cosmological point of view it makes much more sense to keep on working in the original basis. Therefore, we will not have to add the extra term to the action. Instead we will add a deformation to the dual theory to account for the correct boundary conditions. This deformation will induce a flow from the free theory to the interacting one, which we will discuss in the next section. To keep the discussion manageable in this and the following section, we will restrict ourselves to one squashing parameter, i.e. $B = 0$.

In Figure 5.9 the probabilities are plotted first as a function of both the squashing and the deformation and beneath that, different slices of α are shown for the probabilities as a function of the squashing. Notice that we reintroduced the Bolt-like solutions. For large squashing these dominate the partition function, i.e. there is a Hawking-Page like phase transition very similar to the one described for the AdS solutions in Section 3.3. The point where this phase transition happens, more or less stays at the same value of α. From these figures it is clear that the maximum value of the probability distribution always occurs around $A = 0$ for every possible α, meaning that round universes are preferred no matter what the matter content is. This agrees with the three-dimensional plot from which we can learn that the absolute maximum sits at zero squashing and zero matter field.

It is also possible to combine the distribution of the classical histories with the probability distributions. This was done in Figure 5.10 where the probability for a bounce is calculated for a particular value of α for models with one squashing, i.e. marginalised over the values of A. The probability is weighted by the integral over the whole of (A, α)-space. In the no-scalar field case the probability to have a bouncing history is around 10%. As we increase α the probability decreases and reaches zero at the critical value of $\alpha \approx 0.59$ above which there are only singular histories.

Let us briefly summarise our gravitational results before we start our study of the dual field theory in the next section. We started this section by realising that the gravitational solutions constructed in the previous chapter, are not adequate to describe classical dS solutions. For this reason we constructed new solutions, which in the AdS representation correspond to taking an initial

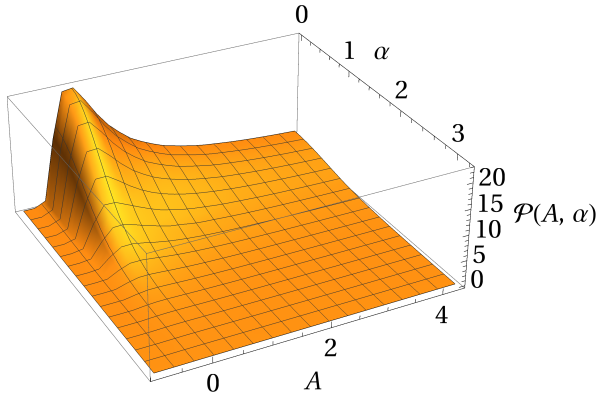

(a) The probability distribution as a function of the squashing A and α.

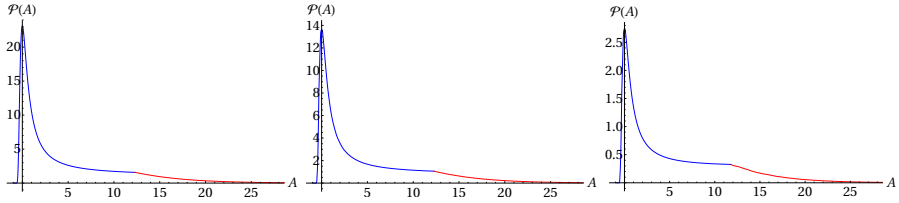

(b) $\mathcal{P}(A)$ for $\alpha = 0$ **(c)** $\mathcal{P}(A)$ for $\alpha = 0.71$ **(d)** $\mathcal{P}(A)$ for $\alpha = 1.51$

Figure 5.9: In the top plot the probabilities for models with one squashing and a scalar deformation are shown as a function of A and α. From this figure it is clear that $A = 0 = \alpha$ is a global maximum. The bottom row shows slicings of this plot for different values of α. The blue lines give the NUT solutions, while the dominant Bolt solution is given in red.

imaginary scalar field. Afterwards, we studied the classical histories related to these classical solution and learned that anisotropies drove the classical histories towards a singularity. By calculating the action, we finally got the probabilities predicted by the NBWF for anisotropic universes. These taught us that isotropic universes with small scalar fields are favoured.

5.3 Critical field theories on the squashed sphere

In this section we will study the dual field theory of the gravitational solutions presented above. Using the relations between the dS and AdS variables (5.3),

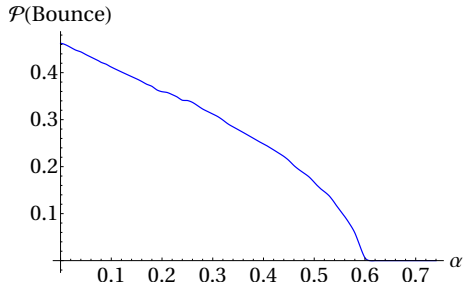

Figure 5.10: The probability to have a bouncing Lorentzian history for the single squashed solutions as a function of α integrated over A.

we can see that the holographic no-boundary conjecture states that for real α

$$|\Psi[\alpha]| = \frac{1}{Z_{\text{AdS}}[-i\alpha]} \ . \tag{5.5}$$

From the holographic principle we know that the deformation α is related to a dual source of dimension one, which means it is a relevant operator that induces a flow from its unstable UV fixed point where it is a free theory to a critical theory in the IR. This implies that the AdS solutions should be dual to the critical $O(N)$ model with a double trace deformation of dimension one.

The critical $O(N)$ model can be obtained from the free model by adding a double trace deformation $f(\phi\cdot\phi)^2/(2N)$ while we keep a source $\rho f\tilde{m}^2$ turned on for the single trace operator $\mathcal{O}\equiv(\phi\cdot\phi)$. Here ρ is a constant that we will fix below and f represents the coupling of the double trace deformation. To see what the relation is between the critical and free model, we start from the free $O(N)$ model partition function

$$Z_{\text{free}}[m^2] = \int \mathcal{D}\phi \mathrm{e}^{-I_{\text{free}}+\int \mathrm{d}^3x\sqrt{g}m^2\mathcal{O}(x)} \ , \tag{5.6}$$

where I_{free} is the action of the conformal, free $O(N)$ model, given by

$$I_{\text{free}} = \frac{1}{2}\int \mathrm{d}^3x\sqrt{g}\left[\partial_i\phi_a\partial^i\phi^a + \frac{1}{8}R\phi_a\phi^a\right] \ , \tag{5.7}$$

with ϕ_a the components of an N-component field transforming as a vector under $O(N)$ rotations. Now introduce $\tilde{m}^2$ as an auxiliary variable over which we have to integrate and which takes the value $\tilde{m}^2 = \frac{m^2}{\rho f} + \frac{\mathcal{O}}{\rho}$:

$$Z_{\text{free}}[m^2] = \int \mathcal{D}\phi\mathcal{D}\tilde{m}^2 \mathrm{e}^{-I_{\text{free}}+N\int \mathrm{d}^3x\sqrt{g}\left[\rho f\tilde{m}^2\mathcal{O}-\frac{f}{2}\mathcal{O}^2-\frac{1}{2f}(m^2-\rho f\tilde{m}^2)^2\right]} \ . \tag{5.8}$$

Notice that this expression makes sense, because integrating out $\tilde{m}^2$ gives back (5.6) and the correct expression in terms of m^2 and $\mathcal{O}$ given above. Rearranging some of the terms in (5.8) gives

$$Z_{\text{free}}[m^2] = \int \mathcal{D}\tilde{m}^2 \mathrm{e}^{-\frac{N}{2f}\int \mathrm{d}^3x\sqrt{g}(m^2-\rho f\tilde{m}^2)^2} Z_{\text{crit}}[\tilde{m}^2] \,, \tag{5.9}$$

with

$$Z_{\text{crit}}[\tilde{m}^2] = \int \mathcal{D}\phi \mathrm{e}^{-I_{\text{free}}+N\int \mathrm{d}^3x\sqrt{g}\left[\rho f\tilde{m}^2\mathcal{O}-\frac{f}{2}\mathcal{O}^2\right]} \,. \tag{5.10}$$

We can also invert (5.9) to find Z_{crit} as a function of Z_{free}

$$Z_{\text{crit}}[\tilde{m}^2] = \mathrm{e}^{\frac{Nf\rho^2}{2}\int \mathrm{d}^3x\sqrt{g}\tilde{m}^4} \int \mathcal{D}m^2 \mathrm{e}^{N\int \mathrm{d}^3x\sqrt{g}\left(\frac{m^4}{2f}-\rho\tilde{m}^2m^2\right)} Z_{\text{free}}[m^2] \,. \tag{5.11}$$

The value of ρ for the $O(N)$ model is given by $\rho = 1$[41], then the expression (5.11) agrees with the transformation from critical to free found in [42].[3] By taking $f \to \infty$ the theory flows to its critical fixed point. If this gets combined with the large N limit, it becomes possible to apply a saddle point approximation to find the critical partition function. In taking the large f limit it is clear that the first term outside the path integral is just a divergent term, which we cancel by adding the appropriate counter terms. The saddle point equation then becomes, for homogeneous deformations

$$\int \mathrm{d}^3x\sqrt{g}\left(\frac{m^2}{f}-\tilde{m}^2\right) = -\frac{\partial \log Z_{\text{free}}[m^2]}{\partial m^2} \,, \tag{5.12}$$

where the first term on the left vanishes for large f. This is the equation we have to solve for m^2 and insert back into (5.11). Notice that for the case we are considering, the deformation is imaginary (see (5.5)) and that we are thus actually solving the following equation:

$$\int \mathrm{d}^3x\sqrt{g}\left(\frac{m^2}{f}+i\tilde{m}^2\right) = -\frac{\partial \log Z_{\text{free}}[m^2]}{\partial m^2} \,, \tag{5.13}$$

where $\tilde{m}^2$ is understood to be real

The saddle point equation has infinitely many solutions for a fixed real value $\tilde{m}_0^2$. There is always one greater than $-R/8$ and the rest is smaller than this value. To make sure we include all the relevant solutions, we need to do a careful study of the m^2-plane to determine where the steepest descent contour for m^2 lies. For the single squashed sphere this was already discussed in detail

[3] The above calculation can be repeated for the $Sp(N)$ model by putting $\rho = -i$[41].

by the authors of [41], in which they found that the relevant steepest descent contour could always be deformed to pass the saddle point that lies to the right of the point where $m^2 = -R/8$. In [41] it was also found that for the $Sp(N)$ model the saddle point contour is ill-defined such that the non-perturbative (in N), critical $Sp(N)$ model does not exist.

To apply the above techniques to our model with one squashing, we first have to calculate Z_{Free} as a function of (complex) m^2 and then numerically invert (5.13) to find the behaviour of the complex deformation m^2 as a function of real $\tilde{m}^2$. The relation between these two deformations is shown in Figure 5.11, where the real and imaginary parts of m^2 are plotted as a function of $\tilde{m}^2$ for three different values of A. Notice that m^2 is restricted to be bigger than $-R/8$, as can be seen from the plot of the real part of m^2 where it is clear that for large $\tilde{m}^2$, m^2 approaches $-R/8$. From the left plot we see that the imaginary part of m^2 goes to zero whenever $\tilde{m}^2$ becomes large.

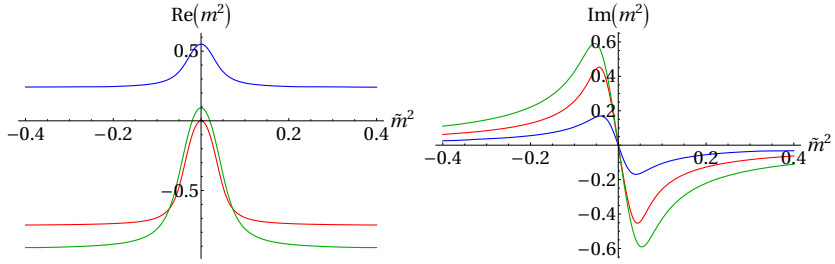

Figure 5.11: Here we show the real and imaginary solutions of the saddle point equation (5.12) for three different values of the squashing. In blue we show the solution for $A = -0.8$, in red $A = 0$ and in green $A = 2.06$. The real parts of m^2 asymptote for large $\tilde{m}^2$ to $-R/8$, which is for the blue curve given by 0.25, for the red curve by -0.75 and for the green curve by -0.92.

Inserting the numerical relation between m^2 and $\tilde{m}^2$ back into (5.11) gives the results we show in Figure 5.12, where in the upper figure the holographic probability distribution as a function of both the deformation and the squashing is plotted, while in the bottom row different slices of this distribution with constant $\tilde{m}^2$ are shown. We took $N = 5$ to let the tail of the zero deformation probability agree with the known dS-Taub Bolt action (with the normalisation $\kappa^2 = 8\pi$). From this figure it is clear that there is a global maximum around zero squashing and zero deformation. Although the top row of this figure suggests that $A = 0$ is always a maximum, the figures of the slices show otherwise. The maximum seems to shift to higher values of A for large values of $\tilde{m}^2$. This is a clear difference with the bulk side! So the partition function seems to prefer zero squashing and deformation, but when the deformation is turned on, zero

squashing is not a maximum any more!

Notice that these plots do not exhibit the feature of the free $O(N)$ model that the distribution functions go exactly to zero when the Ricci curvature disappears. This is of course because, when we did the transformation from free to critical model, the points behind the first divergence were not taken into account. This seems to suggest that the parameter space of the $O(N)$ model should be restricted to regions where $R/8 + m^2 > 0$.

Finally, let us comment on the difference in our approach and the usual one where the wave function is directly related to the partition function of the $Sp(N)$ model[41]. In the case of the free theories, the $O(N)$ and $Sp(N)$ model are related by an analytic continuation of N to $-N$. This means that the partition functions of these are inversely related and therefore the statement that the wave function is equal to the inverse of the AdS dual partition function and the statement that the wave function is equal to the $Sp(N)$ partition function are the same. However, in the strongly interacting limit there seems to be a manifest difference between the two. While it is possible to define a non-perturbative critical $O(N)$ model, the non-perturbative critical $Sp(N)$ model is ill-defined. Therefore our approach of equating the wave function to the inverse of the AdS dual theory and the one where the wave function equals the $Sp(N)$ partition function are not equal any more. Unless if the $Sp(N)$ model parameter space would somehow be restricted to regions that have a positive effective mass.

5.4 Eternal Inflation regulated by the holographic NBWF

In this chapter we computed the NBWF in a homogeneous, but anisotropic minisuperspace. We did this in two ways, in the first one we related the AdS solutions from Chapter 3 to dS, and in the second one, we used the holographic no-boundary proposal to give a holographic measure. The two squashing parameters specify a two parameter set of anisotropic deformations of dS space. The calculations were done in two steps, as a first step we only looked at solutions without scalar deformations. For these we found that the resulting probability distribution over cosmological histories is normalisable and globally peaked at isotropic dS space. Strong squashings lead to boundary geometries with negative scalar curvature which get zero probability from the holographic measure. In this minisuperspace model the overall amplitude of universes with a negative curvature future boundary is nevertheless exponentially small.

In the second step we explored how the addition of a scalar field affected

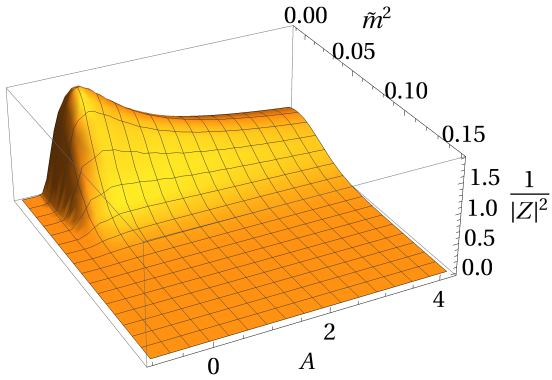

(a) $|Z|^{-2}$ as a function of both the deformation $\tilde{m}^2$ and the squashing A.

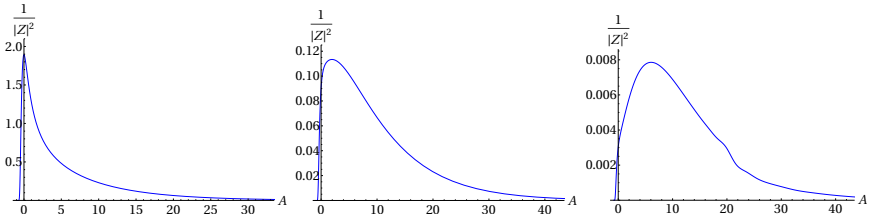

(b) $\tilde{m}^2 = 0.0$ **(c)** $\tilde{m}^2 = 0.05$ **(d)** $\tilde{m}^2 = 0.1$

Figure 5.12: In all these figures we show $|Z|^{-2}$ as a function of A for different values of $\tilde{m}^2$. In the top $|Z|^{-2}$ is a function of both $\tilde{m}^2$ and A and in the bottom row three different $\tilde{m}^2$-slices are shown. We took here $Sp(5)$.

these results. We saw that the gravitational solutions discussed in Chapter 3 are not the saddle points of the NBWF that give classical, cosmological relevant solutions. Instead, we had to work with the second set of saddle points discussed in [44], that were defined by their imaginary scalar field at the SP. With these solutions we observed that the classical histories for this anisotropic minisuperspace were driven to singular histories when anisotropies were present. The probability distributions obtained for these histories showed the same qualitative behaviour as the ones without a scalar field: the negative curvature regime is highly suppressed and there is a NUT to Bolt phase transition for large enough squashings. The global maximum for these distributions is at zero squashing and zero deformation, taking slices with fixed scalar field showed that for every deformation the round sphere is preferred.

Using the holographic no-boundary measure proposal, we found that the inverse of the critical $O(N)$ model with imaginary deformations should resemble dS

space. This is equal to the critical $Sp(N)$ model if we would use a steepest descent contour in the m^2 plane that would only take into account saddle points with $m^2 > -R/8$. This seems to suggest that the full theory should be restricted to where the conformal, effective mass is not tachyonic.

There are a lot of similarities when we compare the wave function calculated from a bulk perspective in Figure 5.9 and from the dual partition function in Figure 5.12. First of all, the distribution functions peak around zero squashing and zero scalar deformation. Secondly, the distributions both go exponentially to zero in the negative curvature regime, suppressing solutions with negative Ricci curvature. Although the global structure has the same properties, there are also some clear differences between the two theories. One of them is the fact that the gravitational theories have a NUT to Bolt phase transition which is not present in the dual field theories. This resembles the situation encountered in Chapter 3 when comparing AdS theories with the free $O(N)$ model. The final difference we want to highlight is that when taking slices of constant deformation the field theory predicts that the probability shifts towards higher values of the squashing, while this feature is absent in the bulk distribution function.

With this comparison in the back of our minds, it is time to finally answer the second question we posed in the introduction: "*What can we learn about eternal inflation using the holographic no-boundary proposal?*". We already saw that in the regime of eternal inflation the dynamics are governed by quantum fluctuations and their backreaction on the background. From Figure 5.4 we know that there will always be eternal inflation in our potential, which implies that when fluctuations get added the above analysis for the bulk should not hold, because the classical evolution of the background calculated above is not valid any more. However, using the holographic no-boundary measure as an alternate formulation of the wave function, it is possible to include these quantum dynamics when the partition function can be calculated non-perturbatively, opening the door to study global features of eternal inflation using the dual field theory.

In this chapter we focused on field theories living on a squashed sphere. This squashed sphere carries some resemblance with the global structure of eternally inflating universes: it is highly anisotropic and contains regions with positive and negative curvature. From this one could expect that the partition functions on the squashed spheres should have common properties with eternally inflating universes. Because we do not know how to calculate the field theory dual to Einstein gravity, we use the results of the $O(N)$ model. Due to the resemblance in the previous chapter between the Euclidean AdS results and the free $O(N)$ model, we expect that the global properties of this vector model carry over to the real dual of Einstein gravity.

In this way we can learn some interesting things about eternally inflating universes from the field theory results of the free $O(N)$ model in Figure 3.13 and the critical $O(N)$ model from Figure 5.12. The main conclusion that can be drawn from these figures is that the holographic measures are peaked around isotropic universes and that the distributions fall off exponentially for negative curvatures. This is not what is expected from eternal inflation, where due to the backreaction of the fluctuations on the geometry one expects a wave function that is very spread out with non-zero probabilities for negative curvature regimes. One could argue that this argument is very model dependent, but in Chapter 4 we showed that the free energy of any three-dimensional CFT partition function on a squashed sphere is always a local maxima as a function of the squashing, see (4.30). From this we can conclude that the holographic measure will always be peaked around isotropic universes. Adding a scalar deformation to the field theory alters these conclusions only slightly, slices of the distribution function with a specific scalar deformation do not peak any more around isotropic universes. However, when the relative values of this get compared with the rest of the distribution it is clear that scalar deformations themselves are not favoured by the holographic no-boundary measure.

Our calculations seem to suggest that the dynamics of eternal inflation do not dominate the global structure of the holographic NBWF, i.e. that the regime of eternal inflation somehow ends such that evolution happens semiclassically again, that is, a smooth exit from eternal inflation. It is not yet clear how the bulk calculations can be adjusted to fit this result.

We would like to stress that the double squashed sphere is just a toy model for the global structure of eternal inflation. It is impossible with this model to capture the entire global structure of eternally inflating universes. For this reason it would be interesting to extend the analysis in Chapter 4 to more general deformations to see if the free energy is in general a local maximum of the geometric deformation in three dimensions. With general proofs like this, we can also circumvent the fact that we were actually calculating the partition function of Vasiliev gravity. Another step in this direction has recently been taken by [109] where it was argued that the holographic amplitude is low for conformal surfaces far from the round conformal class.

As another extension of this work, it would be interesting to calculate the two- and three-point functions from the field theories. These will give us information about the cosmological perturbations during the period of eternal inflation, which could be measurable in the Cosmic Microwave Backgrounds, giving a real observational test for eternal inflation.

CHAPTER 6

QUANTUM TRANSITIONS THROUGH COSMOLOGICAL SINGULARITIES

In this last chapter we will take a step back from the holographic description of the NBWF and instead look at the evolution of the classical histories when we track them back in time before they reach classicality. Quantum mechanics learns us that it becomes possible to transition to another classical region. One could then ask how likely such transitions are, which leads us to the last unsolved question of this thesis: "*What are the probabilities to have a quantum-mechanical transition from one classical solution to another?*".

As we saw in the introductory chapter in Section 1.1.2, classical evolution emerges when the quantum probabilities, predicted by the NBWF, are high for histories that have correlations in time that correspond with the evolution of the classical equations of motion. However, cosmological evolution may not be predicted by the universe's quantum state for all times and in all regions of superspace. Classical behaviour is only expected in limited patches! This means in particular that classical evolution can break down without the breakdown of the classical equations of motion. An example of this is the evolution near the de Sitter like throat in the inflationary histories in the NBWF [17].

Histories of the universe do not simply end when they cease to behave classically. Rather classical evolution is replaced by quantum evolution. In this chapter we will use our minisuperspace methods, used in the previous chapters, to study what happens when classical cosmological evolution breaks down. That is, we

will search for saddle points that predict classical behaviour at late times, but when traced back in time, give transitions to other classically behaving solutions. In this way a classical history in a given patch gets connected with a classical history in another patch. This is schematically illustrated in Figure 6.1.

We will find that the instantons will again be complex, but like the case of the no-boundary instantons the real part of the action will define probabilities for each of these instantons to occur. A classical history typically branches into a continuous set of histories on the other side of the bounce, each with their specific probability.

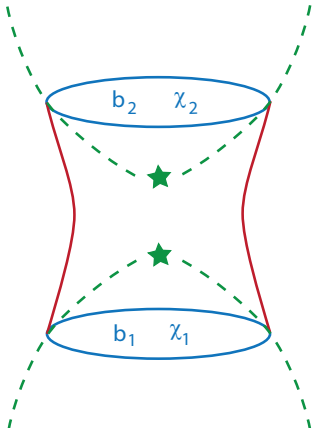

Figure 6.1: We will study quantum transitions (in red) between real, classical boundaries (in blue), here shown for the situation in which the classical evolution (in green) would lead to singularities.

We will apply our method to two qualitatively different cosmological scenarios that are of special interest: quantum transitions between inflationary histories on both ends, and transitions from ekpyrosis to inflation. The latter cosmological models have a classically slow contracting phase, leading to a curvature singularity in its future, while for inflationary models the curvature singularity lies in its past. The quantum transitions we find can thus be viewed as a resolution of the cosmological singularity in these models. This follows the idea that the appearance of singularities is not a breakdown of the quantum theory, but the breakdown of its classical extrapolation.

Transitions between inflationary histories may be argued to be somewhat academic in that the opposite side of the bounce is unlikely to lead to testable predictions on our side of the bounce. This is because the physical arrows of time point away from the bounce on both sides in all quantum states, which implies that perturbations are in their vacuum state near the bounce [110].

By contrast, transitions from ekpyrosis to inflation are central to the theory because the arrow of time does not reverse in ekpyrotic cosmology, where the detailed spectral properties of the perturbations on our side generally depend on the conditions before and at the bounce.

The outline of this chapter is as follows: we start in the following section by describing the general framework that we will work with, namely the semiclassical path integral for the quantum transitions in the minisuperspace approximation. Because our methods can be applied to any quantum state we will construct in Section 6.2 the general saddle points needed to describe transitions between two inflationary histories. Section 6.3 then shows how these transition saddle points can be embedded in the no-boundary quantum state. In Section 6.4 we find transitions between an ekpyrotic contracting phase and an inflationary expanding phase. We conclude with a discussion in Section 6.5 and provide further technical details in Appendix D.

This chapter is based on work with S. Bramberger, J. Lehners and T. Hertog published in [111].

6.1 Quantum transitions of the universe

We will consider in this chapter the simplest minisuperspace models in which the Lorentzian four-geometries are homogeneous, isotropic, and spatially closed, such as those already discussed in detail in Section 1.1.2. For the matter content we take a single homogeneous scalar field ϕ moving in a potential $V(\phi)$, but this time we set the cosmological constant to zero.[1]

The transition amplitudes that we are going to construct can be glued to any quantum state Ψ one prefers, for this reason we will keep the discussions in this and the next section very general. The solutions obtained from Ψ will depend on the specific state one chooses, but their semiclassical behaviour can be obtained in the same way as the we did for the NBWF. That is, by applying a steepest-descent approximation one finds that the quantum state can be approximated by its semiclassical (or WKB) form

$$\Psi(q^A) \approx A(q^A) \exp[iS(q^A)/\hbar] \,, \tag{6.1}$$

where we abbreviated the minisuperspace coordinates (b, χ) to q^A. This form predicts classical histories as long as S varies rapidly compared to A, that is if the classicality conditions (1.14) are satisfied. Similar to the NBWF, the

[1] Putting $\Lambda = 0$ made our numerical work more clear, but nothing prevents us from adding it again.

probability P of the history that passes through q^A is, to leading order in $\hbar$, given by

$$P(q^A) \propto |A(q^A)|^2. \tag{6.2}$$

As we said before, histories need not be all quantum or all classical. Instead the classicality conditions (1.14) may hold in some regions of configuration space but not in other regions. Histories (b, χ) do not end when the classicality conditions (1.14) break down. After all, histories are defined on the whole of the manifold $M = \mathbb{R} \times S^3$. Instead, when the classicality conditions fail deterministic classical evolution is replaced by quantum evolution. This allows for quantum transitions through the region of semiclassical breakdown that connect different parts of histories in the classical region of superspace [17]. Tunnelling through a barrier is a well known example of this.

In minisuperspace quantum cosmology, the quantum transition amplitude between two classical histories is specified by the propagator between an initial spatial hypersurface where $(b, \chi) = (b_1, \chi_1)$ and a final one with data (b_2, χ_2),

$$T(b_2, \chi_2 | b_1, \chi_1) \equiv \int_{(b_1,\chi_1)}^{(b_2,\chi_2)} \delta N \delta a \delta \phi \exp\left\{ i\mathcal{S}[a, \phi]/\hbar \right\}. \tag{6.3}$$

We show below that the transition probabilities derived from this stabilise as the boundary surfaces are moved further into the classical domain of the histories. Hence we obtain a transition matrix $T(b_2, \chi_2 | b_1, \chi_1)$ between classical histories, that in many ways is analogous to an S-matrix. The transition probabilities between specified classical histories are then proportional to

$$p_{\text{trans}}(b_2, \chi_2 | b_1, \chi_1) \propto |T(b_2, \chi_2 | b_1, \chi_1)|^2 . \tag{6.4}$$

Below we calculate this propagator (6.3) in the semiclassical approximation in two different cosmological models.

6.2 Quantum transitions: from inflation to inflation

In this section we consider a positive, quadratic scalar potential $V(\phi) = \frac{m^2\phi^2}{2}$ and evaluate the propagator (6.3) in its saddle point approximation to compute quantum transitions connecting classical, inflationary histories across a de Sitter like throat or a classical singularity. In Section 6.4 we will return to the propagator (6.3) in models with more general potentials that allow for transitions between ekpyrotic contraction to inflationary expansion.

We first consider the semiclassical approximation to the propagator (6.3) interpolating between two identical inflationary histories on both ends. This amounts to finding (complex) "bounce" solutions of the Euclidean equations of motion of gravity coupled to a scalar field given by (1.19).

The symmetry of the problem means it is natural to consider saddle points that are symmetric around the bounce.[2] This translates into the boundary condition that, at the point $\tau_{\rm s}$ of symmetry,

$$a'(\tau_{\rm s}) = 0 \ , \qquad \phi'(\tau_{\rm s}) = 0 \ , \tag{6.5}$$

where we are free to choose $\tau_{\rm s} = 0$. The complex value $\phi(\tau_{\rm s})$ of the scalar field at the surface of symmetry can be varied to obtain the required boundary values (b, χ) of the fields. The bounce value of the (complex) scale factor in turn is determined by the Hamiltonian constraint. Hence we have,

$$\phi(\tau_{\rm s}) = \phi_{\rm s} {\rm e}^{i\theta_{\rm s}} \ , \qquad a(\tau_{\rm s}) = \sqrt{\frac{3}{V(\phi(\tau_{\rm s}))}} \ . \tag{6.6}$$

These constitute a sufficient set of boundary conditions to determine saddle point solutions to the propagator path integral. The bounce solutions can be viewed as solutions in the complex τ-plane, with the bounce located at $\tau = \tau_{\rm s}$ and the boundaries where $(a, \phi) = (b, \chi)$ at some complex value $\pm\upsilon_{\rm s}$ with $\upsilon_{\rm s} = x_{\rm s} + it_{\rm s}$.

To find the saddle points, we will use the same technique for finding NBWF saddle points. That is, we will numerically tune the three free parameters $\phi_{\rm s}, \theta_{\rm s}$ and $x_{\rm s}$ such that the desired boundary values are reached. Figure 6.2 shows an example, for $m = \sqrt{2} \cdot 10^{-2}$. The top panels show the logarithm of the absolute value of ${\rm Im}(\phi)$ and ${\rm Im}(a)$ in the complex τ-plane for $\phi_{\rm s} = 10$ and $\theta_{\rm s} = -0.0637813$. Black lines correspond to large negative values of the logarithm, indicating where the fields become real. Loosely speaking, a classical history corresponds to having vertical black lines (vertical is the Lorentzian time direction) for a and ϕ at the same location in the complex τ-plane. It turns out that the scale factor has in general multiple lines parallel to the y-axis where its imaginary part becomes zero. This is because in a slowly changing potential, the solution for the scale factor is sinusoidal, see (D.5) in Appendix D.2. Then, by tuning the phase $\theta_{\rm s}$ one can ensure the lines of real a and real ϕ coincide. In fact, given there are multiple vertical lines where a is real for a given $\phi_{\rm s}$, one can find several symmetric bouncing saddle points connecting

[2] This saddle point selection principle can be justified in the no-boundary quantum state. We return to this point below in Section 6.3.

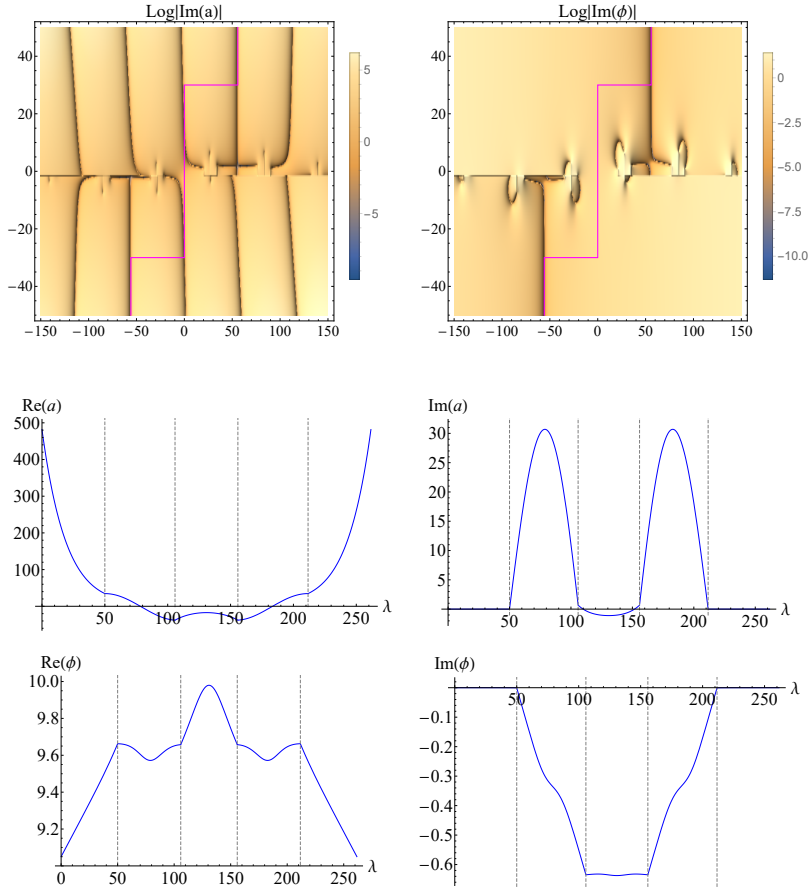

Figure 6.2: For $\phi_s = 10, \theta_s = -0.0637813$ we show on the left side $|\log(\mathrm{Im}(a))|$ and on the right $|\log(\mathrm{Im}(\phi))|$ in the complex τ-plane. These plots show where the scale factor and scalar field become real. The phase θ_s is fine-tuned such that the lines of real values of ϕ and a overlap on the first branch of a to the right of the origin. The contour we chose is drawn in magenta, and the lower panels show the evolution of the fields along this contour as a function of λ, which is related to τ by $\tau = \int N \mathrm{d}\lambda$. Here we took $\lambda = 0$ in the bottom left corner and evaluated the fields from this point to the upper right corner where $\lambda = 261.6$. For the present solution, we have $b_1 = b_2 = 500$, $\chi_1 = \chi_2 = 9.04196$ and at (b_2, χ_2) we have $\mathrm{d}b/\mathrm{d}\tau = -4.00006 \cdot 10^{-7} - 26.1886i$, $\mathrm{d}\chi/\mathrm{d}\tau = 2.18152 \cdot 10^{-8} + 0.0115247i$.

different classical solutions. In Figure 6.2 we have taken θ_s such that the scalar field becomes real on the first branch in the upper right quadrant.[3]

The action of the complex bouncing saddle points determines the quantum transition amplitude between the two classical histories at the endpoints. We have chosen to integrate the action along a contour that is not only symmetric, as required by the NBWF, but which also provides the dominant contribution to the quantum transition. In appendix D.1 we discuss our choice of contour in more detail. We also discuss approximate analytic solutions in appendix D.2.

The contour we selected is shown in Figure 6.2 in magenta in the upper panel. The evolution of the fields along this contour is shown in the lower panels of the figure. The fields indeed become real along the last vertical leg out to the end points, where the saddle points coincide with a classical history. The upper panel shows there are singularities in the complex τ-plane, especially along the real τ axis. Had we chosen a contour encircling one of these singularities, we would have obtained either a different solution on a different Riemann sheet or no solution at all.

Evidently the symmetric bounce solutions can equally well be obtained by integrating the equations of motion from one of the boundaries, instead of starting at the point of symmetry. This proves to be a more useful setup to find interpolating saddle points between different classical histories on both ends. Figure 6.3 shows an example of such an asymmetric bounce, connecting two inflationary histories with a different number of efolds. The contour we selected to compute this asymmetric transition is the one which smoothly changes into the original symmetric contour, without crossing any singularities, when the data on both boundaries are taken to be equal again.

At this point one may wonder whether the quantum transition probabilities (6.4) depend on the boundary value that is taken for the scale factor in the calculation of the propagator (6.3). Clearly this should not be the case as long as the classicality conditions hold on the boundary, since classical evolution preserves the real part of the Euclidean action.

It is therefore a useful consistency check of our method to verify whether the resulting transition probabilities stabilise if we take the boundary surfaces to larger scale factor, deeper into the classical domain of the histories. A first indication that this will indeed be the case for our solutions is provided in Figure 6.4 which shows, for the solution plotted in Figure 6.3, that the real part of the Euclidean action of the interpolating saddle point tends to a constant near both

[3] In the appendix D.1 we show that transitions between branches that are further away are subdominant in the path integral, therefore we will only consider transitions that can lead us from the first branch in the upper right quadrant to the first branch in the lower left quadrant.

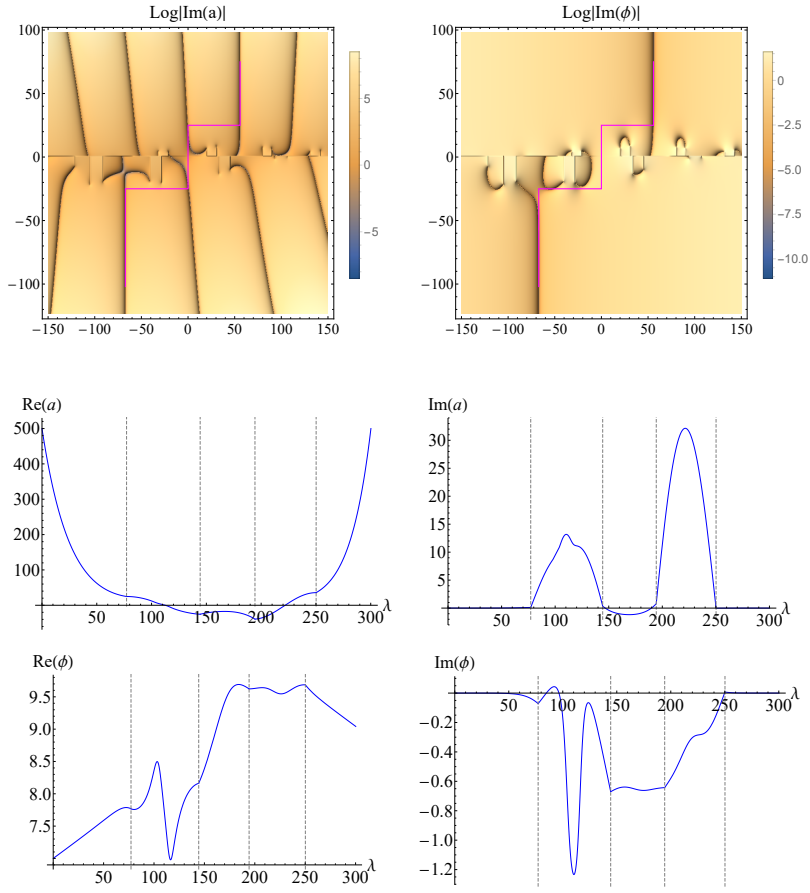

Figure 6.3: An example of an asymmetric bounce with $(b_1 = 500, \chi_1 = 7)$ and $(b_2 = 500, \chi_2 = 9.04196)$. In the upper panel we show the behaviour of the imaginary parts of the fields in the complex τ-plane, together with the contour we chose in magenta. In the lower panels we show the field values along this magenta path. This solution is obtained with the following derivatives imposed at the final boundary: $\mathrm{d}b/\mathrm{d}\tau = 6.93303 \cdot 10^{-6} - 26.1886i$, $\mathrm{d}\chi/\mathrm{d}\tau = -3.7805 \cdot 10^{-7} + 0.011527i$.

boundaries. A more precise assessment is given in Figure 6.5 where the WKB ratio $\nabla_A I_{\mathrm{T}}/\nabla_A S_{\mathrm{T}}$ is plotted as a function of b. We defined here I_{T} and S_{T} as respectively the real and imaginary part of the Euclidean action. The derivatives are estimated from taking finite differences, obtained by calculating successive interpolating instantons matching onto a classical history $(b(\lambda), \chi(\lambda))$, as well

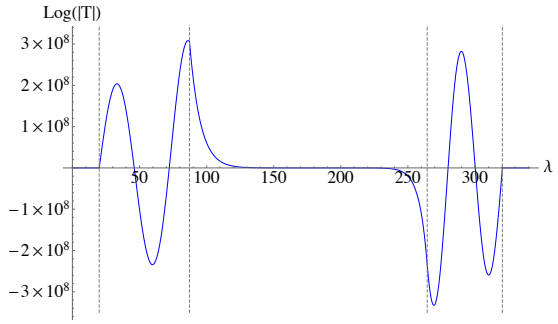

Figure 6.4: The real part of the interpolating saddle point action along the magenta contour shown in Figure 6.3. This tends to a small non-zero constant near the boundaries of the instanton, indicating that the quantum transition probabilities between given classical histories rapidly stabilise in the classical domain away from the bounce.

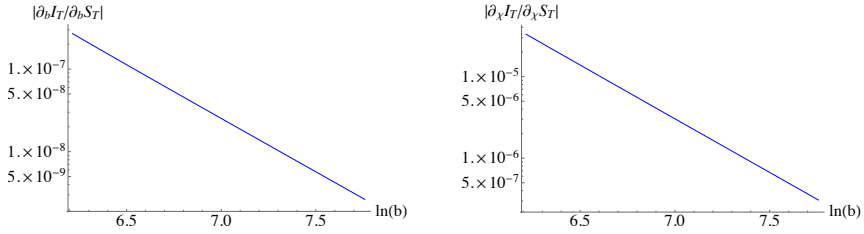

Figure 6.5: Classicality conditions derived from a saddle point describing a quantum bounce, assuming a classical incoming history, as a function of $\ln(b)$. The smallness of these ratios shows that the transition probability stabilises along the outgoing classical history.

as slightly displaced instantons $(b + \delta b, \chi)$ and $(b, \chi + \delta\chi)$. The fact that the WKB conditions are small means the real part of the action is conserved. Thus the transition probability is independent of the slice at which the interpolating instanton is matched onto a given classical history. This also means that to compute asymmetric transitions we can fix b to a convenient value, and let the boundary values of the scalar field vary.

Our results for the semiclassical quantum transitions between inflationary histories in a quadratic potential are summarised in Figures 6.6 and 6.7. Shown in Figure 6.6 are the real parts of the saddle point actions interpolating to different final values of $\chi_2 = 9.3, 7.8, 6.0, 5.0, 3.7, 2.0, 1.3$, as a function of the difference $\chi_2 - \chi_1$ with fixed $b = 500$ on both sides of the bounce. For large initial scalar field values χ_1 the most probable transition is the symmetric one. If we decrease χ_1 the instanton actions increase, giving a lower overall probability

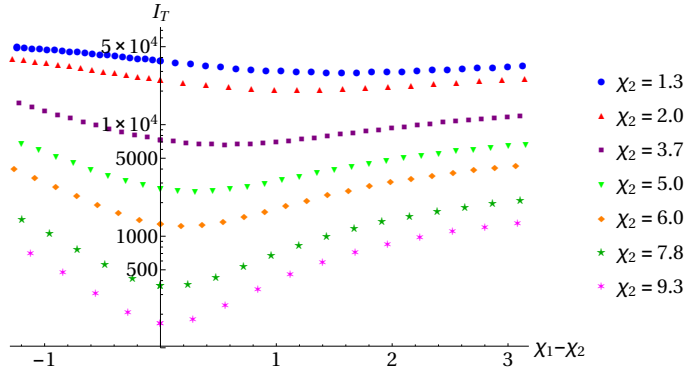

Figure 6.6: Logplot of the real part of the transition actions I_T as a function of the difference $\chi_1 - \chi_2$ for seven different initial values χ_2 shown in the legend. On both sides of the transition we fixed $b = 500$, well into the classical regime.

for a transition to occur. This behaviour is similar to that of probability distributions resulting from the tunnelling wave function in cosmology [20], which one might have expected since the transitions we compute are not unlike tunnelling events. This is illustrated in Fig 6.7 where we integrated over all initial values χ_1 to obtain the total probability to transition as a function of χ_2. Finally we note that the minima shift slightly towards larger values of $\chi_2 - \chi_1$, implying that transitions to universes with a slightly longer period of inflation are preferred.

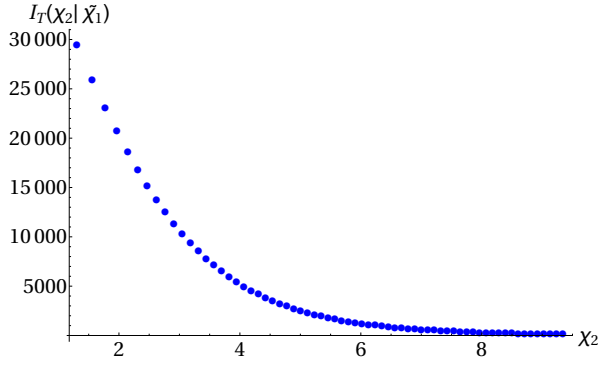

Figure 6.7: The real part of the transition action, as a function of χ_2, for the most probable history on the other side of the bounce. The values $\tilde{\chi}_1$ thus correspond for each χ_2 to the minimum of the curves in Figure 6.6. This shows that transitions are more likely for larger χ_2.

Transition probabilities of this kind can be used to compute probabilities for entire four-dimensional histories in any quantum state that predicts these classical inflationary patches. Let us now specify the quantum state to be the NBWF.

6.3 Bouncing inflationary histories

In this section we combine our results for quantum transitions between inflationary universes with the NBWF. This yields probabilities for an ensemble of complete inflationary histories exhibiting a quantum transition that connects two classical patches on either side.

6.3.1 Classical histories of the no-boundary State

Let us start by repeating some important aspects of the semiclassical approximation to the NBWF needed in this section. The action and equations of motion necessary to evaluate the saddle points are given by respectively (1.18) and (1.19), with the same quadratic potential without a cosmological constant as in the previous section. The NBWF predicts an ensemble of classical histories for saddle points that obey the classicality conditions (1.14), with relative probabilities determined by $\exp[-2I_{\rm R}(b,\chi)/\hbar]$ and (b,χ) the endvalues of the complex saddle point solutions. These classical histories are found by interpolating the Lorentzian equations of motion back in time with endvalues given by the classical solutions. The classical histories will be labelled by the absolute value of the scalar field of the classical solution at the SP, ϕ_0.

As we have seen in the introduction, if $V(\phi)$ is everywhere positive, then the classical NBWF ensemble has the remarkable property that all histories have an early period of scalar field driven inflation [16, 14]. For instance, in our case the solutions can take the approximate slow roll form already given by (1.23) in Chaper 1.

The number of efolds N is $N \sim \phi_0^2$. The right panel of Figure 6.8 shows two examples of classical histories in the NBWF ensemble for this minisuperspace model. For values $\phi_0 \gg \mathcal{O}(1)$ the classically extrapolated histories bounce at a minimum radius $b_{\rm m} \approx (m\phi_0)^{-1}$, never reaching a singularity [14]. By contrast for $3.1 \lesssim \phi_0 \lesssim 3.7$ the classical histories begin with a singularity at infinite scalar field and zero scale factor and expand forever. However, the classicality conditions (1.14) hold neither near the minimum radius nor near the singularity

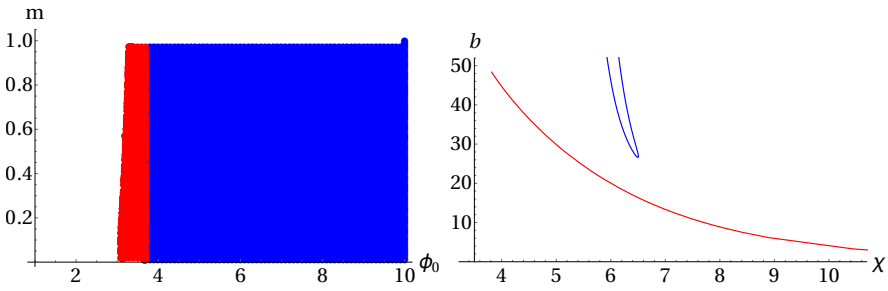

Figure 6.8: Left: The coloured regions are regions of parameter space (m, ϕ_0) that admit classical, inflating histories in the no-boundary state. The value ϕ_0 corresponds roughly to the initial value of the scalar at the start of inflation and m is the mass of the field. Histories in the region in red have an initial singularity when extrapolated classically backwards in time, whereas the classical histories in the blue region have a regular bounce in the past. Notice that there are no classical solutions when ϕ_0 is too small. Right: Two examples of classically extrapolated histories for $m = \frac{\sqrt{2}}{100}$; an initially singular history (red) and a bouncing history (blue).

[112, 14]. The classical extrapolation of the individual histories is thus not justified and must really be replaced by quantum evolution.

Where could quantum evolution lead to? At this point we must remember the NBWF is real. This means that for every saddle point of the form (1.9) there is a complex conjugate saddle point with S replaced by $-S$. Reversing the sign of S amounts to reversing the direction of time in the corresponding classical history [cf. (1.15)].[4]For every classical history in the first ensemble, therefore, its time reversed is in the second. The NBWF thus predicts two identical copies of a set of inflationary histories, with one set interpreted as expanding histories and the other set as contracting histories. Both sets are not connected classically in the no-boundary state, because the classicality conditions fail. But as we now show, we can use our results for the propagator (6.3) above to "connect" a classical history in one ensemble by a quantum transition to a classical history in the other ensemble to make a complete history of the universe.

6.3.2 Probabilities for bouncing no-boundary histories

Probabilities for entire histories of our universe that are in the classical NBWF ensemble in both asymptotic regions and that exhibit a quantum transition

[4]See [17] for a more extensive discussion of this point.

connecting both asymptotic regions take the form,

$$p(\phi_0'', \phi_0') = p_{\rm NB}(\phi_0'') p_{\rm trans}(\phi_0'', \phi_0') p_{\rm NB}(\phi_0'). \tag{6.7}$$

As before the labels ϕ_0' and ϕ_0'' refer to the absolute values of the scalar field at the SP of the saddle points that correspond to the classical histories on both ends, and $p_{\rm trans}(\phi_0'', \phi_0')$ is the transition probability between those histories.

This formula is symmetric under interchanging ϕ_0' and ϕ_0'', or, put differently, under interchanging expanding and contracting. The ensemble of bouncing histories in the NBWF is thus time symmetric by construction, respecting the quantum-mechanical symmetry of the wave function. The individual histories are not symmetric however, because the asymptotic behaviours of the expanding and contracting classical ends are different for different ϕ_0. But for every history in the ensemble the time-reversed is also in the ensemble, with equal probability.

The NBWF probability $p_{\rm NB}(\phi_0)$ of an asymptotically classical inflationary region labelled by ϕ_0, regardless of its past, is approximately given by

$$p_{\rm NB}(\phi_0) \propto \exp[-2I_{\rm R}(\phi_0)] \approx \exp[+3\pi/V(\phi_0)] \tag{6.8}$$

It is well known that the NBWF strongly favours histories with a low amount of slow roll inflation. This is illustrated on the left of Figure 6.9 for a quadratic scalar potential. This figure also shows that the classical domain of the steepest descents wave function is bounded below by a critical value of $\phi_0 \sim \mathcal{O}(1)$, because there are no regular saddle points associated with classical histories for smaller values of ϕ_0.

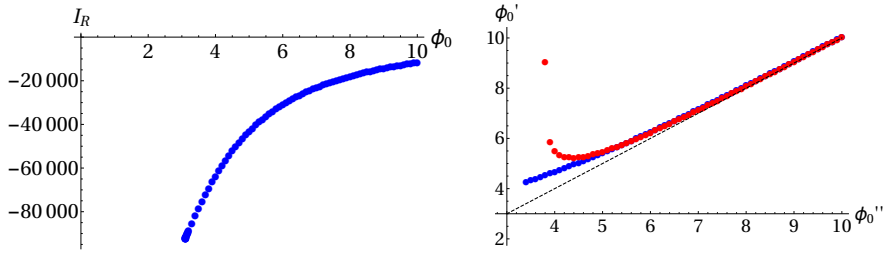

Figure 6.9: Left: The relative probabilities $p_{\rm NB}(\phi_0)$ of classical inflationary histories in the NBWF as a function of ϕ_0, for a quadratic potential with $m^2 = 2.10^{-4}$. Right: The most probable history (labelled by ϕ_0') on the other side of the quantum bounce as a function of the history on our side (labelled by ϕ_0'') is given in blue whereas the classical extrapolation of our side backwards in time is given in red. The classical extrapolation produces a classical bounce for large ϕ_0'' but becomes singular for small values of ϕ_0''.

Our results for the transition probabilities $p_{\rm trans}(\phi_0'', \phi_0')$ between two inflationary histories can be deduced from Figures 6.6 and 6.7, where we plotted $I_{\rm T} =$

$\frac{1}{2}\log p_{\rm trans}$. Applied to the classical NBWF ensemble this yields a quantum connection between both ensembles and in particular a small probability to bounce even in the low ϕ_0 regime of phase space where the classical extrapolation of the individual asymptotic histories backwards in time produces a singularity. We illustrate this in the right panel of Figure 6.9, where we compare the (ϕ_0'', ϕ_0') combinations for the most probable quantum transitions with the combinations resulting from a classical extrapolation through the bounce or into a singularity. For large scalar field values on the boundaries the classical and quantum evolution essentially agree. Both predict a symmetric, regular, approximately classical bounce. This is expected because the classicality conditions only fail in a very narrow regime around the bounce in this regime. By contrast, for low values of the initial scalar field the quantum evolution yields a small probability to bounce whereas the classical evolution produces a singularity.

From the two dimensional probability distribution (6.7) of bouncing histories with no-boundary conditions on both ends one can construct a marginal distribution by integrating over ϕ_0'. This yields a distribution over ϕ_0'' that can be viewed as a refinement of the past of the usual NBWF histories in which one conditions on there being a bounce in the past. This distribution is shown in Figure 6.10. The competition between the no-boundary weighting favouring low ϕ_0'' and the transition probabilities favouring high ϕ_0'' yields a most probable history at an intermediate value of ϕ_0''.

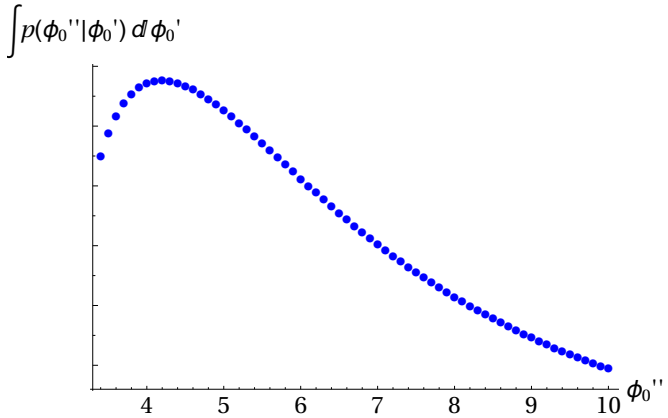

Figure 6.10: The probability distribution over asymptotically classical no-boundary histories labeled by ϕ_0'' that exhibit a quantum bounce, marginalised over the histories on the other side of the bounce labeled by ϕ_0'.

From the probabilities for entire histories (6.7) one can also construct various conditional probabilities. For instance, suppose by measurements of the

expansion we determine that we find ourselves in a late time classical history labelled by $\phi_0'' = \phi_0^*$. What is the probability, with initial and final no-boundary conditions, that this present history arose from a quantum transition from an earlier classical history ϕ_0'? This is given by the conditional probability

$$p(\phi_0'|\phi_0^*) \equiv p(\phi_0', \phi_0^*)/p(\phi_0^*) = p_{\rm trans}(\phi_0^*, \phi_0')p_{\rm NB}(\phi_0') \ . \tag{6.9}$$

We show this in Figure 6.11 for two values of ϕ_0^*.

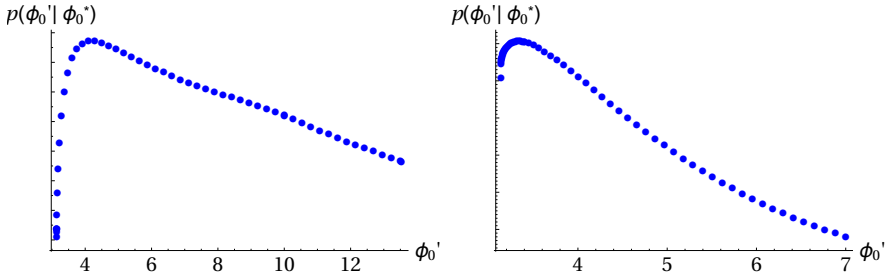

Figure 6.11: The conditional probability (6.9) that our present history labelled by ϕ_0^* arose from a quantum transition from an earlier classical history ϕ_0', for two different values of ϕ_0''. In the left panel $\phi_0^* = 10.0$ and in the right panel $\phi_0^* = 3.4$.

The past evolution on the opposite side of a bounce however, is unlikely to lead to testable predictions on our side of the bounce. This is because the physical arrows of time point away from the bounce on both sides, consistent with overall time symmetry [110]. To have an effect on our observations, signals from events on the far side would have to propagate backwards in the time direction defined by the thermodynamic arrow there and then through a quantum epoch. But the situation is radically different in ekpyrotic cosmology to which we turn next.

6.4 Quantum transitions: from ekpyrosis to inflation

The methods we have developed are not confined to the case of inflationary dynamics. In fact, the inflationary case is slightly special in that the transitions relate classical histories with opposite arrows of time. As a separate road to pursue, one may also consider big crunch singularities, and ask whether it is possible to tunnel out of them into an expanding universe, thereby avoiding the big crunch. The best understood example of a big crunch is that of an ekpyrotic phase, which is a phase of high-pressure contraction during which anisotropies

are suppressed [113, 114]. Thus, during such a phase the universe is driven towards a spatially flat crunch, and this justifies our minisuperspace approach.

We should note that various models for transitions from the contracting into an expanding phase have been investigated to date: in the original ekpyrotic model, the big crunch was modelled as the collision of higher-dimensional branes [113, 115]. At the classical level, the crunch was still singular (even though the singularity is much milder from a higher-dimensional point of view [116]), and thus the precise evolution across such a transition rests on assumptions of how to match a contracting with an expanding universe across a singular surface, see e.g. [117, 118]. To improve the calculational reliability, non-singular bouncing models were also constructed [119, 120, 121, 122]. Such models have the great advantage that one can calculate explicitly and unambiguously what happens to the background evolution and to cosmological perturbations (and it was found, for instance, that long-wavelength cosmological perturbations evolve across the bounce without being altered [123, 124]). However, all of the currently known models include hypothetical forms of matter, such as ghost condensates [125] or Galileons [126, 127], with unusual properties and no clear origin in fundamental physics.

Here we will be concerned with a more direct, and in fact more conservative approach: namely we want to see if one can transition out of an ekpyrotic contraction phase via a quantum transition.[5] As we will demonstrate, this is indeed possible, and in the particular example that we have studied, the ekpyrotic universe performs a quantum transition into an expanding inflationary phase. The reason for transitioning to inflation rather than, say, a kinetic dominated phase, is that the inflationary attractor guarantees a transition to another phase of classical evolution.

The model that we study again contains gravity coupled to a scalar field with a potential. We take the potential to be of the form

$$V(\phi) = V_0 \left(1 - \mathrm{e}^{-c\phi}\right) + 2\tanh(-\phi) \tag{6.10}$$

with the constants chosen to be $V_0 = c = 3$. The potential is shown in Figure 6.12. It contains a steep negative region for negative values of ϕ, separated by a barrier from a region where the potential is positive and flat for positive ϕ. This potential allows for two types of attractor solutions: inflationary slow-roll solutions at positive ϕ, and ekpyrotic contracting solutions at negative ϕ. Let us be slightly more specific about the ekpyrotic solutions: for $\phi \lesssim -1$, we can approximate $V(\phi) \approx -3\mathrm{e}^{-3\phi}$. Assuming a standard flat Robertson-Walker

[5] See e.g. [128, 6, 129, 130, 131] for some earlier work on the quantum resolution of cosmological singularities mostly in the context of the holographic approach to quantum gravity.

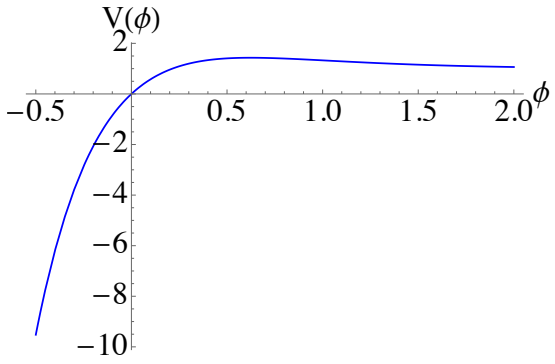

Figure 6.12: The potential $V(\phi) = 3\left(1 - \mathrm{e}^{-3\phi}\right) + 2\tanh(-\phi)$ that we are considering in this section. It allows for ekpyrotic contracting solutions on the left, and for inflationary expanding solutions to the right of the maximum. We wish to show that quantum transitions between these two types of solutions are possible.

metric this model allows for the scaling solutions [51]

$$a(t) = a_0(-t)^{1/\epsilon}\left(1 + \frac{\sqrt{2\epsilon}}{3}\,a_1\,(-t)^{1-3/\epsilon} - \frac{1-3\epsilon}{3(1-\epsilon)}\frac{1}{\sqrt{2\epsilon}}a_2\,(-t)^{2-2/\epsilon} + \dots\right), \tag{6.11a}$$

$$\phi(t) = \sqrt{\frac{2}{\epsilon}}\ln\left(-\sqrt{\frac{\epsilon^2 V_0}{\epsilon-3}}t\right) + a_1\,(-t)^{1-3/\epsilon} + a_2\,(-t)^{2-2/\epsilon} + \dots\,, \tag{6.11b}$$

with a_0 a constant and where we have included the leading correction terms. The parameters a_1, a_2 are fixed by initial conditions. Here $\epsilon = c^2/2 = 9/2$ is the fast-roll parameter, which by definition is always larger than 3 during an ekpyrotic phase. This expression clearly shows that the scaling solution is an attractor, as all correction terms die off in the approach to an eventual big crunch at $t = 0$. Note that the approximation of a spatially flat metric is justified since both the energy of expansion $H^2 \propto t^{-2} \propto a^{-2\epsilon} = a^{-9}$ and the energy density of the scalar field $\dot{\phi}^2 \propto a^{-9}$ grow much faster than the energy density in anisotropic fluctuations (which scales as a^{-6}) as the universe contracts.

The question now is whether, while classically headed for disaster, the big crunch can be avoided by a quantum transition to the other attractor solution, namely the inflationary one at positive scalar field values. Semiclassically, such a quantum transition can be described by a complex saddle point of the path integral, i.e. we will once again look for a complex solution of the equations of motion, this time interpolating between an ekpyrotic starting point and an

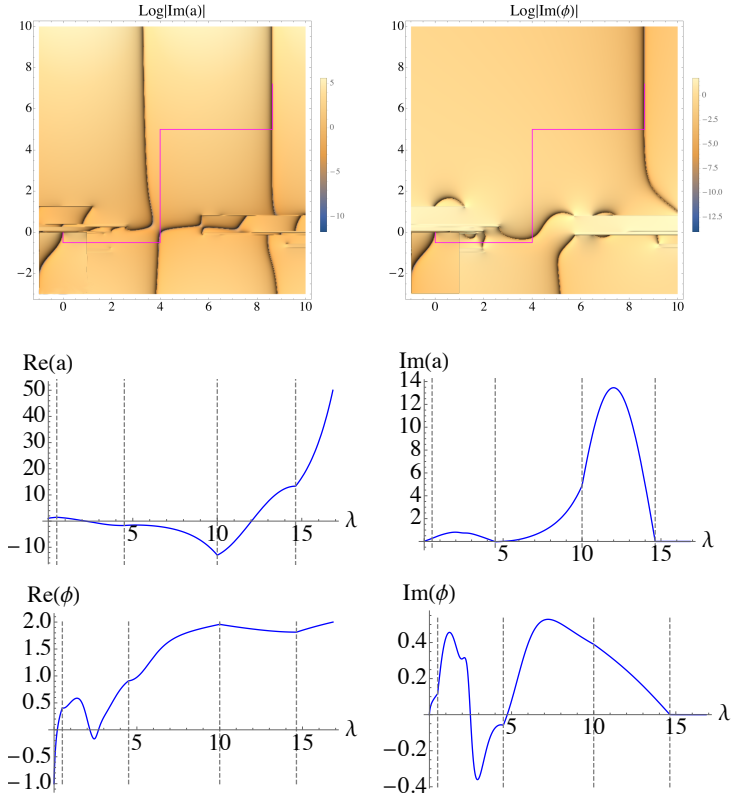

Figure 6.13: These plots show our solution interpolating between a contracting ekpyrotic phase and an expanding inflationary phase over a region of the complex time plane. In the upper panel we show the behaviour of the imaginary parts of the fields in the complex τ-plane, together with the contour we chose in magenta, while in the lower panels the behaviour of the fields along this contour is shown. For this particular solutions, we have $b_1 = 1$, $\chi_1 = -1$ and $b_2 = 50$, $\chi_2 = 2$. The solution corresponds to imposing $\mathrm{d}\chi_1/\mathrm{d}\tau = -1.40549 + 14.1652i$ and $\mathrm{d}b_1/\mathrm{d}\tau = -0.582476 + 5.69670i$. At small λ, the contour first runs down, and accordingly along this first segment the fields undergo a reverse ekpyrotic contraction. Along the middle segments, the evolution is fully complex, and along the final vertical segment a real inflationary expanding history has been reached. The upper graph necessarily only shows one sheet of the full solution function, while one can clearly distinguish several singular points and the associated branch cuts.

inflationary final point. Finding such a solution is complicated in this case by the presence of numerous singularities, which arise because along the ekpyrotic

part of the potential a singularity can be reached within a finite time. Because of these singularities, it is not obvious what the appropriate contour in the complex time plane ought to be, and some trial and error is inevitable. An example of an interpolating solution is shown in Figure 6.13, where in the upper panels the path in the complex plane is drawn with a magenta line and in the lower panels the evolution of the fields along this line is shown. The many singularities mentioned above are immediately apparent in the upper part of this figure, which shows only the relevant sheet of the solution function. Encircling the singularities in different ways typically leads to an entirely different solution, usually containing no region of classicality. This solution is a showcase example of the use of complex time paths in describing quantum tunnelling, as described in more detail in [132, 133].

As one can see from the figures, our solution indeed interpolates between an ekpyrotic and an inflationary history, with a fully complex evolution in between. It is very obvious that a classical inflationary solution is reached near the final boundary, since the scale factor and scalar field remain real in the Lorentzian direction for an extended period of time. On the ekpyrotic side, although at the starting point the fields are real, they rather quickly develop imaginary parts too. This is because the ekpyrotic contraction occurs over a very short time period, and thus appears compressed in the figure. In order to show unambiguously that we are indeed starting from a classical ekpyrotic contraction history, we have evaluated the WKB classicality conditions (1.14) on the ekpyrotic side, keeping the final field values on the inflationary end fixed (while allowing the field derivatives to vary). Corresponding plots are shown in Figure 6.14. As the figures show, the WKB conditions are better and better satisfied as the universe contracts towards a big crunch, which is just as expected for the ekpyrotic attractor [134, 135]. This result also implies that the probability for tunnelling out of an ekpyrotic phase is constant along a classical ekpyrotic contracting solution, analogously to the inflationary case treated in section 6.2.

The solution that we have just presented may be considered as a proof of principle that quantum transitions out of an ekpyrotic contracting phase and into an expanding inflationary phase are possible.

6.5 Discussion and outlook

The final chapter of this thesis was dedicated to the question: Is it possible to learn something about classical histories before these became classical? That is, can the classical cosmological singularity we observe, be resolved by quantum gravity effects? We indeed saw that, using a minisuperspace semiclassical

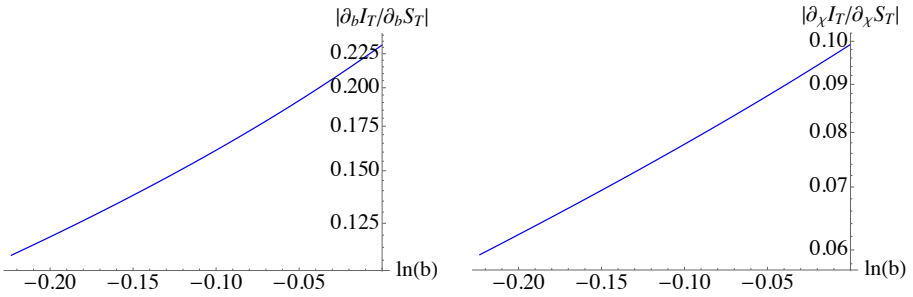

Figure 6.14: A graph of the WKB classicality conditions (1.14). These become small as the universe contracts, i.e. as b decreases, thus demonstrating that the approach to a big crunch is accurately described by a classical ekpyrotic phase.

approximation to quantum gravity, the classical bounce and singularity could be replaced by quantum bounces, complex instantons interpolating between contracting and expanding branches of cosmological histories. With these instantons it was possible to answer the last question we asked in the introduction: "*What are the probabilities to have a quantum-mechanical transition from one classical solution to another?*".

We have focussed on two cases of special interest where classical cosmological evolution often involves a singularity: transitions from inflation to inflation, and transitions from ekpyrosis to inflation. Let us summarise our findings.

The quantum bounces that we have found are mediated by complex saddle points of the action of gravity coupled to a scalar field, interpolating between specified real initial and final classical configurations. For the case of inflationary-to-inflationary transitions, the symmetry of the problem selects the appropriate contour of integration in the complex plane. This provides a clean starting point to identify more general instantons describing asymmetric transitions obtained by smoothly deforming away from the symmetric case. Interestingly, at large values of the inflaton potential, the most likely transition turns out to be the symmetric one, whereas at low values of the potential – the regime where the classical extrapolation produces a singularity – tunnelling to a slightly larger value of the potential is preferred.

Combined with the no-boundary wave function, which provides a measure on inflationary cosmology, our results for the quantum bounces yield probabilities for an ensemble of complete inflationary histories exhibiting a quantum transition that connects two classical inflationary patches on either side. The quantum transitions identified here allow one to refine and differentiate between different possible pasts of the inflationary histories in the NBWF, which are coarse

grained over in the usual treatment.

We have also analysed a potential that contains both ekpyrotic contracting and inflationary expanding solutions. In this case, we have demonstrated the existence of similar quantum transitions from the contracting phase into the expanding one, avoiding the big-crunch singularity that would follow the ekpyrotic contraction in a purely classical context. For the ekpyrotic-to-inflationary transitions we do not have any guidelines as to what the appropriate contour of integration should be, and thus we do not know yet whether the solutions that we have found are the dominant ones. An important question for future work is to clarify this question, perhaps by generalising the treatment of quantum-mechanical tunnelling described in [133] to include gravity. Another question is whether one can transition to other phases of classical evolution, such as a radiation or matter-dominated universe.

Our treatment of quantum transitions has close connections with two papers that recently appeared: in [136] the authors considered a radiation-dominated universe in a theory with a conformal coupling to gravity, which allows for technically very simple complex instantons characterised by $a \propto \eta$, where η denotes the conformal time. Such instantons avoid the big crunch at $\eta = 0$ by choosing a contour that passes around the singularity. Note that these solutions necessarily interpolate between negative and positive values of the scale factor, which appears to be a doubling of phase space in the models we considered in this paper. And in [137] the authors found approximate complex instantons interpolating between two phases of de Sitter expansion in the more restrictive context of gravity coupled to a cosmological constant.

An interesting direction for future research would be the investigation of the evolution of perturbations through the bounce. This could be useful to test the stability of quantum transitions studied here, and possibly to place ekpyrotic cosmology on firmer footing. On the other hand, the study of perturbations is necessary to find possible observational signatures of the pre-bounce era. With the addition of cosmological perturbations we come back to the problem of the possibility of eternal inflation and how this could be incorporated into our model.

Finally, we could also make the connection to holographic cosmology by posing one more question. Namely, how should we describe the transition between two classical solutions from a holographic point of view? Do we need to split up the Hilbert space of the CFT in two? Are these different disconnected pieces, or is there some entanglement between them? This discussion seems to resemble the one for wormholes in AdS [138].

CHAPTER 7

CONCLUDING REMARKS

7.1 Three not so easy questions answered

Mathematical models describing physical processes should consist of two parts, the local laws that govern the dynamics of the theory and boundary conditions that pick out one state from a set allowed by the local laws. In quantum cosmology there are multiple proposals for such boundary conditions. The proposal we focused on in this thesis is the one by Hartle and Hawking which is called the No-Boundary Wave Function. Although it is impossible to calculate this object completely, there are some interesting things that we can deduce from it. One of these is that it is possible to approximate the NBWF in a semiclassical method to get information about the predictions it makes about classical universes. But can we also go beyond these classical solutions and learn something about the quantum regime of the NBWF? As a guiding principle for exploring the physics beyond the classical level, we posed three questions in the introduction. Here we will summarise how these got answered in this thesis.

The first question involved the proposal for the holographic formulation of the NBWF and the question of how to get classical predictions from a holographic point of view, that is: "*Can we derive a sufficient set of conditions on the Euclidean boundary theory in dS/CFT for it to predict classical, Lorentzian bulk evolution at large spatial volumes?*". In Chapter 2 we set out to answer this question by constructing a new wave function in terms of relevant asymptotic variables. This we achieved by performing a canonical transformation of the usual bulk variables to their asymptotic variables. The new asymptotic wave

function allowed us to reformulate the dS/CFT proposal, from which it is immediately clear how to construct the holographic dictionary and find new asymptotic classicality conditions. These give an affirmative answer to the question posed above: if the vevs of the Euclidean boundary theory in dS/CFT obey the new asymptotic classicality condition, see (2.36) and (2.37), it predicts classical, Lorentzian bulk evolution.

For the next question we wanted to explore the dynamics of eternal inflation. The NBWF predicts that in this regime the wave function spreads out due to quantum fluctuations dominating the dynamics, meaning that with the usual methods we cannot get any information of the strucure of the universe. Luckily, with the holographic no-boundary conjecture it becomes possible to relate exact, calculable CFT partition functions with dS universes, including their quantum regime. Therefore, we could ask: "*What can we learn about eternal inflation using the holographic no-boundary proposal?*". To answer this we looked at the double squashed sphere as a toy model for the global structure of eternal inflation, possessing regions of highly negatively and positively curved space.

In Chapter 3 we began our study of these solutions by considering Euclidean bulk theories with a negative cosmological constant, both with and without a scalar field. These are generalisations of previously studied AdS Taub-NUT/Bolt solutions that have as boundary a single squashed sphere. New thermodynamical properties emerged with the addition of a scalar field: we saw that in the alternate quantisation some solutions became multivalued and that for large deformations the region of valid solutions shrinked. We compared these gravitational theories with the $O(N)$ model on the squashed sphere and for the case without scalar deformations found remarkable agreement with the gravitational results. The addition of scalar deformations makes comparison more difficult, because it is not clear how the deformations on both sides of the correspondence agree with each other.

Before we related our newly found AdS solutions to cosmological relevant solutions, using the NBWF, we remarked some interesting properties of field theory partition functions on a squashed sphere in Chapter 4. Namely, we proved that for odd-dimensional CFTs on a background deformed away from a conformal one, the free energy has an extremum in terms of the deformation parameter, where the second derivative of the free energy is controlled by the central charge, C_{T}. For three dimensions in particular, we proved that this extremum is a local maximum, if the geometrical deformation is related to the squashed three-sphere.

In Chapter 5 we then finally used the prescriptions given by the NBWF to turn the AdS/CFT results from Chapter 3 into cosmological relevant solutions. Without the scalar deformation it was possible to directly use the AdS results,

but with the addition of the scalar field the solutions did not obey the classicality conditions along the dS contour any more. Instead, we found that the correct cosmological relevant saddles were the ones with an initial imaginary scalar field. For the dual of this theory we considered the critical $O(N)$ model, whose partition function is inversely related to the NBWF, giving an explicit example of the holographic no-boundary proposal. With this we could finally answer the question stated above. From the dual theory we could see that the holographic distribution peaked around global isotropic universes, meaning that somehow the universe smoothly exits the phase of eternal inflation, giving a localised wave function, not one spread out as expected from the semiclassical analysis.

For the final chapter of this thesis we breached the walls of classicality in a different way. In Chapter 6 we focused on the breakdown of classicality when we track a classical history back in time. When we do this, we eventually end up in a regime where the classicality conditions are not satisfied any more, and a quantum mechanical transition can occur to a different classical history. The question of how probable such quantum transitions are was the main question in Chapter 6, where we formulated an answer to the question:“ *What are the probabilities to have a quantum mechanical transition from one classical solution to another?*”. We answered this by constructing complex saddle points that interpolate between two classical, inflationary histories. The actions of these complex saddle point were then used to infer the probability of a transition between two such histories. At large values of the potential, the most likely transition is a symmetric one, whereas for low values of the potential, transitions to larger values of the potential are preferred. Combined with the no-boundary weighting, this gives conditional probabilities that our universe could have come from another universe with different matter content. As a proof of concept, we also showed it was possible to transition from an ekpyrotic universe to an inflating one.

7.2 More not so easy questions

At the end of each chapter we already presented a detailed outlook to the topics discussed there. Let us summarise these while formulating more questions we would like to answer in the future.

The ultimate goal of a fundamental theory is to make predictions for possible observations. The usual predictions of cosmological models involve the size and behaviour of quantum fluctuations that can be measured in the Cosmic Microwave Background. Therefore, it would be interesting to see how the fluctuations get influenced by taking into account the regime of the NBWF that

is governed by the quantum-mechanical dynamics. This means that we can ask the following question: "*Do the quantum effects discussed in this thesis leave an imprint on the Cosmic Microwave Background?*". It should, for example be possible to use our holographic method to investigate the effect of eternal inflation on the quantum fluctuations that can be measured in the CMB by considering two- and three-point functions. On the other hand, we could also investigate fluctuations of the metric and scalar field to study their behaviour along a quantum transition from one classical universe to another. Could these leave a sign in the CMB? Fluctuations could also be useful to test the stability of these transitions. If fluctuations get preferred that are larger than the transitioning instanton, this could suggest that these transitions are not stable. This seems to be especially important to check for the ekpyrotic to inflationary transitions.

Another interesting avenue of future research would be to obtain more universal properties of field theories on deformed backgrounds by answering the question: "*How do field theory partition functions evolve when general geometric deformations are added?*". This could help us to understand whether the properties of eternal inflation we deduced above from the squashed sphere hold on more general manifolds. Another possible avenue would be to repeat our analysis of Chapter 4 with sources added to the field theory, e.g. a scalar deformation to see if our results for the free $O(N)$ model are more generally applicable. Notice that with universal results, the fact that we do not know the exact form of the field theory dual to Einstein gravity does not matter.

In the last couple of months there has been some excitement about a possible Lorentzian formulation of the no-boundary wave function [139, 140, 141]. The main advantage of this approach is that it is possible to know which saddle points we have to include or exclude when doing the semiclassical approximation. One could then ask the following question: "*Are our holographic methods applicable to Lorentzian wave function proposals?*". If the answer to this question is affirmative, we could go on by asking if this new formulation gives the same probability distributions as the Euclidean formulation? Moreover, would it still be possible, for example, to find the same properties of eternal inflation? The techniques used to determine the correct saddle points will also be interesting to study from the point of view of Chapter 6, to see if the saddle points studied there are indeed the dominant ones.

Related to trying the reformulate the NBWF is the last, non-trivial open question we want to pose: "*Is it possible to use the holographic method to define a mathematically well-defined NBWF?*". That is, a proposal for the NBWF that is not plagued by the issues that are usually related to the Euclidean approach to quantum gravity, e.g. the problem of how to perform the sum over geometries precisely. Checking if the holographic proposal of the NBWF holds beyond the

semiclassical level, would be a first step in this direction. Another problem that comes to mind is what the new, fundamental degrees of freedom would be, and how the classical concepts of geometry, matter and entropy emerge from this dual theory. Our method of how to define the classicality conditions from a holographic perspective already seems a step into this direction.

APPENDIX A

CANONICAL TRANSFORMATIONS AND SYMMETRY ENHANCEMENT

In this appendix we give some supplementary material for Chapter 2. We first discuss a detailed calculation of how canonical transformations can be implemented in non-relativistic quantum mechanics, and in Section A.2 we explain the symmetry enhancement observed in Figure 2.1.

A.1 Canonical transformations of wave functions

The goal of this appendix is to explain how wave functions in terms of different variables are related to each other if these variables are connected by a canonical transformation.

In the most general case, one would consider any even-dimensional phase space $\mathcal{M}$ with a symplectic two-form $J^{(2)}$. However, to simplify the discussion to its essence, we will only consider a two-dimensional phase space parametrised by (x, p), with $J^{(2)} = \mathrm{d}p \wedge \mathrm{d}x$.

We will assume the dynamics are governed by a Hamiltonian $H(x, p)$ which has a discrete spectrum and a unique ground state with energy $E_0 = 0$. The ground state wave function can then be written as a path integral in Euclidean time

$$\psi_0(\mathbf{x}) = \lim_{\tau \to -\infty} \sum_{n \geq 0} \mathrm{e}^{E_n \tau} \psi_n(\mathbf{x})$$

$$\propto \lim_{\tau\to-\infty} \int_{x(\tau)=0}^{x(0)=\mathbf{x}} \mathcal{D}x(\tau)\mathcal{D}p(\tau)\ \mathrm{e}^{i\int p\mathrm{d}x-\int H(x,p)\mathrm{d}\tau}\ . \tag{A.1}$$

We have used the standard method of converting a transition amplitude into a path integral, familiar from calculations of transition amplitudes in real time $t=-i\tau$, i.e. by decomposing the unity operator: $1=\int \mathrm{d}x\ |x\rangle\langle x| = \int \mathrm{d}p\ |p\rangle\langle p|$.

The same ground state can be described using any set of coordinates on phase space, (X,P), which also form a Darboux pair $J^{(2)}=\mathrm{d}P\wedge\mathrm{d}X$. Such coordinates are related to (x,p) by a canonical transformation, i.e. there exist functions

$$\xi:(X,P)\mapsto\xi(X,P)=x\ , \qquad \pi:(X,P)\mapsto\pi(X,P)=p\ , \tag{A.2}$$

that map the (X,P)-coordinates of each point in phase space to its (x,p)-coordinates and that satisfy

$$\pi(X,P)\mathrm{d}\xi(X,P)=P\mathrm{d}X+\mathrm{d}f(X,P)\ . \tag{A.3}$$

Here we introduced f, the "generating function" of this canonical transformation. The goal of the remainder of this appendix is to show that the new wave function $\Psi_0(X)$, describing the same vacuum state, is related to the original wave function as

$$\psi_0(\mathbf{x})=\int \mathrm{d}\mathbf{X}\ \mathrm{e}^{i\tilde{f}(\mathbf{X},\mathbf{x})}\Psi_0(\mathbf{X})\ , \tag{A.4}$$

where $\tilde{f}(X,x)$ is defined as $f[X,\mathcal{P}(X,x)]$, with $\mathcal{P}$ solving the equation $\xi[X,\mathcal{P}(X,x)]=x$.

To derive this relation carefully, we explicitly resolve the path integral measure as a dense set of ordinary integrals. In this discretised way, the path integral is

$$\begin{aligned}\psi_0(\mathbf{x}) &\sim \int\left(\prod_{n=0}^{N+1}\mathrm{d}x_n\right)\left(\prod_{n=0}^{N}\mathrm{d}p_n\right)\delta(\mathbf{x}-x_{n+1})\mathrm{e}^{\sum_{n=0}^{N}[ip_n(x_{n+1}-x_n)-H(x_i,p_i)\Delta\tau]}\\ &= \int\left(\prod_{n=0}^{N}\mathrm{d}x_n\mathrm{d}p_n\right)\mathrm{e}^{ip_N(\mathbf{x}-x_N)+\sum_{n=0}^{N-1}ip_n(x_{n+1}-x_n)-\sum_{n=0}^{N}H(x_n,p_n)\Delta\tau}\ .\end{aligned}$$

On each of these discretised slices, we can change the coordinates from x_n,p_n to X_n,P_n using (A.2). Since the Jacobian of each of these transformations is 1, which is a general property of canonical transformations, we get

$$\psi_0(\mathbf{x})\sim\int\left(\prod_{n=0}^{N}\mathrm{d}X_n\mathrm{d}P_n\right)\mathrm{e}^{i\pi(X_N,P_N)[\mathbf{x}-\xi(X_n,P_N)]-\sum_{n=0}^{N}H(X_n,P_n)\Delta\tau}$$

$$\cdot\, \mathrm{e}^{\sum_{n=0}^{N-1} i[P_n(X_{n+1}-X_n)+f(X_{n+1},P_{n+1})-f(X_n,P_n)]} \tag{A.5}$$

$$= \int \left(\prod_{n=0}^{N} \mathrm{d}X_n \mathrm{d}P_n\right) \mathrm{e}^{i\pi(X_N,P_N)[\mathbf{x}-\xi(X_n,P_N)]+if(X_N,P_N)}$$

$$\cdot\, \mathrm{e}^{\sum_{n=0}^{N-1}[iP_n(X_{n+1}-X_n)-H(X_n,P_n)\Delta\tau]} \,.$$

In these steps we have ignored terms proportional to $\Delta X_n \Delta\tau$ and $H(X_N, P_N)\Delta\tau$ since they will be irrelevant in the limit $\Delta\tau \to 0$.

From (A.3) one can derive that for a canonical transformation,

$$\frac{\partial f}{\partial P} = \pi \frac{\partial \xi}{\partial P}. \tag{A.6}$$

If the functions ξ and π are linear in P, then f will be at most quadratic. This implies that the $\mathrm{d}P_N$-integral in (A.5) is at most Gaussian, so we can solve it exactly by extremising the exponent[1]

$$\frac{\partial \pi}{\partial P_N}[\mathbf{x} - \xi(X_N, P_N)] - \pi \frac{\partial \xi}{\partial P_N} + \frac{\partial f}{\partial P_N} = 0 \,, \tag{A.7}$$

where the last two terms cancel by virtue of (A.6).

For a non-trivial canonical transformation $\partial\pi/\partial P \neq 0$, so we conclude that P_N must solve the equation $\mathbf{x} - \xi(X_N, P_N) = 0$, i.e. $P_N = \mathcal{P}(X_N, \mathbf{x})$. The above integral can thus be rewritten as

$$\int \mathrm{d}\mathbf{X}\ \mathrm{e}^{if[\mathbf{X},\mathcal{P}(\mathbf{X},\mathbf{x})]} \int \left(\prod_{n=0}^{N} \mathrm{d}X_n\right) \left(\prod_{n=0}^{N-1} \mathrm{d}P_n\right) \delta(\mathbf{X} - X_N)$$

$$\mathrm{e}^{\sum_{n=0}^{N-1}[iP_n(X_{n+1}-X_n)-H(X_n,P_n)\Delta\tau]} \,. \tag{A.8}$$

The second integral is of the same form as the first line in (A.5), i.e. (up to the limit $\tau \to -\infty$ and normalisation) it will give the path integral $\Psi_0(\mathbf{X})$ upon taking the limit $\Delta\tau \to 0$. Thus, we have derived (A.4).

A.2 Symmetry enhancement and bifurcation

Figure 2.1 resembles the classic picture of symmetry breaking of a pitchfork bifurcation, where the mass m^2 of the scalar field acts as the order parameter

[1] If the transformation is not linear, the following step is still a good approximation whenever the method of steepest descent is accurate.

and where the symmetric solution is given by $m^2 = 2$. At this point of enhanced symmetry, the diagram seems to be invariant under the transformation

$$(x_{\mathrm{TP}}, \theta) \to (\pi - x_{\mathrm{TP}}, -\theta - \pi) \ . \tag{A.9}$$

In this section we will show that this transformation indeed maps asymptotically real solutions to asymptotically real solutions for $m^2 = 2$.

Consider the scalar field initial value at the SP, $\phi = \phi_0 \mathrm{e}^{i\theta}$ and apply the phase transformation of (A.9). This transforms ϕ to $-\phi^* = -\phi_0 \mathrm{e}^{-i\theta}$. This suggests that the "mirrored" solutions are related to each other by complex conjugation of their initial data. Indeed, this also holds for the scale factor, since the complex conjugation of the no-boundary condition is just the no-boundary condition again. One can see that complex conjugation maps solutions of the equations of motion to other solutions. Furthermore, there is no mixing in the equations between terms that are even and odd in ϕ. This implies that mapping $\phi \to -\phi$ gives a new solution to the equations of motion[2].

Now, we are interested in solutions that become real at late time. Hence we need to study the asymptotic solutions along the Lorentzian axis in the case $m^2 = 2$ (see also (2.38)):

$$\phi = i\eta_0 \mathrm{e}^{i(x_{TP}+it)} \frac{\alpha}{\sqrt{2}\pi} \gamma^3 + \dots \ , \qquad a = \frac{\gamma}{i\eta_0} \mathrm{e}^{-i(x_{TP}+it)} + \dots \ . \tag{A.10}$$

Since we are calculating the wave function of a real de Sitter universe, ϕ and a should asymptote to real values. This is possible if the phase of $i\eta_0 \frac{\alpha}{\sqrt{2}\pi}\gamma^3$ is $-ix_{\mathrm{TP}}$ and that of $\gamma/i\eta_0$ is ix_{TP}. By the θ-transformation in (A.9), these phases will be mapped to $i(x_{\mathrm{TP}} - \pi)$ and $-ix_{\mathrm{TP}} - i\pi$, respectively. Thus we constructed a new solution of the equations of motion in the complex tau-plane,

$$\phi = -|i\eta_0 \frac{\alpha}{\sqrt{2}\pi}\gamma^3| e^{ix_{\mathrm{TP}}} e^{i\tau} \ , \qquad a = |\frac{\gamma}{i\eta_0}| e^{-ix_{\mathrm{TP}}} e^{-i\tau} \ . \tag{A.11}$$

Now one can see that there exists an asymptotic direction in which both of these become real: $\tau = \pi - x_{\mathrm{TP}} + it$, with $t \to \infty$.

Hence, for this value of the mass, we have obtained a set of new solutions with asymptotically real values for the matter field and scale factor. When $m^2 \neq 2$, the symmetry of the solutions is broken because the phases of the exponential in the asymptotic fields change. This explains the pitchfork-like bifurcation in Figure 2.1.

[2]Indeed, the subtraction by π in A.9 is not essential. It serves merely to keep θ within the range $[0, \pi]$.

APPENDIX B

DETAILS OF SQUASHED SPHERE CALCULATIONS

In this appendix we present the details necessary to obtain the solutions from Chapters 3 and 5. In Section B.1 we present the full equations of motion for the generalised AdS-Taub-NUT/Bolt solutions with scalar field. Afterwards we give some more details about the IR and UV asymptotic expansion of the solutions together with a short discussion on the procedure to construct numerical solutions. Section B.2 shows how to find the eigenvalues of the Laplacian of a double squashes sphere which was needed to perform the field theory calculations.

B.1 UV and IR expansions

We start with the full equations of motion for the double squashed case together with a scalar field with potential $V(\phi)$. These can be found by varying the

action in (1.5) with respect to the scale factors and the scalar field respectively:

$$
\begin{aligned}
&\frac{{l_0}^2{l_3}^2}{{l_1}^2{l_2}^2}+\frac{{l_0}^2{l_2}^2}{{l_1}^2{l_3}^2}+\frac{{l_0}^2{l_1}^2}{{l_2}^2{l_3}^2}-\frac{2{l_0}^2}{{l_1}^2}-\frac{2{l_0}^2}{{l_2}^2}-\frac{2{l_0}^2}{{l_3}^2}+4l_0^2\kappa^2V(\phi)\\
&+\frac{4l_1'l_2'}{l_1l_2}+\frac{4l_1'l_3'}{l_1l_3}+\frac{4l_2'l_3'}{l_2l_3}-2\kappa^2\phi'^2=0\ ,\\
&-\frac{4l_0'l_1'}{l_0l_1}-\frac{4l_0'l_3'}{l_0l_3}-\frac{{l_0}^2{l_3}^2}{{l_1}^2{l_2}^2}+\frac{3{l_0}^2{l_2}^2}{{l_1}^2{l_3}^2}-\frac{{l_0}^2{l_1}^2}{{l_2}^2{l_3}^2}-\frac{2{l_0}^2}{{l_1}^2}+\frac{2{l_0}^2}{{l_2}^2}-\frac{2{l_0}^2}{{l_3}^2}\\
&+4{l_0}^2\kappa^2V(\phi)+\frac{4l_1''}{l_1}+\frac{4l_1'l_3'}{l_1l_3}+\frac{4l_3''}{l_3}+2\kappa^2\phi'^2=0\ ,\\
&-\frac{4l_0'l_2'}{l_0l_2}-\frac{4l_0'l_3'}{l_0l_3}-\frac{{l_0}^2{l_3}^2}{{l_1}^2{l_2}^2}-\frac{{l_0}^2{l_2}^2}{{l_1}^2{l_3}^2}+\frac{3{l_0}^2{l_1}^2}{{l_2}^2{l_3}^2}+\frac{2{l_0}^2}{{l_1}^2}-\frac{2{l_0}^2}{{l_2}^2}-\frac{2{l_0}^2}{{l_3}^2}\\
&+4{l_0}^2\kappa^2V(\phi)+\frac{4l_2''}{l_2}+\frac{4l_2'l_3'}{l_2l_3}+\frac{4l_3''}{l_3}+2\kappa^2\phi'^2=0\ ,\\
&-\frac{4l_0'l_1'}{l_0l_1}-\frac{4l_0'l_2'}{l_0l_2}+\frac{3{l_0}^2{l_3}^2}{{l_1}^2{l_2}^2}-\frac{{l_0}^2{l_2}^2}{{l_1}^2{l_3}^2}-\frac{{l_0}^2{l_1}^2}{{l_2}^2{l_3}^2}-\frac{2{l_0}^2}{{l_1}^2}-\frac{2{l_0}^2}{{l_2}^2}+\frac{2{l_0}^2}{{l_3}^2}\\
&+4{l_0}^2\kappa^2V(\phi)+\frac{4l_1''}{l_1}+\frac{4l_1'l_2'}{l_1l_2}+\frac{4l_2''}{l_2}+2\kappa^2\phi'^2=0\ ,\\
&{l_0}^2\frac{\partial V(\phi)}{\partial\phi}+\frac{l_0'\phi'}{l_0}-\frac{l_1'\phi'}{l_1}-\frac{l_2'\phi'}{l_2}-\frac{l_3'\phi'}{l_3}-\phi''=0
\end{aligned}
\tag{B.1}
$$

The relevant equations of motion without a scalar field can be found from these by putting $\phi=0$ and $V(\phi)=\Lambda$.

The IR expansion for the NUT solution with two squashings is given in (3.19). Using the equations of motion leads to the following series expansion

$$
\begin{aligned}
l_0(r) &= 1 \ , \\
l_1(r) &= \frac{1}{2}(r-r^*) + \beta_3 (r-r^*)^3 + \frac{1}{1920}\Big(-4\kappa^4 V(\phi_0)^2 - 576\kappa^2 V(\phi_0)\gamma_3 \\
&\quad - 6912{\gamma_3}^2 + 144\kappa^2 V(\phi_0)\beta_3 - 6912\gamma_3\beta_3 + 4608{\beta_3}^2 - 3\kappa^2 V'(\phi_0)^2 \Big)(r-r^*)^5 \\
&\quad + \mathcal{O}\left((r-r^*)^7\right) \\
l_2(r) &= \frac{1}{2}(r-r^*) + \gamma_3 (r-r^*)^3 + \frac{1}{1920}\Big(-4\kappa^4 V(\phi_0)^2 + 144\kappa^2 V(\phi_0)\gamma_3 \\
&\quad + 4608{\gamma_3}^2 - 576\kappa^2 V(\phi_0)\beta_3 - 6912\gamma_3\beta_3 + 6912{\beta_3}^2 - 3\kappa^2 V'(\phi_0)^2 \Big)(r-r^*)^5 \\
&\quad + \mathcal{O}\left((r-r^*)^7\right) \\
l_3(r) &= \frac{1}{2}(r-r^*) - \left(\frac{\kappa^2}{12}V(\phi_0) + \beta_3 + \gamma_3\right)(r-r^*)^3 + \frac{1}{1920}\Big(16\kappa^4 V(\phi_0)^2 \\
&\quad + 624\kappa^2 V(\phi_0)\gamma_3 + 4608{\gamma_3}^2 + 624\kappa^2 V(\phi_0)\beta_3 + 16128\gamma_3\beta_3 + 4608{\beta_3}^2 \\
&\quad - 3\kappa^2 V'(\phi_0)^2 \Big)(r-r^*)^5 + \mathcal{O}\left((r-r^*)^7\right) \\
\phi(r) &= \phi_0 + \frac{1}{8}V'(\phi_0)(r-r^*)^2 + \left(\frac{\kappa^2 V(\phi_0)V'(\phi_0)}{288} + \frac{V'(\phi_0)V''(\phi_0)}{192}\right)(r-r^*)^4 \\
&\quad + \mathcal{O}\left((r-r^*)^6\right)
\end{aligned}
\tag{B.2}
$$

As explained in the main text this expansion is controlled by the three real parameters β_3, γ_3 and ϕ_0 which are ultimately related to the two squashing parameters A and B and the two free parameters in the UV expansion of the scalar field α and β, at the asymptotic boundary.

The IR expansion for the Bolt solution with two squashings is given in (3.21). Using the equations of motion in (B.1) in the gauge $l_0(r) = 1$ leads to the

following series expansion:

$$
\begin{aligned}
l_1(r) = \gamma_0 + & \left(\frac{1}{4\gamma_0} - \frac{\kappa^2 V(\phi_0)\gamma_0}{4}\right)(r-r^*)^2 - \left(\frac{11}{192{\gamma_0}^3} - \frac{\kappa^2 V(\phi_0)}{24\gamma_0}\right. \\
& \left. + \gamma_4 + \frac{\kappa^2\gamma_0 V'(\phi_0)^2}{32}\right)(r-r^*)^4 + \mathcal{O}\left((r-r^*)^6\right) \\
l_2(r) = \gamma_0 + & \left(\frac{1}{4\gamma_0} - \frac{\kappa^2 V(\phi_0)\gamma_0}{4}\right)(r-r^*)^2 + \gamma_4(r-r^*)^4 + \mathcal{O}\left((r-r^*)^6\right) \\
l_3(r) = & \frac{1}{2}(r-r^*) - \frac{(r-r^*)^3}{12{\gamma_0}^2} + \left(\frac{\kappa^4 V(\phi_0)^2}{160} + \frac{53}{1920{\gamma_0}^4}\right. \\
& \left. - \frac{\kappa^2 V(\phi_0)}{40{\gamma_0}^2} - \frac{\kappa^2 V'(\phi_0)^2}{320}\right)(r-r^*)^5 + \mathcal{O}\left((r-r^*)^7\right) \\
\phi(r) = \phi_0 + & \frac{V'(\phi_0)}{4}(r-r^*)^2 \\
& + \frac{V'(\phi_0)\left(-4 + 3{\gamma_0}^2(2\kappa^2 V(\phi_0) + V''(\phi_0))\right)}{192\gamma_0^2}(r-r^*)^4 + \mathcal{O}\left((r-r^*)^6\right)
\end{aligned}
\tag{B.3}
$$

We chose to parametrise this expansion by the three independent real parameters γ_0, γ_4 and ϕ_0 which are again mapped to the squashing parameters A, B and α, β in the UV. Notice that to get the NUT or Bolt double squashing results without scalar field we have to put $\phi_0 = 0$ and $V(\phi) = \Lambda$ in the initial conditions above. All the results up to now are to find solutions with a negative cosmological constant, but can also be used for the cosmological solutions discussed in Chapter 5. This can be done by plugging in a positive scalar potential and replacing the real coordinate r with the complex coordinate τ.

The general UV expansion is given in (3.15). Plugging this into the equations of motion (B.1) with $l_0(r) = 1$ and using that the potential around $\phi = 0$ looks

like $V(\phi) \approx -3 - \phi^2$, one finds the following consistent series expansion

$$\begin{aligned}
l_1(r) &= A_0 e^r + \frac{1}{16 A_0 {B_0}^2 {C_0}^2}\Big(-5{A_0}^4 + 2{A_0}^2{B_0}^2 + 3{B_0}^4 + 2{A_0}^2{C_0}^2 \\
&\quad - 6{B_0}^2{C_0}^2 + 3{C_0}^4 - 2{A_0}^2{B_0}^2{C_0}^2\tilde{\alpha}^2\Big)e^{-r} + A_3 e^{-2r} + \mathcal{O}(e^{-3r}) \\
l_2(r) &= B_0 e^r + \frac{1}{16 A_0 {B_0}^2 {C_0}^2}\Big(3{A_0}^4 + 2{A_0}^2{B_0}^2 - 5{B_0}^4 - 6{A_0}^2{C_0}^2 \\
&\quad + 2{B_0}^2{C_0}^2 + 3{C_0}^4 - 2{A_0}^2{B_0}^2{C_0}^2\tilde{\alpha}^2\Big)e^{-r} + B_3 e^{-2r} + \mathcal{O}(e^{-3r}) \\
l_3(r) &= C_0 e^r + \frac{1}{16 A_0 {B_0}^2 {C_0}^2}\Big(3{A_0}^4 - 6{A_0}^2{B_0}^2 + 3{B_0}^4 + 2{A_0}^2{C_0}^2 \\
&\quad + 2{B_0}^2{C_0}^2 - 5{C_0}^4 - 2{A_0}^2{B_0}^2{C_0}^2\tilde{\alpha}^2\Big)e^{-r} \\
&\quad - \left(\frac{A_3 C_0}{A_0} - \frac{B_3 C_0}{B_0} - \frac{2}{3}C_0\tilde{\alpha}\tilde{\beta}\right)e^{-2r} + \mathcal{O}(e^{-3r}) \\
\phi(r) &= \tilde{\alpha}e^{-r} + \tilde{\beta}e^{-2r} + \mathcal{O}(e^{-3r})
\end{aligned} \tag{B.4}$$

We have performed this expansion up to eight order and have verified that it is controlled by the seven parameters $\{A_0, B_0, C_0, A_3, B_3, \tilde{\alpha}, \tilde{\beta}\}$. Notice that we introduced new asymptotic coordinates $\tilde{\alpha}, \tilde{\beta}$ to simplify the expressions. Since the equations of motion (B.1) are invariant under constant shifts of the radial coordinate, one can set $A_0 = \frac{1}{4}$ by an appropriate shift of r. The UV expansion could have also been found by inserting the metric Ansatz (3.13) into the general expression for the UV expansion of the metric we obtained in (2.9). One can now identify B_0 and C_0 with the squashing parameters in (3.1) as follows

$$A = \frac{1}{4C_0^2} - 1\,, \qquad\qquad B = \frac{1}{4B_0^2} - 1\,. \tag{B.5}$$

The parameters A_3, B_3 and $\tilde{\beta}$ are independent from the point of view of the UV expansion but are ultimately fixed in terms of A, B and $\tilde{\alpha}$ by the regularity conditions that we imposed for the numerical solutions of the full nonlinear equations of motion.

It is worth discussing how we constructed the numerical solutions of the full nonlinear equations of motion in (B.1). For the AdS-Taub-NUT solutions we picked real values for the parameters β_3, γ_3 and ϕ_0 in the IR expansion (B.2).

For each such value we then numerically integrated the equations of motion from $r = 0$ to some large value of r. If the resulting numerical solution does not exhibit a singularity at an intermediate value of the radial coordinate r we declared the solution to be regular and read of the asymptotic parameters B_0, C_0 and $\tilde{\alpha}$ and $\tilde{\beta}$ in (B.4) which we then related to the squashing parameters A and B using (B.5). As expected we find that there are no restrictions on the parameters A and B, i.e. as we vary β_3 and γ_3 for a fixed ϕ_0 we can explore the whole (A, B) plane. This is illustrated in Figure B.1 for the case that there is no scalar field. If we take a non-zero value for ϕ_0 we will reach the same conclusion with the only difference that the region in the (β_3, γ_3)-plane that gives valid UV solutions shifts to higher values of β_3 and γ_3 when ϕ_0 increases as can be seen in Figure B.2.

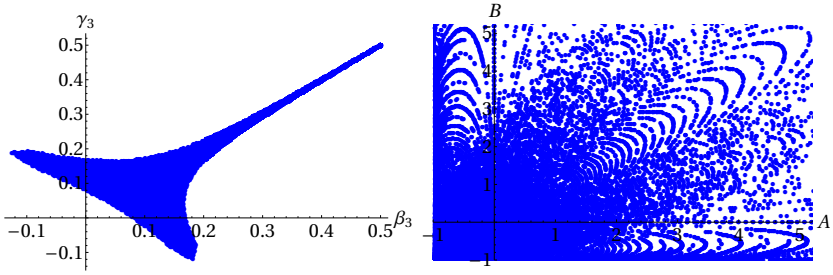

Figure B.1: The range of parameters for the AdS-Taub-NUT solutions with two squashings. Left: the values of γ_3 and β_3 that lead to regular solutions. Right: the resulting values of the squashing parameters α and β.

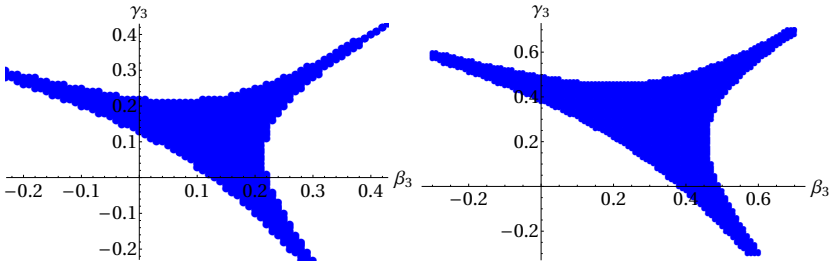

Figure B.2: Initial conditions for γ_3 and β_3 that give rise to non-singular solutions. From the left to the right $\phi_0 = 1, 2$.

The procedure we used to construct the AdS-Taub-Bolt solutions is very similar. We start with the IR expansion in (B.3), vary the parameters γ_0 and γ_4 and integrate numerically the equations of motion. Finally, we read off the

asymptotic parameters B_0 and C_0 from the behaviour of the numerical solutions at large r and deduce the corresponding values of A and B using the relation in (B.5). However, there is an important difference between these solutions and the AdS-Taub-NUT solutions. For a fixed value of B there are critical values of A below/above which there are no AdS-Taub-Bolt solutions. This leads to curves in the (A, B) plane and the AdS-Taub-Bolt solutions exist only for values of the squashing parameters that are below or above these critical curves. Furthermore for every value of (A, B) for which Bolt solutions exist there are two possible solutions of the equations of motion which we dub "positive" and "negative" branch. All of these features are extensions of the familiar behaviour of the analytically known AdS-Taub-Bolt solutions with $B = 0$ discussed in Section 3.2.1. We illustrate the range of the IR and squashing parameters for the "positive" and "negative" branch AdS-Taub-Bolt solutions in Figure B.3 and Figure B.4 respectively for the case withour scalar field. The way the solutions change when we add a scalar field have already been discussed extensively in the main text.

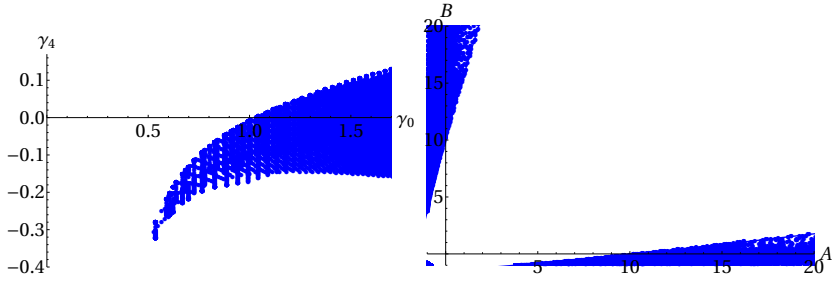

Figure B.3: The range of parameters for the "positive branch" AdS-Taub-Bolt solutions with two squashings and no scalar field. Left: the range of parameters γ_0 and γ_4 that leads to regular solutions. Right: the resulting asymptotic parameters A and B.

B.2 Eigenvalues of the Laplace operator

To calculate the eigenvalues of the Laplacian on the double squashed three sphere we use some of the results in [77]. Their main observation is that the Laplace operator $-\nabla^2$ on the squashed three sphere corresponds to the Hamiltonian $\hat{H}$ of an asymmetric top

$$-\nabla^2 \to \hat{H} = \frac{\hat{L}_1^2}{2I_1} + \frac{\hat{L}_2^2}{2I_2} + \frac{\hat{L}_3^2}{2I_3} \ , \tag{B.6}$$

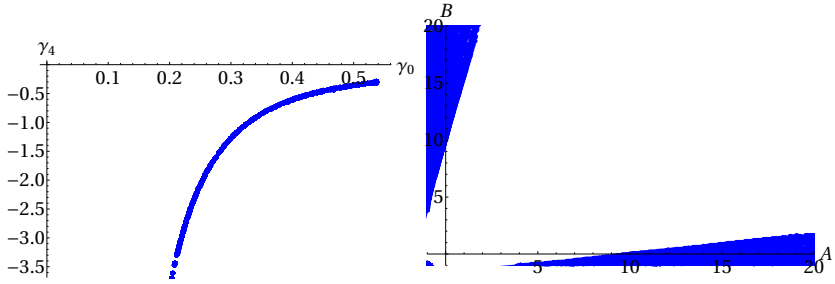

Figure B.4: The range of parameters for the "negative branch" AdS-Taub-Bolt solutions with two squashings and no scalar field. Left: the range of parameters γ_0 and γ_4 that leads to regular solutions. Right: the resulting asymptotic parameters A and B.

with $\hat{L}_1$, $\hat{L}_2$ and $\hat{L}_3$ the components of the angular momentum operator $\hat{L}$ along the three principal axes of inertia. (I_1, I_2, I_3) are the principal moments of inertia of the body. These can be mapped to the squashing parameters in (3.1) in the following way

$$I_1 = \frac{1}{8} , \qquad I_2 = \frac{1}{8(B+1)} , \qquad I_3 = \frac{1}{8(A+1)} . \tag{B.7}$$

The round sphere with $A = B = 0$ is mapped to the spherical top defined by $I_1 = I_2 = I_3$. The sphere with one squashing parameter, say $B = 0$ and $A \neq 0$ is the counterpart of the symmetric prolate top with $I_1 = I_2 \neq I_3$. The problem of finding the eigenvalues of the Laplacian for the sphere with two non-trivial squashing parameters is therefore reduced to finding the eigenvalues of the Hamiltonian of an asymmetric top with three different moments of inertia. This problem is studied to some extent in Section 103 of [142] but since it may not be too familiar we discuss it below in some detail.

Let us start with the simplest case when $I_1 = I_2 = I_3 = I$. The Hamiltonian in this case is reduced to $\hat{H} = \hat{L}^2/(2I)$ for which the eigenvalues of an eigenvector ψ are

$$\hat{H}\psi = \frac{L(L+1)}{2I}\psi , \tag{B.8}$$

with degeneracy[1] $2L+1$. Here L is the rotational quantum number which is related to the quantum number i in (3.52) by $2L+1 = i$.

[1]This is the degeneracy of the energy levels with respect to the $2L+1$ directions of the angular momentum relative to the body itself. There is another $(2L+1)$-fold degeneracy with respect to a fixed coordinate system. These are not really physical, but need to be taken into account when we calculate the partition function.

It is also possible to find analytic expressions for the eigenvalues of the symmetric prolate top with $I_1 = I_2$. In this case the Hamiltonian (B.6) can be rewritten as

$$\hat{H} = \frac{\hat{L}^2}{2I_1} + \frac{1}{2}\left(\frac{1}{I_3} - \frac{1}{I_1}\right)\hat{L}_3^2 \,. \tag{B.9}$$

Since $\hat{L}_3$ commutes with $\hat{L}^2$ it has the same eigenvectors as $\hat{L}^2$, but with eigenvalues

$$\hat{L}_3\psi = k\psi, \qquad k = -L, \ldots, L \,. \tag{B.10}$$

The relation between the quantum number k above and the quantum numbers q and i used in (3.52) is

$$k = q + \frac{1-i}{2} \,. \tag{B.11}$$

With this at hand one can show that the eigenvalues of $\hat{H}$ for the symmetric prolate top are

$$\hat{H}\psi = \left[\frac{L(L+1)}{2I_1} + \frac{1}{2}\left(\frac{1}{I_3} - \frac{1}{I_1}\right)k^2\right]\psi \,. \tag{B.12}$$

Every such eigenvalue is doubly degenerate.

For the completely asymmetric top it is impossible to solve the eigenvalue problem analytically. This is because $\hat{L}_1$, $\hat{L}_2$ and $\hat{L}_3$ do not mutually commute. The degeneracy that was present in the previous examples, is now completely lifted. A possible resolution is to solve the eigenvalue equation in matrix form. This means that we have to find solutions of a secular equation of degree $2L+1$. For general values of L we therefore have to resort to numerical methods to find the eigenvalues. Luckily there are some symmetries that reduce the degree of the secular equation making it more tractable to solve numerically.

The matrix elements of the angular momentum operator can be found in many textbooks on quantum mechanics, see for example [142]. The only non-zero matrix elements are

$$(\hat{L}_1)_{k,k-1} = (\hat{L}_1)_{k-1,k} = \frac{1}{2}\sqrt{(L+k)(L-k-1)} \,, \tag{B.13}$$

$$(\hat{L}_2)_{k,k-1} = -(\hat{L}_2)_{k-1,k} = -i\frac{1}{2}\sqrt{(L+k)(L-k+1)} \,, \tag{B.14}$$

$$(\hat{L}_3)_{k,k} = k. \tag{B.15}$$

From these expressions it is not too difficult to see that the only non-zero elements of $\hat{L}_1^2$, $\hat{L}_2^2$ and $\hat{L}_3^2$ are those for which $k \to k$ or $k \to k \pm 2$. For a given

fixed value of L we have

$$(\hat{H})_{k,k} = \frac{1}{2}\left(\frac{(\hat{L}_1^2)_{k,k}}{I_1} + \frac{(\hat{L}_2^2)_{k,k}}{I_2} + \frac{(\hat{L}_3^2)_{k,k}}{I_3}\right)$$
$$= \frac{1}{4}\left(\frac{1}{I_1} + \frac{1}{I_2}\right)\big(L(L+1) - k^2\big) + \frac{k^2}{2I_3}\,, \tag{B.16}$$

$$(\hat{H})_{k,k+2} = (\hat{H})_{k+2,k}$$
$$= \frac{1}{8}\left(\frac{1}{I_1} - \frac{1}{I_2}\right)\sqrt{(L-k)(L-k-1)(L+k+1)(L+k+2)}\,. \tag{B.17}$$

These matrices are the essential building blocks in our numerical analysis. To continue our simplification of the secular equations, we have to treat the case of integer and half-integer values of L separately.

First, let us consider the case when L can only take integer values. In this case the even and odd values of k will never be mixed. This means that the secular equation for a given L splits into a secular equation of degree L and one of degree $L+1$

$$\det(H_{k,k'} - E\delta_{k,k'}) = \det(H_{k,k'} - E\delta_{k,k'})|_{k\ \text{even}} \times \det(H_{k,k'} - E\delta_{k,k'})|_{k\ \text{odd}}\,. \tag{B.18}$$

It is possible to lower the degrees of the secular equations even further. To this end we have to consider the matrix elements with respect to a new basis

$$\psi^+_{L_k} = \frac{\psi_{L_k} + \psi_{L_{-k}}}{\sqrt{2}}\,, \tag{B.19}$$

$$\psi^-_{L_k} = \frac{\psi_{L_k} - \psi_{L_{-k}}}{\sqrt{2}}\,, \qquad k \neq 0\,. \tag{B.20}$$

This splits everything up in functions that are symmetric or anti-symmetric under sign change of k, which leads to another split in the two secular equations we have. At the end of the day in the new basis we have four independent matrices for which we have to find the eigenvalues. These are denoted by O^+, O^-, E^+ and E^- where O, E stands for odd or even respectively. Furthermore with $k^\pm$ we will distinguish between the eigenbasis spanned by ψ^+ or ψ^-.

The matrix elements in the new basis are then given by

$$(\hat{H})_{k^\pm,k^\pm} = \langle\psi^\pm_{L_k}|H|\psi^\pm_{L_k}\rangle$$

$$= \frac{1}{2}\Big(\langle \psi_{L_k}|H|\psi_{L_k}\rangle \pm \langle \psi_{L_k}|H|\psi_{L_{-k}}\rangle$$

$$\pm \langle \psi_{L_{-k}}|H|\psi_{L_k}\rangle + \langle \psi_{L_{-k}}|H|\psi_{L_{-k}}\rangle \Big)$$

$$= \begin{cases} (\hat{H})_{k,k} & k \neq 1 \\ (\hat{H})_{1,1} \pm (\hat{H})_{1,-1} & k = 1 \end{cases}, \tag{B.21}$$

and

$$(\hat{H})_{k^\pm,k+2^\pm} = \begin{cases} (\hat{H})_{k,k+2} & k \neq 0,-2 \\ \sqrt{2}(\hat{H})_{0,2} \end{cases}. \tag{B.22}$$

This means that, for a given L, the matrices we have to find the eigenvalues of, are

$$O^\pm = \begin{pmatrix} (\hat{H})_{1,1} \pm (\hat{H})_{1,-1} & (\hat{H})_{1,3} & 0 & \dots \\ (\hat{H})_{1,3} & (\hat{H})_{3,3} & (\hat{H})_{3,5} & \dots \\ 0 & (\hat{H})_{3,5} & (\hat{H})_{5,5} & \dots \\ \dots & \dots & \dots & \dots \end{pmatrix},$$

$$E^+ = \begin{pmatrix} (\hat{H})_{0,0} & \sqrt{2}(\hat{H})_{0,2} & 0 & \dots \\ \sqrt{2}(\hat{H})_{0,2} & (\hat{H})_{2,2} & (\hat{H})_{2,4} & \dots \\ 0 & (\hat{H})_{2,4} & (\hat{H})_{4,4} & \dots \\ \dots & \dots & \dots & \dots \end{pmatrix}, \tag{B.23}$$

$$\text{and } E^- = \begin{pmatrix} (\hat{H})_{2,2} & (\hat{H})_{2,4} & 0 & \dots \\ (\hat{H})_{2,4} & (\hat{H})_{4,4} & (\hat{H})_{4,6} & \dots \\ 0 & (\hat{H})_{4,6} & (\hat{H})_{6,6} & \dots \\ \dots & \dots & \dots & \dots \end{pmatrix}.$$

We still have to consider the half-integer values of L. The asymmetric top with half-integer angular momenta has been extensively studied in [143]. In this case there is no transition between elements for which $k + 1/2$ is even and for which this is odd, thus

$$\det(H_{k,k'} - E\delta_{k,k'}) = \det(H_{k,k'} - E\delta_{k,k'})|_{k+1/2 \text{ even}}$$

$$\times \det(H_{k,k'} - E\delta_{k,k'})|_{k+1/2 \text{ odd}} . \tag{B.24}$$

The secular equation is now split into two secular equations of degree $L+1/2$. It is not difficult to see that the set of k's spanned by one of the secular equations

is just minus the one of the other secular equation. On the other hand one can also show that $(\hat{H})_{k,k} = (\hat{H})_{-k,-k}$ and $(\hat{H})_{k+2,k} = (\hat{H})_{-k-2,-k}$. Therefore the two secular equations give the same result, leading to doubly degenerate eigenvalues for the case of half-integer L. The matrix for which we have to find the eigenvalues of is then

$$HI = \begin{pmatrix} (\hat{H})_{-L,-L} & (\hat{H})_{-L,-L+2} & 0 & \cdots \\ (\hat{H})_{-L,-L+2} & (\hat{H})_{-L+2,-L+2} & \hat{H})_{-L+2,-L+4} & \cdots \\ 0 & (\hat{H})_{-L+2,-L+4} & (\hat{H})_{-L+4,-L+4} & \cdots \\ \cdots & \cdots & \cdots & \cdots \end{pmatrix}. \tag{B.25}$$

For the purposes of Section 3.4 we have implemented these eigenvalue problems into a numerical routine which produces all eigenvalues up to a certain quantum number $i = 2L + 1$. To ensure good convergence properties we had to choose values of i that are of the order of 2000.

APPENDIX C

3-POINT FUNCTION OF $T_{\mu\nu}$

In this appendix we give some extra information about the three-point functions that were introduced in Chapter 4. The 2-point function of the energy-momentum tensor was already presented in (4.3) and (4.4). The known expression for the three-point function of the energy-momentum tensor of CFTs in general dimension can be found in [82] (see also [94, 95, 84]). In Euclidean flat space the three-point function is

$$\langle T_{ab}(X)T_{cd}(Y)T_{ef}(Z)\rangle_{\mathbb{R}^d} = \frac{\mathcal{I}_{ab,a'b'}(X-Z)\mathcal{I}_{cd,c'd'}(Y-Z)}{(X-Z)^{2d}(Y-Z)^{2d}}\, t_{a'b',c'd',ef}(W)\,, \tag{C.1}$$

where we have defined

$$\begin{aligned}
\mathcal{I}_{ab,cd}(X) &\equiv \left(\delta_{ae} - \frac{2X_aX_e}{X^2}\right)\left(\delta_{bf} - \frac{2X_bX_f}{X^2}\right)\mathcal{E}_{ef,cd}\,,\\
\mathcal{E}_{ab,cd} &\equiv \frac{1}{2}(\delta_{ac}\delta_{bd}+\delta_{ad}\delta_{bc}) - \frac{1}{d}\delta_{ab}\delta_{cd}\,,\\
W_a &\equiv \frac{(X-Z)_a}{(X-Z)^2} - \frac{(Y-Z)_a}{(Y-Z)^2}\,, \qquad W^2 \equiv \frac{(X-Y)^2}{(X-Z)^2(Y-Z)^2}\,.
\end{aligned} \tag{C.2}$$

The tensor $t_{a'b',c'd',ef}(W)$ is given by the unwieldy expression

$$t_{ab,cd,ef}(W) \equiv \frac{\mathcal{A}}{(W^2)^{d/2}}\mathcal{E}_{ab,gh}\mathcal{E}_{cd,hn}\mathcal{E}_{ef,ng}$$

$$+\,(\mathcal{B}-2\mathcal{A})\,\mathcal{E}_{ef,gh}\mathcal{E}_{cd,hn}\mathcal{E}_{ab,mg}\frac{W_nW_m}{(W^2)^{\frac{d+1}{2}}}$$

$$
\begin{aligned}
&- \mathcal{B}\left(\mathcal{E}_{ab,gh}\mathcal{E}_{cd,hn}\mathcal{E}_{ef,mg} + (ab) \leftrightarrow (cd)\right) \frac{W_n W_m}{(W^2)^{\frac{d+1}{2}}} \\
&+ \frac{\mathcal{C}}{(W^2)^{d/2}}\left(\mathcal{E}_{ab,cd}\left(\frac{W_e W_f}{W^2} - \frac{1}{d}\delta_{ef}\right) + \mathcal{E}_{cd,ef}\left(\frac{W_a W_b}{W^2} - \frac{1}{d}\delta_{ab}\right)\right. \\
&\left. + \mathcal{E}_{ef,ab}\left(\frac{W_c W_d}{W^2} - \frac{1}{d}\delta_{cd}\right)\right) + (\mathcal{D} - 4\mathcal{C})\mathcal{E}_{ab,mn}\mathcal{E}_{cd,mp}\left(\frac{W_e W_f}{W^2} - \frac{1}{d}\delta_{ef}\right)\frac{W_n W_p}{(W^2)^{\frac{d+1}{2}}} \\
&- (\mathcal{D} - 2\mathcal{B})\left(\mathcal{E}_{cd,mn}\mathcal{E}_{ef,mp}\left(\frac{W_a W_b}{W^2} - \frac{1}{d}\delta_{ab}\right) + (ab) \leftrightarrow (cd)\right)\frac{W_n W_p}{(W^2)^{\frac{d+1}{2}}} \\
&+ \frac{(\mathcal{E} + 4\mathcal{C} - 2\mathcal{D})}{(W^2)^{d/2}}\left(\frac{W_a W_b}{W^2} - \frac{1}{d}\delta_{ab}\right)\left(\frac{W_c W_d}{W^2} - \frac{1}{d}\delta_{cd}\right)\left(\frac{W_e W_f}{W^2} - \frac{1}{d}\delta_{ef}\right),
\end{aligned}
\tag{C.3}
$$

where $(\mathcal{A}, \mathcal{B}, \mathcal{C}, \mathcal{D}, \mathcal{E})$ are constants. Only three of these constants are independent. This is made manifest by the following relations

$$
\begin{aligned}
\mathcal{D} &= \frac{(d^2-4)\mathcal{A} + (d+2)\mathcal{B} - 4d\mathcal{C}}{2}, \\
\mathcal{E} &= \frac{d(d+6)\mathcal{B} - 2d(d+10)\mathcal{C} + 4(d^2-4)\mathcal{A}}{4}.
\end{aligned}
\tag{C.4}
$$

There is an alternative parametrisation of these three independent constants which is convenient for the analysis of unitarity bounds in [95]

$$
\begin{aligned}
\mathcal{A} &= 2C_{\mathrm{T}} d^2 \frac{(d(1-d^2) + (d+1)^2 t_2 + (3d+1)t_4)}{(d-1)^3(d+1)^2\mathcal{S}_{d-1}^3}, \\
\mathcal{B} &= C_{\mathrm{T}} d \frac{(2(1+d^2(-2+d+d^2-d^3)) + (3+4d+d^4)t_2 + 2(2+2d-d^2+d^3)t_4)}{2(d-1)^3(d+1)^2\mathcal{S}_{d-1}^3}, \\
\mathcal{C} &= \frac{C_{\mathrm{T}} d}{2(d-1)^3(d+1)^2\mathcal{S}_{d-1}^3}\Big((d(d-1)(d+1)(1-2d(d-1)) \\
&\qquad + (d+1)(d^3-3)t_2 - (4 - d(d-1)(3d+2))t_4)\Big),
\end{aligned}
\tag{C.5}
$$

where $\mathcal{S}_{d-1}$ was defined below (4.3).

The important upshot from these explicit formulae is that the three-point function of the energy-momentum tensor of CFTs in general dimension d is

completely determined by conformal symmetry up to three real constants — C_{T}, t_2, and t_4. The constant C_{T} is the same as the one appearing in the two-point function of the energy-momentum tensor (4.3). For low values of the dimension d, there are kinematical accidents that further reduce the number of independent constants. For example, in $d = 3$ one finds that $t_2 = 0$, which in turn implies that e.g. $\mathcal{A}$ can be written in terms of $\mathcal{B}$ and $\mathcal{C}$.

Finally let us point out that the three-point function of the energy-momentum tensor on a conformally flat manifold can be expressed in terms of the correlator in flat space using the expression

$$\begin{aligned}\langle T_{\mu\nu}(x)T_{\rho\sigma}(y)T_{\gamma\delta}(z)\rangle_{\mathcal{M}} =&\Omega^{d-2}(x)\Omega^{d-2}(y)\Omega^{d-2}(z)M^{ab}_{\mu\nu}M^{cd}_{\rho\sigma}M^{ef}_{\gamma\delta}\times\\ &\langle T_{ab}(X)T_{cd}(Y)T_{ef}(Z)\rangle_{\mathbb{R}^d}\ ,\end{aligned}\tag{C.6}$$

where $\Omega(x)$ and $M^{ab}_{\mu\nu}$ are defined in (4.20) and (4.21).

APPENDIX D

CONTOURS AND PERTURBATIVE RESULTS FOR QUANTUM TRANSITIONS

This appendix gives some additional material for chapter 6. In the first section we show why the contour that was used in the main text is preferred above other possibilities, while in Section D.2 we show some analytic results for large and small scalar field values.

D.1 Contours of integration

For inflationary-to-inflationary transitions, apart from the specific symmetric contour used in the main part of the text, other paths are possible which also lead to potentially valid interpolating solutions. One example is an L-shaped path, as shown in Figure D.1. From the final classical history, this path runs straight down through the point where the big bang singularity would have been, had the solution been real. The fact that the solution is complex now allows one to continue through this point, and connect with an incoming classical history in the bottom left quadrant. However, as shown in Figure D.2, if we look at transitions to different scalar field values, then for the L-shaped path the implied probability distribution would be non-normalisable, indicating that this class of solutions may not be physical. Similar results are obtained for other L-shaped paths that connect with further-removed loci of real a values, and

with upside-down L-shaped paths that run through the would-be singularity from the bottom up. For this reason we focus on the symmetric contour in Chapter 6.

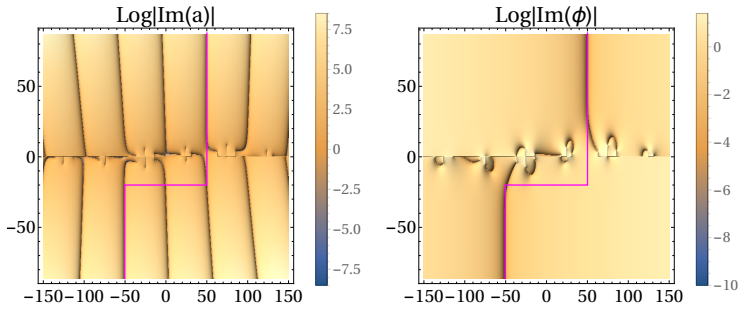

Figure D.1: An instanton with an L-shaped path connecting $\chi_1 = 10$ to $\chi_2 = 10$. This contour first goes up along the contracting inflationary solution, then it goes to the right to reach another line in the complex plane where the scale factor is real, following this path vertically upwards we finally reach another real, inflationary solution.

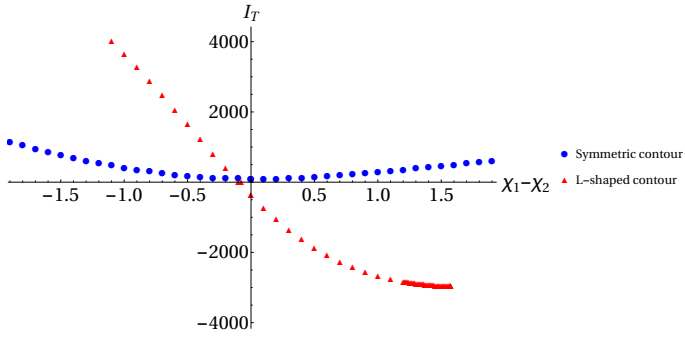

Figure D.2: The real part of the action for transition from $\chi_1 = 10$ to various values of χ_2, plotted as a function of $\chi_1 - \chi_2$ and for two types of integration contour: the L-shaped one (in blue dots) and the symmetric one (in red triangles).

But even for the symmetric contour, we have further possibilities, as we can use it to connect classical histories that are further separated in Euclidean time. Figure D.3 shows the real part of the action for such transitions between increasingly separated "branches" where the scale factor is real, each time with field derivatives optimised such that the locus of real scalar field asymptotically

overlaps with the line of real scale factor. For these higher branches, the action increases monotonically, indicating that these transitions, though also normalisable, are further suppressed. We may thus safely ignore these.

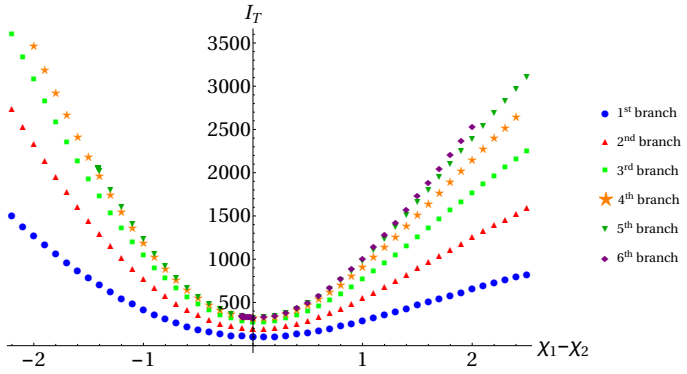

Figure D.3: The real part of the action for symmetric contours connecting classical histories that are ever further separated in Euclidean time, and which we refer to as different branches. These solutions have higher actions and are thus further suppressed.

D.2 Perturbative results

For inflationary-to-inflationary transitions, the equations of motion can be solved analytically in various approximate regimes, allowing us to provide approximate analytic descriptions of the symmetric quantum transitions.

D.2.1 Large scalar field

At large field values we will be in the slow-roll regime, $\phi'^2 \ll V(\phi)$ and $\phi'' \ll \frac{\partial V(\phi)}{\partial \phi}$. If the scale factor is also large, then the spatial curvature can be ignored and the equations of motion simplify to

$$3\frac{a'}{a} = m^2\frac{\phi}{\phi'} \,, \tag{D.1a}$$

$$a'' + \frac{a\kappa^2 m^2 \phi^2}{6} = 0 \,, \tag{D.1b}$$

$$\left(\frac{a'}{a}\right)^2 = -\frac{\kappa^2 m^2 \phi^2}{6} \ . \tag{D.1c}$$

These can be solved explicitly, for example by substituting the first equation into the last,

$$\phi'^2 = -\frac{2}{3}\frac{m^2}{\kappa^2} \ , \tag{D.1d}$$

which can be easily found to give

$$\phi(\tau) = \phi(0) \pm i\frac{m}{\kappa}\sqrt{\frac{2}{3}}\tau \ . \tag{D.2}$$

Notice that again we took the point of symmetry $\tau_{\rm s} = 0$. This result for ϕ can be plugged into (D.1a), from which we then obtain the sale factor

$$\frac{a'}{a} = \mp i\frac{\kappa m}{\sqrt{6}}\left(\phi(0) \pm i\sqrt{\frac{2}{3}}\frac{m\tau}{\kappa}\right) \Rightarrow a(\tau) = C\mathrm{e}^{\mp i\frac{\kappa m\phi(0)\tau}{\sqrt{6}} + \frac{m^2\tau^2}{6}} \ . \tag{D.3}$$

To find the value of C, we will follow [16], who states that when $\mathrm{Re}(\phi(0)) > 0$ in the upper half $\tau-$plane the solutions with the upper sign are valid while in the lower half τ-plane the ones with the lower sign are valid. This means that around $\tau = 0$ both solutions should be matched to one solution,

$$\phi(\tau) \approx \phi(0) \ , \tag{D.4}$$

$$a(\tau) \approx C\cos\left(\frac{\kappa m\phi(0)}{\sqrt{6}}\tau\right) \ . \tag{D.5}$$

Notice that it is clear that these solutions obey the bounce boundary conditions that we impose. To find C we plug a into the Hamiltonian constraint, giving $C = \sqrt{\frac{3}{2}}\frac{1}{\kappa m\phi(0)}$. Collecting our results, the solution is approximately given by

$$\phi(\tau) = \phi(0) + i\sqrt{\frac{2}{3}}\frac{m\tau}{\kappa} \ , \tag{D.6}$$

$$a(\tau) = \sqrt{\frac{3}{2}}\frac{1}{\kappa m\phi(0)}\exp\left(-i\frac{\kappa m\phi(0)}{\sqrt{6}}\tau + \frac{m^2\tau^2}{6}\right) \ . \tag{D.7}$$

From this we can understand the behaviour in our numerics. It is clear that ϕ is real along $\tau = x_{\rm s} + it$ with $x_{\rm s} = -\phi_{\rm sI}\frac{\kappa}{m}\sqrt{\frac{2}{3}}$. Here we have split $\phi(0)$ in its real and imaginary components $\phi(0) = \phi_{\rm sR} + i\phi_{\rm sI}$. It is also interesting to write

$\phi(0) = \phi_{\rm s} e^{i\theta_{\rm s}}$, from which we can see that a change in phase, keeping $\phi_{\rm s}$ fixed, shifts the line of real $\phi(\tau)$:

$$x_{\rm s} = -\phi_{\rm s} \sin(\theta_{\rm s}) \sqrt{\frac{3}{2}} \frac{\kappa}{m} \ . \tag{D.8}$$

Let us now take a closer look at the scale factor. To see where it becomes real, we will try to write it as an amplitude times a phase,

$$\begin{aligned} a(\tau) =& \sqrt{\frac{3}{2}} \frac{1}{\kappa m \phi_{\rm s}} \exp\left[\frac{m^2}{6}(x^2 - t^2) + \frac{\kappa m \phi_{\rm s}}{\sqrt{6}} (\cos(\theta_{\rm s}) t + \sin(\theta_{\rm s}) x) \right] \\ & \times \exp\left[i \left(\frac{m^2 x t}{3} - \theta_{\rm s} - \frac{\kappa m \phi_{\rm s}}{\sqrt{6}} (\cos(\theta_{\rm s}) x - \sin(\theta_{\rm s}) t) \right) \right] \ . \end{aligned} \tag{D.9}$$

This becomes real when the phase is a multiple of π. If t is not too big, the only relevant term is the one without t, therefore we expect that a is real along

$$x_{\rm s} = \frac{n\pi\sqrt{6}}{\kappa m \phi_{\rm s} \cos(\theta_{\rm s})} \ , \tag{D.10}$$

with $n \in \mathbb{Z}$. This explains why we see different lines in the complex $\tau-$plane along which a is real. In the numerical results there are singularities around $\tau = 0$, though these do not appear in our analytic results. The lines of real a and ϕ will coincide if

$$-\phi_{\rm sI} \frac{\kappa}{m} \sqrt{\frac{3}{2}} = \frac{n\pi\sqrt{6}}{\kappa m \phi_{\rm sR}} \Rightarrow \phi_{\rm sI} = -\frac{2n\pi}{\kappa^2 \phi_{\rm sR}} \ , \tag{D.11}$$

or written in terms of the absolute value and the phase of $\phi(0)$

$$\theta_{\rm s} = \frac{1}{2} \sin^{-1}\left(\frac{4n\pi}{\kappa^2 \phi_{\rm s}^2} \right) \ . \tag{D.12}$$

Thus we expect no obstruction to finding such interpolating solutions numerically.

D.2.2 Small scalar field

Another region with possible analytic results is the region where the scalar field is a small perturbation, without backreaction on the metric. Starting with the case for which there is no scalar field at all, the equation of motion for a is solved by

$$a''(\tau) = 0 \Rightarrow a(\tau) = A + B\tau \ . \tag{D.13}$$

Because we demand $a'(0) = 0$ we can conclude that without a scalar field the scale factor is constant, $a(\tau) = A$. If we now add a small scalar field to this background, we get an equation of motion for ϕ:

$$\phi'' - m^2\phi = 0 \ . \tag{D.14}$$

The solution for this, obeying the appropriate boundary condition $\phi'(0) = 0$, is

$$\phi(\tau) = \phi_{\mathrm{s}} \mathrm{e}^{i\theta_{\mathrm{s}}} \cosh(m\tau) \ . \tag{D.15}$$

Plugging this together with a into the Hamiltonian constraint gives $a(\tau) = \pm\frac{\sqrt{6}}{\kappa m \phi_{\mathrm{s}} \mathrm{e}^{i\theta_{\mathrm{s}}}}$.

Now we can look for regions where both a and ϕ are real. The only values of θ_{s} for which a is real are $\theta_{\mathrm{s}} = n\pi$. ϕ can then only be real along the imaginary axis, i.e. $x_{\mathrm{s}} = 0$. This explains why we can not find complex bounce solutions for very small ϕ_{s}, the only possible solutions are those that are real.

BIBLIOGRAPHY

[1] J. Hartle and S. Hawking, *Wave Function of the Universe*, *Phys.Rev.* **D28** (1983) 2960–2975.

[2] A. D. Linde, *Quantum Creation of the Inflationary Universe*, *Lett. Nuovo Cim.* **39** (1984) 401–405.

[3] A. Vilenkin, *Quantum creation of universes*, *Phys. Rev. D* **30** (Jul, 1984) 509–511.

[4] S. Hawking, *The quantum state of the universe*, *Nuclear Physics B* **239** (1984), no. 1 257 – 276.

[5] T. Hertog and G. T. Horowitz, *Towards a big crunch dual*, *JHEP* **07** (2004) 073, [hep-th/0406134].

[6] T. Hertog and G. T. Horowitz, *Holographic description of AdS cosmologies*, *JHEP* **04** (2005) 005, [hep-th/0503071].

[7] A. Bzowski, T. Hertog, and M. Schillo, *Cosmological singularities encoded in IR boundary correlations*, *JHEP* **05** (2016) 168, [arXiv:1512.05761].

[8] P. McFadden and K. Skenderis, *Holography for Cosmology*, *Phys.Rev.* **D81** (2010) 021301, [arXiv:0907.5542].

[9] P. McFadden and K. Skenderis, *The Holographic Universe*, *J. Phys. Conf. Ser.* **222** (2010) 012007, [arXiv:1001.2007].

[10] R. Arnowitt, S. Deser, and C. W. Misner, *Dynamical structure and definition of energy in general relativity*, *Phys. Rev.* **116** (Dec, 1959) 1322–1330.

[11] G. W. Gibbons, *The Einstein Action of Riemannian Metrics and Its Relation to Quantum Gravity and Thermodynamics*, *Phys. Lett.* **A61** (1977) 3–5.

[12] G. W. Gibbons, S. W. Hawking, and J. M. Stewart, *A Natural Measure on the Set of All Universes*, *Nucl. Phys.* **B281** (1987) 736.

[13] S. W. Hawking and D. N. Page, *How probable is inflation?*, *Nucl. Phys.* **B298** (1988) 789–809.

[14] J. Hartle, S. Hawking, and T. Hertog, *The Classical Universes of the No-Boundary Quantum State*, *Phys.Rev.* **D77** (2008) 123537, [arXiv:0803.1663].

[15] J. Hartle, S. W. Hawking, and T. Hertog, *The No-Boundary Measure in the Regime of Eternal Inflation*, *Phys. Rev.* **D82** (2010) 063510, [arXiv:1001.0262].

[16] G. W. Lyons, *Complex solutions for the scalar field model of the universe*, *Phys. Rev.* **D46** (1992) 1546–1550.

[17] J. Hartle and T. Hertog, *Quantum transitions between classical histories*, *Phys. Rev.* **D92** (2015), no. 6 063509, [arXiv:1502.06770].

[18] A. Linde, *The New Inflationary Universe Scenario*, in *Cambridge 1982, Proceedings, The Very Early Universe*, pp. 205–249, 1982.

[19] P. Steinhard, *Natural Inflation*, in *Cambridge 1982, Proceedings, The Very Early Universe*, pp. 251–266, 1982.

[20] A. Vilenkin, *Birth of inflationary universes*, *Phys. Rev. D* **27** (Jun, 1983) 2848–2855.

[21] A. Linde,
Eternal chaotic iflation, *Modern Physics Letters A* **01** (1986), no. 02 81–85, [http://www.worldscientific.com/doi/pdf/10.1142/S0217732386000129].

[22] A. Linde, *Eternally existing self-reproducing chaotic inflanationary universe*, *Physics Letters B* **175** (1986), no. 4 395 – 400.

[23] A. Linde, *A brief history of the multiverse*, *Rept. Prog. Phys.* **80** (2017), no. 2 022001, [arXiv:1512.01203].

[24] M. Aryal and A. Vilenkin, *The fractal dimension of the inflationary universe*, *Physics Letters B* **199** (1987), no. 3 351 – 357.

[25] A. D. Linde, D. A. Linde, and A. Mezhlumian, *From the Big Bang theory to the theory of a stationary universe*, *Phys. Rev.* **D49** (1994) 1783–1826, [gr-qc/9306035].

[26] J. Hartle, S. W. Hawking, and T. Hertog, *Local Observation in Eternal inflation*, *Phys. Rev. Lett.* **106** (2011) 141302, [arXiv:1009.2525].

[27] A. D. Linde, *Inflationary multiverse*, July, 2009.

[28] G. 't Hooft, *Dimensional reduction in quantum gravity*, in *Salamfest 1993:0284-296*, pp. 0284–296, 1993. gr-qc/9310026.

[29] L. Susskind, *The World as a hologram*, *J. Math. Phys.* **36** (1995) 6377–6396, [hep-th/9409089].

[30] J. M. Maldacena, *The Large N limit of superconformal field theories and supergravity*, *Int. J. Theor. Phys.* **38** (1999) 1113–1133, [hep-th/9711200]. [Adv. Theor. Math. Phys.2,231(1998)].

[31] E. Witten, *Anti-de Sitter space and holography*, *Adv. Theor. Math. Phys.* **2** (1998) 253–291, [hep-th/9802150].

[32] S. Kachru, R. Kallosh, A. D. Linde, and S. P. Trivedi, *De Sitter vacua in string theory*, *Phys. Rev.* **D68** (2003) 046005, [hep-th/0301240].

[33] N. Goheer, M. Kleban, and L. Susskind, *The Trouble with de Sitter space*, *JHEP* **07** (2003) 056, [hep-th/0212209].

[34] A. Strominger, *The dS / CFT correspondence*, *JHEP* **10** (2001) 034, [hep-th/0106113].

[35] J. D. Brown and M. Henneaux, *Central charges in the canonical realization of asymptotic symmetries: an example from three-dimensional gravity*, *Comm. Math. Phys.* **104** (1986), no. 2 207–226.

[36] D. Anninos, T. Hartman, and A. Strominger, *Higher Spin Realization of the dS/CFT Correspondence*, *Class. Quant. Grav.* **34** (2017), no. 1 015009, [arXiv:1108.5735].

[37] E. S. Fradkin and M. A. Vasiliev, *On the Gravitational Interaction of Massless Higher Spin Fields*, *Phys. Lett.* **B189** (1987) 89–95.

[38] I. R. Klebanov and E. Witten, *AdS / CFT correspondence and symmetry breaking*, *Nucl. Phys.* **B556** (1999) 89–114, [hep-th/9905104].

[39] I. R. Klebanov and A. M. Polyakov, *AdS dual of the critical O(N) vector model*, *Phys. Lett.* **B550** (2002) 213–219, [hep-th/0210114].

[40] J. M. Maldacena, *Non-Gaussian features of primordial fluctuations in single field inflationary models*, *JHEP* **0305** (2003) 013, [astro-ph/0210603].

[41] D. Anninos, F. Denef, and D. Harlow, *Wave function of Vasiliev's universe: A few slices thereof*, *Phys.Rev.* **D88** (2013), no. 8 084049, [arXiv:1207.5517].

[42] D. Anninos, F. Denef, G. Konstantinidis, and E. Shaghoulian, *Higher Spin de Sitter Holography from Functional Determinants*, *JHEP* **1402** (2014) 007, [arXiv:1305.6321].

[43] T. Hertog and J. Hartle, *Holographic No-Boundary Measure*, *JHEP* **1205** (2012) 095, [arXiv:1111.6090].

[44] J. B. Hartle, S. Hawking, and T. Hertog, *Accelerated Expansion from Negative* Λ, [arXiv:1205.3807].

[45] C. Fefferman and C. Graham, *Conformal invariants*, *Élie Cartan et les Mathématiques d'aujourdhui* **95** (Asterisque, 1985).

[46] A. A. Starobinsky, *Isotropization of arbitrary cosmological expansion given an effective cosmological constant*, *JETP Lett.* **37** (1983) 66–69.

[47] G. Conti, T. Hertog, and E. van der Woerd, *Holographic Tunneling Wave Function*, *JHEP* **12** (2015) 025, [arXiv:1506.07374].

[48] I. Papadimitriou, *Holographic renormalization as a canonical transformation*, *JHEP* **1011** (2010) 014, [arXiv:1007.4592].

[49] T. Hertog, R. Monten, and Y. Vreys, *Lorentzian Condition in Holographic Cosmology*, *JHEP* **01** (2017) 060, [arXiv:1607.07471].

[50] L. Liu, *Holographic renormalization in no-boundary quantum cosmology*, [arXiv:1412.1819].

[51] L. Battarra and J.-L. Lehners, *On the No-Boundary Proposal for Ekpyrotic and Cyclic Cosmologies*, *JCAP* **1412** (2014), no. 12 023, [arXiv:1407.4814].

[52] N. Bobev, T. Hertog, and Y. Vreys, *The NUTs and Bolts of Squashed Holography*, *JHEP* **11** (2016) 140, [arXiv:1610.01497].

[53] G. Conti, T. Hertog, and Y. Vreys, *Holographic Measure on Eternal Inflation*, [arXiv:1707.09663].

[54] E. Sezgin and P. Sundell, *Massless higher spins and holography*, *Nucl. Phys.* **B644** (2002) 303–370, [hep-th/0205131]. [Erratum: Nucl. Phys.B660,403(2003)].

[55] S. Giombi and X. Yin, *Higher Spin Gauge Theory and Holography: The Three-Point Functions*, *JHEP* **09** (2010) 115, [arXiv:0912.3462].

[56] A. H. Taub, *Empty space-times admitting a three parameter group of motions*, *Annals of Mathematics* **53** (1951), no. 3 472–490.

[57] E. Newman, L. Tamburino, and T. Unti, *Empty-Space Generalization of the Schwarzschild Metric*, *Journal of Mathematical Physics* **4** (1963), no. 7 915–923.

[58] N. Hama, K. Hosomichi, and S. Lee, *SUSY Gauge Theories on Squashed Three-Spheres*, *JHEP* **05** (2011) 014, [arXiv:1102.4716].

[59] Y. Imamura and D. Yokoyama, *N=2 supersymmetric theories on squashed three-sphere*, *Phys. Rev.* **D85** (2012) 025015, [arXiv:1109.4734].

[60] Y. Imamura, *Relation between the 4d superconformal index and the S^3 partition function*, *JHEP* **09** (2011) 133, [arXiv:1104.4482].

[61] C. Closset, T. T. Dumitrescu, G. Festuccia, and Z. Komargodski, *Supersymmetric Field Theories on Three-Manifolds*, *JHEP* **05** (2013) 017, [arXiv:1212.3388].

[62] T. Nishioka and K. Yonekura, *On RG Flow of τ_{RR} for Supersymmetric Field Theories in Three-Dimensions*, *JHEP* **05** (2013) 165, [arXiv:1303.1522].

[63] D. Martelli and J. Sparks, *The gravity dual of supersymmetric gauge theories on a biaxially squashed three-sphere*, *Nucl. Phys.* **B866** (2013) 72–85, [arXiv:1111.6930].

[64] D. Martelli, A. Passias, and J. Sparks, *The gravity dual of supersymmetric gauge theories on a squashed three-sphere*, *Nucl. Phys.* **B864** (2012) 840–868, [arXiv:1110.6400].

[65] D. Martelli, A. Passias, and J. Sparks, *The supersymmetric NUTs and bolts of holography*, *Nucl. Phys.* **B876** (2013) 810–870, [arXiv:1212.4618].

[66] D. Martelli and A. Passias, *The gravity dual of supersymmetric gauge theories on a two-parameter deformed three-sphere*, *Nucl. Phys.* **B877** (2013) 51–72, [arXiv:1306.3893].

[67] N. Bobev, P. Bueno, and Y. Vreys, *Comments on Squashed-sphere Partition Functions*, *JHEP* **07** (2017) 093, [arXiv:1705.00292].

[68] R. Emparan, C. V. Johnson, and R. C. Myers, *Surface terms as counterterms in the AdS / CFT correspondence*, *Phys. Rev.* **D60** (1999) 104001, [hep-th/9903238].

[69] H. Stephani, D. Kramer, M. A. H. MacCallum, C. Hoenselaers, and E. Herlt, *Exact solutions of Einstein's field equations*. Cambridge University Press, 2004.

[70] C. W. Misner, *The flatter regions of newman, unti, and tamburino s generalized schwarzschild space*, *Journal of Mathematical Physics* **4** (1963), no. 7 924–937.

[71] M. J. Duff and J. T. Liu, *Anti-de Sitter black holes in gauged N = 8 supergravity*, *Nucl. Phys.* **B554** (1999) 237–253, [hep-th/9901149].

[72] R. B. Mann, *Misner string entropy*, *Phys. Rev.* **D60** (1999) 104047, [hep-th/9903229].

[73] K. Skenderis, *Lecture notes on holographic renormalization*, *Class. Quant. Grav.* **19** (2002) 5849–5876, [hep-th/0209067].

[74] I. Papadimitriou, *Multi-Trace Deformations in AdS/CFT: Exploring the Vacuum Structure of the Deformed CFT*, *JHEP* **05** (2007) 075, [hep-th/0703152].

[75] J. M. Maldacena, *Eternal black holes in anti-de Sitter*, *JHEP* **04** (2003) 021, [hep-th/0106112].

[76] S. A. Hartnoll and S. P. Kumar, *The O(N) model on a squashed S**3 and the Klebanov-Polyakov correspondence*, *JHEP* **06** (2005) 012, [hep-th/0503238].

[77] B. L. Hu, *Scalar Waves in the Mixmaster Universe. I. The Helmholtz Equation in a Fixed Background*, *Phys. Rev. D* **8** (Aug, 1973) 1048–1060.

[78] T. C. Shen and J. Sobczyk, *Higher-dimensional self-consistent solution with deformed internal space*, *Phys. Rev. D* **36** (Jul, 1987) 397–411.

[79] J. S. Dowker, *Effective actions on the squashed three sphere*, *Class. Quant. Grav.* **16** (1999) 1937–1953, [hep-th/9812202].

[80] I. R. Klebanov, S. S. Pufu, and B. R. Safdi, *F-Theorem without Supersymmetry*, *JHEP* **10** (2011) 038, [arXiv:1105.4598].

[81] D. V. Vassilevich, *Heat kernel expansion: User's manual*, *Phys. Rept.* **388** (2003) 279–360, [hep-th/0306138].

[82] H. Osborn and A. C. Petkou, *Implications of conformal invariance in field theories for general dimensions*, *Annals Phys.* **231** (1994) 311–362, [hep-th/9307010].

[83] N. Bobev, S. El-Showk, D. Mazac, and M. F. Paulos, *Bootstrapping SCFTs with Four Supercharges*, *JHEP* **08** (2015) 142, [arXiv:1503.02081].

[84] A. Buchel, J. Escobedo, R. C. Myers, M. F. Paulos, A. Sinha, and M. Smolkin, *Holographic GB gravity in arbitrary dimensions*, *JHEP* **03** (2010) 111, [arXiv:0911.4257].

[85] H. Casini and M. Huerta, *On the RG running of the entanglement entropy of a circle*, *Phys. Rev.* **D85** (2012) 125016, [arXiv:1202.5650].

[86] S. S. Pufu, *The F-Theorem and F-Maximization*, 2016. arXiv:1608.02960.

[87] D. L. Jafferis, I. R. Klebanov, S. S. Pufu, and B. R. Safdi, *Towards the F-Theorem: N=2 Field Theories on the Three-Sphere*, *JHEP* **06** (2011) 102, [arXiv:1103.1181].

[88] E. Perlmutter, *A universal feature of CFT Renyi entropy*, *JHEP* **03** (2014) 117, [arXiv:1308.1083].

[89] J. L. Cardy, *Is There a c Theorem in Four-Dimensions?*, *Phys. Lett.* **B215** (1988) 749–752.

[90] C. Closset, T. T. Dumitrescu, G. Festuccia, Z. Komargodski, and N. Seiberg, *Contact Terms, Unitarity, and F-Maximization in Three-Dimensional Superconformal Theories*, *JHEP* **10** (2012) 053, [arXiv:1205.4142].

[91] M. De Francia, K. Kirsten, and J. S. Dowker, *Effective actions on squashed lens spaces*, *Class. Quant. Grav.* **18** (2001) 955–968, [hep-th/0008059].

[92] G. Gibbons, *Spectral asymmetry and quantum field theory in curved spacetime*, *Annals of Physics* **125** (1980), no. 1 98 – 116.

[93] N. Hitchin, *Harmonic spinors*, *Advances in Mathematics* **14** (1974), no. 1 1 – 55.

[94] J. Erdmenger and H. Osborn, *Conserved currents and the energy momentum tensor in conformally invariant theories for general dimensions*, *Nucl. Phys.* **B483** (1997) 431–474, [hep-th/9605009].

[95] D. M. Hofman and J. Maldacena, *Conformal collider physics: Energy and charge correlations*, *JHEP* **05** (2008) 012, [arXiv:0803.1467].

[96] P. Bueno, R. C. Myers, and W. Witczak-Krempa, *Universality of corner entanglement in conformal field theories*, *Phys. Rev. Lett.* **115** (2015), no. 2 021602, [arXiv:1505.04804].

[97] P. Bueno and R. C. Myers, *Corner contributions to holographic entanglement entropy*, *JHEP* **08** (2015) 068, [arXiv:1505.07842].

[98] H. Casini, M. Huerta, and R. C. Myers, *Towards a derivation of holographic entanglement entropy*, *JHEP* **05** (2011) 036, [arXiv:1102.0440].

[99] J. S. Dowker, *Entanglement entropy for odd spheres*, [arXiv:1012.1548].

[100] A. Allais and M. Mezei, *Some results on the shape dependence of entanglement and Renyi entropies*, *Phys. Rev.* **D91** (2015), no. 4 046002, [arXiv:1407.7249].

[101] M. Mezei, *Entanglement entropy across a deformed sphere*, *Phys. Rev.* **D91** (2015), no. 4 045038, [arXiv:1411.7011].

[102] V. Rosenhaus and M. Smolkin, *Entanglement Entropy: A Perturbative Calculation*, *JHEP* **12** (2014) 179, [arXiv:1403.3733].

[103] V. Rosenhaus and M. Smolkin, *Entanglement Entropy for Relevant and Geometric Perturbations*, *JHEP* **02** (2015) 015, [arXiv:1410.6530].

[104] A. Lewkowycz and E. Perlmutter, *Universality in the geometric dependence of Renyi entropy*, *JHEP* **01** (2015) 080, [arXiv:1407.8171].

[105] R.-X. Miao, *A holographic proof of the universality of corner entanglement for CFTs*, *JHEP* **10** (2015) 038, [arXiv:1507.06283].

[106] P. Bueno and R. C. Myers, *Universal entanglement for higher dimensional cones*, *JHEP* **12** (2015) 168, [arXiv:1508.00587].

[107] T. Faulkner, R. G. Leigh, and O. Parrikar, *Shape Dependence of Entanglement Entropy in Conformal Field Theories*, *JHEP* **04** (2016) 088, [arXiv:1511.05179].

[108] G. Conti and T. Hertog, *Two wave functions and dS/CFT on* $S^1 \times S^2$, *JHEP* **06** (2015) 101, [arXiv:1412.3728].

[109] S. W. Hawking and T. Hertog, *A Smooth Exit from Eternal Inflation*, [arXiv:1707.07702].

[110] J. Hartle and T. Hertog, *Arrows of Time in the Bouncing Universes of the No-boundary Quantum State*, *Phys. Rev.* **D85** (2012) 103524, [arXiv:1104.1733].

[111] S. F. Bramberger, T. Hertog, J.-L. Lehners, and Y. Vreys, *Quantum Transitions Through Cosmological Singularities*, *JCAP* **1707** (2017), no. 07 007, [arXiv:1701.05399].

[112] J. B. Hartle, S. Hawking, and T. Hertog, *No-Boundary Measure of the Universe*, *Phys.Rev.Lett.* **100** (2008) 201301, [arXiv:0711.4630].

[113] J. Khoury, B. A. Ovrut, P. J. Steinhardt, and N. Turok, *The Ekpyrotic universe: Colliding branes and the origin of the hot big bang*, *Phys. Rev.* **D64** (2001) 123522, [hep-th/0103239].

[114] J.-L. Lehners, *Ekpyrotic and Cyclic Cosmology*, *Phys. Rept.* **465** (2008) 223–263, [arXiv:0806.1245].

[115] J. Khoury, B. A. Ovrut, N. Seiberg, P. J. Steinhardt, and N. Turok, *From big crunch to big bang*, *Phys. Rev.* **D65** (2002) 086007, [hep-th/0108187].

[116] J.-L. Lehners, P. McFadden, and N. Turok, *Colliding Branes in Heterotic M-theory*, *Phys. Rev.* **D75** (2007) 103510, [hep-th/0611259].

[117] C. Cartier, R. Durrer, and E. J. Copeland, *Cosmological perturbations and the transition from contraction to expansion*, *Phys. Rev.* **D67** (2003) 103517, [hep-th/0301198].

[118] A. J. Tolley, N. Turok, and P. J. Steinhardt, *Cosmological perturbations in a big crunch / big bang space-time*, *Phys. Rev.* **D69** (2004) 106005, [hep-th/0306109].

[119] E. I. Buchbinder, J. Khoury, and B. A. Ovrut, *New Ekpyrotic cosmology*, *Phys. Rev.* **D76** (2007) 123503, [hep-th/0702154].

[120] P. Creminelli and L. Senatore, *A Smooth bouncing cosmology with scale invariant spectrum*, *JCAP* **0711** (2007) 010, [hep-th/0702165].

[121] J.-L. Lehners, *Cosmic Bounces and Cyclic Universes*, *Class. Quant. Grav.* **28** (2011) 204004, [arXiv:1106.0172].

[122] A. Ijjas and P. J. Steinhardt, *Fully stable cosmological solutions with a non-singular classical bounce*, [arXiv:1609.01253].

[123] M. Koehn, J.-L. Lehners, and B. A. Ovrut, *Cosmological super-bounce*, *Phys. Rev.* **D90** (2014), no. 2 025005, [arXiv:1310.7577].

[124] L. Battarra, M. Koehn, J.-L. Lehners, and B. A. Ovrut, *Cosmological Perturbations Through a Non-Singular Ghost-Condensate/Galileon Bounce*, *JCAP* **1407** (2014) 007, [arXiv:1404.5067].

[125] P. Creminelli, M. A. Luty, A. Nicolis, and L. Senatore, *Starting the Universe: Stable Violation of the Null Energy Condition and Non-standard Cosmologies*, *JHEP* **12** (2006) 080, [hep-th/0606090].

[126] T. Qiu, J. Evslin, Y.-F. Cai, M. Li, and X. Zhang, *Bouncing Galileon Cosmologies*, *JCAP* **1110** (2011) 036, [arXiv:1108.0593].

[127] D. A. Easson, I. Sawicki, and A. Vikman, *G-Bounce*, *JCAP* **1111** (2011) 021, [arXiv:1109.1047].

[128] B. Craps, T. Hertog, and N. Turok, *On the Quantum Resolution of Cosmological Singularities using AdS/CFT*, *Phys. Rev.* **D86** (2012) 043513, [arXiv:0712.4180].

[129] J. L. Barbón and E. Rabinovici, *AdS crunches, CFT falls, and cosmological complexity*, in *Lecture Notes, Les Houches Summer School, 97th Session: Theoretical Physics to Face the Challenge of LHC: Les Houches, France, August 1-26, 2011*, pp. 367–394, 2015.

[130] A. Awad, S. R. Das, A. Ghosh, J.-H. Oh, and S. P. Trivedi, *Slowly Varying Dilaton Cosmologies and their Field Theory Duals*, *Phys. Rev.* **D80** (2009) 126011, [arXiv:0906.3275].

[131] L. Battarra and T. Hertog, *Particle Production near an AdS Crunch*, *JHEP* **12** (2010) 017, [arXiv:1009.0992].

[132] N. Turok, *On Quantum Tunneling in Real Time*, *New J. Phys.* **16** (2014) 063006, [arXiv:1312.1772].

[133] S. F. Bramberger, G. Lavrelashvili, and J.-L. Lehners, *Quantum tunneling from paths in complex time*, *Phys. Rev.* **D94** (2016), no. 6 064032, [arXiv:1605.02751].

[134] L. Battarra and J.-L. Lehners, *On the Creation of the Universe via Ekpyrotic Instantons*, *Phys. Lett.* **B742** (2015) 167–171, [arXiv:1406.5896].

[135] J.-L. Lehners, *Classical Inflationary and Ekpyrotic Universes in the No-Boundary Wavefunction*, *Phys. Rev.* **D91** (2015), no. 8 083525, [arXiv:1502.00629].

[136] S. Gielen and N. Turok, *Perfect Quantum Cosmological Bounce*, *Phys. Rev. Lett.* **117** (2016), no. 2 021301, [arXiv:1510.00699].

[137] P. Chen, Y.-C. Hu, and D.-h. Yeom, *Fuzzy Euclidean wormholes in de Sitter space*, [arXiv:1611.08468].

[138] K. Skenderis and B. C. van Rees, *Holography and wormholes in 2+1 dimensions*, *Commun. Math. Phys.* **301** (2011) 583–626, [arXiv:0912.2090].

[139] J. Feldbrugge, J.-L. Lehners, and N. Turok, *Lorentzian Quantum Cosmology*, *Phys. Rev.* **D95** (2017), no. 10 103508, [arXiv:1703.02076].

[140] J. Feldbrugge, J.-L. Lehners, and N. Turok, *No smooth beginning for spacetime*, [arXiv:1705.00192].

[141] J. Diaz Dorronsoro, J. J. Halliwell, J. B. Hartle, T. Hertog, and O. Janssen, *The Real No-Boundary Wave Function in Lorentzian Quantum Cosmology*, [arXiv:1705.05340].

[142] L. D. Landau, *Quantum mechanics : non-relativistic theory*. Pergamon Press, Oxford New York, 1977.

[143] J. S. Dowker and D. F. Pettengill, *The quantum mechanics of the ideal asymmetric top with spin (frozen mixmaster universe)*, *Journal of Physics A: Mathematical, Nuclear and General* **7** (1974), no. 13 1527.

LIST OF PUBLICATIONS

1. T. Hertog, R. Monten, and Y. Vreys, *Lorentzian Condition in Holographic Cosmology*, *JHEP* **01** (2017) 060, [arXiv:1607.07471]

2. N. Bobev, T.Hertog, and Y. Vreys, *The NUTs and Bolts of Squashed Holography*, *JHEP* **11** (2016) 140, [arXiv:1610.01497]

3. S. F. Bramberger, T. Hertog, J. Lehners, and Y. Vreys, *Quantum Transitions Through Cosmological Singularities*, *JCAP* **07** (2017) 007, [arXiv:1701.05399]

4. N. Bobev, P. Bueno, and Y. Vreys, *Comments on Squashed-Sphere Partition Functions*, *JHEP* **07** (2017) 093, [arXiv:1705.00292]

5. G. Conti, T. Hertog, and Y. Vreys, *Holographic Measure on Anisotropic Minisuperspace*, *In publication*, [arXiv:1707.09663]

FACULTY OF SCIENCE
DEPARTMENT OF PHYSICS AND ASTRONOMY
INSTITUUT VOOR THEORETISCHE FYSICA
Celestijnenlaan 200D
B-3001 Leuven
https://fys.kuleuven.be/itf